Spring 1-1-2012

An Investigation of Optimal Control of Desiccant-Enhanced Evaporative Air Conditioning

Aaron Patrick Boranian
University of Colorado at Boulder, flyn.hawyn@gmail.com

An Investigation of Optimal Control of Desiccant-Enhanced Evaporative Air Conditioning

by

Aaron P. Boranian

B. Eng., Colorado School of Mines, 2009

A thesis submitted to the

Faculty of the Graduate School of the

University of Colorado in partial fulfillment

of the requirements for the degree of

Masters of Science

Department of Civil, Environmental, and Architectural Engineering

2012

This thesis entitled:
An Investigation of Optimal Control of Desiccant-Enhanced Evaporative Air Conditioning
written by Aaron P. Boranian
has been approved for the Department of Civil, Environmental and Architectural Engineering

_____
Michael Brandemuehl, PhD, P.E.

_____
Jay Burch, PhD

_____
Gregor Henze, PhD, P.E.

Date _____

The final copy of this thesis has been examined by the signatories, and we find that both the content and the form meet the acceptable presentation standards of scholarly work in the above mentioned discipline.

Boranian, Aaron P. (M.S., Civil, Environmental, and Architectural Engineering)

An Investigation of Optimal Control of Desiccant-Enhanced Evaporative Air Conditioning

Thesis directed by Prof. Michael Brandemuehl, PhD, P.E.

The purpose of this research is to determine an optimal control strategy for an air conditioner that simultaneously uses liquid desiccant dehumidification and indirect evaporative cooling. The advantages posed by liquid desiccant dehumidification are numerous: significant reduction (80-90%) in electricity consumption, air pollutant removal, potential to use low-grade energy for regeneration, and avoiding a need for excessive cooling and reheating of process air. The National Renewable Energy Laboratory in Golden, CO has developed an innovative air conditioner that combines liquid desiccant dehumidification and indirect evaporative cooling, referred to as Desiccant-Enhanced Evaporative Air Conditioning, or DEVap. In the first stage of the device, process air is dehumidified with a liquid desiccant film and simultaneously cooled with an evaporatively-cooled airstream. In the second stage of the device, another evaporatively-cooled airstream removes sensible energy from the process air without changing the humidity of the process air. This second evaporatively-cooled airstream is siphoned off from the cool-dry process air exiting the device, providing a large cooling potential.

Latent and sensible cooling loads can be met independently by adjusting four control variables: mixed air flow ratio (R_{ma}), first stage exhaust flow ratio (R_{e1}), outdoor air fraction (OAF), and inlet liquid desiccant concentration ($C_{LD,in,DEVap}$). A wide range of outdoor and return air conditions and sensible heat ratio values were simulated with the intent of optimizing

source coefficient of performance (COP_{source}) by changing control variable values. From these simulations, optimal control strategies were developed.

Control strategies are divided into three cases: (1) latent cooling only, (2) sensible cooling only, and (3) both sensible and latent cooling. A simple strategy concerning R_{ma} and $C_{LD,in,DEVap}$ was developed for case (1). For case (2), it was determined that return air states had less influence than outdoor air states and that holding OAF and R_{e1} constant while linearly increasing R_{ma} would be satisfactory for most cases. For case (3), optimal control was divided into two phases: a ramping phase where OAF and R_{e1} are held constant while R_{ma} linearly increases and a final phase where R_{ma} is held at its maximum value and OAF slightly shifts value to provide larger cooling capacities.

Acknowledgements

The author would like to thank: the National Renewable Energy Laboratory (NREL) for providing the opportunity to work on this project, their monetary support and their patience; Jay Burch, Eric Kozubal, and Jason Woods at NREL for their constant guidance and willingness to offer assistance; Andy Lowenstein and AIL Research for performing experiments concerning desiccant regenerators; Matt Duffy from Thermal Energy System Specialists for his technical support and knowledge concerning the Transient System Simulations software; Michael Brandemuehl, PhD, P.E., for his advice, support and motivation; Gregor Henze, PhD, P.E., for his extensive insight and tutelage concerning control strategies; and finally, the Boranian family for their endless supply of love and support throughout this process and my life.

Table of Contents

List of Tables

List of Figures

Glossary

Accronyms and Abbreviations

AAHX	Air-to-air heat exchanger
AILR	AIL Research
A/C	Air conditioning
COP	Coefficient of performance
DEVap	Desiccant-enhanced evaporative cooling
DX	Direct expansion
ICHX	Interchange heat exchanger
IEC	Indirect evaporative cooling
LDAC	Liquid desiccant air conditioner
NREL	National Renewable Energy Laboratory
OAF	Outdoor air fraction
RH	Relative humidity
SHR	Sensible heat ratio

Variable Definitions

C	Concentration
m	Mass flow rate
R	Ratio of actual mass flow rate to design mixed air mass flow rate

Subscripts

e1	First stage exhaust air
e2	Second stage exhaust air
in	Inlet state
LD	Liquid desiccant
ma	Mixed air
near-opt	Variable value to use in near-optimal control strategy
oa	Outdoor air
out	Outlet state
ra	Return air
reg	Regenerator

Chapter 1: Introduction

1.1 Air-Conditioning Background

Today's air-conditioning (A/C) is primarily based on the direct expansion (DX) process invented more than 100 years ago. Due to its ability to maintain comfortable environments, it has become commonplace in many areas around the world. However, the widespread use of DX A/C, which is powered solely by electricity, has multiple consequences. For example, A/C uses approximately 10.5 out of 38.8 quadrillion Btu (quads) of the source energy used for annual electricity production in the United States alone, which results in the release of about 620 million tons of carbon dioxide into the atmosphere (EIA 2009). Also, with a current source-to-site energy ratio of approximately 3.4 for electricity production, only 3.1 quads of electrical energy are actually delivered to users out of the 10.5 quads of energy used to generate electricity. The remaining 7.4 quads of thermal energy are rejected as waste heat to the environment during the processes of generating, transmitting, and distributing electricity.

Another major drawback to DX A/C is that it does not currently have the capability to meet latent and sensible loads independently at reasonable costs. Humidity is reduced by cooling air below the dew point temperature of the space, causing moisture to condense out of the air on the cooling coil. The air is then heated to an appropriate temperature before being discharged into the space. This process of sensibly over-cooling and then heating air requires unnecessary consumption of energy.

1.2 Liquid Desiccant Background

Developments to incorporate liquid desiccants into cooling systems were first made in the 1930s [2]. Liquid desiccants, which include glycols and halide salt solutions, have a strong capability to dehumidify air streams. This is due to the fact that desiccants typically have an equilibrium vapor pressure that is lower than the vapor pressure of air, and this vapor pressure difference creates a driving potential for moisture transfer. The mass concentration of desiccant material decreases as desiccant solutions absorb moisture, causing the equilibrium vapor pressure to increase and reduce the driving potential for moisture transfer. Energy must be consumed to heat the desiccant to a temperature where its equilibrium vapor pressure is greater than air so that moisture can be released, but this regeneration process can be accomplished with low-quality energy sources such as waste heat or solar energy.

1.3 DEVap Technology

The National Renewable Energy Laboratory (NREL) has been developing, primarily with AIL Research (AILR) as an industry partner, liquid-desiccant-based A/C (LDAC) for over 15 years. The technology uses liquid desiccants to utilize water as the refrigerant instead of chlorofluorocarbon-based refrigerants to drive the cooling process. Since desiccants drive dehumidification processes, evaporative cooling devices can be used in novel ways in all climates. This type of desiccant A/C system decouples the sensible and latent cooling loads, allowing each to be met independently. NREL's desiccant-enhanced evaporative cooling (DEVap) concept enhances LDAC technology through the use of membranes separating

channels and novel heat and mass exchangers (HMX) [3]. The DEVap concept is explained in detail in Section 3.1 of this thesis.

1.4 Why DEVap?

There are multiple benefits to incorporating the DEVap concept to meet cooling loads. One benefit is that it will substitute electricity use with thermal energy use for liquid desiccant regeneration, which can be powered by many types of energy sources, including natural gas, solar thermal, biofuels, and waste heat. This results in generally lower source energy use, much lower peak electricity demand, and lower carbon emissions, especially when a renewable fuel is used. Also, since sensible and latent cooling loads can be met independently, occupant comfort will be better than during the use of conventional DX A/C technology.

A key benefit of DEVap is that it combines dehumidification, air conditioning, and ventilation into one packaged unit, simplifying the installation process. DEVap also does not require a cooling tower, which reduces maintenance. Figure 1.1 shows how DEVap would replace conventional DX A/C units. The left half shows possible regeneration strategies.

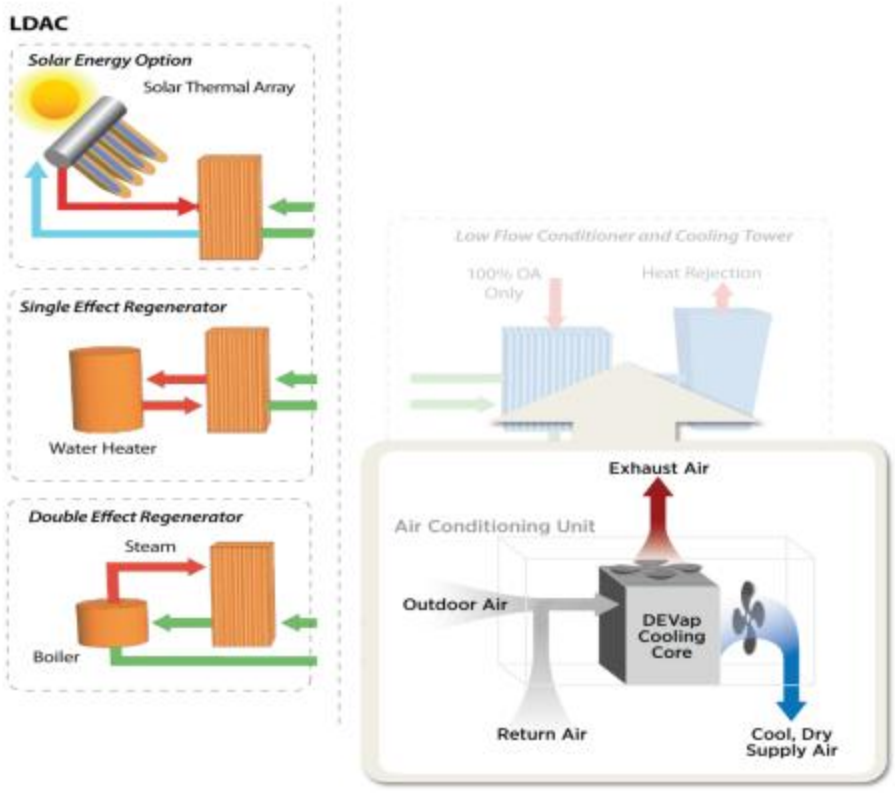

Figure 1.1: DEVap enhancement for LDAC [3]

1.5 Objective

This project has the overall objective of devising a method to ascertain optimal control strategies for the operation of a cooling system that employs the DEVap concept with a two-stage regenerator. In October 2010, the author had performed annual simulations comparing energy consumption for houses in eight different US cities using DX A/C and DEVap using the Transient System Simulations (TRNSYS) software [3]. While the results showed that DEVap did consume less source energy than DX A/C, time constraints imposed on the author led to the application of simple initial control strategies without an investigation into how to achieve optimal operation. In order to determine optimal control strategies, the independent and dependent variables that affect DEVap's cooling performance must be identified, as well as the

expected range of values for each variable that DEVap can experience. For a given set of independent variable values, the dependent variables that can be controlled must be altered in order to determine what combination yields optimal cooling performance. Since capturing all optimal events in one algorithm is extremely difficult, the final step of this project is to devise "near-optimal" control strategies that capture trends observed in optimal operation while being easier to implement in future work.

1.6 Thesis Organization

The following first presents a review of relevant research into the areas of desiccant technology, recent LDAC technology advancements, DEVap simulation, and optimal control strategies for LDAC systems similar to DEVap.

Next, detailed descriptions of DEVap's components and control variables are presented. The operation of different cooling modes for DEVap is discussed next. Since latent and sensible loads can be met independently, DEVap has the option to only dehumidify in a nearly adiabatic fashion, only sensibly cool, or do both at the same time. For each mode, the working components and control variables of DEVap and typical air states are explained. The components and control variables of the modeled regenerator system are also described.

The computer modeling methodologies for DEVap and the regenerator system are discussed next. Two-dimensional nodal heat and mass transfer equations were utilized to ensure accuracy in the DEVap model. Results from the models were then used in a "design of

experiments" approach in order to develop correlations for DEVap operation and simplify future work.

The thesis continues by discussing the methodology employed to determine optimal operating strategies. The correlations from the design of experiments were used to expedite the process in Microsoft Excel. An explanation of expected value ranges for control variables for each mode of operation is given.

This is followed by simulation results for optimal operation and near-optimal strategies that were developed from these results. An overview of how these control strategies can be practically implemented is given.

Finally, general conclusions of near-optimal control strategies for DEVap and areas of future research are presented.

Chapter 2: Literature Review

This chapter presents research previously performed that provides supplementary information pertaining to this thesis. Liquid desiccant technology is presented first, followed by systems that combine liquid desiccant with a sensible cooling technology. Research analyzing the DEVap concept where liquid desiccants and evaporative cooling are combined in an air conditioning system follows. Finally, research examining optimal control of such air conditioning systems is analyzed.

2.1 LDAC Background

Desiccants have been proven to have a strong capability to dehumidify air streams. This is due to the fact that desiccants typically have an equilibrium vapor pressure that is lower than the vapor pressure of air, and this vapor pressure difference creates a driving potential for moisture transfer. When air comes into equilibrium with a liquid desiccant of fixed concentration, the plotted air states on a psychrometric chart mimic a line of constant relative humidity. Figure 2.2 shows this relationship for solutions of lithium chloride (LiCl) and calcium chloride ($CaCl_2$).

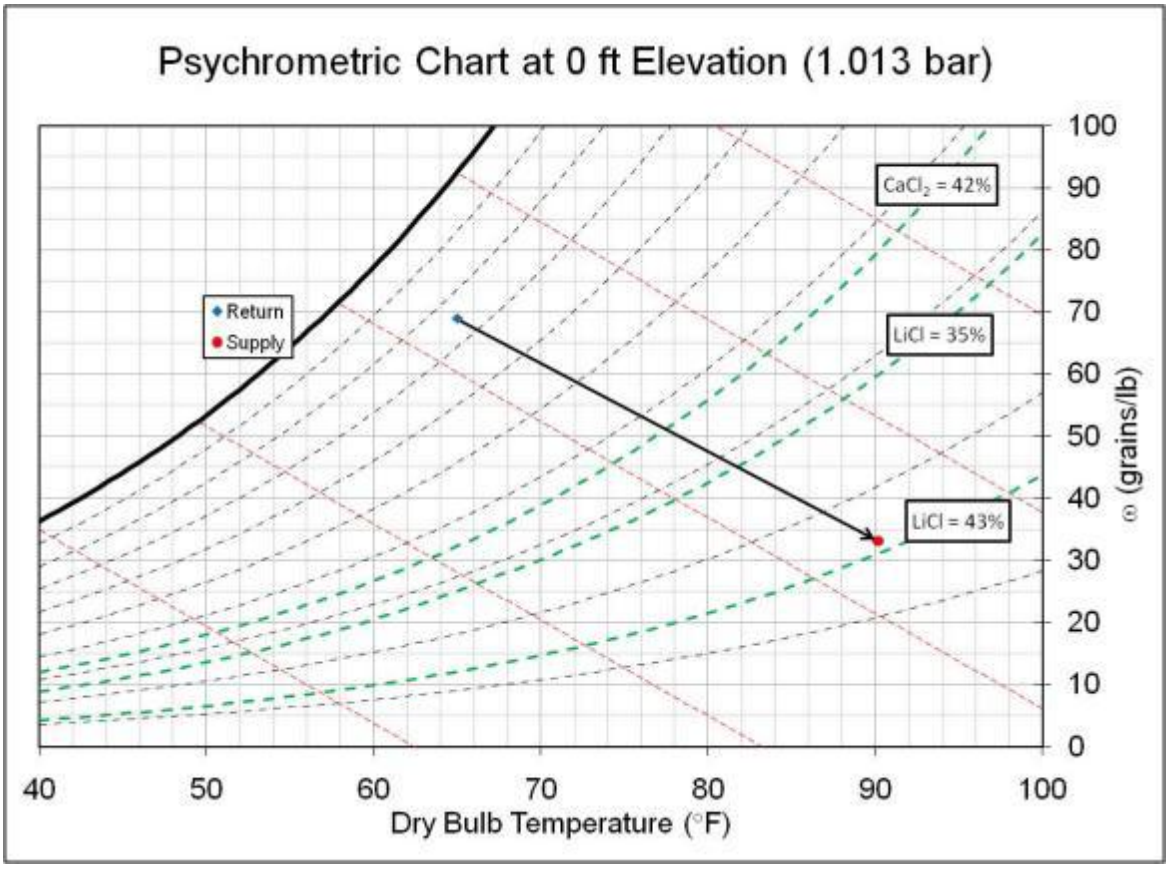

Figure 2.2: Psychrometric chart showing the dehumidification process using desiccants

If a desiccant is held at a constant concentration, then air at a higher vapor pressure will release moisture into the desiccant. As this occurs, the desiccant releases heat and warms the air in a nearly adiabatic process. The supply air will have a slightly higher enthalpy than the return air because the released heat from the desiccant includes the chemical heat of mixing between the desiccant and water as well as the vapor-liquid latent heat for water vapor.

The arrow in Figure 2.2 illustrates the process that return air at 65°F and 75% relative humidity (RH) follows when it comes into contact with lithium chloride that is held at 43% concentration. As desiccants absorb water and become less concentrated, their equilibrium vapor pressure increases and causes the equilibrium line of constant relative humidity to shift towards

the saturation line, diminishing dehumidification potential. Energy must be consumed to heat the desiccant to a temperature where its equilibrium vapor pressure is greater than air so that moisture can be released, restoring the desiccant back to a higher concentration. However, this regeneration process can be accomplished with low-quality energy sources such as waste heat or solar energy.

Desiccants can be in solid and liquid form. Liquid desiccants pose multiple advantages: lower air-side pressure drop during dehumidification, lower regeneration temperature, and the ability to remove air pollutants from the process air stream [4]. Over the past 10 years, an increasing amount of research has been performed on incorporating liquid desiccants into A/C systems. Lowenstein [2] compiled a paper reviewing the most readily available literature on incorporating liquid desiccant into heating, ventilation, and air-conditioning (HVAC) devices. The review covers liquid desiccant technology, advanced liquid desiccants, advancements in conditioners and regenerators using liquid desiccant, and areas requiring further research to achieve important advances for LDAC to be widely used.

Lowenstein [5] proposes that the most important maintenance issue when using a halide salt solution such as LiCl or $CaCl_2$ as liquid desiccant in an absorber is possibility of liquid droplet carryover from the absorber into other sections of the air handling system. This is because halide salts are very corrosive and can damage metal components. Lower desiccant flow rates paired with wetting of the contact surface instead of spraying allows for zero carryover, but contact surfaces must be internally cooled instead of adiabatic to have high dehumidification capacity.

Such a device is proposed by Lowenstein [6], where the flooding rate of the contact surface is reduced by an order of magnitude and contact surfaces are continually cooled in the absorber and continually heated in the regenerator. At these low liquid desiccant flow rates, liquid films are contained within wicking surfaces that ensure even distribution. Since the contact surface is continually cooled in the absorber, there is no need to cool the liquid desiccant before entering the absorber. This allows for heat and mass transfer to occur simultaneously between process air and liquid desiccant in the absorber. Compared to other liquid desiccant dehumidification systems, this device can provide the same amount of cooling at lower liquid desiccant concentrations and with air-side pressure drop values that are approximately 10% of those observed in conventional systems [6].

2.2 Combining LDAC with Sensible Cooling

Since liquid desiccants adiabatically dehumidify process air, the resulting supply air is hot and often requires the application of a sensible cooling technology (chilled ceiling, evaporative cooling, etc.) to ensure occupant comfort. Different combinations of liquid desiccant dehumidification with a viable sensible cooling technology have been previously researched. Zhang and Niu [7] experimentally studied the performance of a system that combined a pre-cooling Munters environmental control cycle (PMEC) that used a membrane-based enthalpy exchanger to pre-cool process air before it entered a desiccant dehumidification region with a chilled ceiling arrangement for sensible cooling. Compared to a conventional system, simulation results in a typical office room in a south-facing high-rise building in Hong

Kong resulted in 72% less fan energy use and 50% less chiller energy use, which amounted to 40% source energy savings.

Indirect evaporative cooling (IEC) has become an attractive alternative to conventional cooling systems for sensible cooling for multiple reasons: lower energy consumption, cheaper and easier operation and maintenance, and the use of water as a working fluid instead of a CFC-based refrigerant that is detrimental to the ozone layer [8]. The major challenge in the design of an indirect evaporative cooling system is to achieve high heat and mass transfer rates and low air-side pressure drop so that the cooling device can be efficient and compact [9]. High mass transfer rates will occur if the inlet secondary air that absorbs moisture is dry, since dry air has a greater ability to absorb moisture than humid air. For this reason, IEC alone is not an optimal cooling method in hot and humid climates and requires the accompaniment of a dehumidification process in order to become a viable cooling technology under such conditions. For this reason, the combination of liquid desiccant dehumidification with IEC technology has been researched.

Saman and Alizadeh [10,11] conducted a performance analysis of a cross-flow type plate heat exchanger for use as a liquid desiccant dehumidifier and indirect evaporative cooler. This device is described as a direct contact, cross-flow heat and mass exchanger with flow passages separated from each other by thin plastic plates. The device was inclined at 45° to allow both liquid desiccant and water to naturally flow downward due to gravity with primary air flowing in a counter arrangement with desiccant and secondary air flowing in a counter arrangement with water. This device proved to perform well under a wide range of air states and desiccant concentrations. This device differs from DEVap mainly in its channel orientation: primary air flows in a cross-flow arrangement with desiccant in DEVap instead of a counter arrangement and secondary air flows in the same direction as water in DEVap instead of in a counter arrangement.

Also, DEVap is not inclined at 45° and has a secondary IEC section to provide further cooling of process air.

2.3 DEVap Technology

Desiccant-enhanced evaporative cooling (DEVap) marries a low-flow liquid desiccant absorber with IEC technology, such that both dehumidification and sensible cooling can be provided independently by one device. Due to this ability to independently provide latent and sensible cooling, DEVap has multiple modes of operation. This technology was developed by NREL, and initial simulations comparing DEVap to conventional air conditioning technology in eight different US cities were done expediently in response to program requests [3]. DEVap is explained in detail in Section 3.1 of this thesis.

A simulation was performed in standard cooling mode under a conservative design condition in order to determine design values for mixed air flow rate and liquid desiccant flow rate. These design flow rate values were important for two reasons: they were used as a maximum flow rate to size pump and fan equipment to be paired with DEVap, and they were embedded in the initial proportional control logic. Proportional control logic was used in order to relate a deviation from cooling set point temperature or humidity to a ratio of actual mixed air flow rate to design mixed air flow rate. The conservative design condition and resulting design flow rates are shown in Table 2.1.

Table 2.1: DEVap Design Conditions

Parameter	Value
Return air temperature, T_{ra}	76°F
Return air relative humidity, RH_{ra}	56%
Outdoor air temperature, T_{oa}	95°F
Outdoor air humidity ratio, ω_{oa}	0.0200
SHR	0.6
OAF	0.3
Enthalpy change ($h_{ra} - h_{sa}$)	7 Btu/lbm
Design liquid desiccant flow rate	0.0280 kg/s
Design process air flow rate	0.285 kg/s

The following sections explain the initial control strategy used in these initial simulations for each mode of operation.

2.3.1 Initial Control Strategy: Dehumidification Only Mode

Providing only latent cooling through liquid desiccant technology is appropriate for a building when the space is sufficiently cool and humid, since the supply air is hot and dry. A common control strategy is to allow for only dehumidification when the relative humidity (RH) in the space is above a set point and the dry bulb temperature in the space is below a set point. For the original DEVap study [3], those set points were an RH_{set} of 54% and T_{set} of 74°F. As long as the space remained at a temperature below this set point, the flow rate of process air being dehumidified through DEVap increased from 40% of maximum flow to 100% as RH increased from 54% to 60% for a constant inlet liquid desiccant concentration of 38%. When this mode of operation is used, the process air is dehumidified and heated using liquid desiccant in the first section of DEVap in a nearly adiabatic process. It is not exactly adiabatic due to the release of the chemical heat of mixing as water is absorbed by the liquid desiccant. A simplified

schematic of dehumidification mode operation is shown in Figure 2.3. RA and SA denote return air and supply air states, respectively.

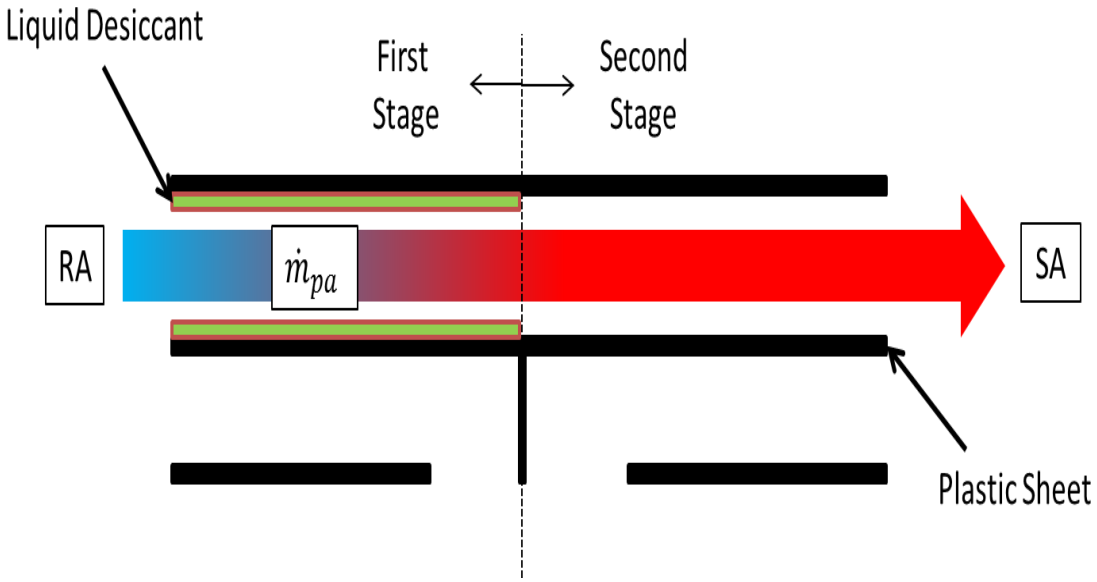

Figure 2.3: Simplified schematic of dehumidification mode operation

2.3.2 Initial Control Strategy: Indirect Evaporative Cooling (IEC) Only Mode

Providing only sensible cooling through indirect evaporative technology is appropriate for a building when the space is hot and dry, since the supply air is cold and dry. A common control strategy for sensible cooling is the opposite of that for dehumidification: operate when the RH in the space is below set point and the dry bulb temperature in the space is above set point. As long as the space remained at an RH below 54% in the initial simulations, the scavenging air flow siphoned off of the supply air stream in the second stage increased from a minimum outdoor air ventilation rate of 1.5% of supply air flow rate to 30% and process air flow rate increased from 40% to 100% of design flow rate as temperature of return air increased from 74°F to 76°F. When this mode of operation is used, the mixed air entering DEVap is only sensibly cooled in both sections of DEVap. To ensure that mixing return air with outdoor air

doesn't introduce excessive humidity to the space, sensible cooling without dehumidification is prohibited whenever the outdoor air is at a dew point temperature above 56°F. A simplified schematic of IEC mode operation is shown in Figure 2.4. OA, MA, E1, and E2 denote outdoor air, mixed air, first stage exhaust air, and second stage exhaust air, respectively.

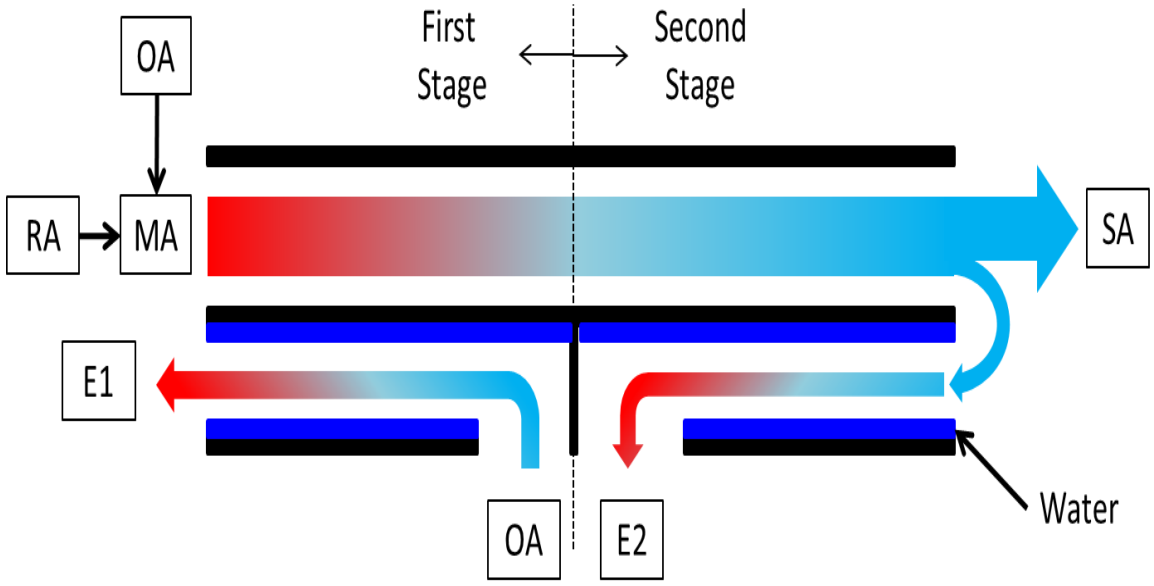

Figure 2.4: Simplified schematic of IEC mode operation

2.3.3 Initial Control Strategy: Standard Cooling Mode

Providing both latent and sensible cooling simultaneously is appropriate for a building when the space is hot and humid, since the supply air is cold and dry. The initial control strategy for this standard cooling was to operate whenever both the RH and temperature in the space were above their respective set points with the same proportional logic explained above: process air flow rate increases from 40% to 100% of design flow rate and outdoor air ventilation rate increases from 1.5% to 30% of process air flow rate as return air RH increases from 54% to 60% or as return air temperature increases from 74°F to 76°F, whichever deviates more from its respective set point. A simplified schematic of standard mode operation is shown in Figure 2.5.

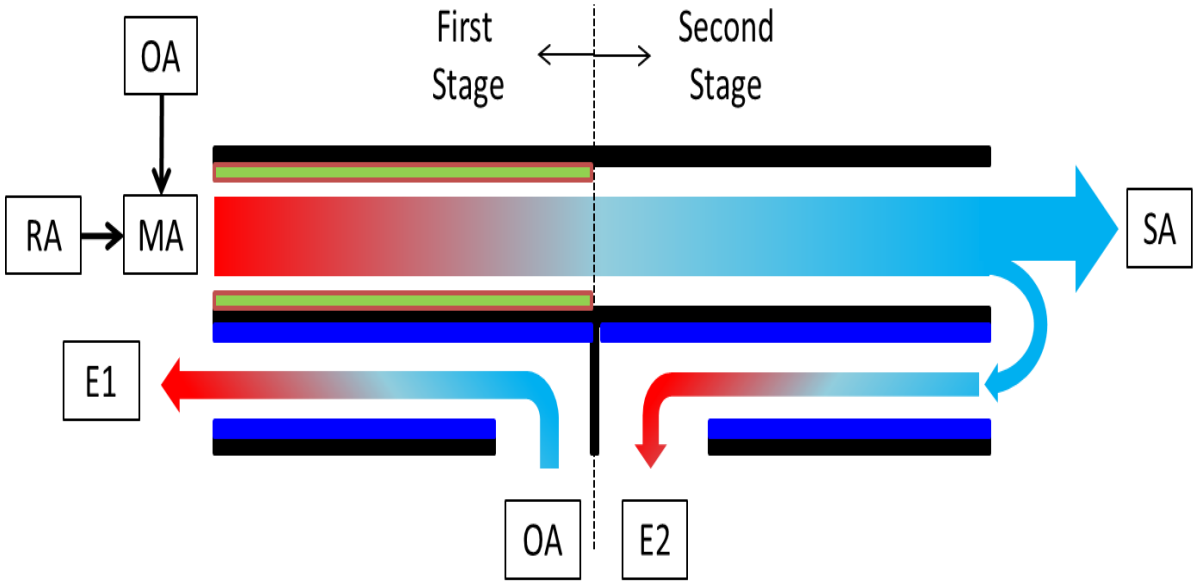

Figure 2.5: Simplified schematic of standard mode operation

For standard cooling, there was no dew-point limitation on the outdoor air state like in sensible only cooling. However, the supply air leaving DEVap was set to have a dew point temperature of 51°F. This was a simple strategy that served as an educated guess for a reasonable supply humidity level in order to eliminate an unknown variable from the equations in order to expedite the simulation process. An example of return and supply air states encountered for each mode of operation in an annual simulation for Houston, TX is shown in a psychrometric chart in Figure 2.6.

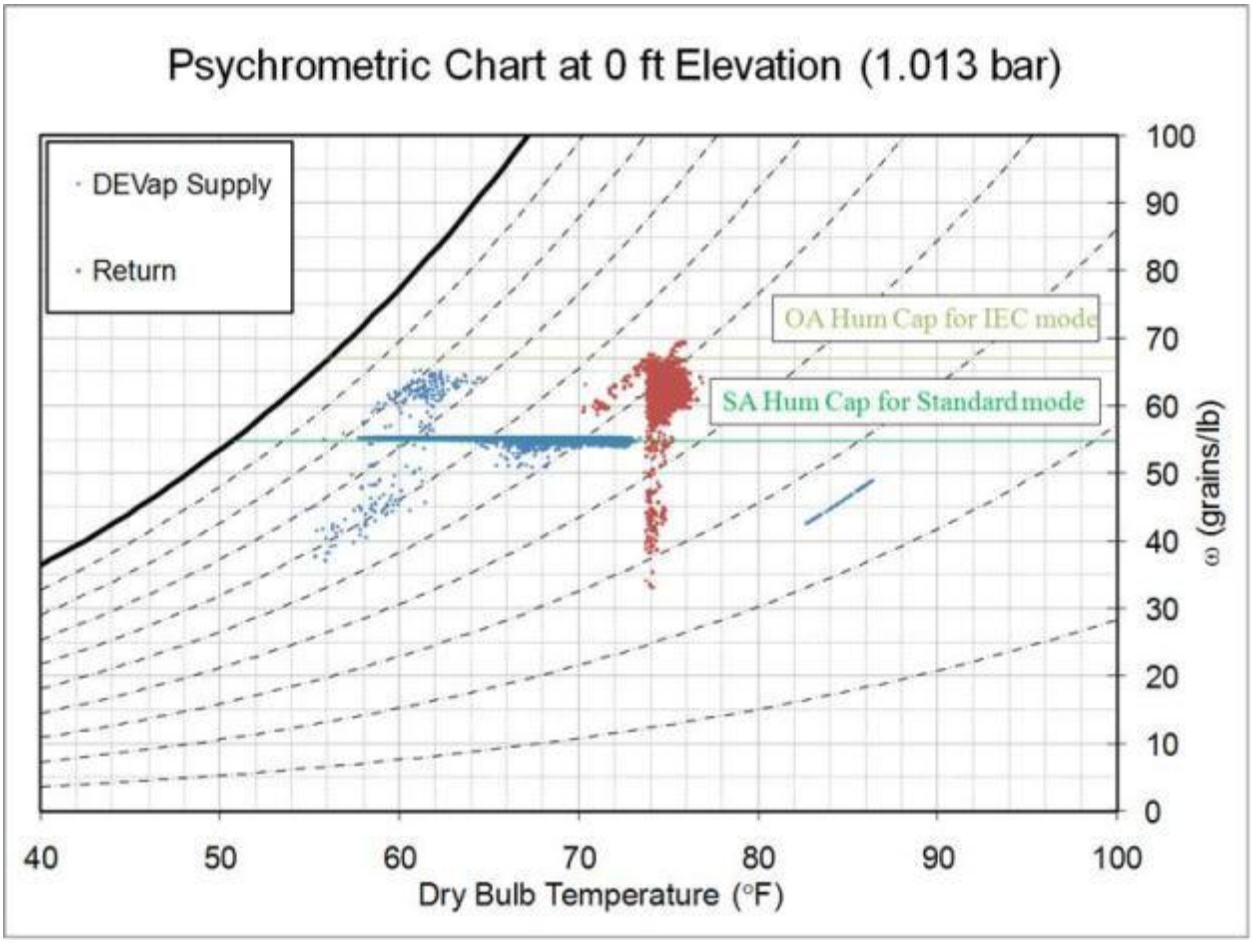

Figure 2.6: Return and supply air states for annual DEVap simulation in Houston, TX [3]

Both return and supply air states are organized according to operation modes. Return air states that are colder than 74°F but at a RH of at least 54% translate into hot and dry supply air states during dehumidification mode. They are at a constant RH since the inlet liquid desiccant concentration to DEVap was constant, translating to equal dehumidification potential. Likewise, return air states that are hotter than 74°F but at a RH below 54% translate into cold supply air states for IEC mode. The absolute humidity value of the supply air states differ from those of return air states due to mixing of return air with outdoor air before being sensibly cooled. All return air states that are hotter than 74°F and at an RH at least 54% translate into cold and dry

supply air states for standard mode. The dew point temperature of the supply air states in standard mode is a constant 51°F, adhering to the initial control strategy mentioned earlier.

These initial control strategies were applied without any research performed on optimal control, leading to the justification for the research performed in this thesis. The following section provides a summary of previous research performed on optimal operation of air conditioning systems similar to DEVap.

2.4 Optimal Control Studies

Numerous studies have been performed that analyze optimization of liquid desiccant dehumidification. Fumo and Goswami [12] and Liu et al [13] determined that the single variable that impacted absorber dehumidification the most is inlet desiccant concentration. Liu et al [14] determined that specifically for a cross-flow type absorber using low liquid desiccant flow, moisture removal rate is affected most by inlet desiccant concentration. This is beneficial information, since the dehumidification section of DEVap is in a cross-flow arrangement.

Guo and Zhao [9] conducted a parametric study of an indirect evaporative air cooler in a cross flow arrangement, similar to the indirect evaporative cooling arrangement in the first section of DEVap. In this study it was determined that heat transfer effectiveness is greatly affected by wettability of the exhaust channel. This is because greater contact area between water and secondary air results in secondary air absorbing more moisture. As more moisture is absorbed by the secondary air, the surface separating primary air from secondary air is increasingly cooled, which provides a greater cooling effect for primary air. This indicates that it

is important to ensure wetting of exhaust air channels in DEVap and that it is more effective to use dry exhaust air during indirect evaporative cooling in both sections of DEVap.

Saman and Alizadeh [10] determined that for a cross-flow type plate heat exchanger using liquid desiccant and indirect evaporative cooling, the ratio of water flow to primary air flow and the ratio of desiccant solution flow to primary air flow had little impact for a constant ratio of primary air flow to secondary air flow. This indicates that water flow and liquid desiccant flow can be held constant in DEVap and result in little performance loss. In this study it was also determined that the ratio of primary air flow to secondary air flow had a significant impact on absorber performance. This is explained as follows: as secondary air flow increases, more moisture is absorbed and a greater cooling effect occurs for both primary air and liquid desiccant. If liquid desiccant is cooled, then its vapor pressure decreases and dehumidification potential increases. This indicates that secondary air should be increased as long as the benefit of increased cooling potential outweighs the negative impact of increased fan energy use.

It was also determined in this study that as primary air inlet temperature increases, mass transfer effectiveness decreases. This is explained as follows: as primary air inlet temperature increases, liquid desiccant is increasingly heated. This heating increases the vapor pressure of the desiccant and reduces the dehumidification potential. This indicates that as mixed air entering DEVap becomes hotter, desiccant concentration will have to increase to maintain dehumidification potential.

Saman and Alizadeh [11] in a different study determined that heat and mass transfer effectiveness for the same cross-flow plate heat exchanger initially increases with primary air flow rate to a certain point, after which there is no further increase or even a decrease in

effectiveness in some cases. This is explained as follows: coefficients of heat and mass transfer increase as air velocity increases, but the rate with which they increase is reduced at higher air velocity. This indicates that the greatest cooling capacities may not be achieved at maximum air flow rates, since maximum heat and mass exchange effectiveness could potentially be at a lower flow rate.

Vitte et al [15] performed a study on a model of a solar desiccant evaporative cooler in order to determine a control strategy for switching between natural ventilation and desiccant cooling. In this study it was determined that enthalpy difference between return air and outdoor air was a better indicator of when to switch between cooling methods compared to return air temperature alone. Using the developed control strategy, it was calculated that the modeled system would save 45% of the primary energy used in a conventional system over the cooling season in Paris. This indicates that enthalpy difference between return and outdoor air may serve as a satisfactory control function concerning when to switch between the three modes of operation in DEVap.

From these previous studies, it can be assumed that the following control strategies should contribute to optimal operation of DEVap:

- Inlet desiccant concentration should be at an optimal value, since it is the control variable with the largest impact on moisture removal rate
- Since secondary air flow has the largest impact on cooling potential, it should be increased before other control variables to provide increased cooling potential. This strategy should hold as long as the increased cooling potential outweighs the resulting increase in fan energy consumption

- As mixed air entering DEVap becomes hotter, liquid desiccant concentration should increase to maintain dehumidification potential. This should hold when both return air and outdoor air become hotter
- Maximum cooling potential may not occur at maximum flow rates of primary or secondary air
- Enthalpy difference between return air and outdoor air may serve as a better control function than return air temperature

Chapter 3: System Components and Control Variables

This thesis examines DEVap, a concept developed by NREL that combines liquid desiccant and evaporative cooling technology [3]. This chapter describes the components and variables affecting performance of the conditioner (DEVap), as well as DEVap's three modes of operation. The components and variables affecting performance of the regenerator are also explained.

3.1 DEVap Operation

The DEVap concept can be simplified down to two sections: a dehumidification section using liquid desiccant technology followed by a sensible cooling section that is solely used for indirect evaporative cooling (IEC). These two sections use porous membranes to construct channels for each fluid to flow and prevent mixing while still allowing for heat and mass transfer between channels. Increasing the amount of channels in the device increases the cooling capacity that can be provided.

3.1.1 Dehumidification Section

Dehumidification in DEVap is accomplished with liquid desiccant in the first stage of the device. Vapor-permeable membranes keep liquid desiccant contained in one channel and process air in an adjacent channel while allowing moisture to transfer between the two channels. The difference in vapor pressure between the liquid desiccant and process air creates a driving potential for moisture to exit the process air and enter the liquid desiccant. For DEVap, liquid desiccant is applied onto a wicked surface to ensure even distribution. The liquid desiccant then

naturally trickles down through the channel due to gravity and is collected at the bottom before being delivered to the regeneration system.

Process air flows horizontally through a channel, eventually exiting the first stage as warm and dry air. Unaltered outdoor air enters at the top of the device and acts as a scavenging air stream until exhausted as hot and humid air at the bottom, similar to the liquid desiccant flow pattern. This scavenging air stream is used primarily to cool the liquid desiccant in order to maintain a low vapor pressure and, consequently, a high dehumidification potential. This air stream does also evaporatively cool the process air stream, but not as effectively as in the second stage. This is because the liquid desiccant channel separates the process air stream from the scavenging air stream and heat exchange between process air and scavenging air occurs in a cross-flow pattern that is less efficient. An impermeable plastic sheet separates the liquid desiccant channel from the water channel and a vapor-permeable membrane separates the water channel from the scavenging air channel to ensure that water vapor will only transfer from the water channel into the scavenging air channel.

The vapor-permeable membrane separating the water channel from the scavenging air channel is in place to resist biological growth, but creates a small resistance to moisture transfer. According to strong evidence from companies that have developed similar systems using wicked surfaces to create successful evaporative coolers (e.g., Coolerado Cooler, Speakman – OASys), this water-side membrane may not be necessary. The desiccant-side membrane, however, is essential in order to ensure liquid desiccant does not become entrained in the process air.

The preceding description is for one channel pair. However, the design cooling capacity of DEVap determines the amount of channels to be used. The physical arrangement for a

channel pair in the first stage is shown in Figure 2.2. Bold lines indicate impermeable plastic sheets.

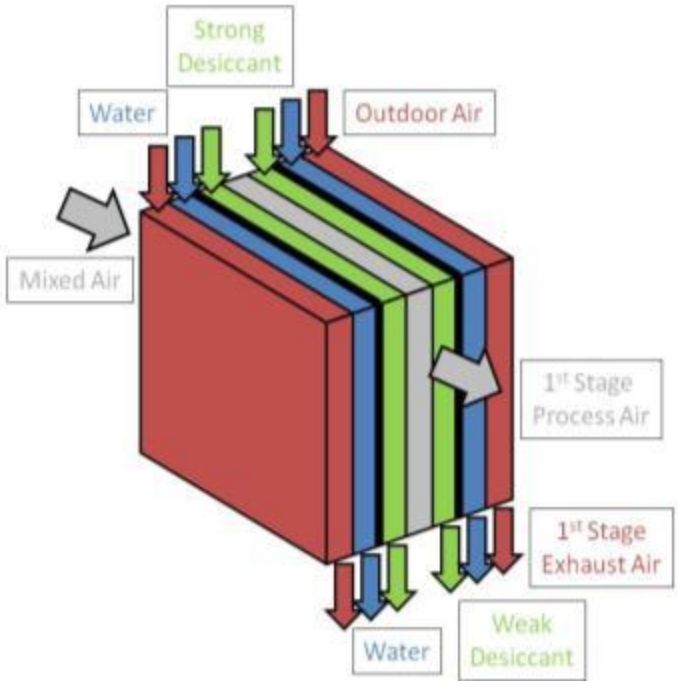

Figure 3.7: Channel pair orientation in first stage of DEVap

3.1.2 Sensible Cooling Section

The sensible cooling section in DEVap is immediately after the dehumidification setion. One channel pair in this section is comprised of a process air channel, water channel, and scavenging air channel. An impermeable plastic sheet separates the process air channel from the water channel and a vapor-permeable membrane separates the water channel from the scavenging air channel to ensure that water vapor will transfer from the water channel into the scavenging air channel and not the process air channel. Scavenging air is initially cold and dry supply air that is siphoned off after exiting DEVap and brought back through parallel channels in a counter-flow arrangement before exiting as hot and humid air at the bottom of the device. Another reason that IEC of process air is more efficient in this second section compared to the

first section is that the scavenging air stream is much drier since it has been previously dehumidified in the first section. The physical arrangement for a channel pair in the second stage is shown in Figure 3.8. Bold lines indicate impermeable plastic sheets.

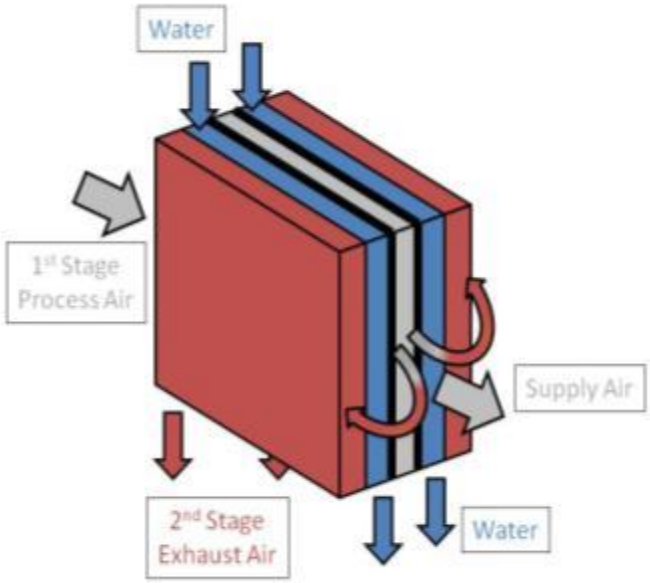

Figure 3.8: Channel pair orientation in second stage of DEVap

3.1.3 DEVap Device

An overview of the DEVap concept and how the two stages interact with each other is shown in Figure 3.9. A top view of one channel pair is shown in the upper right corner, while an isometric view of a SolidWorks model of the device is shown on the left. Process and exhaust air states are shown in blue and red, respectively, on a psychrometric chart in the lower right corner.

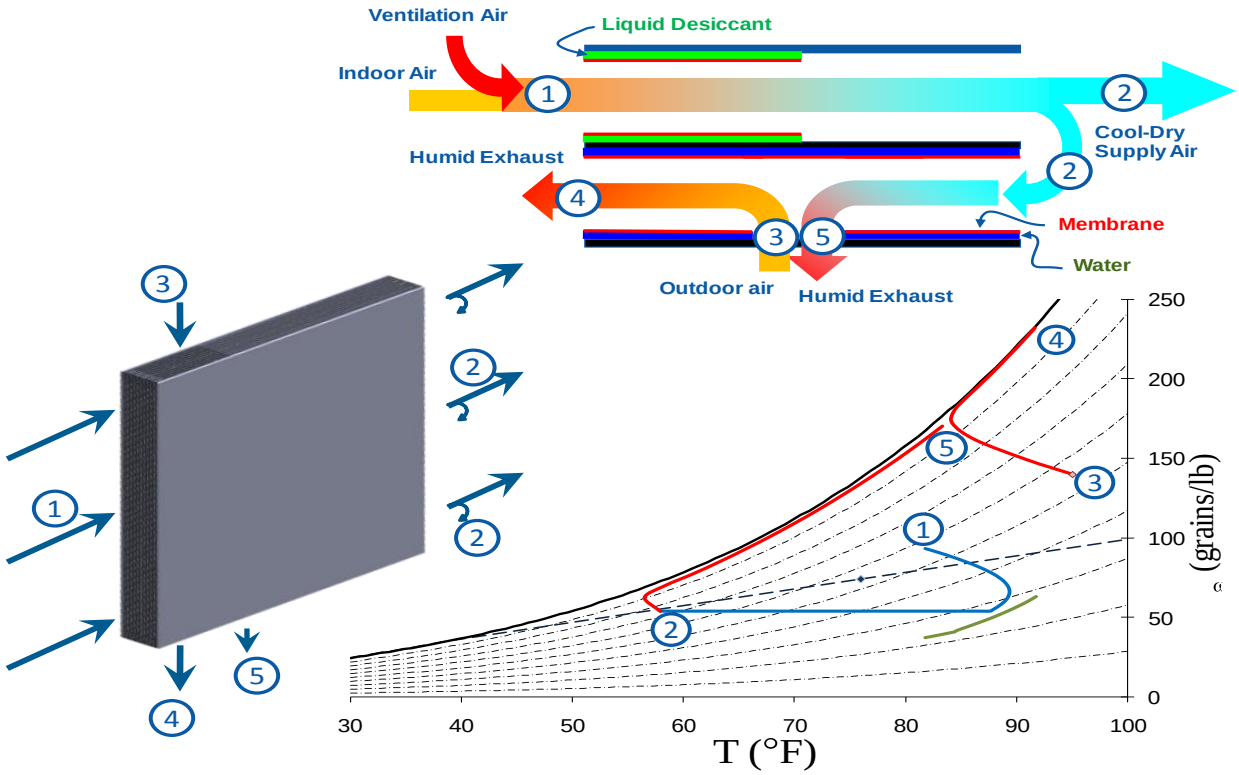

Figure 3.9: DEVap concept [3]

Before entering the device, return air is mixed with outdoor air. The portion of mixed air entering DEVap that is comprised of outdoor air is called the outdoor air fraction (OAF), defined using Equation 6.15, where m_{oa}, m_{ra} , and m_{ma} are the mass flow rates of outdoor air, return air, and mixed air, respectively.

$$OAF = \frac{m_{oa}}{m_{oa} + m_{ra}} = \frac{m_{oa}}{m_{ma}}$$

Equation 3.1

Warm and humid mixed air enters the first stage of DEVap and becomes process air as it is dehumidified by liquid desiccant. The amount of dehumidification provided can be increased by increasing the inlet liquid desiccant concentration to DEVap ($C_{LD,in,DEVap}$). Outdoor air enters an adjacent channel and behaves as a scavenging air stream to cool the liquid desiccant. This

cooling of the desiccant slightly cools the mixed air, since the two streams are only separated by a vapor-permeable membrane. The amount of cooling provided by this stream can be increased by increasing the flow rate through the exhaust channel in the first stage (m_{e1}) and using cold, dry air in the scavenging air stream. Since the scavenging air stream is unaltered outdoor air, the latter method cannot be implemented. It is important to note that process air exiting the first stage is hotter than mixed air entering the first stage, due to the nearly adiabatic dehumidification process being used.

After exiting the first stage as hot and dry air, the process air then immediately enters the second stage where it is evaporatively cooled and exits DEVap as cold and dry supply air. The flow rate of air siphoned from the supply air stream exiting the second stage (m_{e2}) is equal to m_{oa}. This ensures that the amount of air sent from the space to be conditioned is equal to the amount of conditioned air sent back to the space, preventing a need to pressurize or depressurize and consume energy unnecessarily. Under constant conditions, the amount of cooling provided by DEVap can be increased by increasing m_{ma}. Since the previously dehumidified air from the first stage is used as the evaporative sink in the second stage, DEVap has the ability to operate in hot and humid climates.

3.2 DEVap Control Variables

The performance of DEVap is determined by many variables. For example, as previously explained, the amount of dehumidification in the first stage can be adjusted by changing $C_{LD,in,DEVap}$. This is one example of a control variable that can be adjusted during

operation. However, there are also independent variables that cannot be controlled. The impact that both of these types of variables have on DEVap's performance is explained below.

3.2.1 Independent Variables

The independent variables for DEVap's operation are namely air states and cooling loads. These include return air and outdoor air states, as well as the sensible heat ratio (SHR) associated with the amount of total cooling required. The return air state during DEVap's operation will not vary greatly, since DEVap will only operate when either the temperature or humidity in the space is above its respective set point. The outdoor air state during DEVap's operation will cover a tremendous range, since DEVap will ideally be implemented in any climate. The outdoor air state will affect the mixed air state entering DEVap, so outdoor air that is cold and dry will reduce the total cooling load imposed on DEVap compared to outdoor air that is hot and humid. Also, since outdoor air is used as the scavenging air in the first stage, cold and dry outdoor air offers more cooling potential for liquid desiccant than hot and humid outdoor air.

The cooling load and SHR imposed on DEVap will change depending upon location, building function, day of the year, and time of day. As the cooling load increases, DEVap's performance will gradually decline. As the SHR associated with the cooling load increases, less dehumidification and more IEC is required.

The control variables that can be adjusted during operation are explained in detail below. From the explanation following Figure 3.9, it can be determined that there are four control variables: m_{ma}, OAF, m_{e1}, and $C_{LD,in,DEVap}$. To simplify future simulations, a ratio is used to express each of the two mass flow rates. R_{ma} is defined as the ratio of actual mixed air flow rate to maximum mixed air flow rate, and R_{e1} is defined as the ratio of actual first stage exhaust air

flow rate to maximum mixed air flow rate. For each of these four control variables, minimum and maximum values are assigned based on educated assumptions pertaining to DEVap's operation. These minimum and maximum values are summarized in Table 3.2.

Table 3.2: Minimum and Maximum Control Variables Values

Control Variable	Minimum Value	Maximum Value
R_{ma}	0.3	1.0
OAF	0.05	0.5
R_{e1}	0.1	0.7
$C_{LD,in,DEVap}$	0.24	0.4

3.2.2 Control Variables: Mixed Air Flow Rate Ratio, R_{ma}

Increasing R_{ma} results in process air flowing faster through DEVap. Figure 3.10 shows the impact of adjusting R_{ma} from 0.3 to 1.0 while holding all other control variables constant for a given combination of outdoor and return air. ratio A visual representation of where R_{ma} impacts DEVap is shown in the upper left corner, while a graph of how source coefficient of performance (COP_{source}) and total cooling capacity (Q_{tot}) change with R_{ma} is shown in the lower left corner. A psychrometric chart showing how air states are affected by R_{ma} is shown on the right. On this psychrometric chart, "PA,1" corresponds to the process air state exiting the first stage of DEVap and entering the second stage of DEVap. COP_{source} and Q_{tot} are calculated using Equation 3.2 and Equation 3.3, respectively. It was assumed that site-to-source ratios of 3.4 for electricity and 1.1 for natural gas were appropriate.

$$\boldsymbol{COP_{source} = \frac{Q_{tot}}{(Q_{electricity} * 3.4 + Q_{natural\ gas} * 1.1)}}$$

Equation 3.2

$$Q_{tot} = m_{sa} * \ h_{ra} - h_{sa} \ = m_{ma} * \ 1 - OAF \ * \ h_{ra} - h_{sa}$$

Equation 3.3

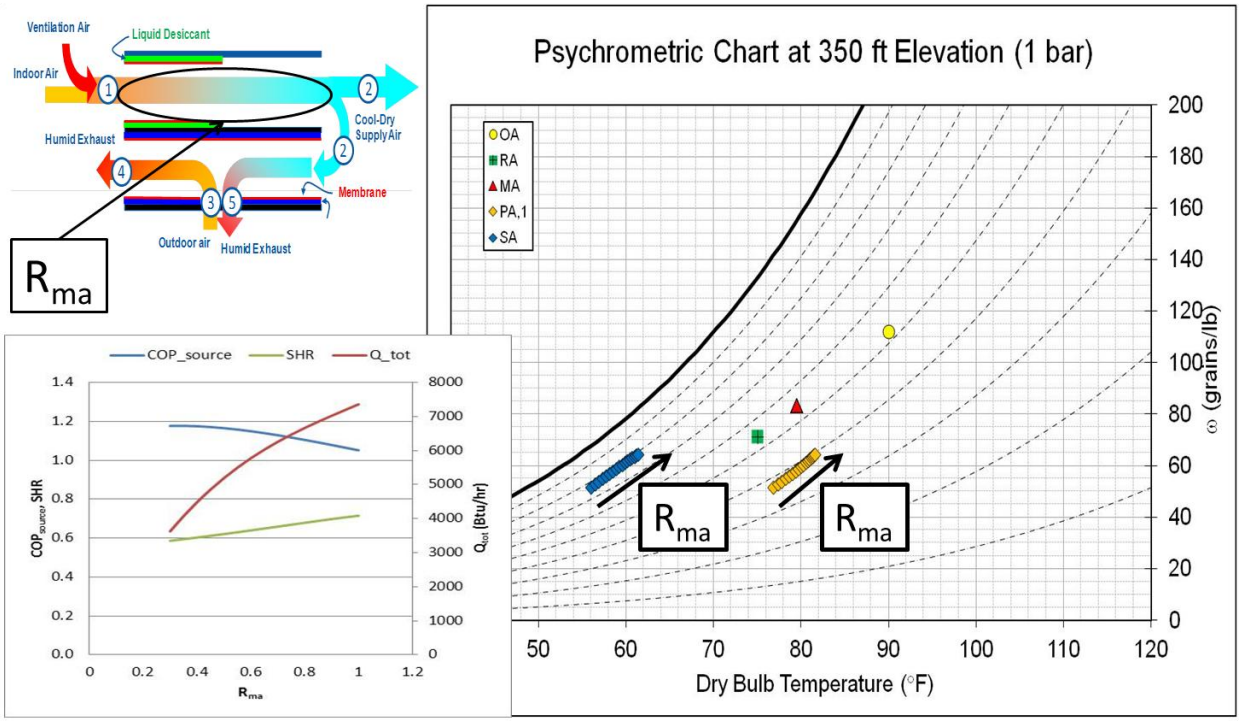

Figure 3.10: Impact of adjusting R_{ma} during DEVap operation for T_{ra} = 75°F, RH_{ra} = 55%, T_{oa} = 90°F, and ω_{oa} = 0.0054 kg/kg

From Figure 3.10, it is determined that as R_{ma} increases, Q_{tot} increases. This is because as air flows through DEVap faster, there is a greater amount of conditioned air being sent to the space. However, this greater Q_{tot} is met with a reduced COP_{source}, but not a drastic reduction. It should be noted that the SHR provided doesn't change much as R_{ma} increases.

The mixed air state entering DEVap remains constant because the OAF remains constant. It is important to note that as R_{ma} increases, the amount of dehumidification and sensible cooling provided decreases. This is due to the fact that the process air spends less time in the device, reducing the amount of time that process air is in contact with liquid desiccant and exchanging

heat with an exhaust air stream, which is a similar to that of increasing flow rate of one fluid through a heat exchanger. It is also important to note that the temperature difference between air exiting the first stage in orange and supply air exiting DEVap in blue remains relatively constant. This is because the OAF was held constant, meaning that the amount of cooling provided in the second stage is held constant.

3.2.3 Control Variables: Outdoor Air Fraction, OAF

Increasing OAF causes two reactions: mixed air entering DEVap becomes more similar to outdoor air, and more supply air is siphoned off to be used as scavenging air in the second stage. Figure 3.11 shows the impact of adjusting OAF from 0.05 to 0.50 while holding all other control variables constant for a given combination of outdoor and return air. A visual representation of where OAF impacts DEVap is shown in the upper left corner, while a graph of how COP_{source} and Q_{tot} change with OAF is shown in the lower left corner. A psychrometric chart showing how air states are affected by OAF is shown on the right.

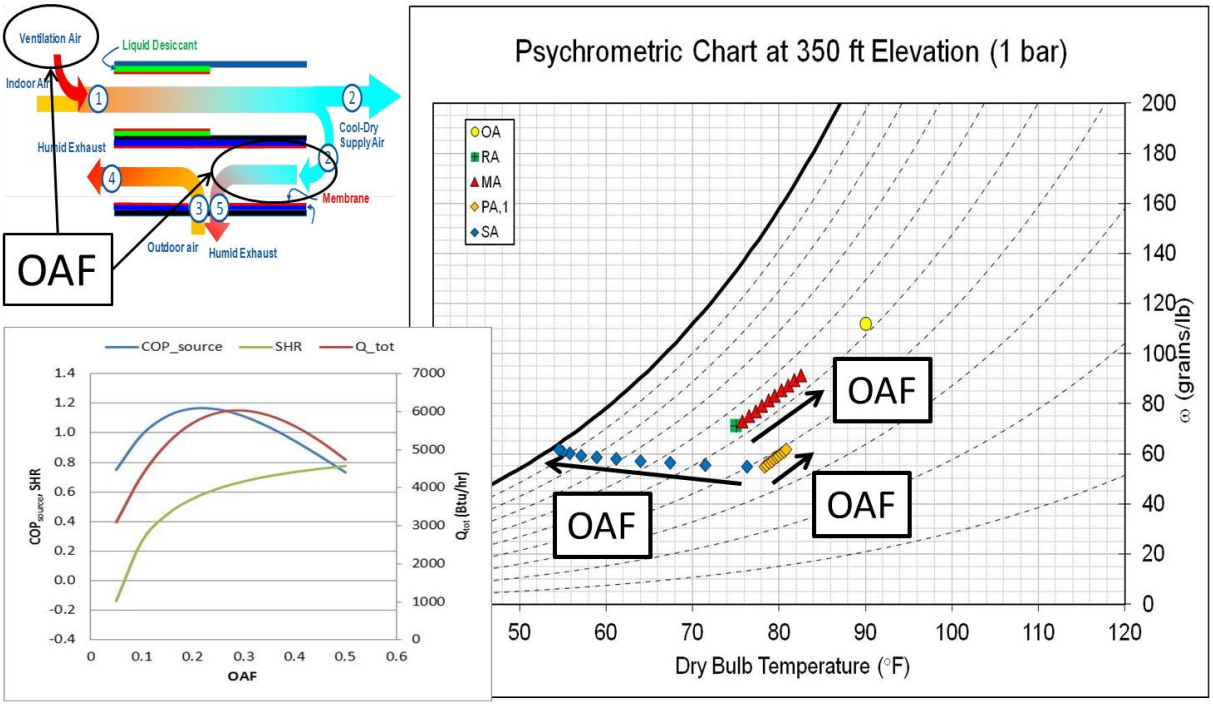

Figure 3.11: Impact of adjusting OAF during DEVap operation for T_{ra} = 75°F, RH_{ra} = 55%, T_{oa} = 90°F, and ω_{oa} = 0.0054 kg/kg

From Figure 3.11, it is determined that as OAF increases, Q_{tot} increases, but only to a certain point. After this point, the provided cooling capacity begins to decline. This is because as more air is siphoned off the supply air stream for second stage cooling, the amount of conditioned air that is actually sent to the space is reduced. Eventually there is a point where the benefit of sending a high amount of conditioned supply air to the space outweighs the benefit of using dry supply air for second stage cooling. However, before this point is reached, the COP increases with Q_{tot}. This indicates that situations where higher OAF is required, such as higher SHRs, greater values for COP_{source} are expected. It should also be noted that the ranges of COP_{source} and SHR values encountered are also larger than those encountered previously for R_{ma}, indicating that COP_{source} and SHR are more sensitive to OAF.

The mixed air state entering DEVap becomes more and more similar to the outdoor air state because the OAF is increasing. It is important to note that even as OAF increases, the process air exiting the first stage doesn't change much. This is due to the fact that $C_{LD,in,DEVap}$ and R_{ma} remain constant. It is also important to note that the temperature difference between process air exiting the first stage and supply air exiting DEVap increases. This is because more supply air is being siphoned off for second stage cooling, increasing the amount of cooling provided in the second stage.

3.2.4 Control Variables: First-Stage Exhaust Air Flow Ratio, R_{e1}

An increase in R_{e1} results in an increase in the flow rate of the scavenging air in the first stage. Figure 3.12 shows the impact of adjusting R_{e1} from 0.1 to 0.7 while holding all other control variables constant for a given combination of outdoor and return air. ratio A visual representation of where R_{e1} impacts DEVap is shown in the upper left corner, while a graph of how COP_{source} and Q_{tot} change with R_{e1} is shown in the lower left corner. A psychrometric chart showing how air states are affected by R_{e1} is shown on the right.

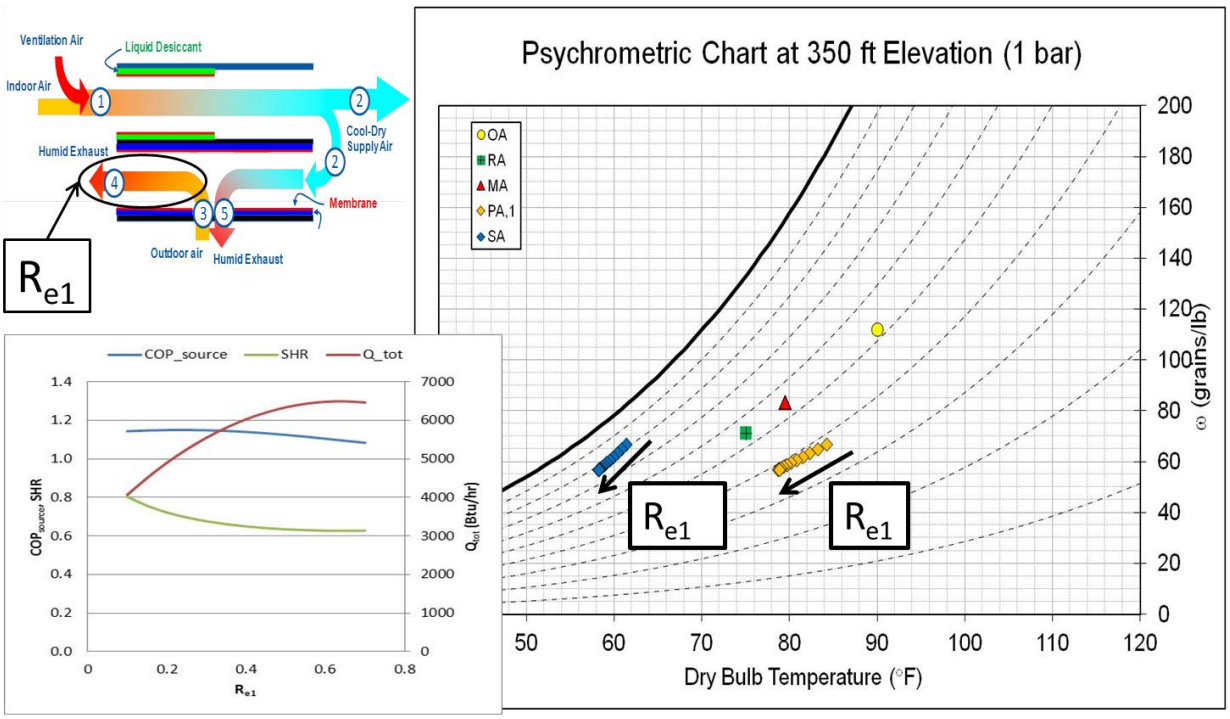

Figure 3.12: Impact of adjusting m_{e1} during DEVap operation for T_{ra} = 75°F, RH_{ra} = 55%, T_{oa} = 90°F, and ω_{oa} = 0.0054 kg/kg

From Figure 3.12, it is determined that as the R_{e1} ratio increases to approximately a value of 0.6, Q_{tot} increases to a maximum value. This is because the benefit of using hot and humid outdoor air as a scavenging air stream in the first stage is limited. However, if the outdoor air was cold and dry, this scavenging air stream would be much more beneficial. It should be noted that COP_{source} reaches a maximum value at an R_{e1} ratio of approximately 0.25, indicating that there is an optimal value to achieve for R_{e1}. The range of values for both COP_{source} and SHR is small, indicating that COP_{source} and SHR are not too sensitive to R_{e1}.

The mixed air state entering DEVap remains constant because the OAF remains constant. It is important to note that as R_{e1} increases, the amount of dehumidification provided increases. This is due to the fact that liquid desiccant is being increasingly cooled, reducing its vapor pressure and increasing the dehumidification potential in the first stage. This reduction in the

liquid desiccant temperature also results in lower temperatures for air exiting the first stage. It is also important to note that the temperature difference between air exiting the first stage and supply air exiting DEVap slightly decreases. This is because even though the process air is being increasingly dehumidified before used as scavenging air in the second stage, it is also being increasingly cooled, slightly reducing the cooling potential in the second stage.

3.2.5 Control Variables: Inlet Liquid Desiccant Concentration to DEVap, $C_{LD,in,DEVap}$

Increasing $C_{LD,in,DEVap}$ results in increased dehumidification potential in the first stage of DEVap. Figure 3.13 shows the impact of adjusting $C_{LD,in,DEVap}$ from 0.24 to 0.40 while holding all other control variables constant for a given combination of outdoor and return air. A visual representation of where $C_{LD,in,DEVap}$ impacts DEVap is shown in the upper left corner, while a graph of how COP_{source} and Q_{tot} change with $C_{LD,in,DEVap}$ is shown in the lower left corner. A psychrometric chart showing how air states are affected by $C_{LD,in,DEVap}$ is shown on the right.

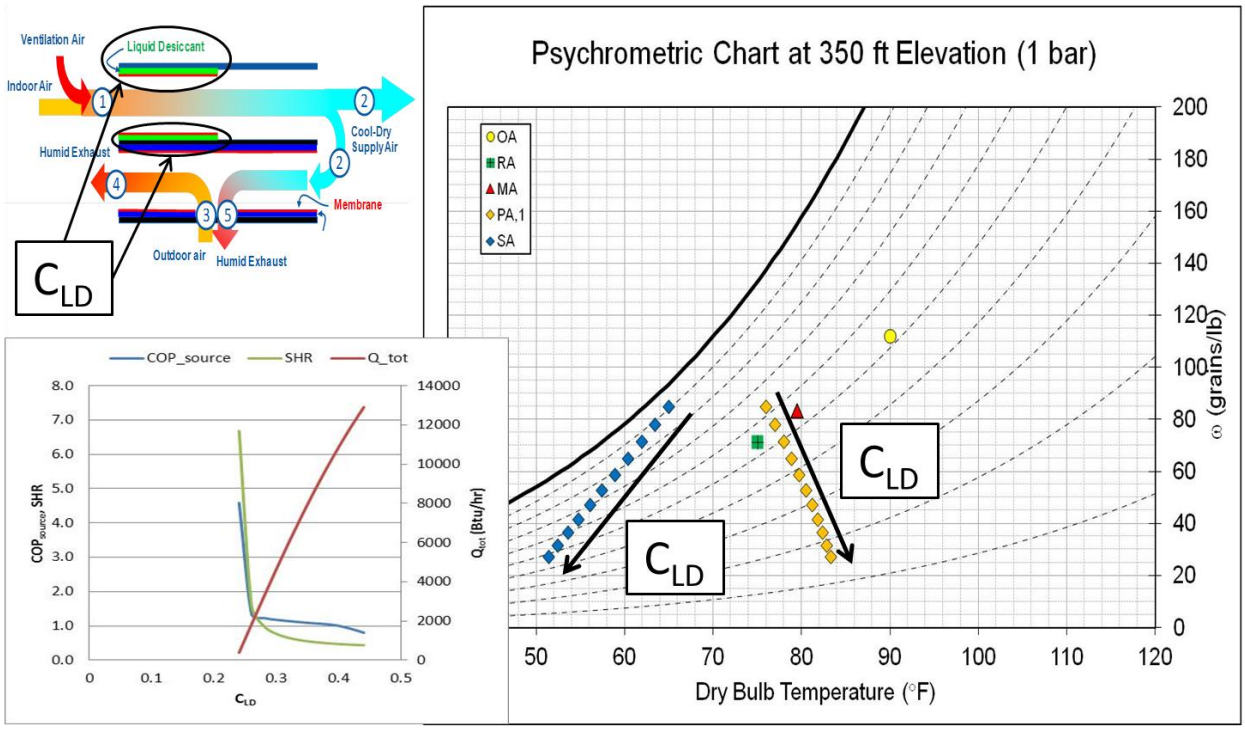

Figure 3.13: Impact of adjusting $C_{LD,in,DEVap}$ during DEVap operation for T_{ra} = 75°F, RH_{ra} = 55%, T_{oa} = 90°F, and ω_{oa} = 0.0054 kg/kg

From Figure 3.13, it is determined that as $C_{LD,in,DEVap}$ increases, Q_{tot} increases. In fact, the range of Q_{tot} achieved here is much greater than those obtained for varying the other three control variables. This is because for a low value for $C_{LD,in,DEVap}$, process air is actually humidified before being cooled in the second stage, indicating that the liquid desiccant vapor pressure is greater than that of the process air. For this case, the enthalpy difference between return air and supply air is small, resulting in a low Q_{tot} and high SHR. Since the process air is actually being humidified, there is no energy input needed to regenerate the liquid desiccant, resulting in a very high COP_{source}. For a high value for $C_{LD,in,DEVap}$, a high amount of dehumidification is provided to the process air. This very dry air is then used as scavenging air in second stage cooling, providing a high cooling potential. For this case, the enthalpy difference between return air and supply air is high, resulting in a high Q_{tot} and low SHR. It should be

noted that COP_{source} changes very little, due to the fact that increasing the amount of dehumidification provided in the first stage leads to natural gas with a low site-to-source ratio to be consumed in order to regenerate the liquid desiccant.

The mixed air state entering DEVap remains constant because the OAF remains constant. As $C_{LD,in,DEVap}$ increases, the amount of dehumidification provided increases. This is due to the fact that higher concentrations result in lower vapor pressure, increasing dehumidification potential in the first stage. It is also important to note that the temperature difference between process air exiting the first stage and supply air exiting DEVap increases as $C_{LD,in,DEVap}$ increases. This is because the process air becomes drier before being siphoned off and used as the scavenging air stream in second stage cooling, increasing the cooling potential in the second stage.

3.3 DEVap Modes of Operation

Since the amount of dehumidification and sensible cooling provided by DEVap can be adjusted freely during operation, latent and sensible cooling loads can be met independently. As a result, there are multiple modes of operation. DEVap can only utilize liquid desiccant for dehumidification in the first stage, only use water and scavenging air for IEC in both stages, or use all simultaneously to dehumidify and cool the process air in a standard cooling mode.

In dehumidification mode, there is no need to supply any sensible cooling and there is only a latent load (Q_{lat}) of interest. For this reason, there are no exhaust air flows in either the first or second stage. This means that both R_{e1} and OAF are set to zero in dehumidification

mode. Therefore, the only control variables to adjust in dehumidification mode are R_{ma} and $C_{LD,in,DEVap}$ to meet Q_{lat}. Since there is no mixing of outdoor and return air and there is only a latent load of interest, the only independent variables that impact dehumidification mode are return air temperature and humidity and Q_{lat}. Q_{lat} is a function of R_{ma}, the humidity difference between return and supply air, and the latent heat of regeneration ($h_{fg,regen}$), as shown in Equation 3.4. $h_{fg,regen}$ is a function of the boiling temperature of liquid desiccant, which is relatively constant for different desiccant concentrations.

$$\boldsymbol{Q_{lat} = m_{sa} * h_{fg,regen} * \ \omega_{ra} - \omega_{sa} \ = R_{ma} * m_{ma,des} * h_{fg,regen} * (\omega_{ra} - \omega_{sa})}$$

Equation 3.4

In IEC mode, there is no need to supply any dehumidification and there is only a sensible load (Q_{sens}) of interest. For this reason, there is no flow of liquid desiccant in the first stage and $C_{LD,in,DEVap}$ is not a control variable in IEC mode. This means that R_{ma}, R_{e1}, and OAF are all control variables to be adjusted in IEC mode to meet Q_{sens}. Since there is mixing of outdoor and return air and there is only a sensible load of interest, the independent variables that impact IEC mode are outdoor and return air temperature and humidity and Q_{sens}. Q_{sens} is a function of R_{ma}, OAF, the average specific heat of process air in DEVap ($c_{p,avg}$), and the temperature difference between return and supply air, as shown in Equation 3.4.

$$\boldsymbol{Q_{sens} = m_{sa} * c_{p,avg} * \ T_{ra} - T_{sa} \ = R_{ma} * m_{ma,des} * \ 1 - OAF \ * c_{p,avg} * \ T_{ra} - T_{sa}}$$

Equation 3.5

In standard mode, there is simultaneous dehumidification and sensible cooling in order to meet a combination of Q_{tot} and SHR. Standard mode is a combination of dehumidification mode and IEC mode, so all four control variables discussed previously are adjusted to meet the

required combination of Q_{tot} and SHR. Since there is mixing of outdoor and return air and there is a combination of latent and sensible cooling, the independent variables that impact standard mode are outdoor and return air temperature and humidity, Q_{tot}, and SHR. An example of air states observed for each mode of operation is shown in Figure 3.14.

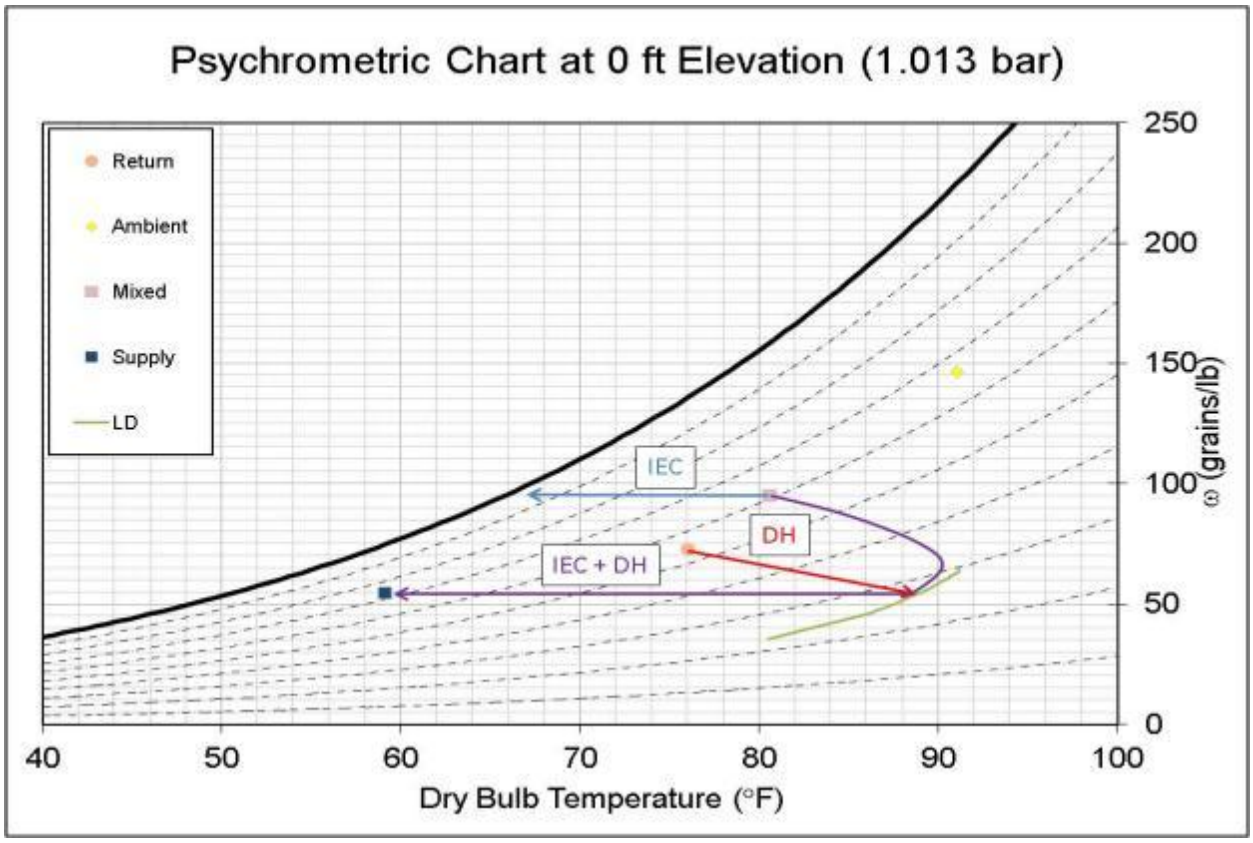

Figure 3.14: Example air states for DEVap's modes of operation (DH = Dehumidification, IEC = Indirect Evaporative Cooling)

Notice that dehumidification mode is the only mode where return air is the initial process air state. This is because dehumidification mode is the only mode where no sensible cooling is performed in the second stage. Since the amount of scavenging air siphoned off of the supply air stream for second stage cooling is equal to the OAF, this means there is no mixing of return air with outdoor air in dehumidification mode. For IEC mode, the process air is only sensibly

cooled starting at the mixed air state. For standard mode, process air is simultaneously dehumidified and sensibly cooled starting at the mixed air state until exiting the first stage, at which point it is only sensibly cooled until exiting as supply air. Ideally, standard mode provides the full range of SHRs between those observed in dehumidification mode (~ $-\infty$) and IEC mode (>1 when outdoor air is more humid than return air). A summary of pertinent independent and control variables for each mode of operation is shown in Table 3.3. An "x" indicates a variable of interest.

Table 3.3: Summary of Independent and Control Variables for DEVap

	Mode of Operation	DH	IEC	Standard
Independent Variables	T_{ra}	x	x	x
	RH_{ra}	x	x	x
	T_{oa}		x	x
	ω_{oa}		x	x
	SHR			x
	Load of Interest	Q_{lat}	Q_{sens}	Q_{tot}
Control Variables	R_{ma} ratio	x	x	x
	R_{e1} ratio		x	x
	OAF		x	x
	$C_{LD,in,DEVap}$	x		x

3.4 Regenerator Components

The regenerator that will be used to drive moisture away from liquid desiccant is a two-stage system that employs a gas-fired boiler and a scavenging air regenerator (SAR) that are used in parallel [16]. The SAR is comprised of a scavenging air stream, a liquid desiccant stream, and a heat source stream, which will be steam from the boiler. Interchange heat exchangers (ICHXs) and an air-to-air heat exchanger (AAHX) are also incorporated in the liquid desiccant stream and

scavenging air stream to improve operating performance. A simplified schematic of the regenerator system is shown in Figure 3.15. Each component is explained below.

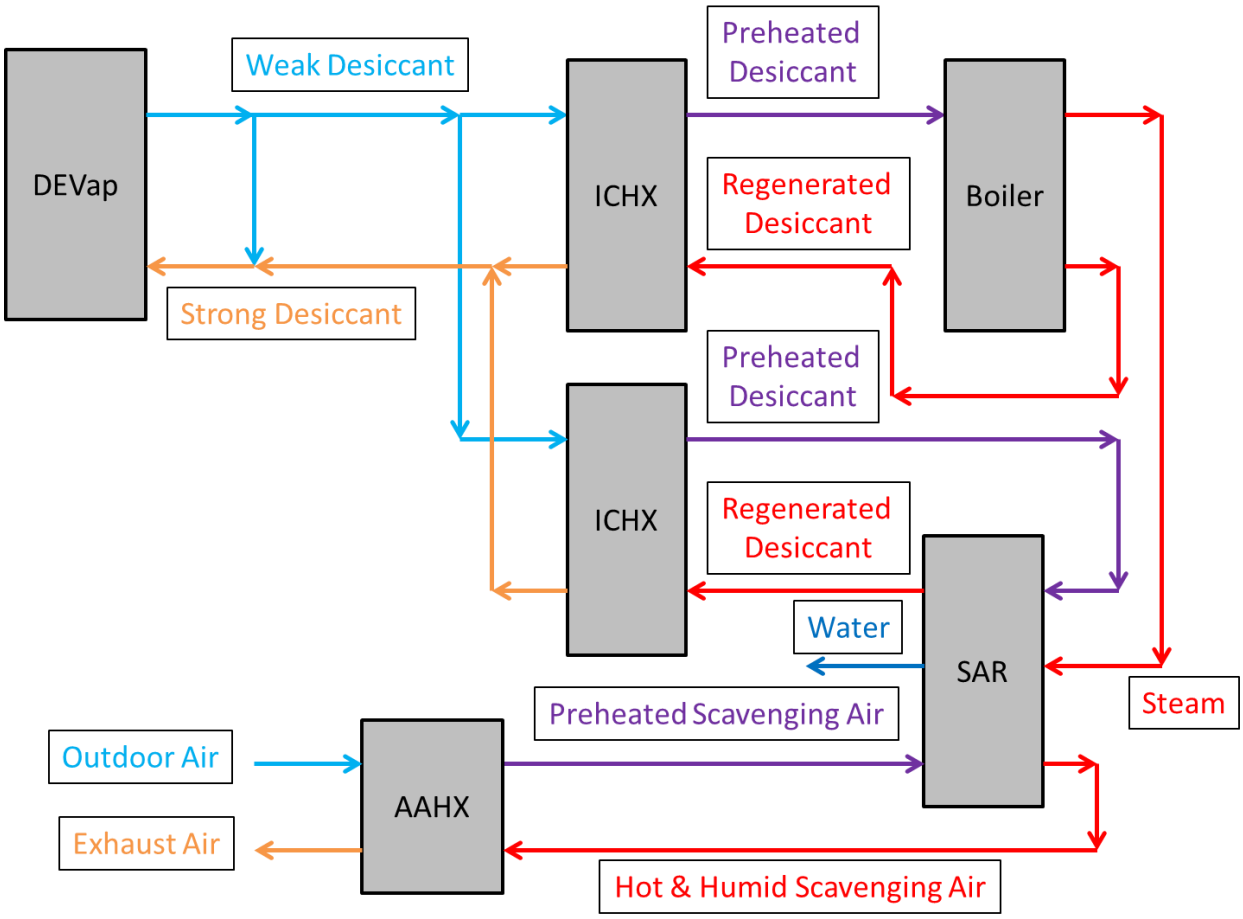

Figure 3.15: Regenerator system schematic

It should be noted that there is a recirculation loop for the liquid desiccant to avoid the regenerator and be recycled through DEVap. Since the design concentration change for the liquid desiccant is 2% across DEVap and 8% across the regenerator, this recirculation loop has been set to always siphon off 75% of the desiccant flow exiting DEVap for recirculation and allow the remaining 25% to pass through the regenerator. After this recirculation split, there is a split in the desiccant flow between a loop using the boiler for regeneration and a loop using the SAR for regeneration. Each of these loops contains its own ICHX to provide maximum heat

recovery. The regenerated desiccant from both loops is mixed together first and then mixed with the recirculated desiccant that wasn't regenerated before finally being sent to DEVap to dehumidify process air.

3.4.1 Gas-Fired Boiler

A gas-fired boiler is the primary method of regenerating the liquid desiccant, since it can achieve high temperatures and the steam exiting the boiler is the heat source to regenerate liquid desiccant in the SAR. In situations where little regeneration is required, the portion of liquid desiccant being passed through the boiler is minimal, resulting in reduced gas consumption.

3.4.2 Scavenging Air Regenerator (SAR)

The SAR utilizes a system of tubes for steam and scavenging air to flow in a cross flow orientation. Liquid desiccant is sprayed onto a wicking surface at the top of a vertical plate and allowed to trickle down one side to the bottom where it is collected. The liquid desiccant film comes into contact with the scavenging air as it trickles down the plate, allowing moisture transfer between these two fluids. The plate separates steam from the liquid desiccant to ensure that there is no mass transfer between these two fluids. Steam is used in the SAR as the heat source instead of hot water because steam has higher enthalpy at the same temperature. As liquid desiccant is heated by the steam from the boiler, its vapor pressure increases. This increases the vapor pressure difference between liquid desiccant and scavenging air, causing moisture to exit the liquid desiccant and enter the scavenging air stream. Eventually the steam loses enthalpy and condenses into hot liquid water when it exits the SAR. The physical arrangement for the channels in the SAR is shown in Figure 3.16.

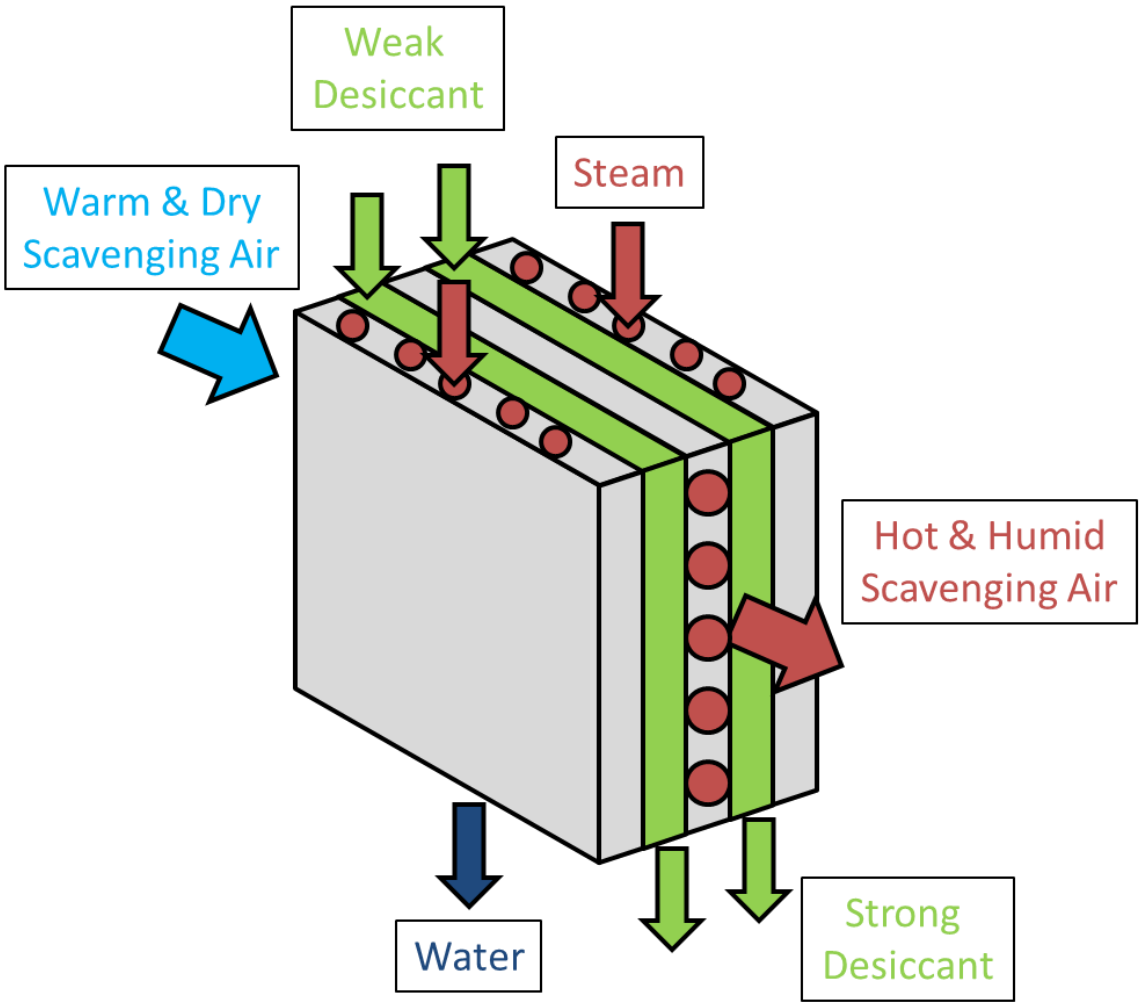

Figure 3.16: Channel orientation for SAR

3.4.3 Heat Exchangers

Heat exchangers are utilized for the liquid desiccant streams connected to the boiler and SAR as well as the scavenging air stream of the SAR. For liquid desiccant, an ICHX serves the purpose of preheating before entering the regenerator system and precooling before entering DEVap to improve the performance of both systems. For scavenging air, an AAHX exclusively preheats the scavenging air before entering the SAR to increase vapor pressure, which results in increased moisture absorption potential.

3.5 Regenerator Control Variables

The regenerator described in the previous section also has control variables that can be adjusted during operation and independent variables that cannot be controlled. The only two control variables are the inlet liquid desiccant concentration to the regenerator, $C_{LD,in,reg}$, and the desired concentration change across the regenerator, $\Delta C_{LD,reg}$. Both of these control variables affect how much moisture the regenerator must drive off of the desiccant. As $C_{LD,in,reg}$ increases, the vapor pressure of the desiccant entering the regenerator decreases, making it increasingly more difficult to raise the vapor pressure of the desiccant to the point where moisture will transfer to a scavenging air stream in either the boiler or SAR. This translates into more energy being consumed in order to regenerate the desiccant, which causes COP_{reg} to decline. As $\Delta C_{LD,reg}$ increases, then the amount of moisture that is driven off of the desiccant increases. This results in higher steam flow exiting the boiler. Since the SAR uses steam from the boiler as a heat source, this translates into greater regeneration in the SAR. This increase in "free" regeneration in the double-stage regenerator system results in an increase in COP_{reg}. These two trends are shown in Figure 3.17.

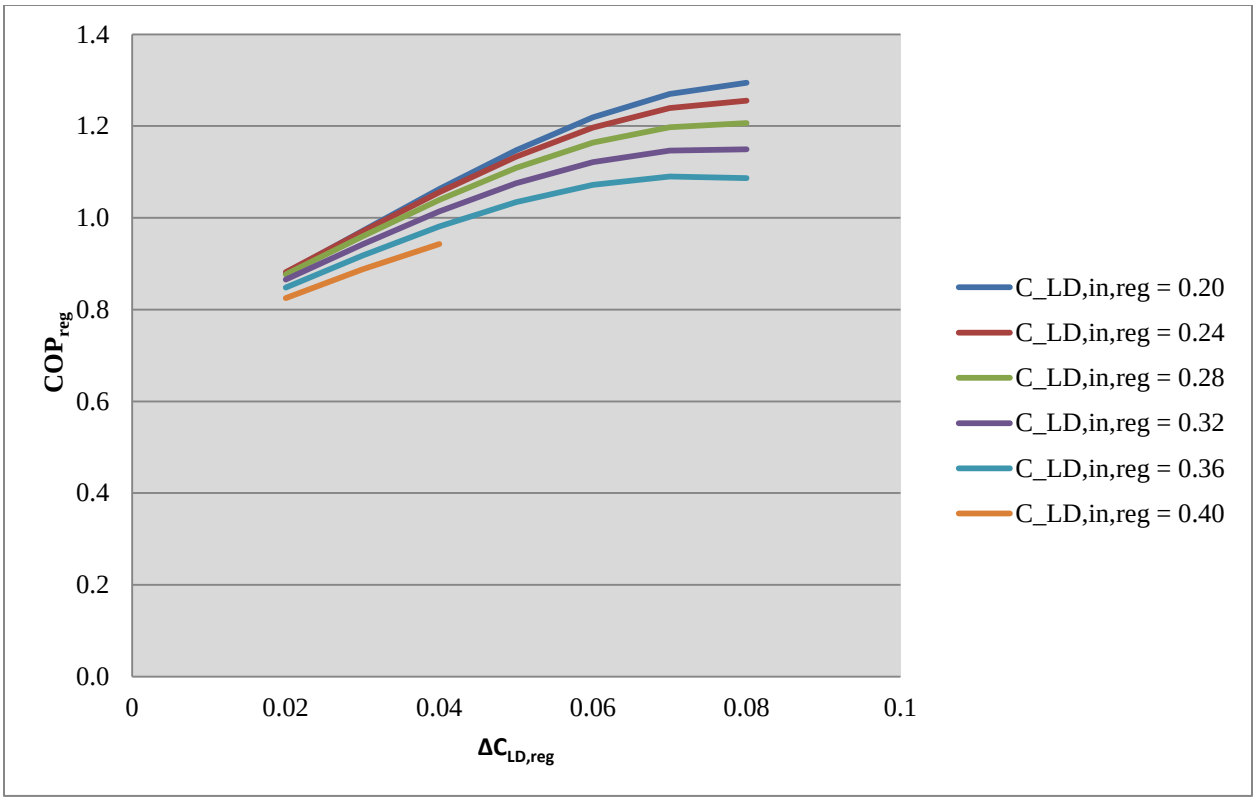

Figure 3.17: Impact of adjusting CLD,in,reg and ΔCLD,reg on COPreg for constant outdoor air

The only two independent variables affecting regenerator performance that cannot be controlled are outdoor air temperature and humidity. As outdoor air becomes hotter and drier, it offers greater potential to absorb moisture as a scavenging air stream in the SAR. However, since regeneration will likely occur whenever dehumidification is required in DEVap, and since return air states mimic outdoor air states, it is expected that outdoor air will be humid during regeneration.

Now that the DEVap and regenerator system are described, the following chapter describes how these two systems were modeled in computer simulation tools.

Chapter 4: Methods – Research Preparation

This chapter presents methods used for computer simulation of DEVap and the regenerator whose results were described in the previous chapter. The original modeling of DEVap and the regenerator are discussed first. This is followed by an explanation of the procedure used to devise correlations for DEVap and regenerator performance. These correlations avoid the need to use iterative computer simulation processes, thereby expediting the research for this thesis. The expected range of values for independent and control variables during the operation of DEVap and the regenerator are discussed, along with the accuracy of the correlations that were developed.

4.1 DEVap Modeling

The DEVap concept is modeled using the Engineering Equation Software (EES) framework. The model developed by Woods employs two-dimensional nodal heat and mass balances for exchanges between liquid desiccant, process air, water, and exhaust air channels [20]. The two-dimensional nodal grid is oriented from the top to the bottom of the device along the direction of air flow through the device, as shown in Figure 4.18.

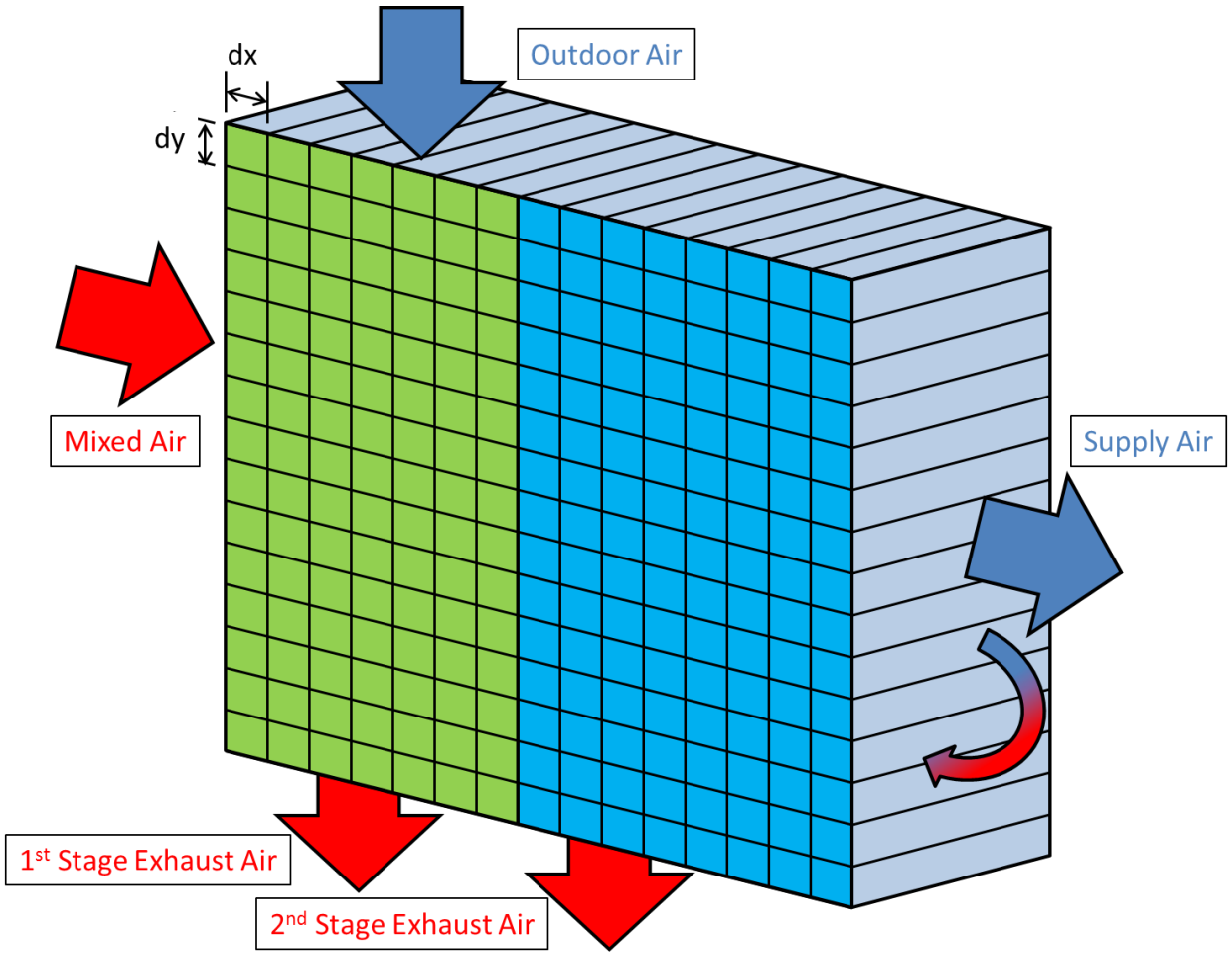

Figure 4.18: Two-dimensional nodal scheme for DEVap modeling

Starting with inlet conditions for mixed air, outdoor air, and liquid desiccant, the model solves sets of equations pertaining to heat and mass exchange between each node. This ultimately results in solving for outlet conditions for supply air, exhaust air in the both the first and second stage, and liquid desiccant. Two-dimensional nodal analysis was employed in order to reduce run time for simulations compared to three-dimensional nodal analysis. The transport properties for the membrane are estimated using standard practice from the membrane-science field for similar vapor-transport processes [20]. The convection coefficient and friction factors for the air channels are based on experimental data measured at NREL of the Dais ConsERV

energy recovery ventilator that uses a similar air flow arrangement used in DEVap [3]. Properties of lithium chloride at different concentrations and temperatures were determined in the DEVap EES model using a table of properties of aqueous solutions of liquid desiccants [21]. Heat transfer with the environment is not included in the model. Parameter values for the spacers separating vertical channels and membranes within DEVap are shown in Table 4.4.

Table 4.4: Membrane Parameter Values for DEVap [20]

Parameter	Value
Spacer conductivity, k_{spacer}	0.15 W/m*°C
Membrane conductivity, k_{mem}	0.25 W/m*°C
Average membrane pore diameter, $d_{pore,avg}$	1.0 µm
Void fraction of hydrophobic layer	0.7

The optimization of a control strategy for DEVap requires that the device not change dimensions. Device dimensions used for this thesis are shown in

Table 4.5. These parameter values are fixed for all following simulations used to develop control strategies for optimal DEVap operation. Theoretically, if these dimension values change, the optimal control strategy developed in this thesis would not apply to the new device. DEVap dimensions are illustrated in Figure 2.2.

Table 4.5: DEVap Device Dimensions

Parameter	Value
Total length, L	1.64 ft
Length of first stage, L_1	0.45 ft
Length of second stage, L_2	1.19 ft
Height, H	1.64 ft
Width, W	2.00 ft
Number of channel pairs	100
Supply air channel width	2.5 mm
Membrane thickness	0.03 mm
Desiccant flow thickness	0.25 mm
Plastic sheet thickness	0.25 mm
Water flocking thickness	0.25 mm
Exhaust air channel width	2.0 mm

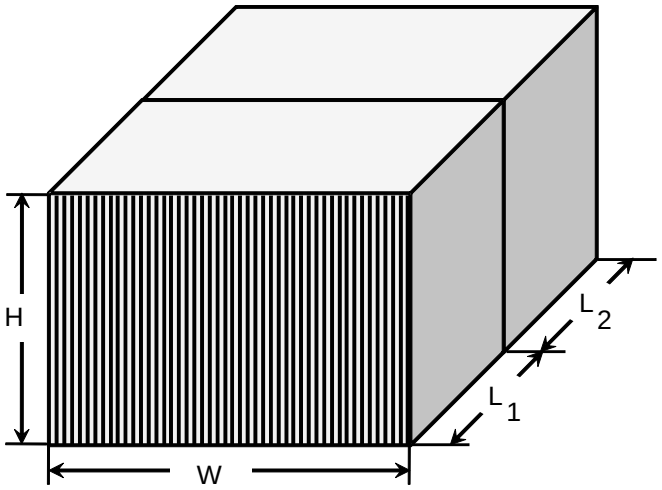

Figure 4.19: DEVap device design [3]

For the research performed in this thesis, the same design condition from the original DEVap study was used [3]. Therefore, the design process air flow rate of 0.285 kg/s and design liquid desiccant flow rate of 0.0280 kg/s apply. The design mixed air flow rate impacts both R_{ma} ratio and R_{e1} ratio, while the liquid desiccant flow rate for all future simulations will be set to the design desiccant flow rate since it has little impact on dehumidification performance.

4.2 Regenerator Modeling

The two-stage regenerator was modeled using the EES framework and the same library of liquid desiccant properties as the DEVap model [21]. The modeling approach utilized a simple thermodynamic approach with a control volume defined around each individual part of the regenerator system, with the assumption of lossless piping. The SAR was modeled as one body with one steam channel, one liquid desiccant channel, and one scavenging air channel instead of as multiple channel pairs. Heat transfer with the environment was not included in the model for any component of the regenerator system. It was assumed that the inlet steam temperature would be the boiling temperature of the inlet liquid desiccant, since the steam fed into the SAR comes from the boiler. It was also assumed that steam would maintain temperature of 100°C throughout the SAR and eventually exit as liquid water at 90°C, which is also the assumed exiting temperature of liquid desiccant. The code for this EES model can be found in Appendix A.

Lowenstein of AIL has constructed a first principle finite difference model of a SAR that is identical to the one modeled here, except that the heat source is hot water instead of steam [22]. Since Lowenstein has been researching and constructing recent breakthroughs in LDAC

equipment, this model is considered to be very accurate. Data from this model was used to calibrate the effectiveness of heat and mass exchange within the SAR, defined by Equation 4.6 and Equation 4.7, respectively.

$$\varepsilon_{SAR,T} = \frac{T_{air,out} - T_{air,in}}{T_{steam} - T_{air,in}} = \frac{T_{air,out} - T_{air,in}}{100°C - T_{air,in}}$$

Equation 4.6

$$\varepsilon_{SAR,\omega} = \frac{\omega_{air,out} - \omega_{air,in}}{\omega_{LD,max} - \omega_{air,in}} = \frac{\omega_{air,out} - \omega_{air,in}}{(\omega_{LD} @ T = 100°C \,\&\, C_{LD,in}) - \omega_{air,in}}$$

Equation 4.7

It was assumed that the SAR would behave similar to a cross-flow heat exchanger with unmixed streams and that the NTU-effectiveness relationship for such a heat exchanger would apply. The heat exchange and mass exchange coefficients for the two effectivenesses defined above are then calculated using Equation 4.8 and Equation 4.9, respectively.

$$NTU_{SAR,T} = \frac{UA_{SAR,T}}{(m * c_p)_{min}}$$

Equation 4.8

$$NTU_{SAR,\omega} = \frac{KA_{SAR,\omega}}{m_{min}}$$

Equation 4.9

The streams used to determine the minimum heat transfer capacity and flow rate are the air stream and liquid desiccant stream. In order to ensure that the SAR model behaves correctly,

a range of input conditions for both the air stream and liquid desiccant stream from Lowenstein's data was imposed on the SAR model. This range of conditions is outlined in Table 3.3.

Table 4.6: AIL Comparison Conditions for Scavenging Air Regenerator

Parameter	Value
Inlet liquid desiccant concentration	0.35 – 0.39
Outlet liquid desiccant concentration	0.41 – 0.45
Inlet liquid desiccant temperature	156°F
Air flow rate	12 scfm
Standard air density	0.08 lbm/ft^3
Inlet scavenging air temperature	60 – 120°F
Inlet scavenging air RH	25 – 60%
Outlet scavenging air temperature	174.9 – 184.2°F
Outlet scavenging air humidity ratio	0.0835 – 0.1124
Water removal rate	3.87 – 5.30 lbm/hr

Forcing the SAR model and Lowenstein's data to have the same inlet and outlet air conditions will cause them to also have the same water removal rate as Lowenstein's data, since the moisture change in the air stream is the same. A comparison of COP_{reg} between the SAR model and Lowenstein's data for different water removal rates is shown in Figure 4.20.

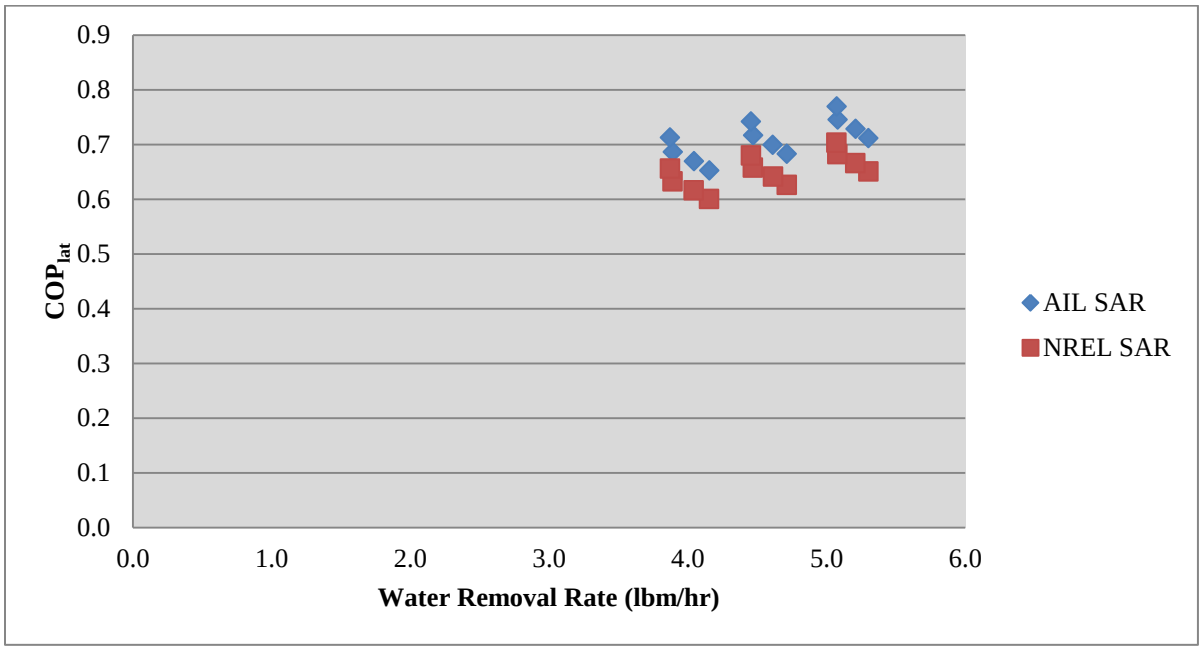

Figure 4.20: Latent COP vs water removal rate comparison for SAR models

From Figure 4.20 it can be determined that the SAR model removes water at a COP_{reg} that is comparable to Lowenstein's data and therefore gives satisfactory results. In order to determine the heat and mass exchange coefficients in the SAR model, a design case from Lowenstein's data was imposed on the SAR model. ???You are forcing agreement here The design case for modeling the SAR is outlined in Table 4.7. The resulting heat and mass exchange coefficients calculated by the SAR model under the design case are outlined at the bottom of Table 4.7.

Table 4.7: Scavenging Air Regenerator Design Parameters

Parameter	Value
Inlet liquid desiccant concentration	0.37
Outlet liquid desiccant concentration	0.43
Inlet air temperature	100°F
Inlet air RH	40%
Inlet air flow rate	12 scfm
Standard air temperature	290 K
Standard air pressure	100 kPa
Inlet steam temperature	254°F
Outlet water temperature	194°F
Inlet liquid desiccant temperature	156°F
Outlet liquid desiccant temperature	194°F
Outlet air temperature	180.6°F
Outlet air humidity ratio	0.0993
Heat exchange coefficient for SAR, $UA_{SAR,T}$	9.665 W/°C
Mass exchange coefficient for SAR, $KA_{SAR,\omega}$	0.001525 kg/s

Now that the heat and mass exchange coefficient for the SAR is known, the heat exchange coefficient for each heat exchanger in the rest of the regenerator system can be determined for a given design case. The design case for the regenerator system is outlined in Table 4.8.

Table 4.8: Regenerator System Design Parameters

Parameter	Value
Inlet liquid desiccant concentration	0.36
Inlet liquid desiccant temperature	25°C
Outlet liquid desiccant concentration	0.44
Inlet liquid desiccant flow rate	0.0280 kg/s
Effectiveness of ICHX	0.80
Effectiveness of AAHX	0.60
Boiler efficiency	0.82
$UA_{SAR,T}$	9.665 W/°C
$KA_{SAR,\omega}$	0.001525 kg/s
Outdoor air temperature	95°F
Outdoor air humidity	55% RH
Heat exchange coefficient for ICHX in boiler loop, $UA_{ICHX,boiler}$	26.87 W/°C
Heat exchange coefficient for ICHX in SAR loop, $UA_{ICHX,SAR}$	19.01 W/°C
Heat exchange coefficient for AAHX, UA_{AAHX}	7.56 W/°C

Now that all the heat and mass exchange coefficients in the regenerator system are determined, simulations can be performed in order to derive performance correlations for both DEVap and the regenerator system. These performance correlations will allow further simulations to be conducted in Excel instead of EES and reduce simulation time.

4.3 Design Expert Correlations

For further research, it will be beneficial to develop performance correlations so that simulating combinations of air states and operating parameter values can be performed in Excel instead of EES. This will avoid using a slower iterative solution process and therefore expedite the optimization process. The desired correlations will be able to calculate outputs of both

DEVap and the regenerator system that are necessary to determine the cooling load provided and required amount of energy input. These are required to calculate the source coefficient of performance of DEVap's operation (COP_{source}) and the cooling load provided by DEVap (Q_{tot}), which are calculated as shown previously in Equation 4.9 and Equation 4.93, respectively.

For DEVap, the only electricity consumption is due to fan energy use to move supply air and exhaust air in both the liquid desiccant dehumidification section as well as the indirect evaporative cooling section. A general formula for fan energy consumption is given in Equation 4.10.

$$\boldsymbol{Q_{fan}} = \frac{\boldsymbol{V_{air}} * \Delta \boldsymbol{P_{air}}}{\boldsymbol{\eta_{fan}}}$$

Equation 4.10

From Equation 4.10, the fan energy can be calculated using the volumetric flow rate of air, the air-side pressure drop, and the fan efficiency. For all simulations, it was assumed that the fan efficiency was a constant 0.5. The volumetric flow rate of air can be determined from the mass flow rate of air and density of air. The mass flow rate of air can be set in simulations, so two independent air parameters, such as temperature and humidity ratio, must be known to determine the density of air. The inlet air states and outlet air states for each section are used to determine the average air state, which is assumed to be constant for one given section. Therefore, it is necessary to develop correlations for temperature and humidity of air exiting the dehumidification section and entering the indirect evaporative cooling section as well as supply air exiting the indirect evaporative cooling section. It is also necessary to develop correlations for the air-side pressure drops in the supply channel of both sections and each exhaust channel,

which are calculated and output in the DEVap EES model. Any cooling load provided by DEVap can be calculated using the mass flow rate of air through the device and the difference between inlet and outlet air states, so no further correlations for DEVap are required. The input variables to these correlations should be the temperature and humidity of the mixed air entering DEVap, temperature and humidity of outdoor air, and the four control variables: outdoor air fraction (OAF), concentration of liquid desiccant entering DEVap ($C_{LD,in,DEVap}$), first stage exhaust air flow rate ratio (R_{e1}), and mixed air flow rate ratio (R_{ma}). Since DEVap has three modes of operation, there will be three different sets of correlations for mixed air exiting the first stage, supply air exiting DEVap, and air-side pressure drops across the different channels.

The only other energy that will be consumed during the operation of DEVap is natural gas consumption due to the regeneration process. It was assumed that the amount of required regeneration energy would be equal to the latent load provided by DEVap divided by the COP of the regenerator (COP_{reg}), calculated using Equation 4.11.

$$\boldsymbol{Q_{reg} = \frac{Q_{lat}}{COP_{reg}} = \frac{R_{ma} * m_{ma,des} * h_{fg,regen} * (\omega_{ra} - \omega_{sa})}{COP_{reg}}}$$

Equation 4.11

COP_{reg} is expected to change as the concentration of liquid desiccant exiting DEVap and entering the regeneration system does, since it is easier to drive moisture off of desiccant at lower concentrations. Similarly the desired amount of liquid desiccant concentration change across the regenerator will also have an impact on latent COP. Since the SAR does employ ambient air drawn through an AAHX as the scavenging air stream to absorb moisture driven from the liquid desiccant, ambient air states also need to be included as independent variables

that affect regenerator performance. Therefore, the inlet liquid desiccant concentration to the regenerator ($C_{LD,in,reg}$), desired change in concentration across the regenerator ($\Delta C_{LD,reg}$), and ambient air conditions should all be input variables into the correlation for regenerator performance.

Once ranges of expected values for input variables to each correlation are determined, a design of experiments using the Box-Behnken method can be developed in order to avoid simulating every possible combination of expected conditions to derive correlations from. The Box-Behnken method uses the minimum and maximum expected value as well as the average of those two values for each input variable of interest. If the "space" of the experiment is thought of as a cube, with each axis as an input variable, then the Box-Hehnken method will use information from the cube's center, the center of each face, and the center of each edge in order to gather enough information about how the remainder of the cube will behave. This is illustrated in Figure 4.21.

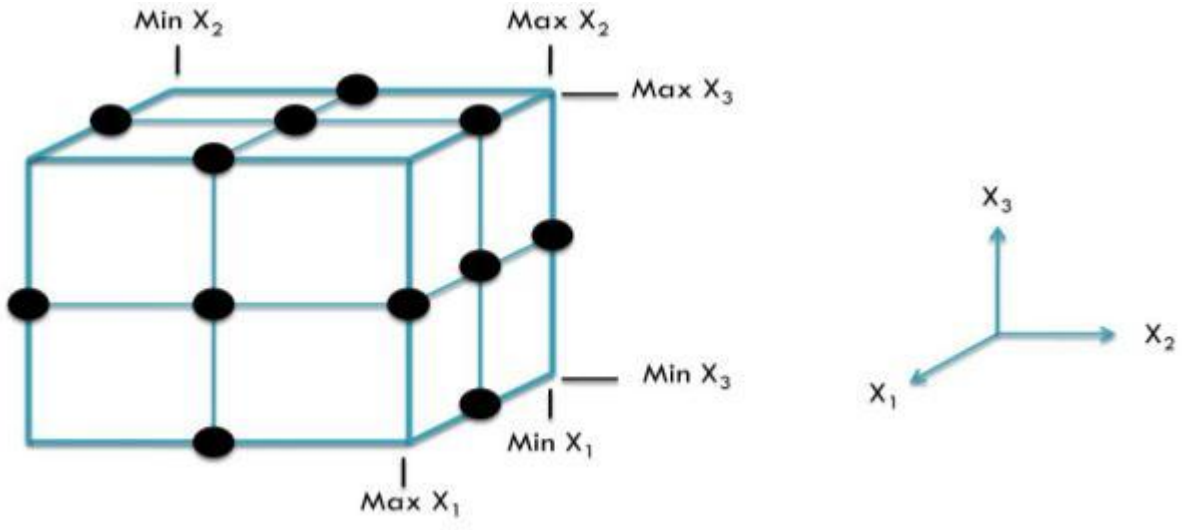

Figure 4.21: Diagram of Box-Behnken design

The Design Expert software takes a minimum and maximum value for each input variable for a correlation and generates a design of experiments based upon the Box-Behnken method. This design of experiments can now be simulated in a parametric table in EES using the appropriate model. If certain combinations of input variables results in the EES model not being able to simulate, then the input variable values can be slightly adjusted from the design of experiments until simulation is successful. Once complete, the results from the parametric table offer insight into relationships between independent variables and dependent variables for which correlations must be developed. These results are then entered back into the same Design Expert model that generated the design of experiments so that the appropriate coefficient values for the initial quadratic equation can be determined without an exponential transform. However, Design Expert outputs an appropriate exponent value to use that will reduce the most bias in the correlation. Once that transform is applied, then the final correlation is the ultimate result. A diagram of this design of experiments process is shown in Figure 4.22.

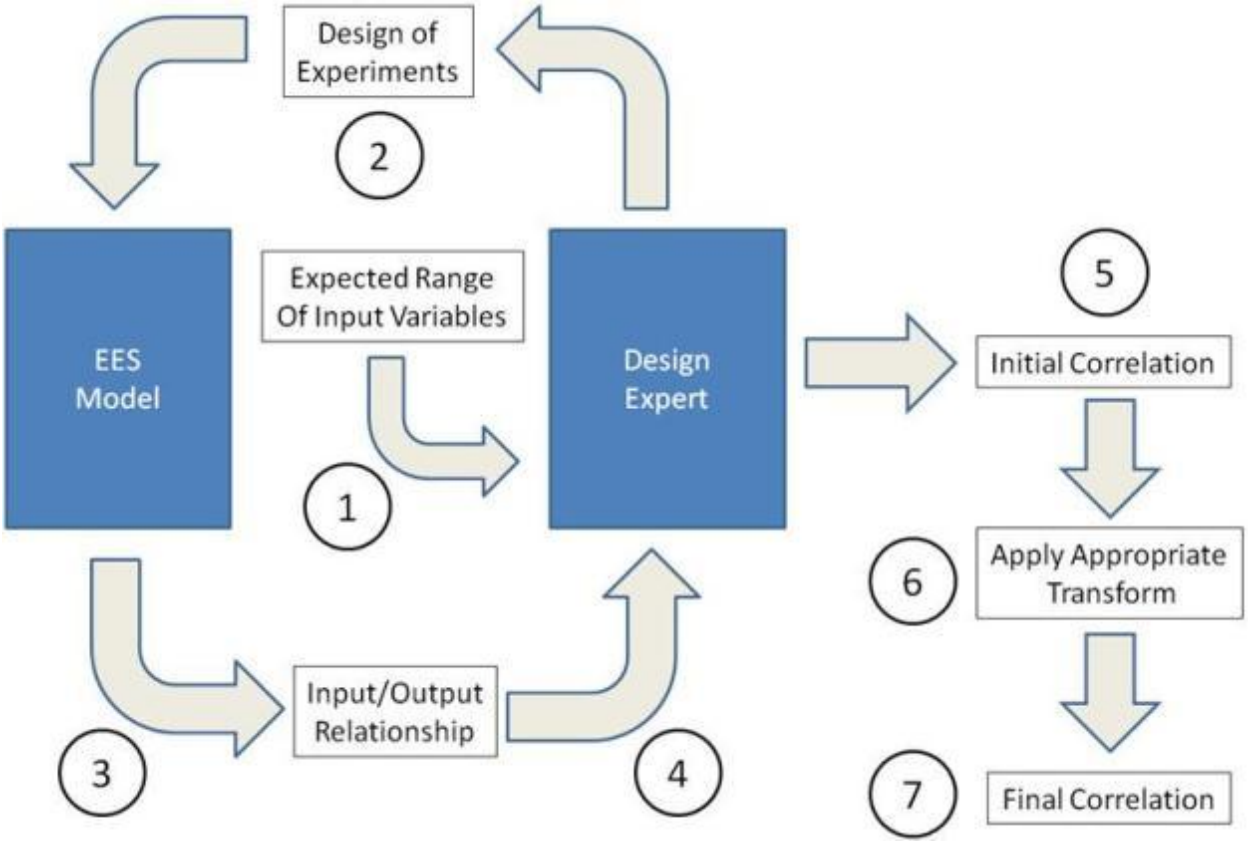

Figure 4.22: Diagram of correlation development process

To simplify the correlation creation process, it was assumed that quadratic correlations would be satisfactory. This is because they are more accurate than linear correlations with much less coefficients and terms than cubic correlations, so they will be easier to implement in Excel.

4.3.1 Design Expert Correlations: Dehumidification Mode

In dehumidification mode, there is no air flow in either of the exhaust channels. This is because there is no need to have exhaust flow absorb any moisture and cool down the process air stream since no cooling is required. This means that both R_{e1} and OAF are set to zero and that there is no air-side pressure drop across the exhaust channels. Since there is no outdoor air being used as exhaust air in the first stage, and there is no mixing of outdoor air with return air, outdoor

air conditions are not relevant either. This leaves the return air conditions, R_{ma}, and C_{LD} as the relevant input variables for correlations used to calculate DEVap's performance as a dehumidifier. In this mode of operation, the mixed air exiting the first stage and the supply air exiting the second stage are the same, since there is no cooling being done in the second stage. Therefore, only one of the two state points requires correlations. This results in a requirement of three correlations: supply air temperature (T_{sa}), supply air humidity ratio (ω_{sa}), and air-side pressure drop across the supply air channel (ΔP_{sa}).

To determine an appropriate range of input variable values, the situations in which only dehumidification is required must be analyzed. This occurs when the space is at or above a relative humidity set point (usually 55% RH) but below a cooling set point temperature, which is typically 75°F. This information was used to create a range of values for each input variable to enter into Design Expert in order to create a design of experiments, as shown in Table 4.9.

Table 4.9: Expected Dehumidification Mode Operating Conditions

Parameter	Range
Return air temperature, T_{ra} (°F)	50 – 80
Return air relative humidity, RH_{ra}	0.50 – 1.00
Ratio of mixed air mass flow rate to design mass flow rate, R_{ma} ratio	0.3 – 1.0
Inlet liquid desiccant concentration, $C_{LD,in,DEVap}$	0.30 – 0.44

It was assumed that a range of 50°F - 80°F for return air temperature and 50% RH - 100% RH for return air relative humidity would cover all possible situations where occupants change set points or turn off equipment while they are gone. These return air states are shown on a psychrometric chart in Figure 4.23.

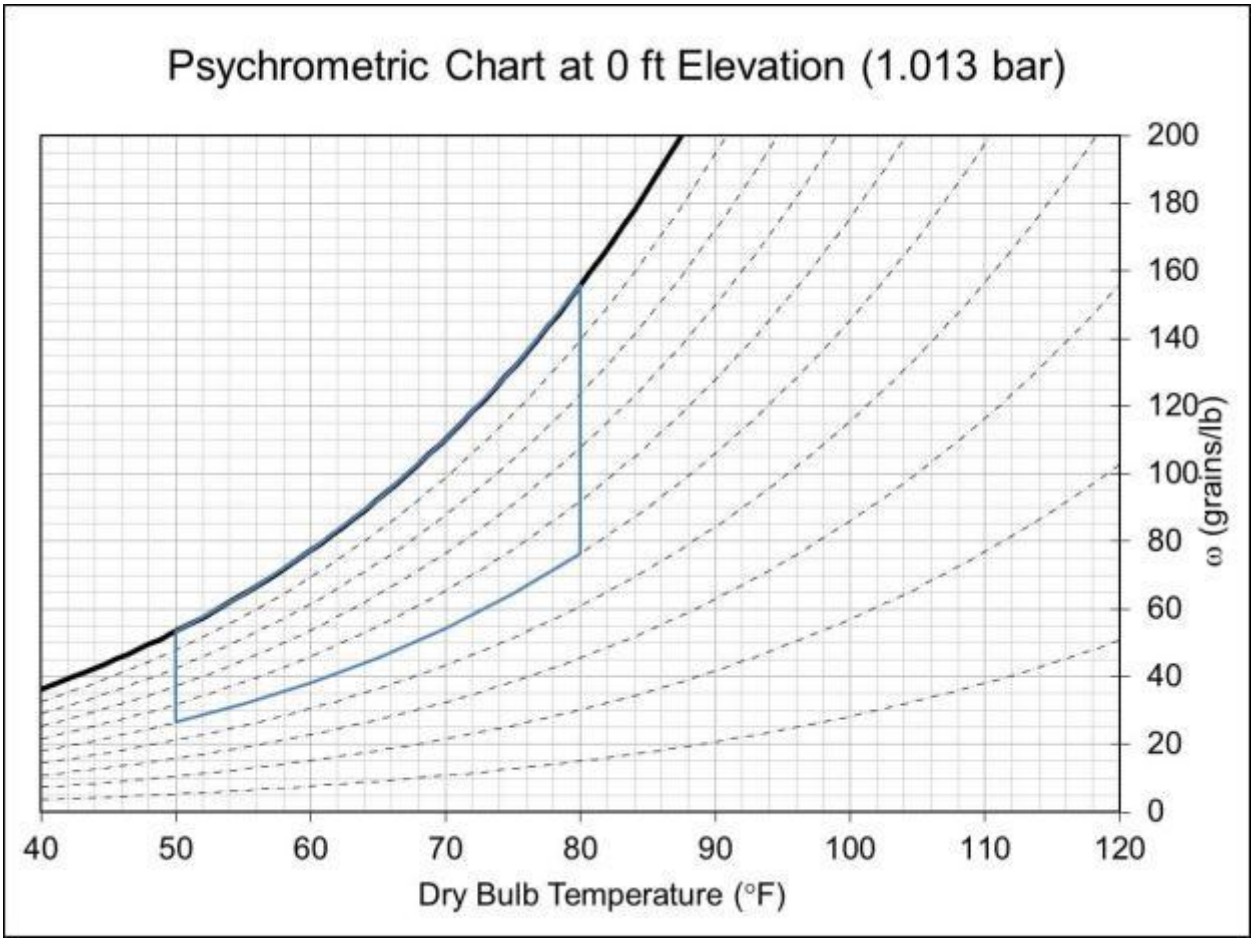

Figure 4.23: Possible return air conditions during dehumidification mode

It was also assumed that R_{ma} would be allowed to vary between 30% and 100% and that C_{LD} would vary between 0.30, where its vapor pressure is close to that of air and little dehumidification is possible, and 0.44 (an assumption of the maximum concentration that the regenerator can output). Entering Table 4.9 into Design Expert resulted in the generation of a design of experiments for dehumidification mode. Once this design of experiments was entered into a parametric table in the EES model and simulated, the following results were obtained. The full design of experiments results for dehumidification mode and all other correlations can be found in Appendix B.

Table 4.10: Dehumidification Mode Design of Experiments Results

T_{ra} (°F)	RH_{ra}	R_{ma} ratio	$C_{LD,in,DEVap}$	T_{sa} (°F)	ω_{sa}	ΔP_{sa} (in H_2O)
50	0.5	0.65	0.37	57.01	0.002351	0.3039
50	0.75	0.65	0.3	57.3	0.004165	0.3056
50	0.75	1	0.37	62.67	0.003067	0.5346
50	0.75	0.3	0.37	63.26	0.002947	0.1147
65	0.5	0.65	0.3	67.6	0.006047	0.3181
…	…	…	…	…	…	…
80	0.75	0.65	0.44	113.8	0.009546	0.357

Entering these simulation results back into the Design Expert model allowed the relationships between input variables and each output variable to be characterized into quadratic correlations. The coefficients for each correlation are outlined in

Table 4.11, with highlighted cells representing correlation terms deemed insignificant by Design Expert.

$$f\ A, B, C, \dots, n = x_0 + x_A * A + x_B * B + \cdots + x_{A^2} * A^2 + x_{B^2} * B^2 + \cdots + x_{AB} * A * B + x_{AC} * A * C + \cdots + x_{n-1\ n} * (n-1) * n$$

Equation 4.12

Table 4.11: Dehumidification Mode Correlation Coefficients

Coefficient	T_{sa} (°F)	ω_{sa}	ΔP_{sa} (in H_2O)
x_0	0.2154	0.1640	-3.5030
x_A (A: T_{ra})	-0.0021	-0.0009	0.0009
x_B (B: RH_{ra})	-0.0420	-0.0476	-0.0418
x_C (C: R_{ma})	-0.0001	-0.0113	4.5203
x_D (D: C_{LD})	-0.1285	-0.1713	-0.0607
x_A^2	0.0000	0.0000	0.0000
x_B^2	0.0087	-0.0092	-0.0144
x_C^2	0.0006	0.0009	-1.7910
x_D^2	0.0645	-0.2316	-0.0361
x_{AB}	0.0002	0.0016	0.0020
x_{AC}	0.0000	0.0000	0.0000
x_{AD}	0.0002	0.0012	0.0033
x_{BC}	0.0001	0.0045	0.0027
x_{BD}	0.0077	0.0426	0.0503
x_{CD}	0.0009	0.0282	0.0116

The previous tables outlining the expected range of input variables, design of experiments results, and correlation coefficients for dehumidification mode can be found in Appendix B, along with tables for all further correlations. A test for correlation accuracy was conducted by entering the original values for input variables from the design of experiments into the correlations. The resulting output values for T_{sa}, ω_{sa}, and ΔP_{sa} were then compared to those values calculated from the DEVap EES model for the same input variable values. The following statistical data outlined in

Table 4.12 were realized.

Table 4.12: Dehumidification Mode Correlation Accuracy

Correlation	Max Δ	Min Δ	Avg Δ	Max %Δ	Min %Δ	Avg %Δ	R^2
T_{sa} (°F)	0.32	-0.43	0.00	0.36%	-0.37%	0.00%	1.000
ω_{sa}	0.0002	-0.0001	0.0000	1.86%	-2.53%	-0.23%	1.000
ΔP_{sa} (in H_2O)	0.001	-0.001	0.000	0.12%	-0.17%	0.00%	1.000

Max, min, and avg Δ represent the maximum, minimum, and average difference between correlation output and model calculation, respectively. Max, min, and avg %Δ represent the maximum, minimum, and average percent difference between correlation output and model calculation, respectively. Percent difference was calculated using Equation 4.13 and the square of the Pearson product moment correlation coefficient, R^2, was calculated using Equation 4.14.

$$\%\Delta = \frac{x - y}{y}$$

Equation 4.13

$$R^2 = \left(\frac{x-\bar{x}\ \ y-\bar{y}}{(x-\bar{x})^2\ \ (y-\bar{y})^2}\right)^2 ???$$

Equation 4.14

In these equations, x denotes correlation output values from Design Expert and y denotes model output values from the DEVap EES model [20], while a bar above a variable denotes the mean value for that variable. From

Table 4.12, it can be determined that all the correlations for dehumidification mode are satisfactory.

4.3.2 Design Expert Correlations: Indirect Evaporative Cooling Mode

In IEC mode, cooling occurs in both sections of DEVap. In the first section, the process air is cooled by untreated outdoor air absorbing water in a cross-flow arrangement. Therefore, the first stage exhaust air flow ratio (R_{e1}) is a control variable. In the second stage, the process air exiting the first stage is further cooled by air that is siphoned off of the supply air stream in a counter flow arrangement. Since the amount of air siphoned off is equal to the amount of outdoor air mixed with return air, OAF is a control variable as well. Since outdoor air becomes influential in both the mixed air state entering DEVap as well as the cooling potential in the first stage exhaust stream, outdoor air conditions are important. The final control variable is the mixed air flow ratio (R_{ma}). There is no flow of liquid desiccant due to a lack of latent cooling required, resulting in $C_{LD,in,DEVap}$ losing relevance as a control variable.

In this mode of operation, the process air exiting the first stage and the supply air exiting the second stage are not the same, since there is cooling being done in the second stage. Therefore, correlations are required for each of the two state points. However, since no dehumidification occurs, the humidity ratio of supply air exiting DEVap is the same as the humidity ratio of mixed air entering DEVap. This results in a requirement of six correlations: supply air temperature (T_{sa}), process air temperature exiting the first stage ($T_{pa,1}$), air-side pressure drop across the supply air channel in the first stage (ΔP_{s1}), air-side pressure drop across the supply air channel in the second stage (ΔP_{s2}), air-side pressure drop across the exhaust air channel in the first stage (ΔP_{e1}), and air-side pressure drop across the exhaust air channel in the

second stage (ΔP_{e2}). Correlations for process air exiting the first stage will use mixed air state, outdoor air state, R_{ma} ratio, and R_{e1} ratio, and OAF as input variables. Correlations for supply air exiting DEVap will use process air exiting the first stage, R_{ma} ratio, and OAF as input variables.

To determine an appropriate range of input variable values, the situations in which only indirect evaporative cooling is required must be analyzed. This occurs when the space is below a relative humidity set point (usually 55% RH) but above a cooling set point temperature, which is typically 75°F. This information was used to create a range of values for each input variable to enter into Design Expert in order to create a design of experiments, as shown in

Table 4.13.

Table 4.13: Expected Indirect Evaporative Cooling Mode Operating Conditions

Parameter	Range
Outdoor air fraction, OAF	0.05 – 0.50
Ratio of mixed air mass flow rate to design mass flow rate, R_{ma} ratio	0.3 – 1.0
Ratio of first stage exhaust air mass flow rate to design mass flow rate, R_{e1} ratio	0.1 – 0.7
Return air temperature, T_{ra} (°F)	65 – 80
Return air relative humidity, RH_{ra}	0.15 – 0.65
Outdoor air temperature, T_{oa} (°F)	60 – 120
Outdoor air humidity ratio, ω_{oa}	0.0003 – 0.0110

It was assumed that a range of 65°F - 80°F for T_{ra} and 15% - 65% for RH_{ra} would cover all possible situations where occupants change set points or turn off equipment while they are gone. Including relative humidity values of 55% will allow insight into DEVap's usefulness as an indirect evaporative cooler just before dehumidification is required. Outdoor air humidity values were kept low since first stage cooling is much more attractive when outdoor air is drier

and more able to absorb moisture. These return and outdoor air states are shown on a psychrometric chart in Figure 4.24.

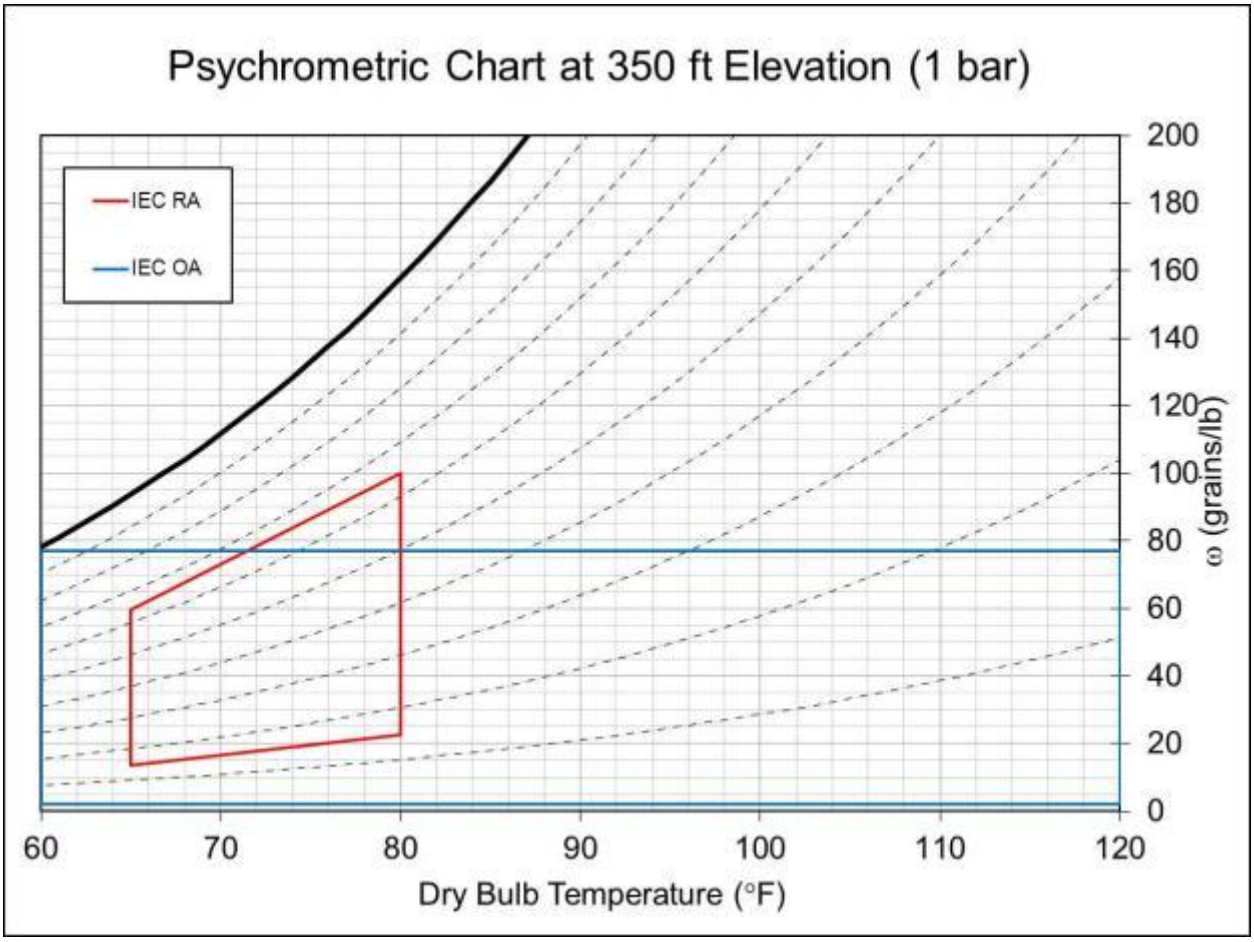

Figure 4.24: Possible return and outdoor air conditions during IEC mode

It was also assumed that R_{ma} ratio would be allowed to vary between 30% and 100% and that R_{e1} ratio would be allowed to vary between 10% and 70% since the exhaust fan should be sized smaller than the mixed air fan. The minimum OAF value of 0.05 represents a minimum ventilation level during cooling, and the OAF is not expected to go higher than 0.5 because that would indicate that half of the supply air stream that was cooled is being siphoned off for second stage cooling, resulting in a huge loss of cooling load provided.

Entering

Table 4.13 into Design Expert resulted in the generation of a design of experiments for indirect evaporative cooling mode. After completing the process of developing correlations outlined by Figure 4.21, the final correlations for temperatures and air-side pressure drops in IEC mode are developed. The design of experiments results and correlation coefficient values are shown in Appendix B.

A test for correlation accuracy was conducted by entering the original values for input variables from the design of experiments into the correlations. The resulting output values for $T_{pa,1}$, ΔP_{e1}, ΔP_{s1}, T_{sa}, ΔP_{e2}, and ΔP_{s2} were then compared to those values calculated from the DEVap EES model for the same input variable values. The following statistical data outlined in Table 4.14 were realized.

Table 4.14: IEC Mode Correlation Accuracy

Correlation	Max Δ	Min Δ	Avg Δ	Max %Δ	Min %Δ	Avg %Δ	R^2
$T_{pa,1}$ (°F)	1.56	-1.35	0.03	2.45%	-2.20%	0.06%	0.996
ΔP_{e1} (in H_2O)	0.002	-0.001	0.000	0.44%	-0.37%	0.02%	1.000
ΔP_{s1} (in H_2O)	0.001	-0.002	0.000	0.36%	-0.41%	0.05%	1.000
T_{sa} (°F)	1.35	-2.01	0.09	2.39%	-2.68%	0.18%	0.991
ΔP_{e2} (in H_2O)	0.001	-0.001	0.000	1.22%	-1.36%	0.31%	0.992
ΔP_{s2} (in H_2O)	0.002	-0.003	0.000	1.41%	-1.27%	0.26%	0.990

From Table 4.14, it can be determined that the correlations developed for the outlet conditions from the second stage are not as accurate as those developed for outlet conditions from the first stage in IEC mode. This is because second stage correlations use calculated values from first stage correlations, so any inaccuracies in first stage correlations are compounded in the

second stage correlations. It should be noted that the cases where maximum and minimum differences occur are highly unlikely situations generated by the design of experiments, such as low OAF and R_{e1} ratio when both outdoor and return air are hot. On average, all correlations result in little difference from EES results and are deemed satisfactory for future work.

4.3.3 Design Expert Correlations: Standard Cooling Mode

In standard cooling mode, latent and sensible cooling occurs simultaneously. For this reason, all input variables for correlations discussed earlier are now relevant. Since there is dehumidification taking place in the first stage, the humidity ratio of air will change across that section, requiring a correlation for humidity of process air exiting the first stage. This adds one more correlation to those required for indirect evaporative cooling mode, resulting in the need for seven correlations: supply air temperature (T_{sa}), process air temperature exiting the first stage ($T_{pa,1}$), process air humidity ratio exiting the first stage ($\omega_{pa,1}$), air-side pressure drop across the supply air channel in the first stage (ΔP_{s1}), air-side pressure drop across the supply air channel in the second stage (ΔP_{s2}), air-side pressure drop across the exhaust air channel in the first stage (ΔP_{e1}), and air-side pressure drop across the exhaust air channel in the second stage (ΔP_{e2}). Correlations for process air exiting the first stage will use mixed air state, outdoor air state, R_{ma} ratio, R_{e1} ratio, and $C_{LD,in,DEVap}$ as input variables. Correlations for supply air exiting DEVap will use process air exiting the first stage, R_{ma} ratio, and OAF as input variables.

To determine an appropriate range of input variable values, the situations wherestandard cooling is required must be analyzed. This occurs when the space is simultaneously above a relative humidity set point (usually 55% RH) and above a cooling set point temperature, which is typically 75°F. This information was used to create a range of values for each

input variable to enter into Design Expert in order to create a design of experiments, as shown in

Table 4.15. A lower minimum $C_{LD,in,DEVap}$ value is assumed in standard mode compared to dehumidification mode to allow for high sensible heat ratio values to be provided.

Table 4.15: Expected Standard Cooling Mode Operating Conditions

Parameter	Range
Outdoor air fraction, OAF	0.05 – 0.50
Inlet liquid desiccant concentration to DEVap, $C_{LD,in,DEVap}$	0.20 – 0.44
Ratio of mixed air mass flow rate to design mass flow rate, R_{ma} ratio	0.3 – 1.0
Ratio of first stage exhaust air mass flow rate to design mass flow rate, R_{e1} ratio	0.1 – 0.7
Return air temperature, T_{ra} (°F)	65 – 80
Return air relative humidity, RH_{ra}	0.15 – 0.65
Outdoor air temperature, T_{oa} (°F)	60 – 120
Outdoor air humidity ratio, ω_{oa}	0.0076 – 0.0267
Outdoor air humidity ratio, WB_{oa} (°F)	56 – 84

It was assumed that a range of 65°F - 80°F for T_{ra} and 15% - 65% for RH_{ra} would cover all possible situations where occupants change set points or turn off equipment while they are gone. Outdoor air humidity values were kept high since return air states mimic outdoor air states, therefore latent cooling is likely required when it is humid outside. These return air states are shown on a psychrometric chart in Figure 4.25.

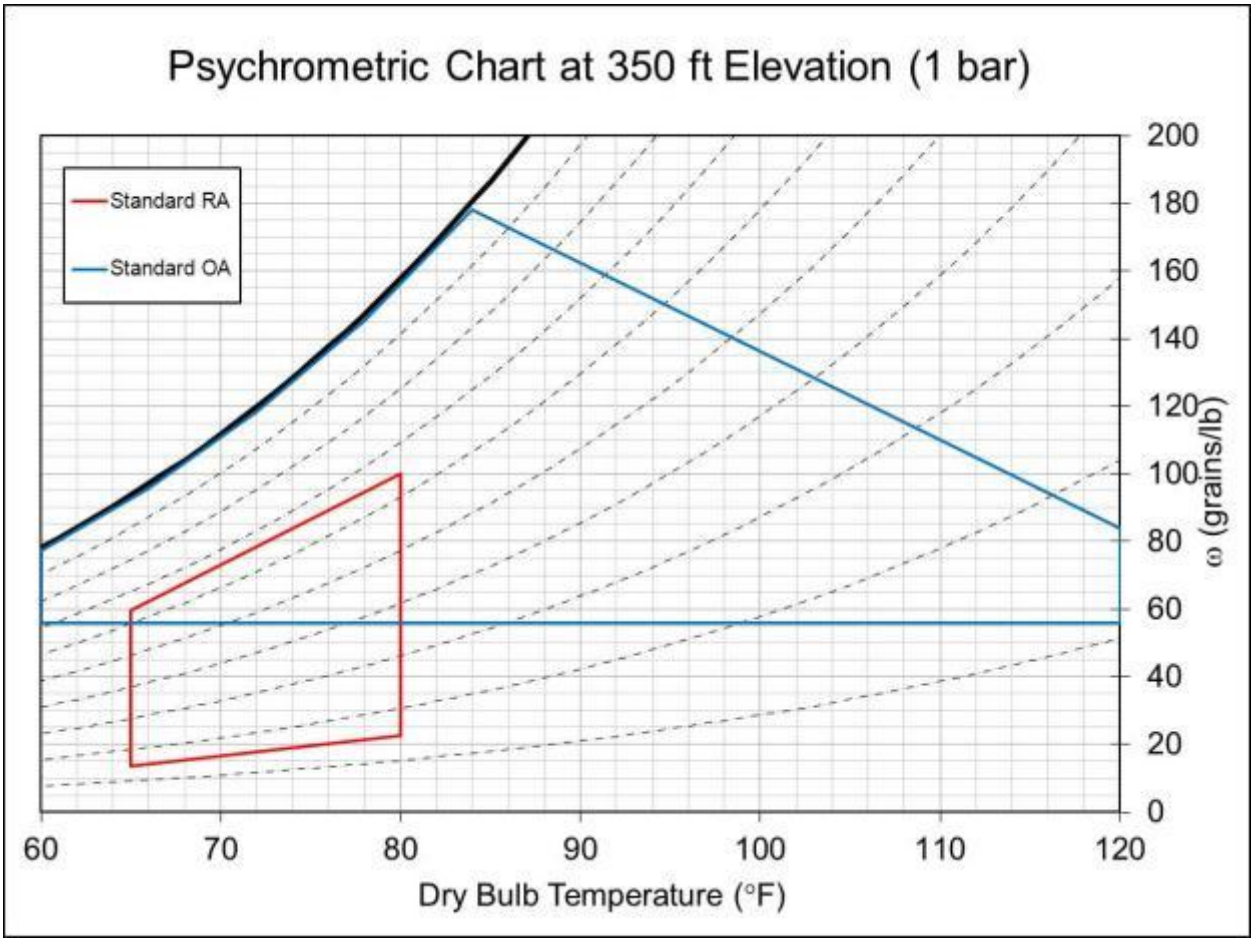

Figure 4.25: Possible return and outdoor air conditions during standard cooling mode

It was also assumed that R_{ma} ratio would be allowed to vary between 30% and 100% and that R_{e1} ratio would be allowed to vary between 10% and 70% since the exhaust fan should be sized smaller than the mixed air fan. The minimum OAF value of 0.05 represents a minimum ventilation level during cooling, and the OAF is not expected to go higher than 0.5 because that would indicate that half of the supply air stream that was cooled is being siphoned off for second stage cooling, resulting in a huge loss of cooling load provided.

Entering Table 4.15 into Design Expert resulted in the generation of a design of experiments for indirect evaporative cooling mode. After completing the process of developing

correlations outlined by Figure 4.21, the final correlations for temperatures, humidity ratios, and air-side pressure drops in standard mode are developed. The design of experiments results and correlation coefficient values are shown in Appendix B.

A test for correlation accuracy was conducted by entering the original values for input variables from the design of experiments into the correlations. The resulting output values for $T_{pa,1}$, ω_{sa}, ΔP_{e1}, ΔP_{s1}, T_{sa}, ΔP_{e2}, and ΔP_{s2} were then compared to those values calculated from the DEVap EES model for the same input variable values. The following statistical data outlined in Table 4.16 were realized.

Table 4.16: Standard Cooling Mode Correlation Accuracy

Correlation	Max Δ	Min Δ	Avg Δ	Max %Δ	Min %Δ	Avg %Δ	R^2
$T_{pa,1}$ (°F)	1.46	-1.40	0.00	1.88%	-1.83%	0.01%	0.995
ω_{sa} (-)	0.0003	-0.0003	0.0000	3.89%	-4.29%	0.02%	0.997
ΔP_{e1} (in H_2O)	0.001	-0.001	0.000	0.20%	-0.23%	0.00%	1.000
ΔP_{s1} (in H_2O)	0.001	-0.003	0.000	1.62%	-2.55%	0.00%	1.000
T_{sa} (°F)	2.79	-2.55	0.00	4.72%	-4.65%	0.01%	0.993
ΔP_{e2} (in H_2O)	0.000	0.000	0.000	0.85%	-1.65%	-0.01%	1.000
ΔP_{s2} (in H_2O)	0.004	-0.005	0.000	1.63%	-2.09%	0.00%	1.000

From Table 4.16, it can be determined that the correlations developed for the outlet conditions from the second stage are not as accurate as those developed for outlet conditions from the first stage in standard mode. This is because second stage correlations use calculated values from first stage correlations, so any inaccuracies in first stage correlations are compounded in the second stage correlations. It should be noted that the cases where maximum and minimum differences occur are highly unlikely situations generated by the design of

experiments, such as low $C_{LD,in,DEVap}$ when RH_{ra} = 65%. On average, all correlations result in little difference from EES results and are deemed satisfactory for future work.

4.3.4 Design Expert Correlations: Regenerator Performance

As explained earlier, regenerator performance is a function of four control variables: the inlet liquid desiccant concentration to the regenerator ($C_{LD,in,reg}$), desired change in concentration across the regenerator ($\Delta C_{LD,reg}$), and ambient air conditions (since ambient air is passed through an AAHX before used as a scavenging air stream). The range of values that is expected for these four variables is outlined in Table 4.17. A psychrometric chart outlining the ambient air conditions is shown in Figure 4.26.

Table 4.17: Expected Regenerator System Operating Conditions

Parameter	Range
Inlet liquid desiccant concentration to regenerator, $C_{LD,in,reg}$	0.20 – 0.42
Liquid desiccant concentration change across regenerator, $\Delta C_{LD,reg}$	0.02 – 0.08
Ambient air temperature, T_{oa} (°F)	60 – 120
Ambient air humidity, ω_{oa}	0.0076 – 0.0260

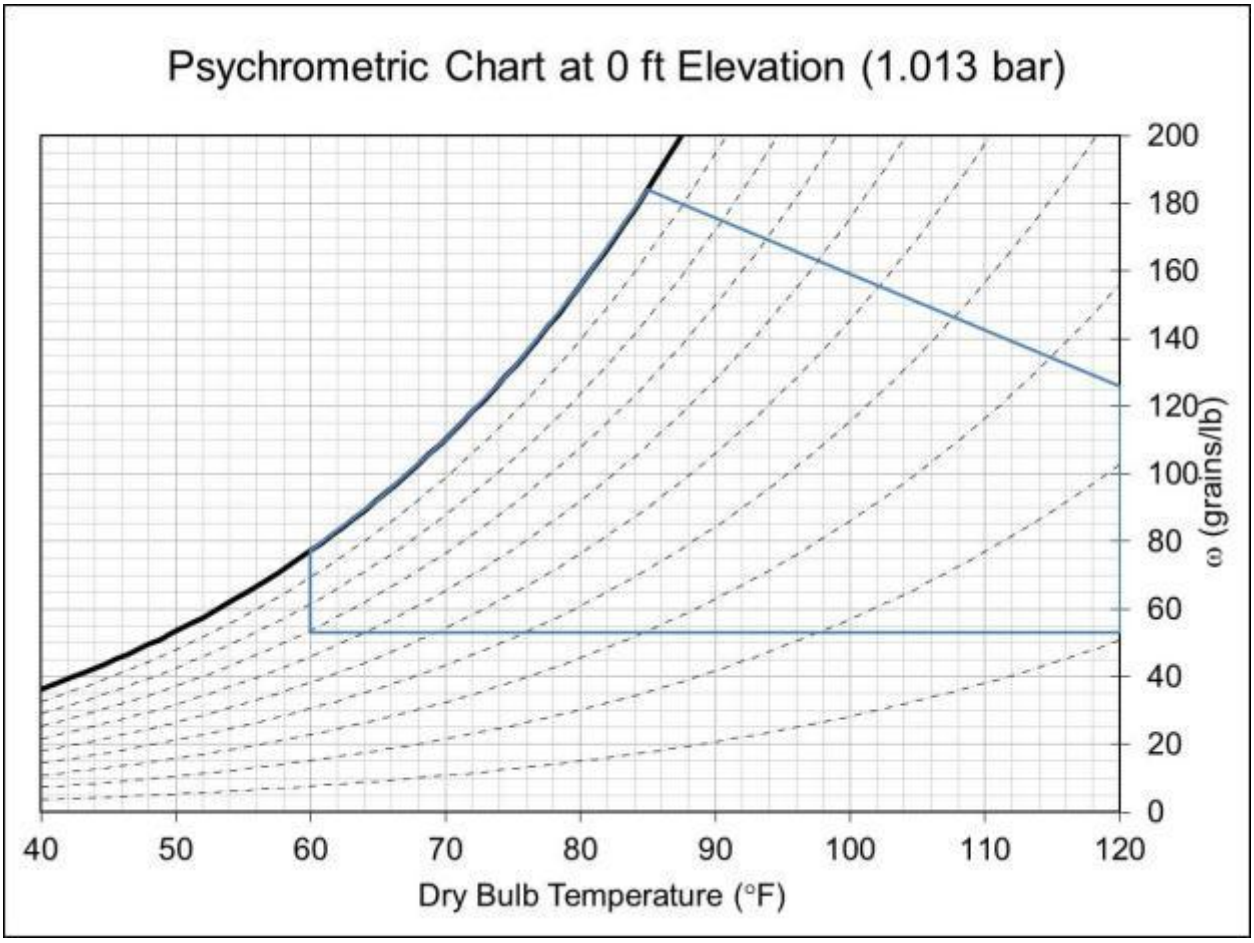

Figure 4.26: Expected outdoor air conditions during regeneration

It was assumed that the maximum possible concentration change of liquid desiccant across the regenerator would be 0.08 and that the maximum possible concentration exiting the regenerator would be 0.44, based upon data from AIL. It was also assumed that if the regenerator was operating, then it would increase the desiccant concentration as much as possible. The assumed ambient air states are humid because that is likely to be when a building will require dehumidification.

Entering Table 4.17 into Design Expert resulted in the generation of a design of experiments for indirect evaporative cooling mode. After completing the process of developing

correlations outlined by Figure 4.21, the final correlation for COP_{reg} is developed. The design of experiments results and correlation coefficient values are shown in Appendix B.

From the coefficients it was determined that ambient air conditions were insignificant input variables. Therefore, only $C_{LD,in,reg}$ and $\Delta C_{LD,reg}$ were used as input variables to the correlation. A test for correlation accuracy with only these two input variables was conducted by entering the original values for input variables from the design of experiments into the correlations. The resulting output values for COP_{reg} were then compared to those values calculated from the DEVap EES model for the same input variable values. The following statistical data outlined in Table 4.18 was realized.

Table 4.18: Regenerator Performance Correlation Accuracy

Correlation	Max Δ	Min Δ	Avg Δ	Max %Δ	Min %Δ	Avg %Δ	R^2
COP_{reg} (-)	0.02	-0.03	0.00	2.69%	-3.74%	0.19%	0.996

From Table 4.18, it can be determined that the correlation for regenerator performance is satisfactory. The correlations developed in this chapter are used in an optimization that maximizes source coefficient of performance. This optimization process is described in the following chapter.

Chapter 5: Methods – Procedure for Finding Optimal Operation

This chapter presents the methods used to determine the combinations of control variables for given combinations of independent variables that result in optimal performance using correlations developed in the previous chapter. First, the general procedure of finding optimal control variable combinations is explained. This is followed by an explanation of how the general procedure was applied to each mode of operation for DEVap. This includes the reasoning for the maximum and minimum values applied to each independent and control variable during the optimization process. Finally, an explanation of how degrees of freedom influence the optimization process is given.

5.1 General Procedure

Development of correlations allows for combinations of variables that can't be controlled, such as air states and cooling loads, to be simulated in Excel and determine the combination of control variables that results in optimal performance. The Solver tool in Excel allows for multiple cells to be changed within a range of constraint values to maximize, minimize, or set another cell's value. In this case, the constraint values are the minimum and maximum expected values for each control variable outlined earlier in the design of experiments process. Using this tool, the general procedure for determining optimal combinations of control variables is as follows:

- Set values for return and outdoor air temperature and humidity. In standard mode, set SHR as well
- Within the constrained range of values for each control variable, use Solver to determine the combination of control variables that results in maximum COP
- Within the constrained range of values for each control variable, use Solver to slightly increase the cooling load and determine the combination of control variables that results in maximum $\frac{dCOP_{source}}{dQ_{tot}}$ (which in this case is the lowest negative value, since COP decreases as cooling load increases)
- Continue until the maximum possible cooling load is achieved

The constrained values for control variables are outlined in Table 5.19.

Table 5.19: Expected Dehumidification Mode Operating Conditions

Control Variable	Range
Ratio of mixed air mass flow rate to design mass flow rate, R_{ma} ratio	0.3 – 1.0
Outdoor air fraction, OAF	0.05 – 0.60
Ratio of 1st stage exhaust air mass flow rate to design mass flow rate, R_{e1} ratio	0.3 – 1.0
Inlet liquid desiccant concentration, $C_{LD,in,DEVap}$	0.30 – 0.44

In this optimization process, the Solver tool is setting control variable values such that cooling capacity provided and source coefficient of performance adhere to restrictions. Cooling capacity increases by set increments, and the rate at which source coefficient of performance decreases is minimized. Setting independent variables to values allows for Solver to have degrees of freedom in adjusting control variable values to meet these restrictions. There may be possible scenarios where developing a near-optimal strategy removes degrees of freedom to the point where these restrictions can no longer be met.

5.2 Dehumidification Mode

For dehumidification mode, the outdoor air state is not a factor since there is no mixing with return air and no evaporative cooling in the first stage. Therefore, only the return air states likely to be encountered were simulated. It was assumed that simulating a range of 65°F - 80°F for T_{ra} and 50% - 60% for RH_{ra} would cover all likely scenarios where dehumidification mode will be used. Increments of 5°F and 5% RH were used to create a performance grid. These air states are shown in Figure 5.27.

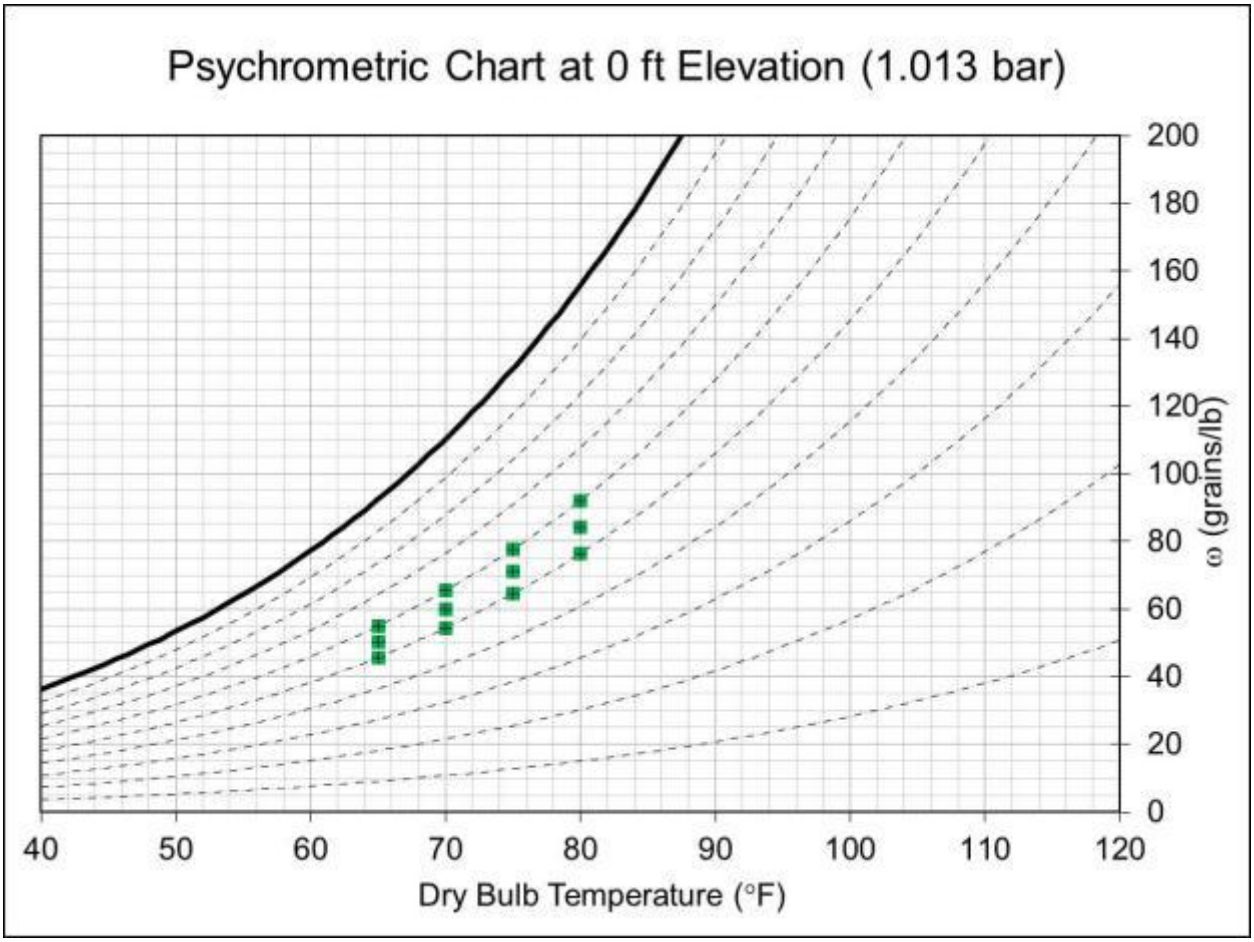

Figure 5.27: Psychrometric chart of return air states simulated in dehumidification mode

The only two control variables that apply are R_{ma} ratio and $C_{LD,in,DEVap}$. No constraints were placed on supply air conditions in order to observe "true" performance trends without control interference.

Since the purpose of dehumidification mode is to perform latent cooling, Solver was used to set values for latent cooling loads using Equation 3.4 instead of total cooling loads. In any case, the total cooling capacity provided in dehumidification mode would be essentially zero since it is a nearly adiabatic process. COP_{source} is still calculated in the same manner as shown in Equation 3.2, where Q_{tot} is replaced by Q_{lat}. Return air state will be held constant during the optimization simulation, leaving R_{ma} ratio and $C_{LD,in,DEVap}$ as correlation variables that Solver can adjust to calculate supply air state and air-side pressure drops to adhere to the restriction of minimizing decrease in COP_{source} for a given incremental increase in Q_{lat}. Therefore, two floating control variables combined with one constraint results in one degree of freedom in the optimization process for dehumidification mode.

5.3 Indirect Evaporative Cooling Mode

For IEC mode, both the outdoor and return air states are independent variables that must be set. It was assumed that simulating a range of 70°F - 80°F for T_{ra}, 25% - 55% for RH_{ra}, 60°F - 120°F for T_{oa}, and 0.0003 – 0.0100 kg/kg for ω_{oa} would cover all likely scenarios where IEC mode will be used. Increments of 5°F and 10% RH for return air states and 15°F with variable humidity ratio increments for outdoor air states were used to create a performance grid. These air states are shown in Figure 5.28.

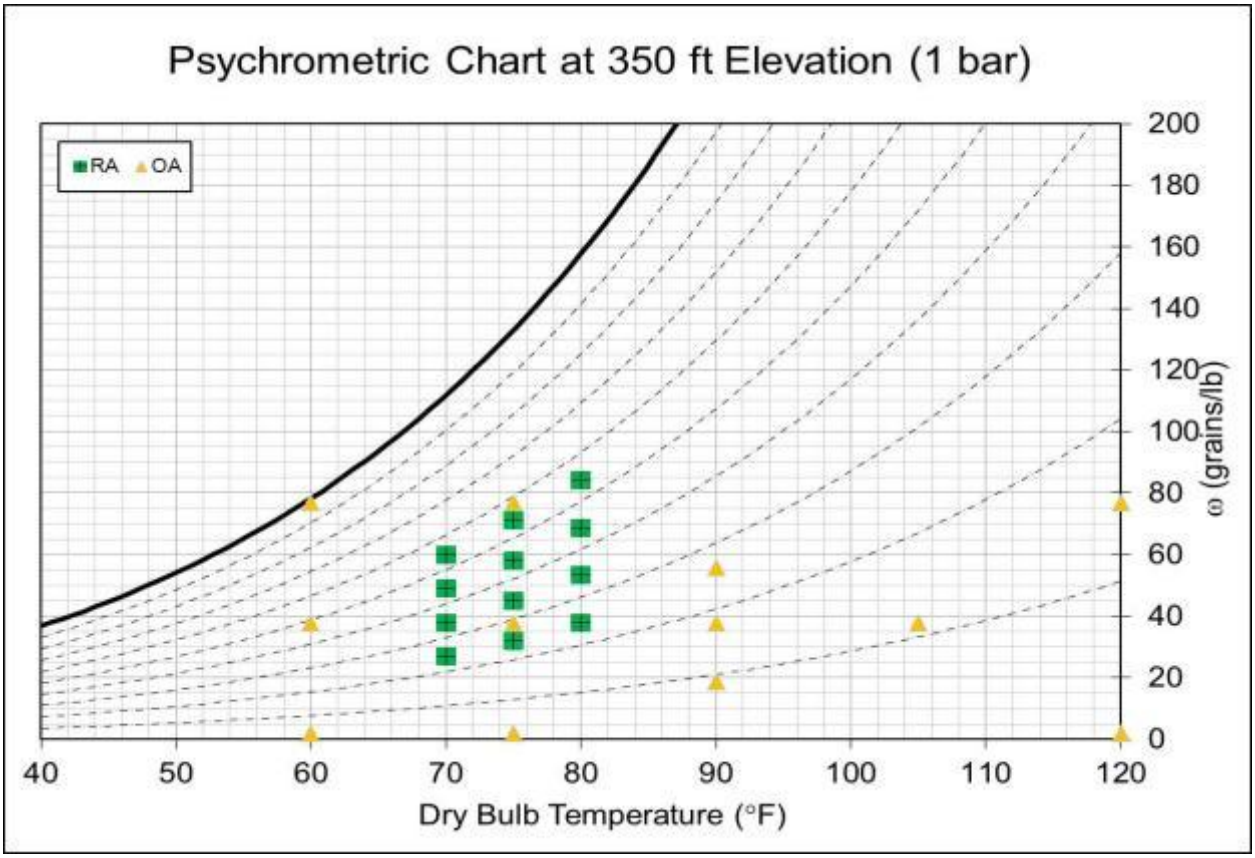

Figure 5.28: Psychrometric chart of return and outdoor air states simulated in indirect evaporative cooling mode

The control variables that apply are R_{ma} ratio, R_{e1} ratio, and OAF. No constraints were placed on supply air conditions in order to observe "true" performance trends without control interference. For this thesis, no energy penalty was applied for situations where supply air needs to be reheated before sent to the space.

Since the purpose of IEC mode is to perform sensible cooling, Solver was used to set values for sensible cooling loads using Equation 3.5 instead of total cooling loads. COP_{source} is still calculated in the same manner as shown in Equation 3.2, where Q_{tot} is replaced by Q_{sens}. Since no desiccant dehumidification occurs in this mode, no regeneration energy is required and only electricity is consumed in the form of fan energy. Since the return and outdoor air state will

be set, R_{ma} , R_{e1} ratio, and OAF are the three variables left that are inputs to correlations for both first stage and second stage processes in IEC mode. Solver can adjust these three values to calculate supply air state and air-side pressure drops to adhere to the restriction of minimizing decrease in COP_{source} for a set incremental increase in Q_{sens}. Therefore, three floating control variables combined with one constraint results in two degrees of freedom in the optimization process for IEC mode.

5.4 Standard Cooling Mode

For standard cooling mode, both the outdoor and return air states are independent variables that must be set. It was assumed that simulating a range of 70°F - 80°F for T_{ra}, 50% - 60% for RH_{ra}, 60°F - 120°F for T_{oa}, and 0.0080 – 0.0240 kg/kg for ω_{oa} with a maximum of 84°F for outdoor air wet bulb temperature would cover all likely scenarios where standard cooling mode will be used. Increments of 5°F and 5% RH for return air states and 15°F for outdoor air states were used to create a performance grid. The increments for outdoor air humidity ratio varied depending upon outdoor air temperature. These air states are shown in Figure 5.29.

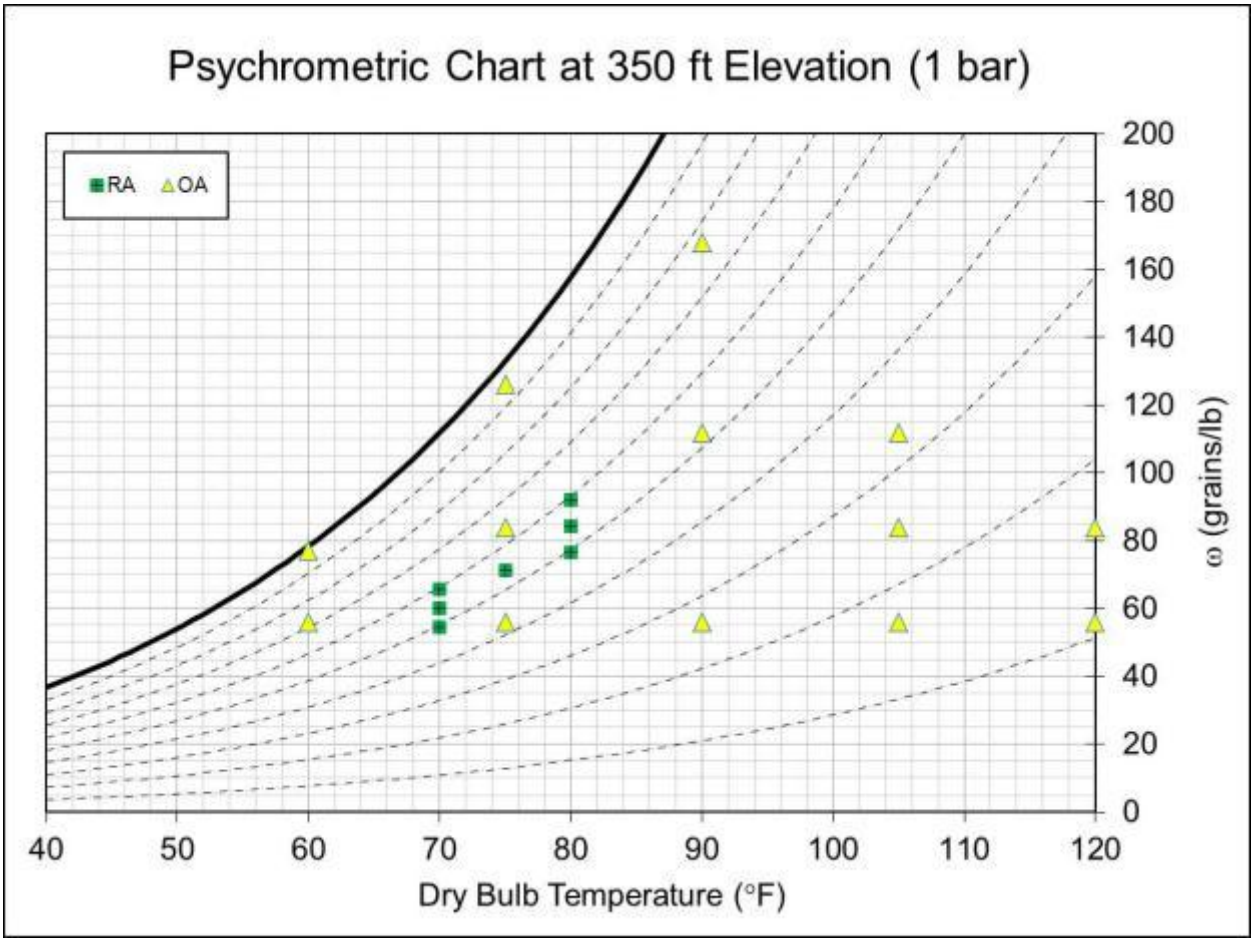

Figure 5.29: Psychrometric chart of return and outdoor air states simulated in standard cooling mode

The SHR provided by DEVap is also important and must be set as well. It was assumed that simulating a range of 0.50 – 0.80 in increments of 0.15 would compile enough information for all likely scenarios where standard cooling mode will be used. All control variables mentioned earlier apply (R_{ma} rat, R_{e1} ratio, OAF, and $C_{LD,in,DEVap}$). No constraints were placed on supply air conditions in order to observe "true" performance trends without control interference. For this thesis, no energy penalty was applied for situations where supply air needs to be reheated before sent to the space.

For standard cooling mode, Solver was used to set values for total cooling loads using Equation 3.3 and COP_{source} is calculated in the same manner as shown in Equation 3.2. Since both desiccant dehumidification and fan energy use occurs in this mode, regeneration energy and electricity are both consumed. Since the return and outdoor air state will be set, R_{ma} , R_{e1} ratio, OAF, and $C_{LD,in,DEVap}$ are the four variables left that are inputs to correlations for both first stage and second stage processes in standard mode. Solver can adjust these four values to calculate supply air state and air-side pressure drops to adhere to the restrictions of minimizing decrease in COP_{source} and supplying a given SHR value for a set incremental increase in Q_{tot}. Therefore, four floating control variables combined with two constraint results in two degrees of freedom in the optimization process for standard mode.

Chapter 6: Results and Discussion

This chapter presents some of the simulation results for optimal control of DEVap using the methodology described in Chapter 5. These results are accompanied by an explanation of how control variable behavior changes for different return and outdoor air states and cooling loads. An analysis of near-optimal control strategies that are easier to implement is also presented. The first three sections describe the control strategies developed for dehumidification mode, IEC mode, and standard mode. The final section discusses how these control strategies can be implemented.

6.1 Dehumidification Mode

Since only return air states affect performance and there are only two control variables (R_{ma} ratio and $C_{LD,in,DEVap}$) to adjust during operation in dehumidification mode, it will be easiest of the three operation modes to analyze. Any control strategies that are developed for dehumidification mode should also be useful in standard mode, since desiccant dehumidification occurs for both modes. The trends observed for optimal operation of one return air state in dehumidification mode are described first. This is followed by the sensitivity of these observed trends to changing return air state, ending with near-optimal operation strategies that were derived.

6.1.1 Optimal Trends

As explained in Section 5.1, the Solver tool in Excel was used to incrementally increase cooling load provided while maximizing COP_{source} by adjusting combinations of values for control variables. For dehumidification mode, the cooling load of interest is the latent load. It is expected that as return air becomes hotter and more humid, the latent capacity that can be provided by DEVap will increase because the dehumidification potential is greater. Since the dehumidification potential is greater, this should also translate into hotter and more humid return air states yielding a higher COP_{source} compared to colder and drier return air states when trying to provide an equal Q_{lat}.

It is expected that DEVap will operate in dehumidification mode when RH_{ra} reaches 55% and T_{ra} is below 75°F, since these are typical RH and temperature set points, respectively. An example of how optimal values for R_{ma} ratio, $C_{LD,in,DEVap}$, T_{sa}, and COP_{source} change as the latent cooling capacity increases for a typical operating condition of T_{ra} = 70°F and RH_{ra} = 55% is shown in Figure 6.30, which is referred to as a latent capacity curve for dehumidification mode. A psychrometric chart outlining supply air states during the optimal simulation for the same return air state is shown in Figure 6.31. Since there is no second stage cooling in dehumidification mode, the process air state exiting the first stage and the supply air state exiting DEVap are identical.

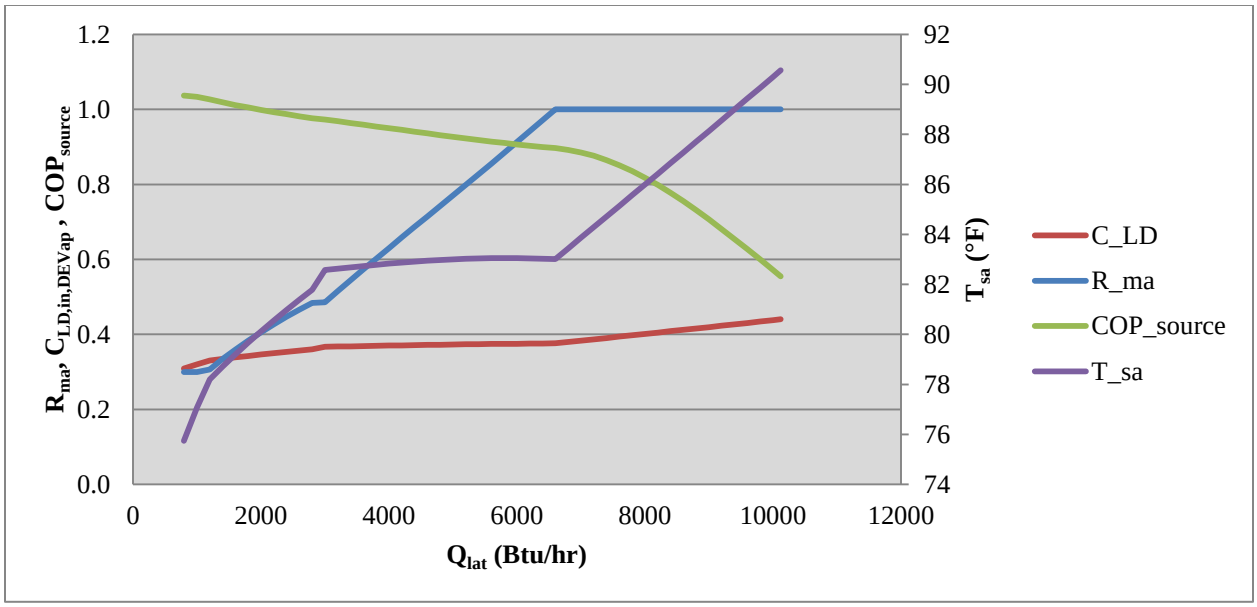

Figure 6.30: Optimal control variable trends for T_{ra} = 70°F and RH_{ra} = 55% in dehumidification mode

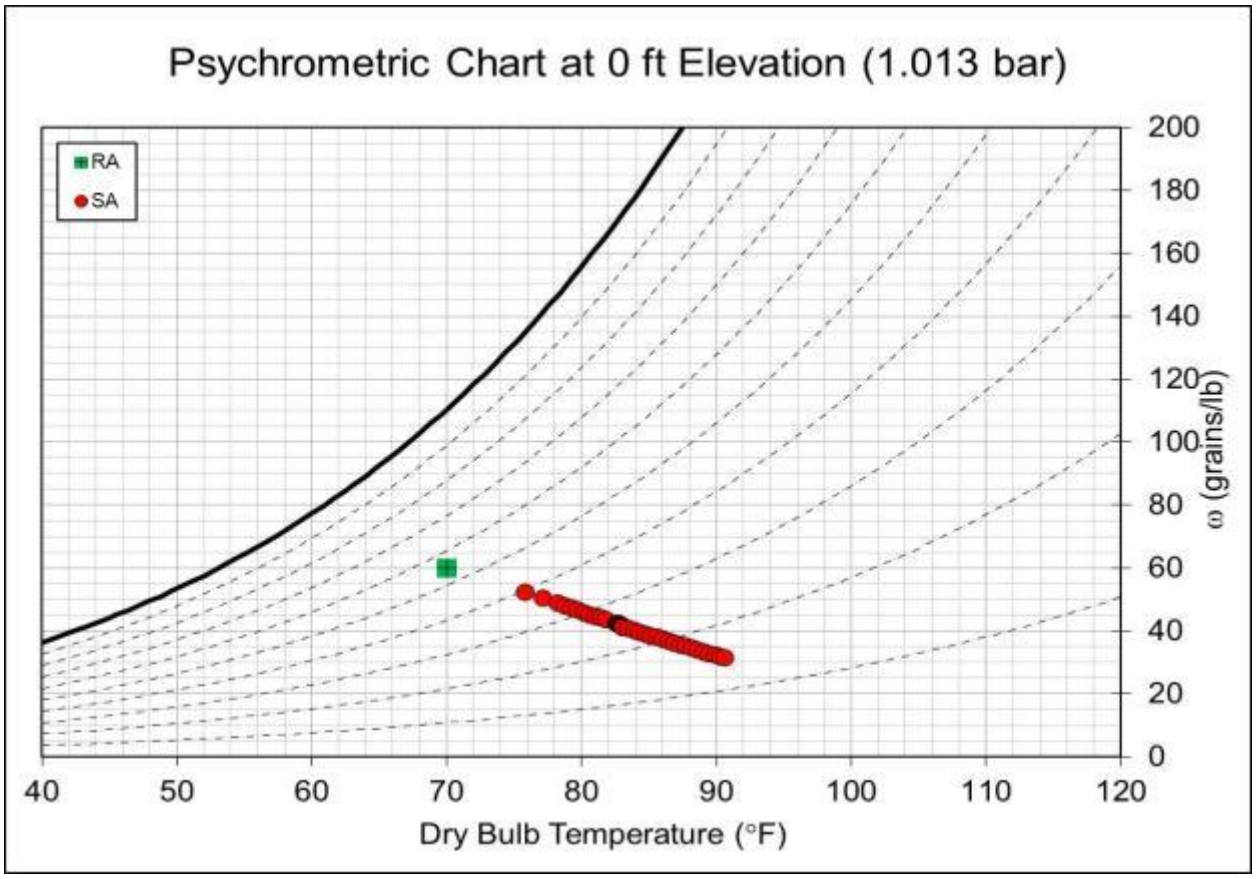

Figure 6.31: Optimal air states for T_{ra} = 70°F and RH_{ra} = 55% in dehumidification mode

In order to explain the optimal trends that occur, it is important to remember that increasing R_{ma} ratio results in more electricity consumption to power fans to blow air through DEVap at an increased rate, and increasing $C_{LD,in,DEVap}$ results in more natural gas consumption to regenerate liquid desiccant that starts at a higher concentration upon entering the regenerator. Since it is a source coefficient of performance that is maximized, and electricity consumption is associated with a larger site-to-source ratio than natural gas consumption, the optimal combination of control variables is the minimum R_{ma} ratio and the appropriate $C_{LD,in,DEVap}$ to meet the required latent load.

From Figure 6.30, it can be determined that for minimum latent capacity at the given return air state, it is most efficient to minimize R_{ma} ratio and have $C_{LD,in,DEVap}$ set to approximately 31%. $C_{LD,in,DEVap}$ is not its minimum value of 30% because the benefit of increased dehumidification potential in DEVap outweighs the negative impact of increased regeneration energy required. This minimum latent capacity corresponds to the supply air state that is closest to the return air state in Figure 6.31, since $C_{LD,in,DEVap}$ is at its lowest value, resulting in the lowest dehumidification potential during the simulation. As $C_{LD,in,DEVap}$ increases, the supply air state becomes drier and hotter in a nearly adiabatic process.

For cases where greater latent capacity is required, it is most efficient to increase $C_{LD,in,DEVap}$ as R_{ma} ratio remains 30%. It should be noted that during this trend, $C_{LD,in,DEVap}$ increases at a higher rate than at any other instance on the latent capacity curve. This rapid increase in $C_{LD,in,DEVap}$ at the beginning of the latent capacity curve corresponds to supply air states close to return air becoming rapidly hotter and drier in Figure 6.31.

This trend continues until an initial transition point is reached when $C_{LD,in,DEVap}$ reaches approximately 33%. At this point, it is most efficient to begin increasing R_{ma} ratio and keep increasing $C_{LD,in,DEVap}$, but at a slower rate than previously. This is because the benefit of increasing dehumidification potential at the same rate as previously no longer outweighs the negative impact of increasing regeneration energy input at the same rate. Instead, the benefit of increasing the flow rate of air through DEVap to increase latent capacity outweighs the negative impact of increased fan energy use. Since R_{ma} ratio begins to increase, the rate at which $C_{LD,in,DEVap}$ increases is forced to be reduced in order to meet latent loads increasing at the same increments as before. In Figure 6.31, this lower rate of increase for $C_{LD,in,DEVap}$ results in supply air states being grouped closer together than previously.

This trend continues until a second transition point is reached when $C_{LD,in,DEVap}$ reaches approximately 36.5% and R_{ma} reaches approximately 48%. At this point, R_{ma} ratio begins to increase at a slightly higher rate and $C_{LD,in,DEVap}$ increases at a very low rate. This is because $C_{LD,in,DEVap}$ has reached a value that results in the liquid desiccant exiting the regenerator at a concentration close to its maximum value of 44%. This is assuming a 2% concentration change for liquid desiccant across DEVap, resulting in an inlet concentration of 35% to the regenerator and an outlet concentration of 43% from the regenerator. Once $C_{LD,in,DEVap}$ increases past 38%, the inlet concentration to the regenerator increases past 36%, and the concentration change of liquid desiccant across the regenerator begins to decrease below 8% in order to still output desiccant at a concentration of 44%. This results in increased regenerator energy input and reduced regenerator efficiency, as shown previously in Figure 3.11. Since $C_{LD,in,DEVap}$ is almost held constant, the rate at which R_{ma} ratio increases is forced to be raised in order to meet latent

loads increasing at the same increments as before. In Figure 6.31, holding $C_{LD,in,DEVap}$ almost constant results in a black grouping of supply air states that are almost constant as well.

This trend continues until R_{ma} ratio reaches its maximum possible value of 100%. If more latent capacity is still required, the only way to provide it is to increase $C_{LD,in,DEVap}$ to its maximum value of 44%. In Figure 6.31, this increase in $C_{LD,in,DEVap}$ results in supply air states being hotter and drier, grouped apart from each other once again. It should be noted that during this final trend of the latent capacity curve, COP_{source} decreases at the highest rate. This is because the regenerator is being forced to regenerate desiccant from an increasingly higher concentration to the maximum possible concentration, resulting in the need for rapidly increasing regenerator energy input.

6.1.2 Sensitivity of Optimal Trends to Control Variables

In order to illustrate how sensitive DEVap's performance is to control variables, dehumidification mode will be used as an example due to the fact that it has less independent and control variables than the other two modes of operation. If the Solver tool was not used to solve the set of equations to maximize COP_{source}, then a grid of different combinations of R_{ma} and $C_{LD,in,DEVap}$ for a constant return air state could be simulated to determine how Q_{lat} and COP_{source} change. This is illustrated in Figure 6.32 and Figure 6.33, respectively for T_{ra} = 70°F and RH_{ra} = 55%. The bold black line indicates the optimal trends discussed previously for the same return air state.

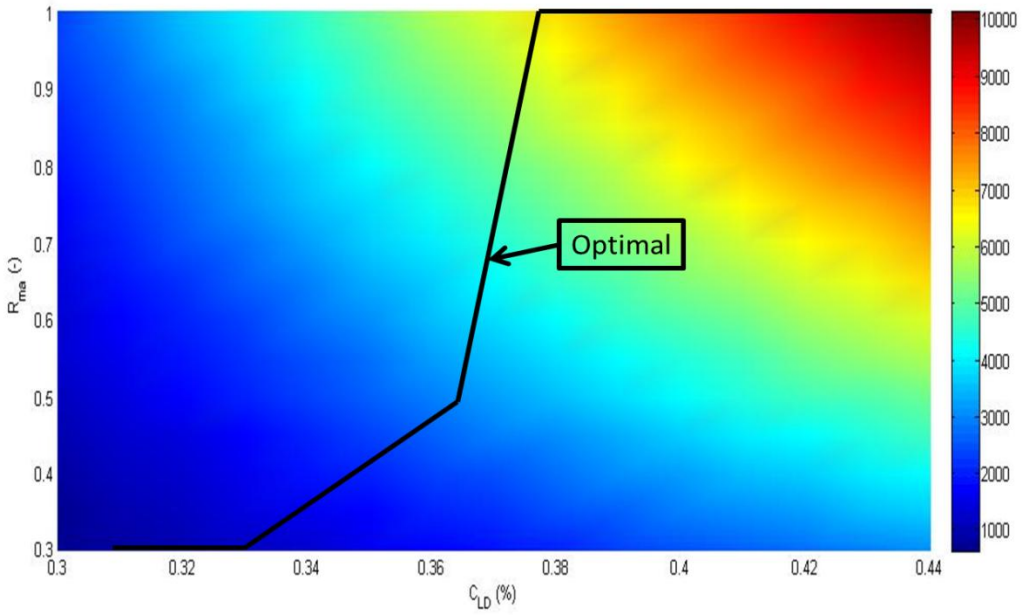

Figure 6.32: Sensitivity of Q_{lat} to R_{ma} and $C_{LD,in,DEVap}$ in dehumidification mode for T_{ra} = 70°F and RH_{ra} = 55%

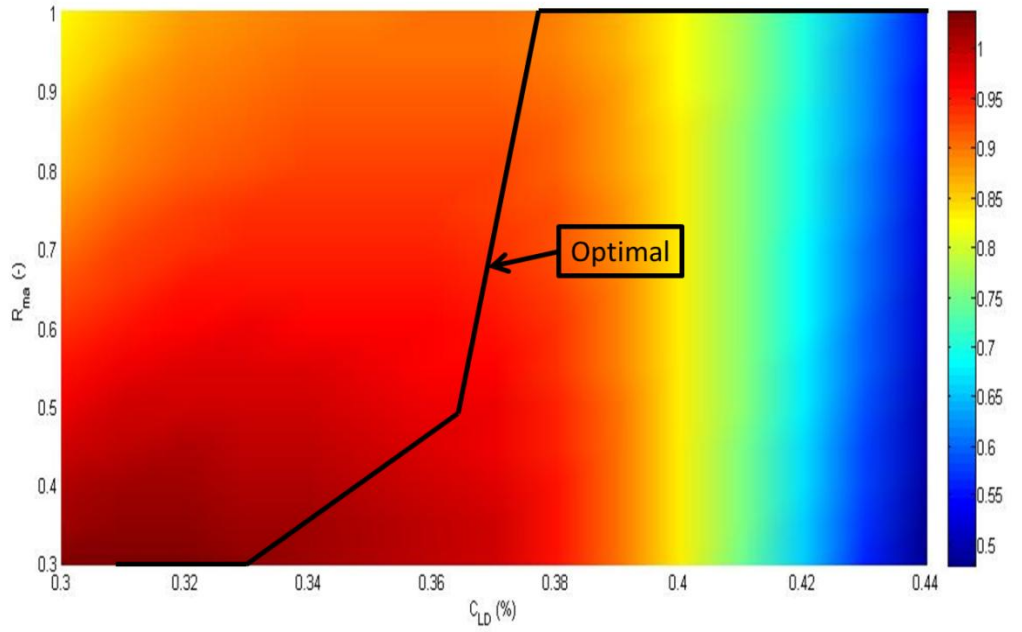

Figure 6.33: Sensitivity of COP_{source} to R_{ma} and $C_{LD,in,DEVap}$ in dehumidification mode for T_{ra} = 70°F and RH_{ra} = 55%

From Figure 6.32, it can be determined that Q_{lat} increases in an approximately linear fashion as R_{ma} and $C_{LD,in,DEVap}$ increase. This indicates that Q_{lat} is approximately equally sensitive to both control variables. From Figure 6.33, it can be determined that COP_{source} is matginally more sensitive to R_{ma} at $C_{LD,in,DEVap}$ values below approximately 0.37. At $C_{LD,in,DEVap}$ values above 0.37, COP_{source} is almost insensitive to changes in R_{ma}. This reiterates the point made previously that the COP of the regeneration process significantly decreases once $C_{LD,in,DEVap}$ increases past 37%, which in turn makes DEVap's performance sensitive to $C_{LD,in,DEVap}$ when trying to meet high latent loads that require higher liquid desiccant concentrations. At lower Q_{lat} values, straying from the optimal trend towards different R_{ma} and $C_{LD,in,DEVap}$ values has a small impact. However, once Q_{lat} surpasses approximately 6,500 Btu/hr, straying from the optimal trend towards different $C_{LD,in,DEVap}$ values specifically does have a significant impact on DEVap's performance in dehumidification mode. This indicates that in the near-optimal strategy, it is more important to mimic optimal $C_{LD,in,DEVap}$ trends than optimal R_{ma} trends at higher Q_{lat} values.

6.1.3 Sensitivity of Optimal Trends to Return Air State

To determine if these trends are true for other return air states, a latent capacity curve for each control variable can be plotted for multiple return air states. Optimal trends for R_{ma} ratio, $C_{LD,in,DEVap}$, and COP_{source} for all simulated return air states expressed as T_{ra}/ RH_{ra} are shown in Figure 6.34, Figure 6.35, and Figure 6.36, respectively.

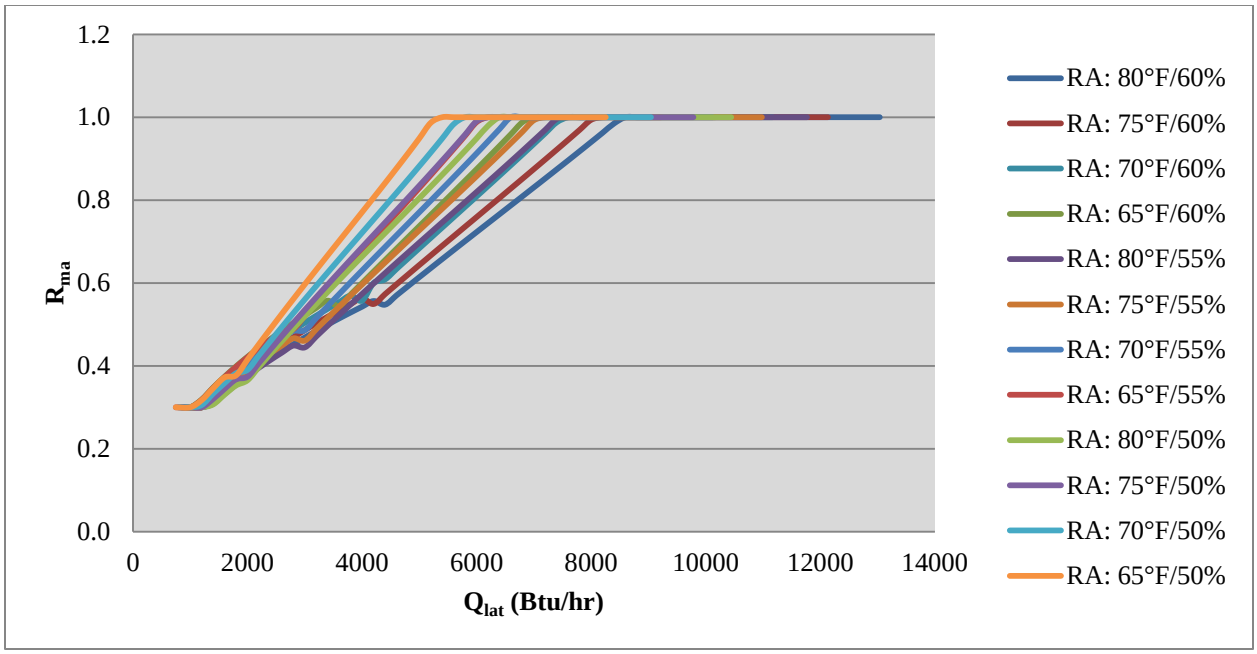

Figure 6.34: Optimal trends for R_{ma} ratio in dehumidification mode for variable return air states

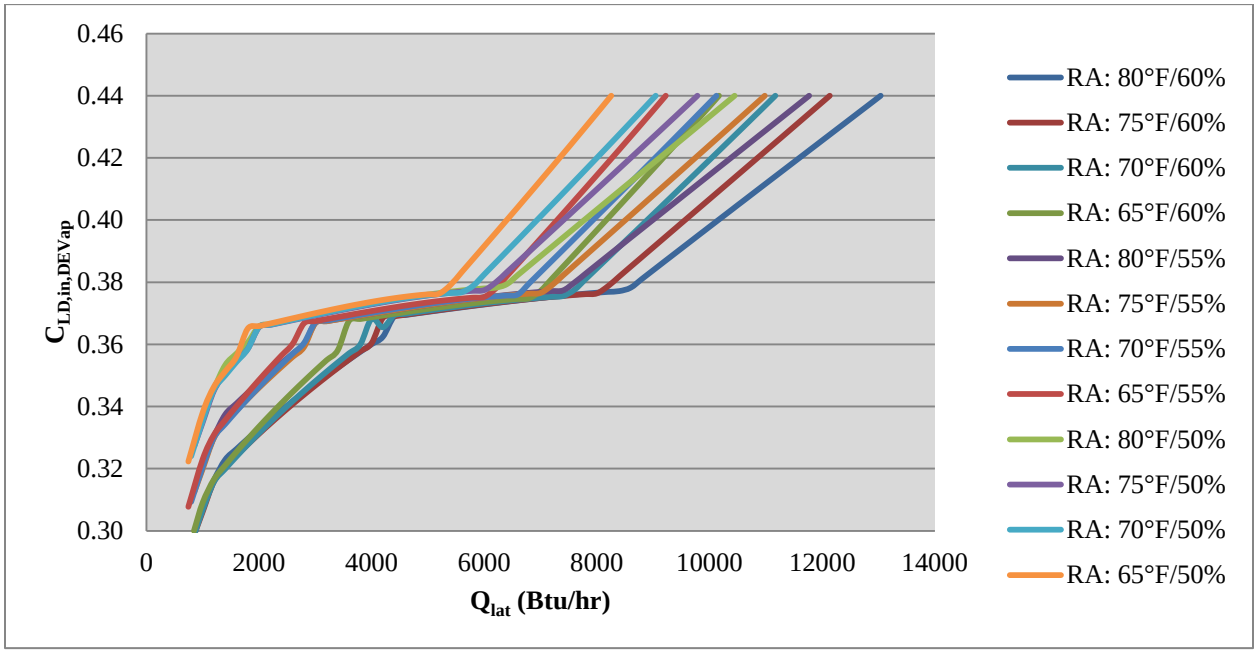

Figure 6.35: Optimal trends for $C_{LD,in,DEVap}$ in dehumidification mode for variable return air states

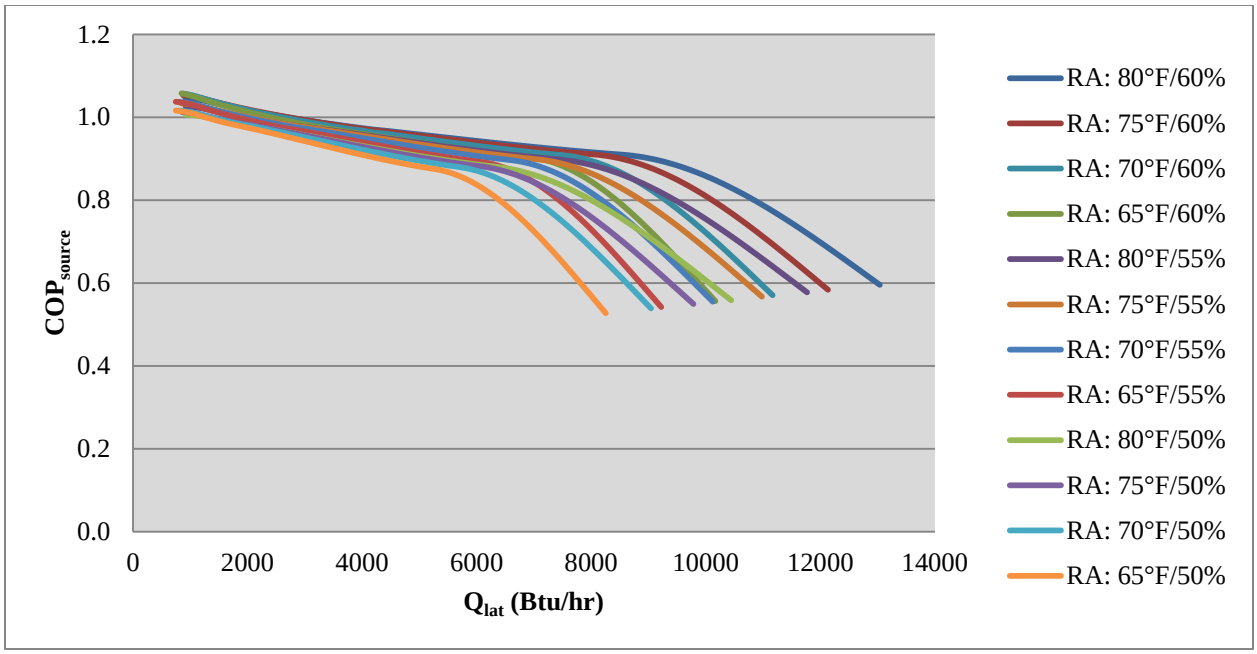

Figure 6.36: Optimal trends for COP_{source} in dehumidification mode for variable return air states

From Figure 6.36, it can be determined that both assumptions of increased latent capacity and COP_{source} for hotter and more humid return air states are valid. From Figure 6.34 and Figure 6.35, the trends discussed previously are also proved to apply to all return air states. There is a slight change in the initial value for $C_{LD,in,DEVap}$, but R_{ma} ratio always increases from 30% at an initial transition point to 100% with a slight change in slope at a second transition point, where $C_{LD,in,DEVap}$ is approximately 36.5% for all return air states. When R_{ma} ratio reaches 100%, $C_{LD,in,DEVap}$ is approximately 37.5% for all return air states. It should be noted that for all return air states the maximum latent capacity is always achieved with the combination of a R_{ma} ratio of 100% and $C_{LD,in,DEVap}$ of 44%.

After examining Figure 6.34 and Figure 6.35, it can be determined that there are three distinct groups of secondary transition points where R_{ma} ratio begins to increase at a higher rate and $C_{LD,in,DEVap}$ reaches approximately 36.5% and begins to very slowly increase. Each of these groups has four curves associated with them, organized according to RH_{ra}. The group with

secondary transition points occurring for the lowest Q_{lat} values is for RH_{ra} = 50% and the group with transition points occurring for the highest Q_{lat} values is for RH_{ra} = 60%. This is explained by the fact that for a given latent capacity, return air states with a lower relative humidity require a greater $C_{LD,in,DEVap}$ value in order to maintain the same dehumidification potential. This explains why $C_{LD,in,DEVap}$ is initially at higher values at the left end of the latent capacity curve and meets the secondary transition point at a value of 36.5% at lower Q_{lat} values for drier return air states. This behavior also occurs as T_{ra} increases, but to a smaller effect. This is because dehumidification potential lines for liquid desiccant are close to lines of constant relative humidity. Therefore, as return air states shift towards higher temperatures along a constant relative humidity, only a small increase in dehumidification potential is required.

6.1.4 Near-optimal Strategy

For near-optimal strategies in general, we try to simplify optimal trends while remaining close to optimal results. This is especially true for instances where greater cooling capacities are required, since devices inherently operate at lower efficiency values under higher loads.

Using this logic, the initial optimal trend of holding R_{ma} ratio at its minimum value while increasing $C_{LD,in,DEVap}$ can be discarded in the near-optimal strategy. This is because this trend occurs for the first 10% - 15% of the latent capacity possible for each return air state. The portion of each latent capacity curve where R_{ma} ratio increases from its minimum 30% to 100% encompasses 15% - 60% of the latent capacity possible for each return air state, therefore making it important to capture in the near-optimal strategy. The final 60% - 100% of each latent capacity curve is simple to adopt in a near-optimal strategy: once R_{ma} ratio has reached 100%, linearly increase $C_{LD,in,DEVap}$ to meet greater latent cooling loads until $C_{LD,in,DEVap}$ reaches 44%.

The portion of the near-optimal strategy that must be simplified is the process of increasing both R_{ma} ratio and $C_{LD,in,DEVap}$. The transition point where R_{ma} ratio increases at a higher rate and $C_{LD,in,DEVap}$ increases at a very low rate shifts depending largely upon RH_{ra}. An ideal approach would be to avoid having a transition point at all, and just maintain one strategy to apply to $C_{LD,in,DEVap}$ while R_{ma} ratio linearly "ramps" from 30% to 100%. Since $C_{LD,in,DEVap}$ only increases from slightly less than 37% when the secondary transition point is reached to slightly greater than 37% when R_{ma} ratio reaches 100%, holding $C_{LD,in,DEVap}$ at a constant value of 37% while R_{ma} ratio linearly ramps from 30% to 100% is sensible. Since $C_{LD,in,DEVap}$ is in the range of 32% - 36% for lower Q_{lat} values, there will be greater variation from optimal trends for these scenarios. However, it is more important to mimic optimal trends at higher cooling capacities, as stated earlier. Using this logic, the near-optimal strategy for dehumidification mode is outlined as follows:

- Initially set R_{ma} ratio to 30% and $C_{LD,in,DEVap}$ to 37%
- If greater latent capacity is required, linearly ramp R_{ma} to 100%
- If greater latent capacity is still required once R_{ma} ratio reaches 100%, linearly increase $C_{LD,in,DEVap}$ to 44%

This near-optimal strategy for dehumidification mode is illustrated in Figure 6.37 and Figure 6.38.

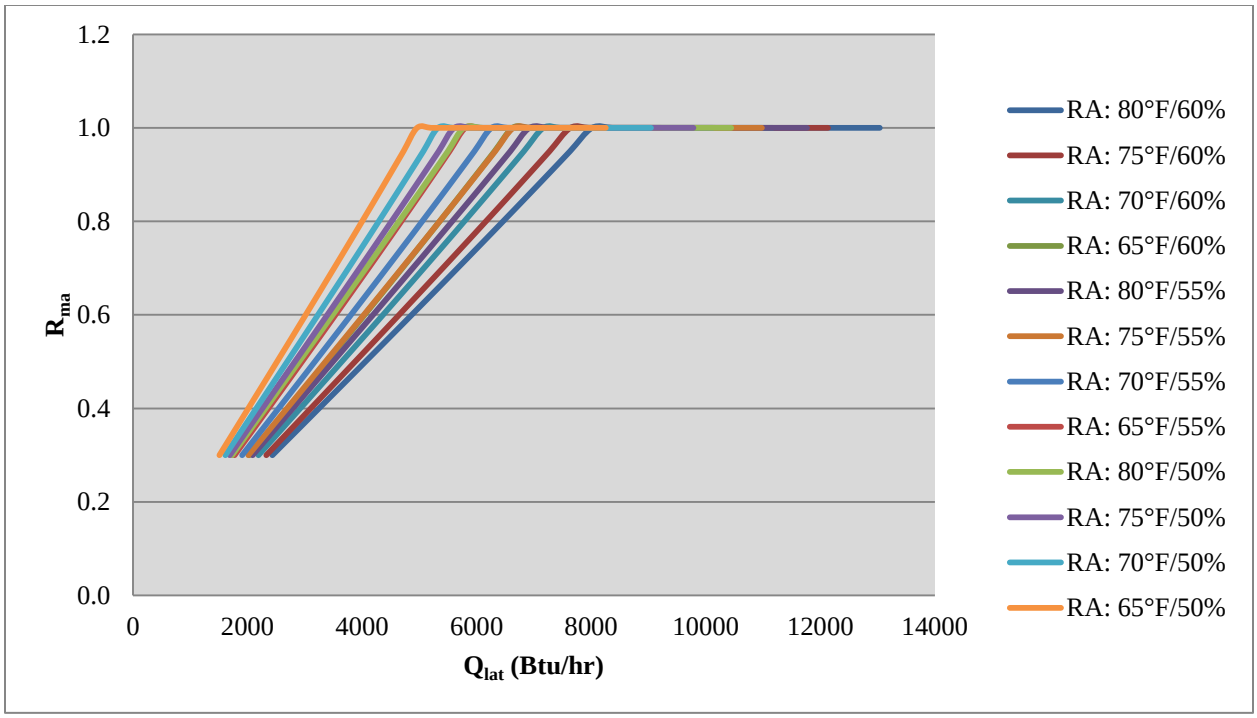

Figure 6.37: Near-optimal trends for R_{ma} ratio in dehumidification mode for variable return air states

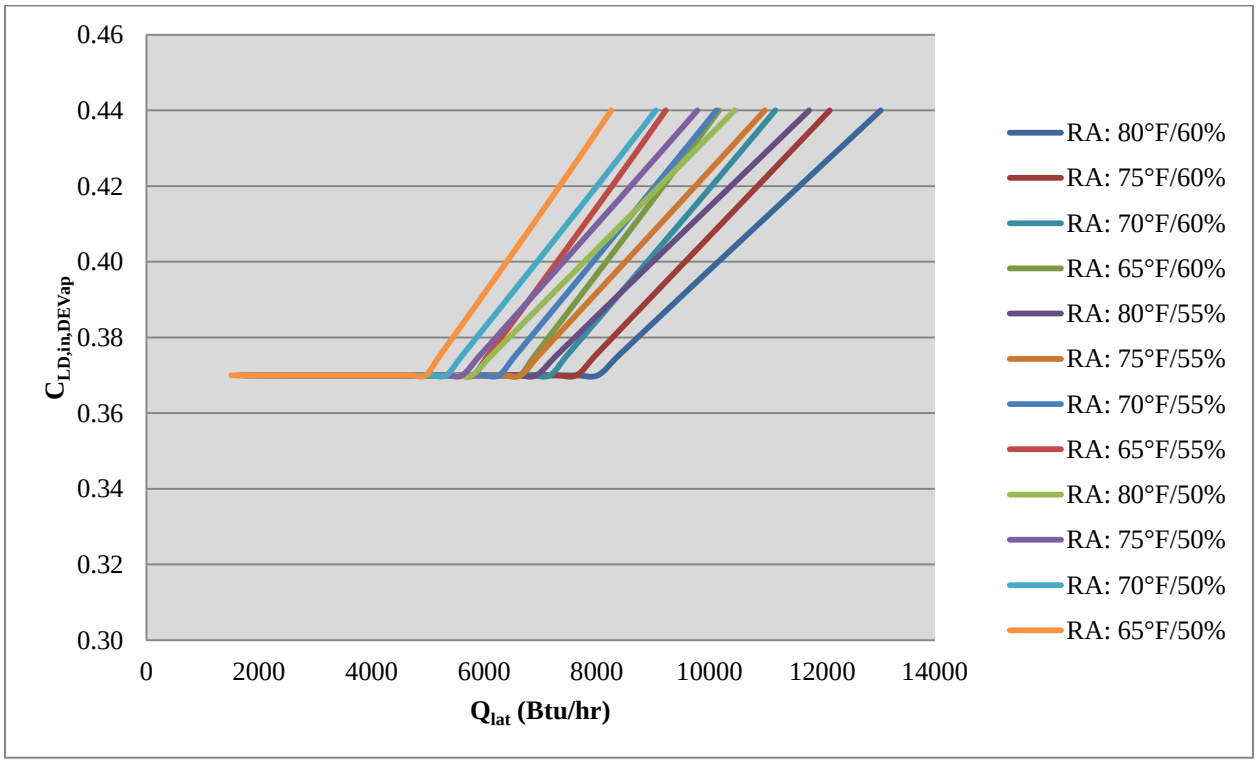

Figure 6.38: Near-optimal trends for $C_{LD,in,DEVap}$ in dehumidification mode for variable return air states

6.1.5 Analysis of Near-optimal Performance

If these near-optimal trends are applied to R_{ma} ratio and $C_{LD,in,DEVap}$ for the same return air states previously simulated, then the resulting performance is nearly identical to optimal performance. A COP_{source} comparison between the optimal simulation and near-optimal strategy for the typical operating condition of T_{ra} = 70°F and RH_{ra} = 55% is shown in Figure 6.39.

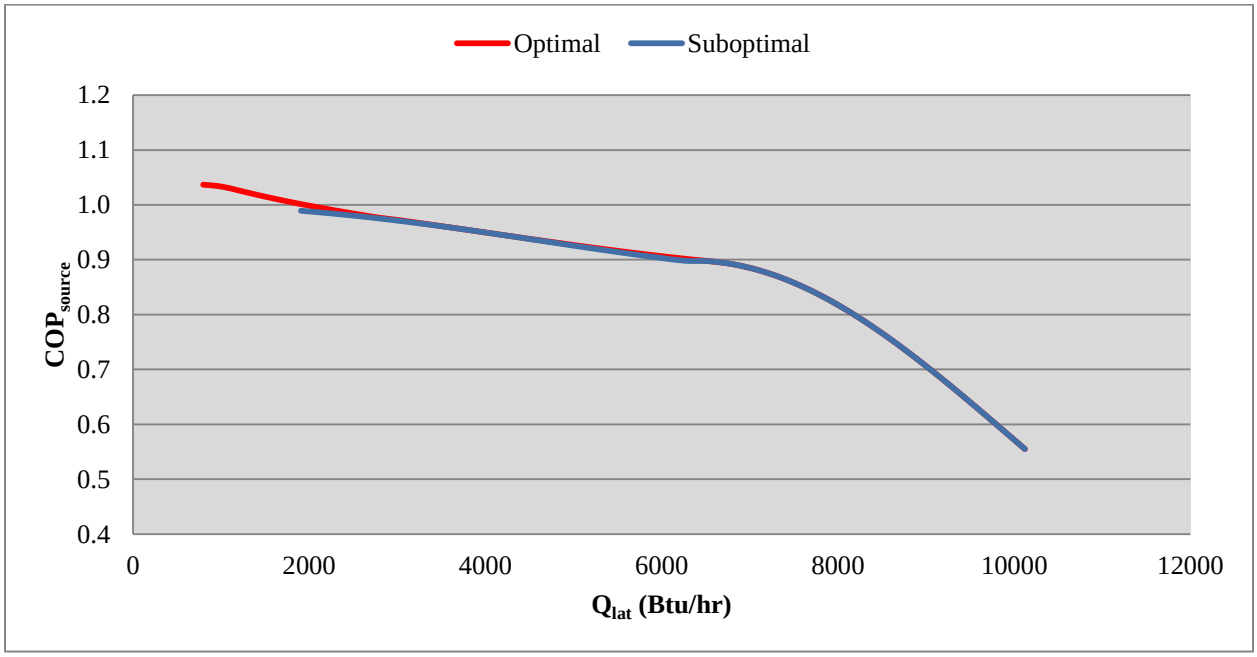

Figure 6.39: Comparison of COP_{source} for optimal and near-optimal trends in dehumidification mode for typical operating condition (T_{ra} = 70°F and RH_{ra} = 55%)

From Figure 6.39, it can be determined that for $Q_{lat,norm}$ ranging from approximately 30% to 100%, the near-optimal strategy defined previously for dehumidification mode results in nearly identical performance compared to the optimal trends. The portion of the latent capacity curve where the near-optimal strategy yields reduced performance is for $Q_{lat,norm}$ ranging from

approximately 20% to 30%, with the largest performance penalty occurring at the minimum $Q_{lat,norm}$. The largest difference in COP_{source} between the optimal simulation and near-optimal strategy occurs for all return air states at the minimum latent capacity provided by the near-optimal strategy, where $Q_{lat,norm}$ is approximately 20%. For the typical operating conditions of T_{ra} = 70°F and RH_{ra} = 55%, the COP_{source} difference at this latent capacity is still only 1.1%. The largest COP_{source} differential is 1.9% for T_{ra} = 70°F and RH_{ra} = 60%, and the least COP_{source} differential is 0.3% for T_{ra} = 80°F and RH_{ra} = 50%. This indicates that the near-optimal strategy for dehumidification mode is more than satisfactory.

It should be noted that by applying the near-optimal strategy, an initial portion of the latent capacity curve for $Q_{lat,norm}$ ranging from approximately 10% to 20% that was met in the optimal simulation is no longer met. This is because the near-optimal strategy has an initial $C_{LD,in,DEVap}$ value of 37% instead of 32% when R_{ma} ratio is initially 30% before increasing, thereby providing a greater latent capacity. If a latent capacity lower than the minimum latent capacity provided by the near-optimal strategy is required, then DEVap will have to cycle instead of operate continuously.

6.2 Indirect Evaporative Cooling Mode

For IEC mode, both return and outdoor air states affect performance and the three control variables of interest are R_{ma} ratio, R_{e1} ratio, and OAF. Any control strategies that are developed for IEC mode should also be useful in developing strategies in standard mode, since sensible cooling occurs for both modes. The trends observed for optimal operation of IEC mode are

described first, followed by the near-optimal operation strategies derived from those optimal trends.

6.2.1 Optimal Trends

As explained in Section 5.1, the Solver tool in Excel was used to incrementally increase cooling load provided while maximizing COP_{source} by adjusting combinations of values for control variables. For IEC mode, the cooling load of interest is the sensible load. It is expected that as both return and outdoor air become hotter and drier, the sensible capacity that can be provided by DEVap will increase because there is greater potential to sensibly cool from a hotter and drier mixed air state towards the saturation line on a psychrometric chart. Since the cooling potential is greater, this should also translate into hotter and drier return and outdoor air states yielding a higher COP_{source} compared to colder and more humid return and outdoor air states when trying to provide an equal Q_{sens}.

It is expected that DEVap would operate in IEC mode when RH_{ra} is below 55% and T_{ra} reaches 75°F, since these are typical RH and temperature set points, respectively. An example of how optimal values for R_{ma} ratio, R_{e1} ratio, OAF, $T_{pa,1}$, T_{sa}, and COP_{source} change as the sensible cooling capacity increases for a typical operating condition of T_{ra} = 75°F, RH_{ra} = 45%, T_{oa} = 90°F, and ω_{oa} = 0.0054 kg/kg is shown in Figure 6.40, which is referred to as a sensible capacity curve for IEC mode. A psychrometric chart outlining all process air states during the optimal simulation for the same combination of return and outdoor air state is shown in Figure 6.41.

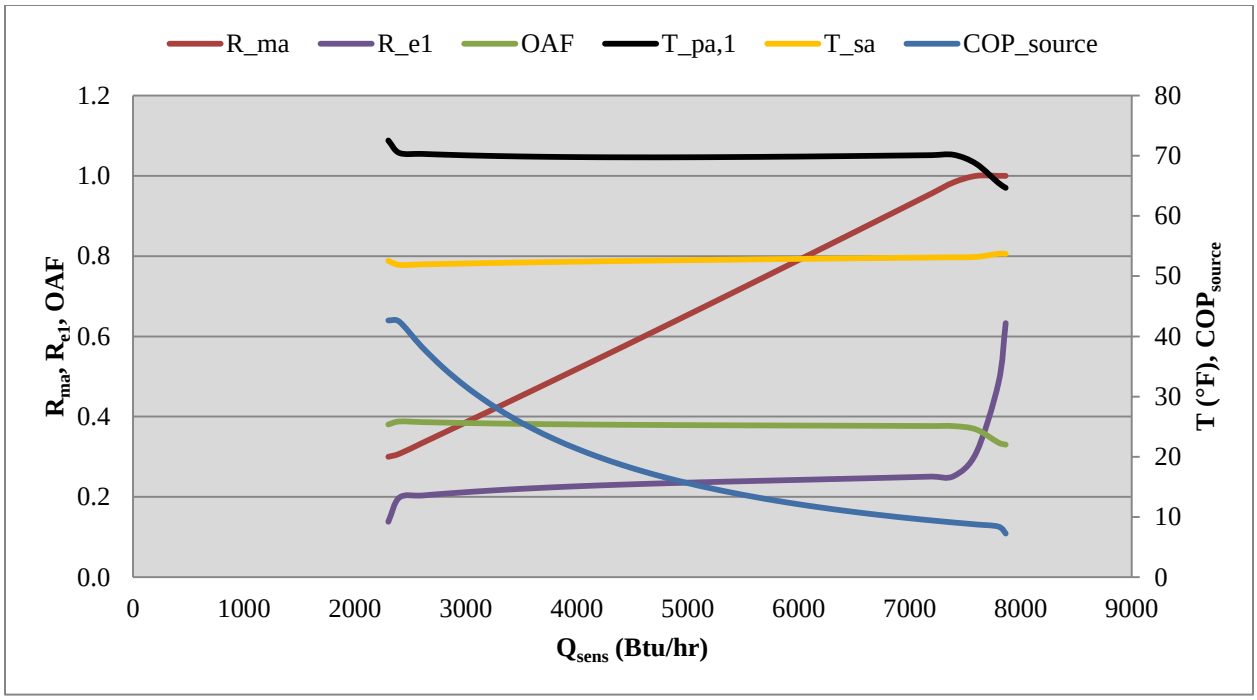

Figure 6.40: Optimal control variable trends for T_{ra} = 75°F, RH_{ra} = 45%, T_{oa} = 90°F, and ω_{oa} = 0.0054 kg/kg in IEC mode

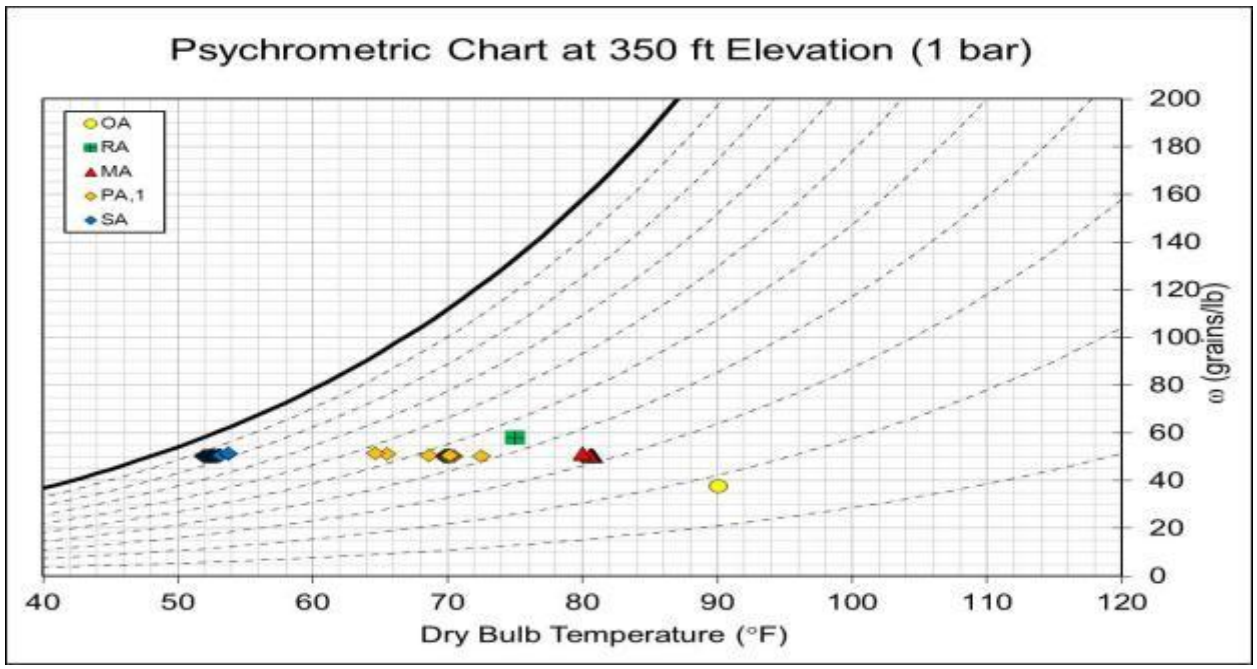

Figure 6.41: Optimal air states for T_{ra} = 75°F, RH_{ra} = 45%, T_{oa} = 90°F, and ω_{oa} = 0.0054 kg/kg in IEC mode

From Figure 6.40, it can be determined that for minimum sensible capacity at the given return and outdoor air states, it is most efficient to minimize R_{ma} ratio while setting R_{e1} ratio to approximately 14% and OAF to approximately 38% . OAF is not set to a small value because it is better to use second stage cooling that is in a counter flow arrangement and uses air that has been previously cooled as an evaporative sink compared to first stage cooling that is in a less efficient cross flow arrangement and using relatively hot outdoor air as an evaporative sink. In Figure 6.41, this minimum sensible capacity provided is shown as the combination of a mixed air state that is grouped with the majority of other mixed air states, the hottest process air exiting the first stage, and a supply air state that is grouped with the majority of other supply air states. The mixed air state is almost identical throughout this simulation because the OAF is relatively constant throughout the sensible capacity curve. The process air exiting the first stage is hottest because R_{e1} ratio is the lowest for minimum sensible capacity at the left end of the sensible capacity curve. Since OAF is relatively constant, the humidity of mixed air entering DEVap is relatively constant as well, so the cooling potential in the second stage is dependent upon $T_{pa,1}$.

For cases where greater sensible capacity is required, it is most efficient to rapidly increase R_{e1} ratio and very slightly increase OAF as R_{ma} ratio remains at its minimum value of 30%. This is because the benefit of increasing the flow rate of dry outdoor air used as an evaporative sink in first stage cooling outweighs the benefit of increasing the flow rate of process air being cooled through DEVap. OAF remains relatively constant because an optimal balance between the mixed air state entering DEVap, amount of second stage cooling provided, and amount of supply air siphoned off to provide that second stage cooling has been attained.

This trend of rapidly increasing R_{e1} ratio and very slightly increasing OAF while holding R_{ma} ratio to its minimum continues for a short period until R_{e1} ratio reaches approximately 20%.

At this initial transition point, both R_{e1} ratio and OAF are held relatively constant while R_{ma} ratio linearly ramps from 30% to 100%. This is because the benefit of increasing the flow rate of process air being cooled through DEVap outweighs the benefit of increasing the flow rate of dry outdoor air used as an evaporative sink in first stage cooling. R_{e1} ratio stops increasing at a low value of 20% because even though the outdoor air is dry, it is also hot, making first stage cooling less effective. In Figure 6.41, the different air states associated with this ramping R_{ma} ratio trend are grouped together. The mixed air states are grouped together because OAF is almost constant. Since R_{e1} ratio is also almost constant, the amount of cooling provided in the first stage remains the same, so process air states exiting the first stage are grouped together. Since OAF is constant, this also means that the amount of cooling provided in the second stage remains the same as well, so supply air states exiting DEVap are grouped together. It should be noted that this trend of increasing R_{ma} ratio while holding R_{e1} ratio and OAF relatively constant occupies the majority of the sensible capacity curve.

This trend of ramping R_{ma} ratio while holding R_{e1} ratio and OAF almost constant continues until R_{ma} ratio reaches 100%. If more sensible capacity is still required, both R_{e1} ratio and OAF can still be adjusted, and the most efficient method to do so depends upon the combination of return and outdoor air states. For this specific combination of return and outdoor air states, it is most efficient to rapidly increase R_{e1} ratio and slowly decrease OAF until R_{ma} ratio reaches approximately 65% and OAF reaches approximately 34%. R_{e1} ratio increases because the benefit of increasing the flow rate of dry outdoor air used as an evaporative sink in first stage cooling outweighs the negative impact of increasing fan energy use. OAF decreases because R_{ma} ratio has reached its maximum value, so the only way to provide more sensible capacity is to begin siphoning off less supply air. In Figure 6.41, this final trend is shown by the air states that

are most humid, since OAF has decreased to its lowest value throughout the sensible capacity curve. Since R_{e1} ratio has increased to its highest value throughout the sensible capacity curve, the process air states exiting the first stage are increasingly colder than in previous trends. Supply air states become increasingly hotter because OAF is decreasing, resulting in less counter flow second stage cooling that is more efficient than cross flow first stage cooling.

6.2.2 Sensitivity of Optimal Trends to Return Air State

To determine if these trends are true for other combinations of return and outdoor air states, a sensible capacity curve for each control variable is be plotted. First the impacts of adjusting return air states for a constant outdoor air state are analyzed. Optimal trends for R_{ma} ratio, R_{e1} ratio, OAF, and COP_{source} for T_{oa} = 90°F and ω_{oa} = 0.0054 under all simulated return air states expressed as T_{ra}/ RH_{ra} are shown in Figure 6.42 through **Error! Reference source not found.**.

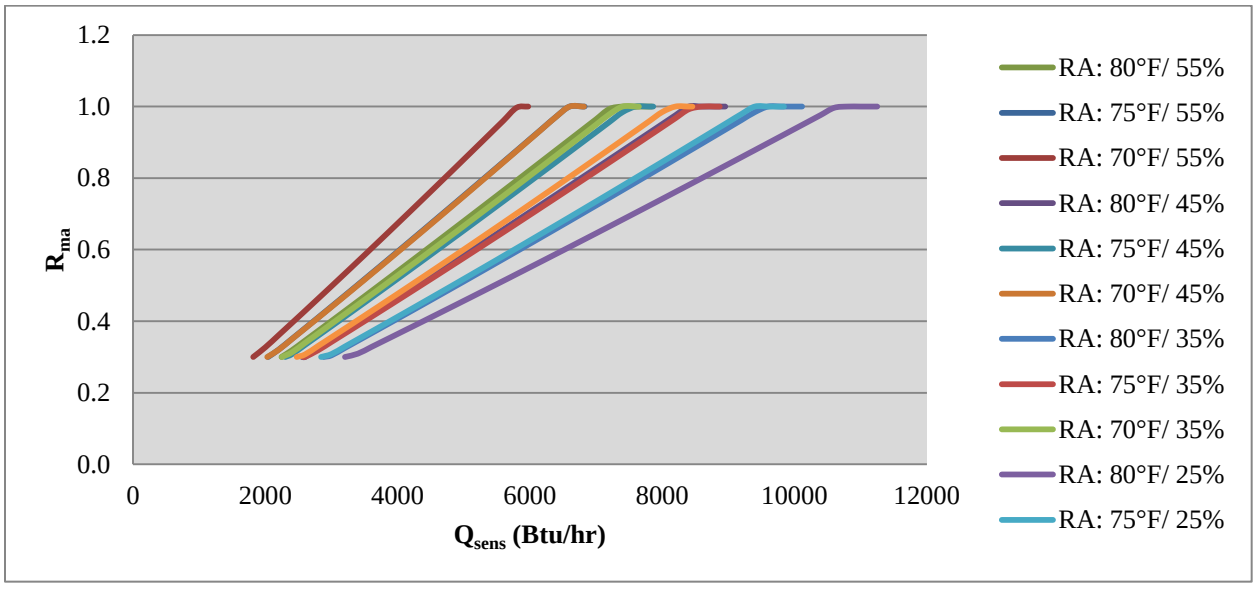

Figure 6.42: Optimal R_{ma} ratio trends in IEC mode for T_{oa} = 90°F and ω_{oa} = 0.0054 kg/kg at variable return air states

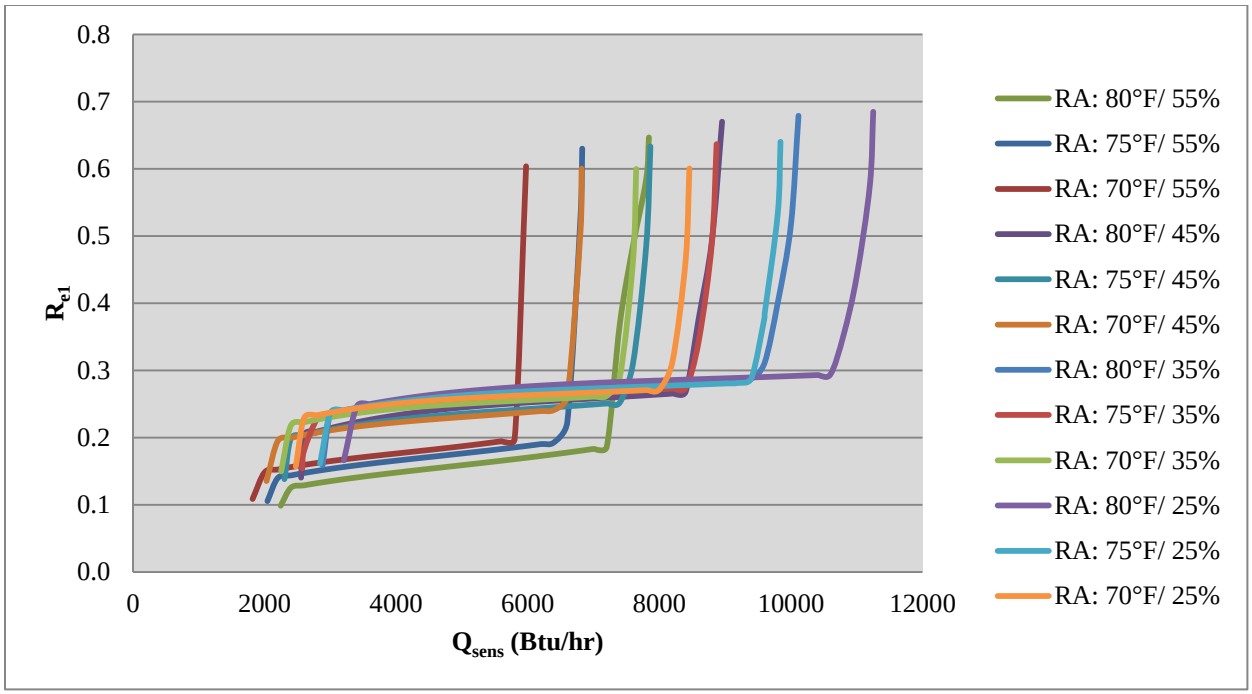

Figure 6.43: Optimal R_{e1} ratio trends in IEC mode for T_{oa} = 90°F and ω_{oa} = 0.0054 kg/kg at variable return air states

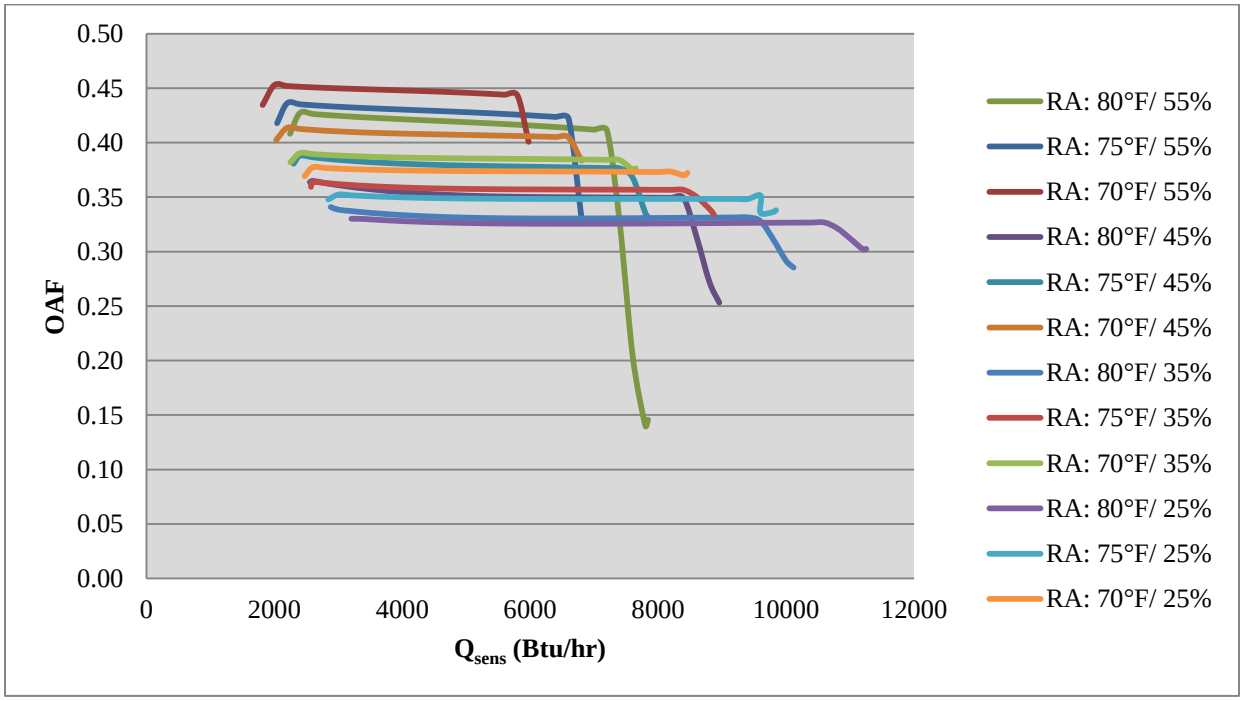

Figure 6.44: Optimal OAF trends in IEC mode for T_{oa} = 90°F and ω_{oa} = 0.0054 kg/kg at variable return air states

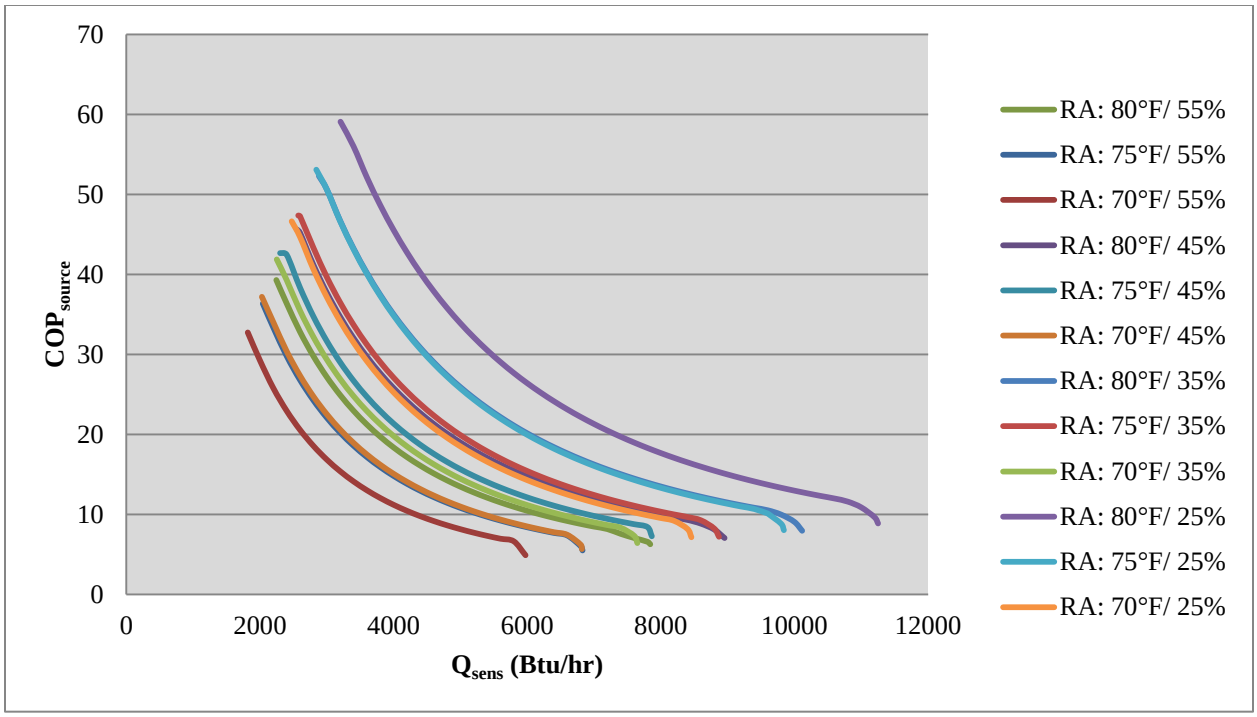

Figure 6.45: Optimal COP_{source} trends in IEC mode for T_{oa} = 90°F and ω_{oa} = 0.0054 kg/kg at variable return air states

From **Error! Reference source not found.**, it can be determined that the assumption of ncreased Q_{sens} and COP_{source} for hotter and drier return air states is correct. From examining **Error! Reference source not found.**, it can be determined that the trend of linearly ramping R_{ma} atio from 30% to 100% is applicable to all return air states. Some return air states have a slightly longer region where R_{ma} ratio is pegged at 100%, but the majority of the sensible capacity curve for each return air state is occupied by R_{ma} ratio linearly ramping from 30% to 100% and the other two control variables remaining relatively constant.

Both Figure 6.43 and Figure 6.44 should be examined together, since trends observed for R_{e1} ratio and OAF are a result of their being intricately linked. From Figure 6.43 it is deduced that all three trends in R_{e1} ratio discussed earlier (rapidly increasing R_{e1} ratio initially, then very slowly increasing R_{e1} ratio while R_{ma} r ramps from 30% to 100%, then again rapidly increasing

R_{e1} ratio) holds true for all return air states. From Figure 6.44, it is deduced that all three trends in OAF discussed earlier (very slowly increasing OAF initially, then holding OAF relatively constant while R_{ma} ratio ramps from 30% to 100%, then decreasing OAF) holds true for all return air states. It should be noted that a clear trend of OAF values increasing as RH_{ra} increases occurs. This trend is explained as follows: it is most beneficial to mix a high amount of dry outdoor air with humid return air since the resulting mixed air state entering DEVap has a greater temperature differential between the saturation line, increasing DEVap's cooling potential.

There is a very slight change in R_{e1} ratio initially and relatively constant values while R_{ma} ratio ramps between most return air states except for when RH_{ra} is equal to 55%, at which point R_{e1} ratio values are markedly lower. This is explained by the fact that these humid return air states result in humid mixed air states with a smaller temperature difference to the saturation curve on a psychrometric chart. Since optimizing OAF is a higher priority due to its multiple implications for DEVap's cooling performance, the high OAF values for humid return air states results in high amounts of second stage cooling, forcing first stage cooling to decrease as a result.

6.2.3 Sensitivity of Optimal Trends to Outdoor Air State

Since outdoor air states affect both the mixed air state entering DEVap and the cooling potential in the first stage, they are expected to have a larger impact on optimal control variable trends than return air states. Optimal trends for R_{ma} r, R_{e1} ratio, OAF, and COP_{source} for T_{ra} = 75°F and RH_{ra} = 45% under all simulated outdoor air states expressed as T_{oa}/ WB_{oa} are shown in Figure 6.46 through Figure 6.49.

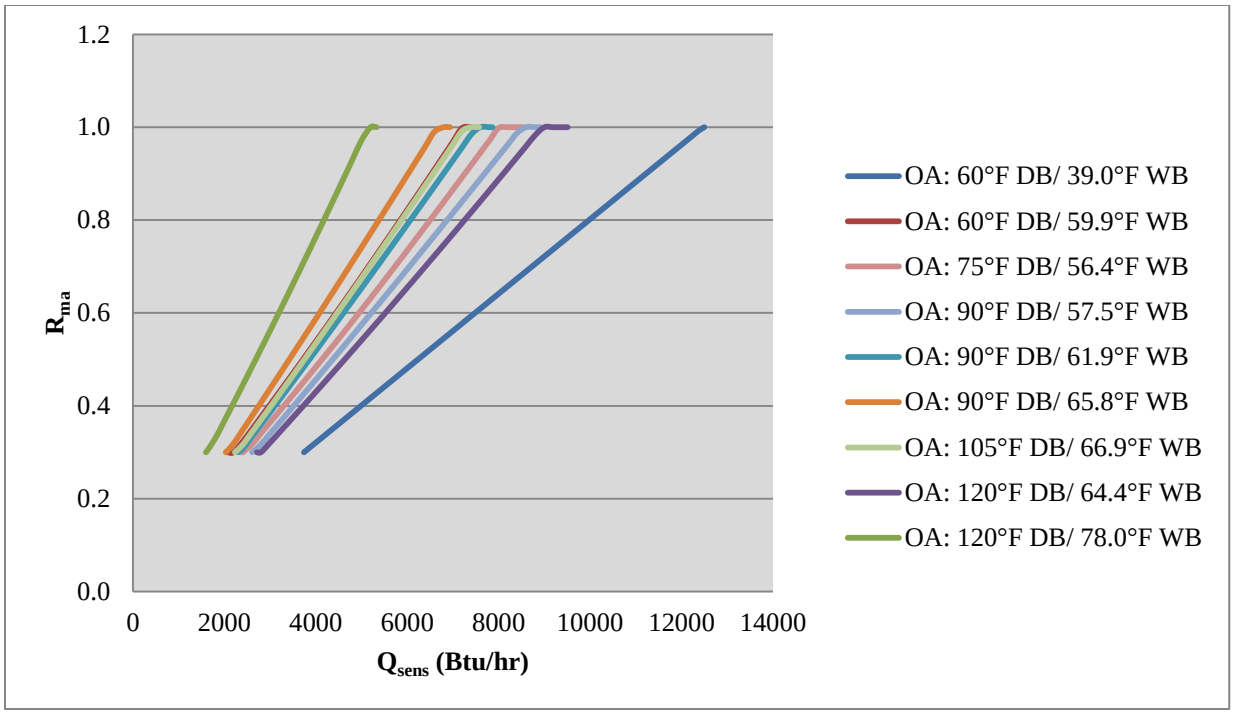

Figure 6.46: Optimal R_{ma} ratio trends in IEC mode for T_{ra} = 75°F and RH_{ra} = 45% at variable outdoor air states

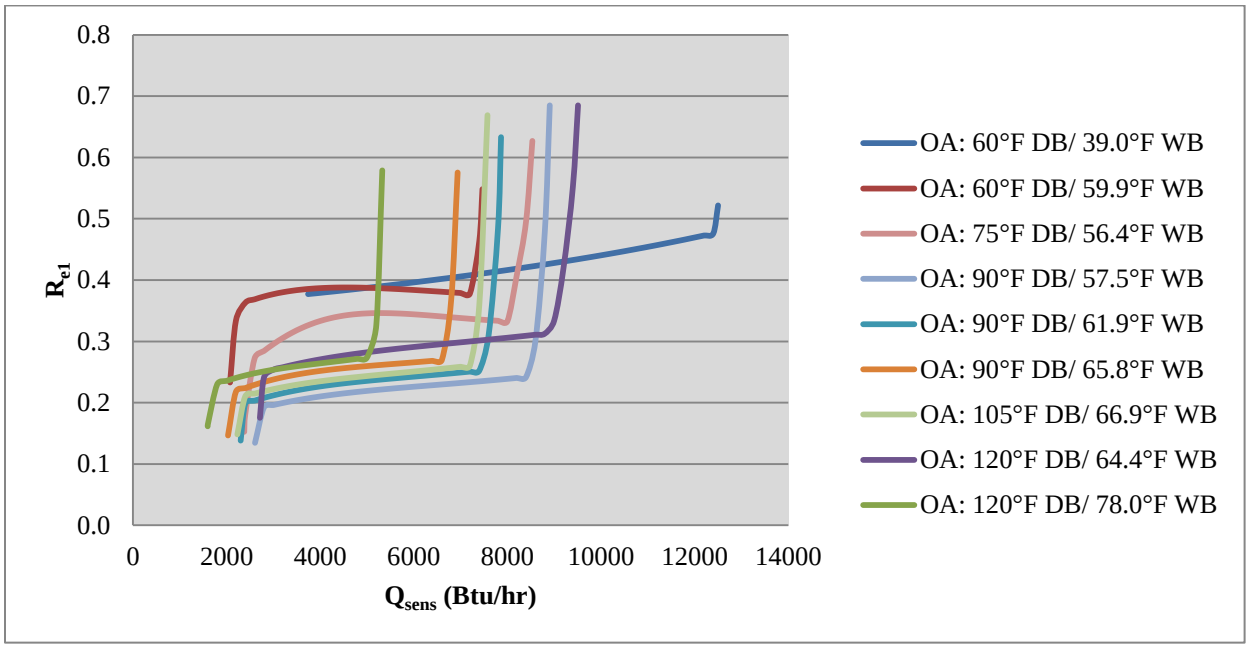

Figure 6.47: Optimal R_{e1} ratio trends in IEC mode for T_{ra} = 75°F and RH_{ra} = 45% at variable outdoor air states

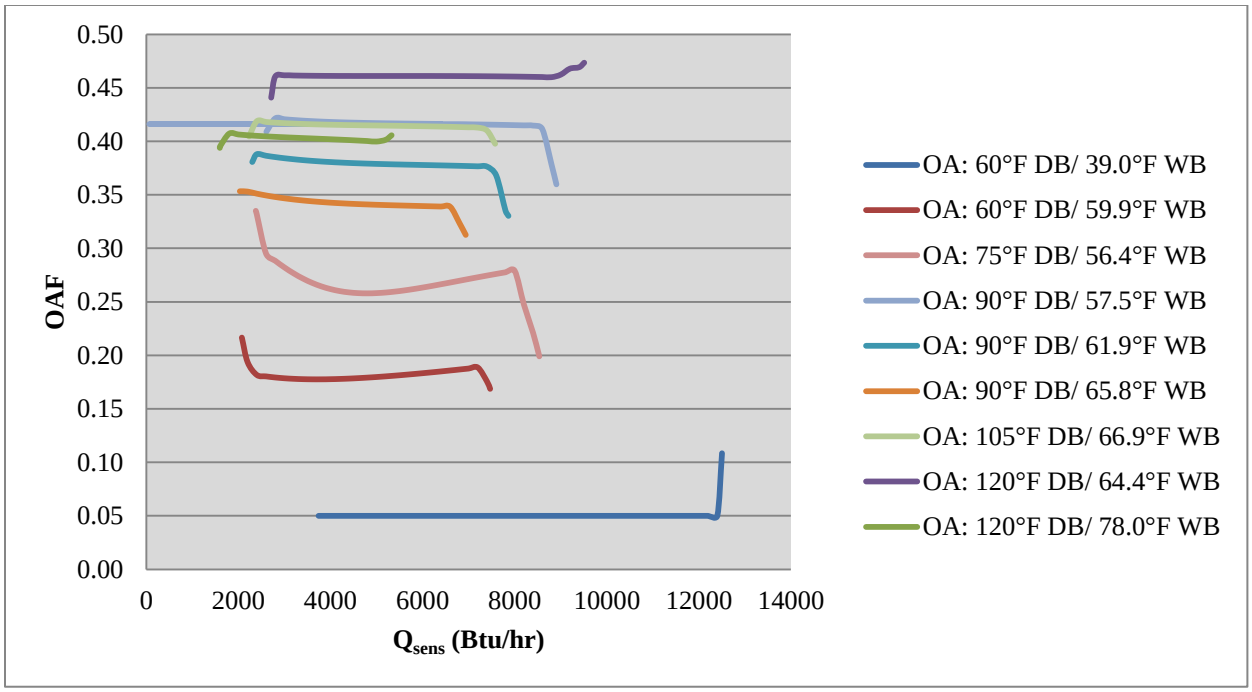

Figure 6.48: Optimal OAF trends in IEC mode for T_{ra} = 75°F and RH_{ra} = 45% at variable outdoor air states

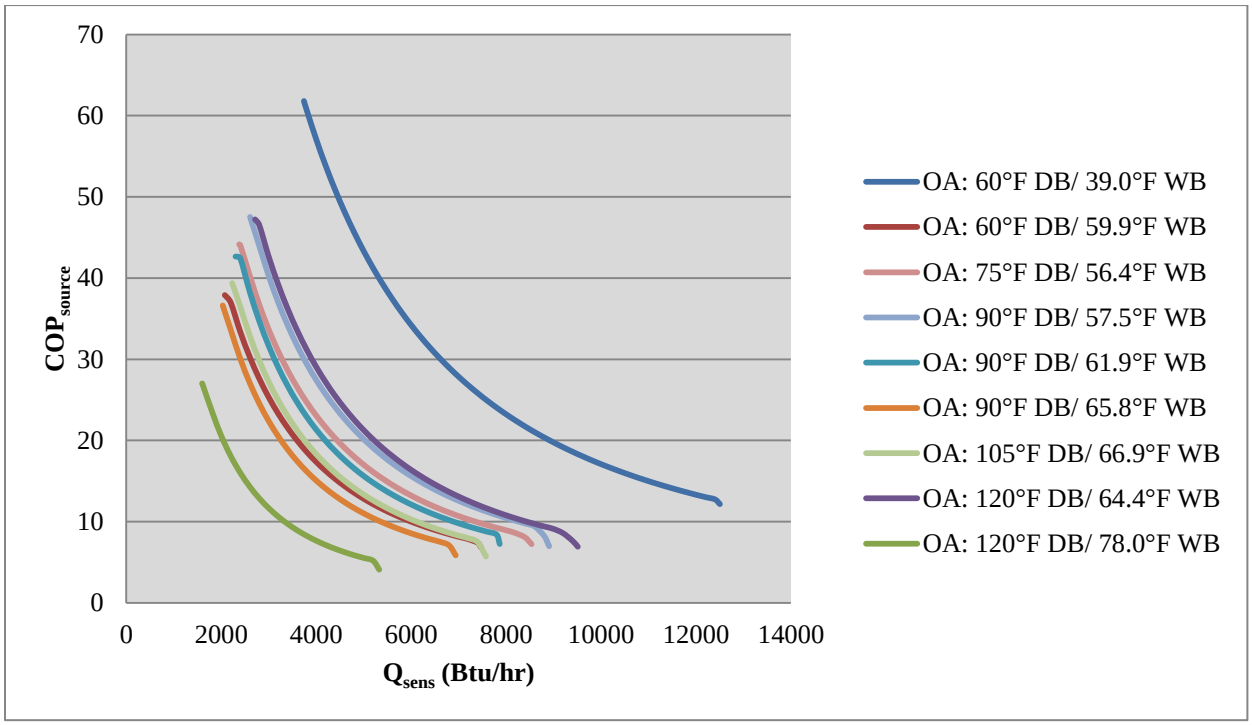

Figure 6.49: Optimal COP_{source} trends in IEC mode for T_{ra} = 75°F and RH_{ra} = 45% at variable outdoor air states

From Figure 6.49, it can be determined that the assumption of increased Q_{sens} and COP_{source} for hotter and drier outdoor air states was incorrect and instead occurs for colder and drier outdoor air states. This can be explained by the fact that colder and drier air is a better evaporative sink in first stage cooling than hotter and drier air. If more of the sensible capacity can be met using first stage cooling, then less second stage cooling is required. This results in less energy spent siphoning off conditioned supply air for second stage cooling, saving a large amount of energy.

From examining Figure 6.46, it can be determined that the trend of linearly ramping R_{ma} ratio from 30% to 100% is applicable to all outdoor air states. Some outdoor air states have a slightly longer region where R_{ma} ratio is pegged at 100%, but the majority of the sensible capacity curve for each outdoor air state is occupied by R_{ma} ratio linearly ramping from 30% to 100% and the other two control variables remaining relatively constant.

Upon examining Figure 6.47, it can be determined that the trends of rapidly increasing R_{e1} ratio initially, then very slowly increasing R_{e1} ratio while R_{ma} ratio ramps from 30% to 100%, then rapidly increasing R_{e1} ratio again holds true for all outdoor air states. There is a slight change in the initial and relatively constant values while R_{ma} ratio ramps between most outdoor air states except for when T_{oa} is equal to or less than T_{ra}, at which point R_{e1} ratio values are markedly higher. This is explained by the fact that when outdoor air is colder than return air, then the outdoor air will serve as both an evaporative sink to absorb moisture and a heat sink for heat transfer from process air to exhaust air in the first stage. This increased cooling potential in the first stage results in the optimal values of R_{e1} ratio being greater than those for hotter outdoor air states.

After examining Figure 6.48, it can be determined that the trend of holding OAF relatively constant while R_{ma} ratio ramps applies to all outdoor air states, but initial and final trends discussed previously for OAF aren't widely applicable across outdoor air states. The initial trend of increasing OAF applies to all outdoor air states that have T_{oa} greater than T_{ra}, and the opposite case where initially OAF decreases occurs when T_{oa} is less than or equal to T_{ra}. This can be explained by the increased first stage cooling potential under this situation, as discussed previously. Greater R_{e1} ratio values taking advantage of increased first stage cooling potential result in reduced need for second stage cooling and lower OAF values. This also explains why R_{e1} ratio and OAF are generally inversely proportional.

For hot outdoor states with T_{oa} equal to or greater than 105°F, greater R_{e1} ratio values are paired with greater OAF values instead of lower ones. This is because when hot outdoor air is used as an evaporative sink in first stage cooling and transferring heat into the process air stream, it is most beneficial to have a hot mixed air state entering DEVap, simultaneously reducing the heat transfer between exhaust and process air in the first stage and creating greater second stage cooling potential. The final trend of decreasing OAF once R_{ma} ratio reaches 100% holds true for all outdoor air states except for the hottest and driest ones. This is because it is most beneficial to force mixed air entering DEVap to be hotter and drier, increasing cooling potential in both stages for different reasons. In the first stage, hotter mixed air results in increased evaporation of moisture and heat transfer into the exhaust air. In the second stage, drier mixed air results in drier supply air being siphoned off and used as a more effective evaporative sink.

6.2.4 Near-optimal Strategy

Using the previously discussed logic for near-optimal control strategies from Section 6.1.3, the initial and final optimal trends of adjusting R_{e1} ratio and OAF while holding R_{ma} ratio to its minimum and maximum value, respectively, can be discarded. This is because these trends account for a combined 15% of the sensible capacity curve with the remainder occupied by the "ramping" phase for R_{ma} ratio as it increases from 30% to 100%. Therefore the near-optimal strategy for IEC mode has the intent of creating a simple method of knowing what values to hold constant for R_{e1} ratio and OAF while R_{ma} ra ramps from 30% to 100%.

Since the values for R_{e1} ratio and OAF while R_{ma} ratio ramps are relatively constant, the average of all values over the region of the sensible capacity curve where R_{ma} ratio ramps for each control variable is used as the value to hold constant in the near-optimal strategy. This usually translates to the value for each control variable when R_{ma} ratio = 65%, since there is approximately a linear change in each control variable's value while R_{ma} ratio ramps. These values to hold constant in the near-optimal strategy for IEC mode are referred to as $R_{e1,near\text{-}opt,IEC}$ and $OAF_{near\text{-}opt,IEC}$.

After determining values for $R_{e1,near\text{-}opt,IEC}$ and $OAF_{near\text{-}opt,IEC}$ by taking the average of R_{e1} ra and OAF values during the ramping phase of R_{ma} ratio for all combinations of return and outdoor air states, it is difficult to show all the information in one figure. One option is to show $R_{e1,near\text{-}opt,IEC}$ values for all simulated outdoor air states under different RH_{ra} values and one T_{ra} value plotted as bar charts on one psychrometric chart as shown in Figure 6.50, then show $OAF_{near\text{-}opt,IEC}$ values for all simulated outdoor air states under different RH_{ra} values and one T_{ra} value plotted as bar charts on another psychrometric chart as shown in Figure 6.51. Using this

methodology, three $R_{e1,near\text{-}opt,IEC}$ charts and three $OAF_{near\text{-}opt,IEC}$ charts are required, one of each for each T_{ra} value that was simulated. Figure 6.50 and Figure 6.51 are charts for T_{ra} = 75°F, which is a typical cooling set point DEVap will operate at.

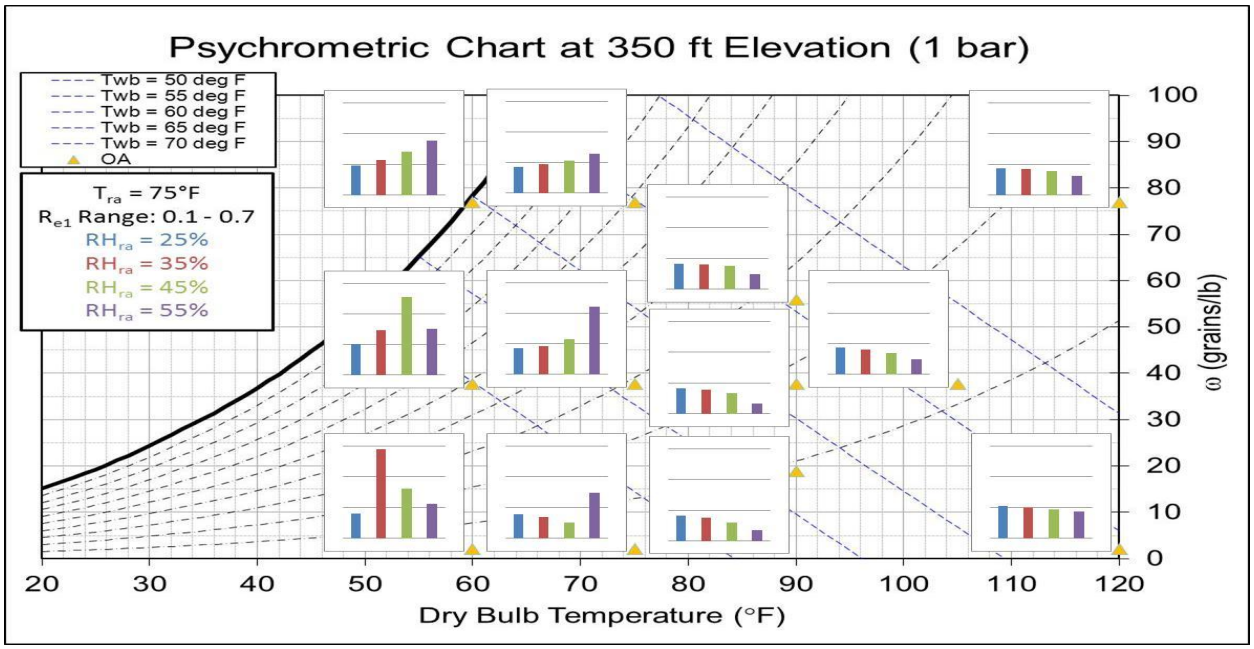

Figure 6.50: Values held constant for $R_{e1,near\text{-}opt,IEC}$ when T_{ra} = 75°F under variable RH_{ra} and outdoor air states

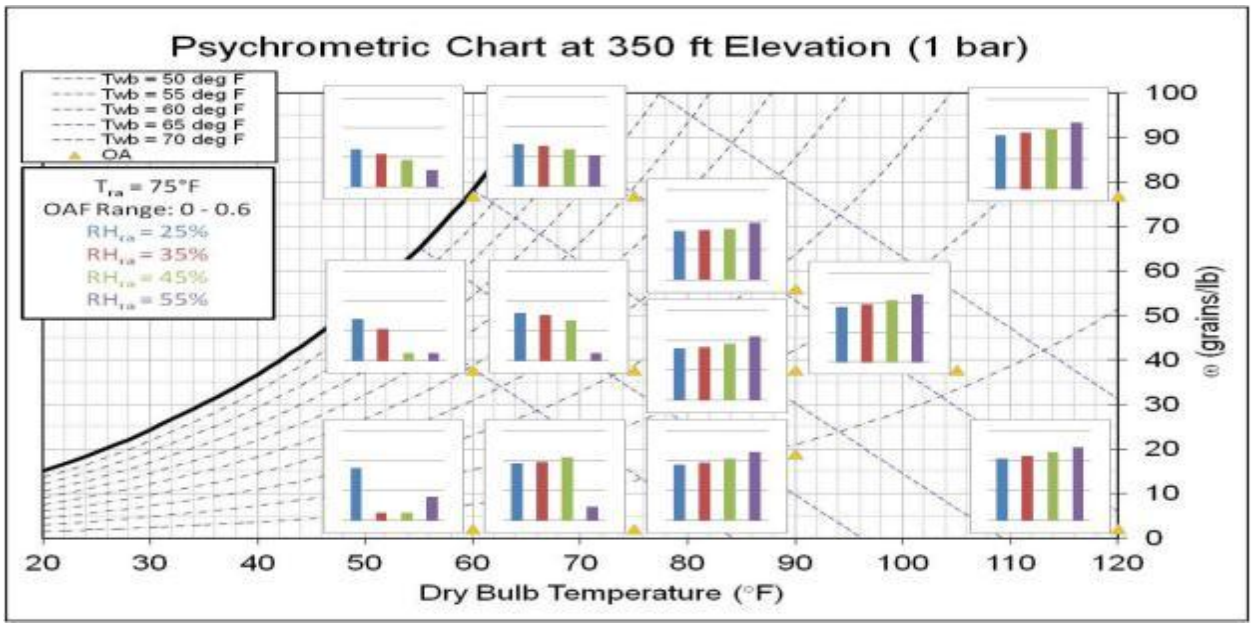

Figure 6.51: Values held constant for $OAF_{near\text{-}opt,IEC}$ when T_{ra} = 75°F under variable RH_{ra} and outdoor air states

Both of these figures show the inverse relationship between R_{e1} ratio and OAF. They also show that RH_{ra} has a small impact on both $R_{e1,near\text{-}opt,IEC}$ and $OAF_{near\text{-}opt,IEC}$ for cases where T_{oa} is greater than T_{ra}. For these situations, as RH_{ra} increases, $OAF_{near\text{-}opt,IEC}$ slightly increases and $R_{e1,near\text{-}opt,IEC}$ slightly decreases. This is explained as follows: as RH_{ra} increases, the mixed air state becomes more humid as well regardless of outdoor air humidity. As the mixed air state becomes more humid, the ability of supply air siphoned off for second stage cooling to serve as an evaporative sink is diminished. Due to this diminished cooling potential, more second stage cooling is required and OAF increases. As more second stage cooling is required, less first stage cooling is required and R_{e1} ratio decreases. The values for $R_{e1,near\text{-}opt,IEC}$ are lower for these hotter outdoor air conditions because first stage cooling actually induces an adverse effect of heat transfer from the outdoor air into the process air.

Another trend occurs for cases where T_{oa} is greater than T_{ra} in which as RH_{oa} decreases, $R_{e1,near\text{-}opt,IEC}$ and $OAF_{near\text{-}ubopt,IEC}$ both slightly increase. This is explained as follows: as RH_{oa} decreases, there are multiple effects. Mixed air becomes hotter and drier, resulting in increased cooling potential of outdoor air in first stage cooling and increased ability of supply air siphoned off for second stage cooling to serve as an evaporative sink. At the same time, the temperature difference between the mixed air state and saturation line increases. Due to this combination of increased cooling potential in both stages and increased temperature difference that can be provided, more cooling is required in both stages and both R_{e1} ratio and OAF increase as a result.

For cases where T_{oa} is equal to or less than T_{ra}, there exist very dry outdoor air states where $OAF_{near\text{-}opt,IEC}$ slightly increases and $R_{e1,near\text{-}opt,IEC}$ slightly decreases as RH_{ra} increases, and

more humid outdoor air states where $OAF_{near\text{-}opt,IEC}$ slightly decreases and $R_{e1,near\text{-}opt,IEC}$ increases as RH_{ra} increases. This is explained as follows: as return air becomes more humid, mixing with cold and slightly dry outdoor air causes the mixed air state to have decreased temperature differential to the saturation curve. This results in reduced need for second stage cooling and OAF decreases. Since OAF decreases, the mixed air state becomes hotter and more humid, making first stage cooling more effective and R_{e1} ratio increases. If the outdoor air were very dry, then mixed air would be dry enough to have a large temperature differential to the saturation curve and more second stage could be employed. It should be noted that these cases where IEC mode is used and T_{oa} is equal to or less than T_{ra} are not likely to occur, since return air states mimic outdoor air states and cooling is usually required when outdoor air is hot. Similar curves for T_{ra} = 80°F and T_{ra} = 70°F are found in Appendix C, and they show that there is little difference in $OAF_{near\text{-}opt,IEC}$ and $R_{e1,near\text{-}opt,IEC}$ values for different T_{ra} values.

Since RH_{ra} has a larger impact on $OAF_{near\text{-}opt,IEC}$ and $R_{e1,near\text{-}opt,IEC}$ values than T_{ra} values, the near-optimal strategy should incorporate RH_{ra} with outdoor air state as the dependent variables to determine what control variable values should be. If $R_{e1,near\text{-}opt,IEC}$ and $OAF_{near\text{-}opt,IEC}$ values for the three T_{ra} values are averaged together for each RH_{ra} and outdoor air state, then the result is Figure 6.52 and Figure 6.53. Averaging the three T_{ra} values causes the near-optimal strategy to mimic optimal trends for T_{ra} = 75°F, since values for $R_{e1,near\text{-}opt,IEC}$ and $OAF_{near\text{-}opt,IEC}$ observed in which is beneficial since this is a typical cooling set point temperature. These two graphs contain all information concerning what values to hold for each control variable as R_{ma} ratio ramps under all simulated return and outdoor air states. If DEVap operates in an outdoor air state not shown in these figures, then linear interpolation can be used to determine what values to set for R_{e1} ratio and OAF.

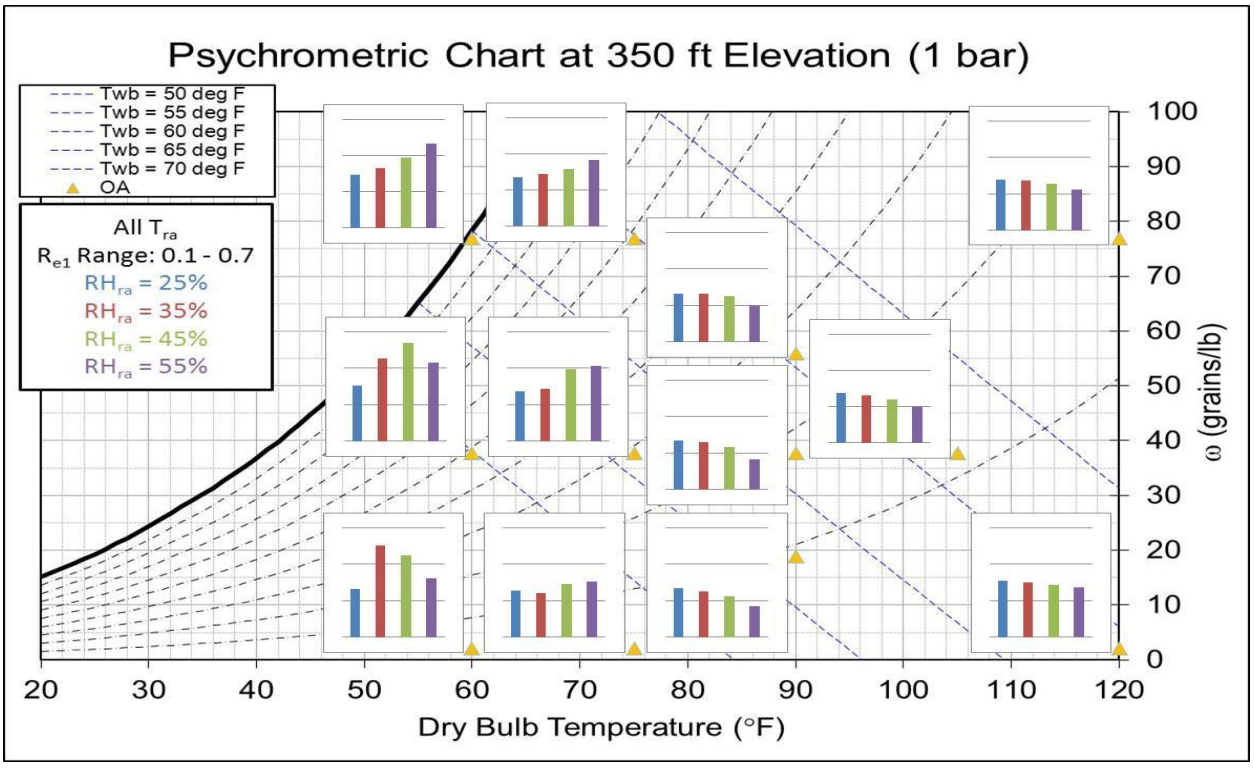

Figure 6.52: Average values across all T_{ra} held constant for $R_{e1,near\text{-}opt,IEC}$ under variable RH_{ra} and outdoor air states

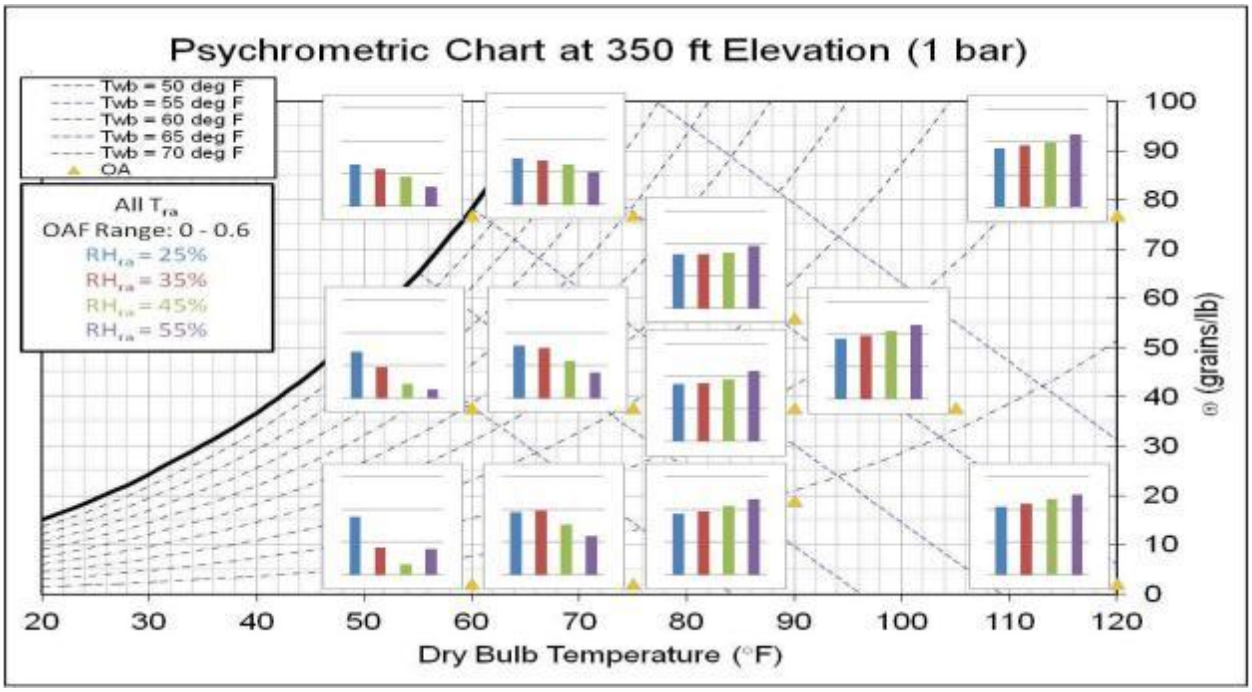

Figure 6.53: Average values across all T_{ra} held constant for $OAF_{near\text{-}opt,IEC}$ under variable RH_{ra} and outdoor air states

It should be noted that the same trends observed in Figure 6.50 and Figure 6.51 occur in Figure 6.52 and Figure 6.53, indicating a near-optimal strategy that mimics optimal trends. The final near-optimal strategy for IEC mode is outlined as follows:

- Knowing values for RH_{ra}, T_{oa}, and ω_{oa}, set R_{e1} ratio and OAF to values according to Figure 6.52 and Figure 6.53, respectively.
- Begin to initially provide Q_{sens} by setting R_{ma} ratio to 30%
- If greater values of Q_{sens} are required, accordingly increase R_{ma} ratio
- The greatest Q_{sens} that can be provided is achieved when R_{ma} ratio reaches 100%

An example of how near-optimal values for R_{ma} ratio, R_{e1} ratio, OAF, $T_{pa,1}$, T_{sa}, and COP_{source} change as the sensible cooling capacity increases under the typical IEC mode operating condition of T_{ra} = 75°F, RH_{ra} = 45%, T_{oa} = 90°F, and ω_{oa} = 0.0054 kg/kg is shown in Figure 6.54. A psychrometric chart outlining all process air states during near-optimal control for the same return and outdoor air state is shown in Figure 6.55.

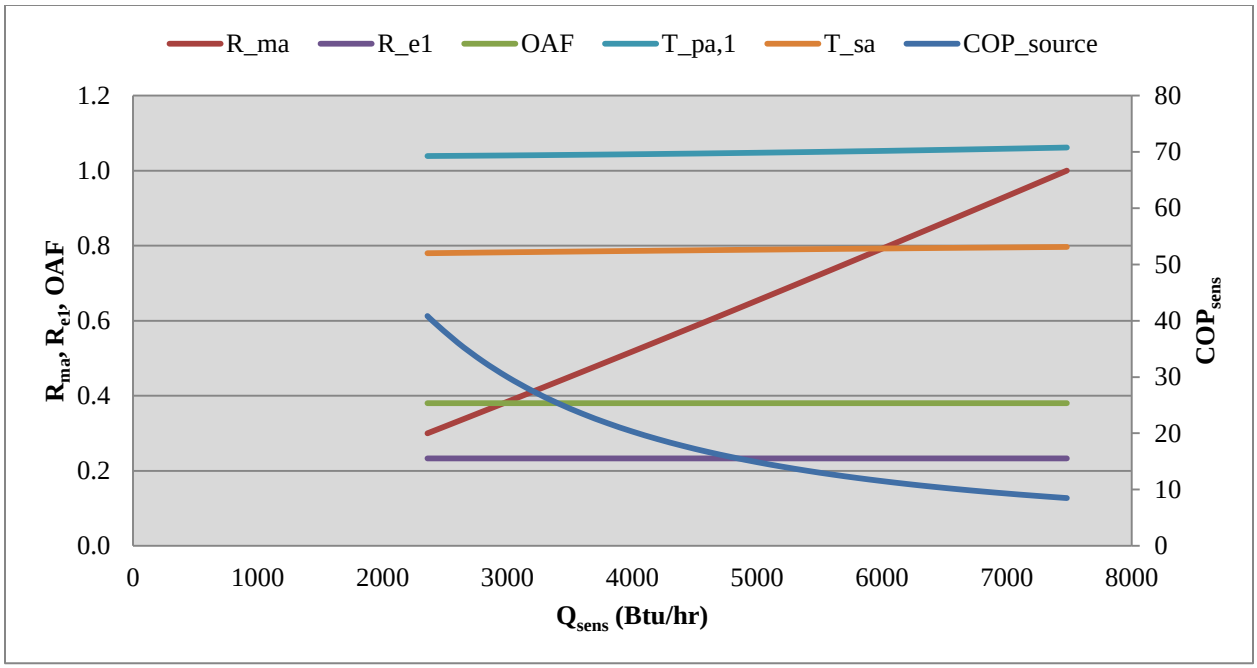

Figure 6.54: Near-optimal control variable trends for T_{ra} = 75°F, RH_{ra} = 45%, T_{oa} = 90°F, and ω_{oa} = 0.0054 kg/kg in IEC mode

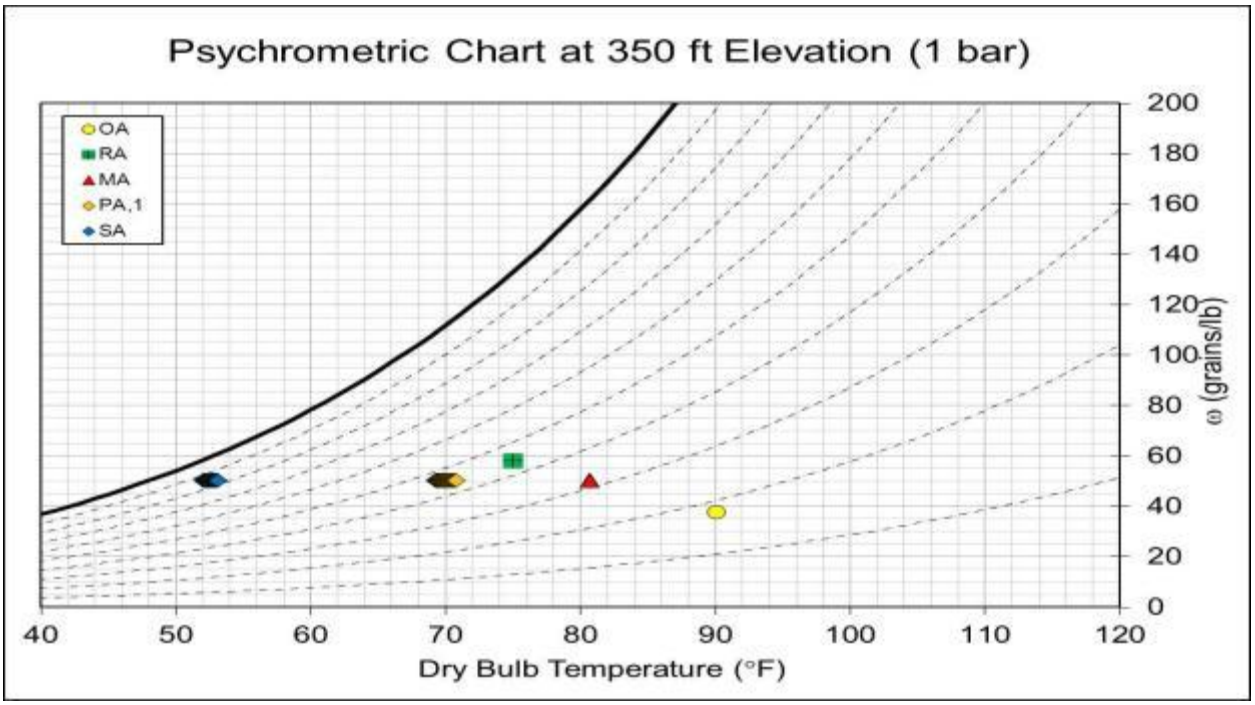

Figure 6.55: Near-optimal air states for T_{ra} = 75°F, RH_{ra} = 45%, T_{oa} = 90°F, and ω_{oa} = 0.0054 kg/kg in IEC mode

From Figure 6.54 and Figure 6.55, it can be determined that mixed air does not change due to constant OAF and both process air exiting the first stage and supply air become slightly hotter as Q_{sens} increases. This is because the only way to increase Q_{sens} is to increase R_{ma} ratio, which causes process air to spend less time in DEVap and therefore reduces the heat exchange effect between process air and exhaust air streams. It should be noted that COP_{source} values in Figure 6.54 are comparable to those found in Figure 6.40 under the same Q_{sens} values, indicating a satisfactory near-optimal strategy that should be applied to all return and outdoor air states.

6.2.5 Analysis of Near-optimal Performance

In order to analyze the performance of the near-optimal strategy for IEC mode, the Solver tool must be used in a similar fashion as the optimization process. The difference is that for this analysis, both R_{e1} ratio and OAF are set to values according to Figure 6.52 and Figure 6.53, respectively. Therefore, the only way for the Solver tool in Excel to set the value of Q_{sens} provided is to adjust R_{ma} ratio accordingly. The Solver tool allows for Q_{sens} to incrementally increase in the same manner as described in Chapter 5, which allows for a comparison of COP_{source} values between optimal control and near-optimal control at equal Q_{sens} values.

Using the near-optimal strategy described in the previous section and holding constant values shown in for $R_{e1,near\text{-}opt,IEC}$ and $OAF_{near\text{-}opt,IEC}$, it is expected that there will be reduced performance and maximum Q_{sens} of IEC mode. A COP_{source} comparison between the optimal simulation and near-optimal strategy for the typical operating condition of T_{ra} = 75°F, RH_{ra} = 45%, T_{oa} = 90°F, and ω_{oa} = 0.0054 kg/kg is shown in Figure 6.56.

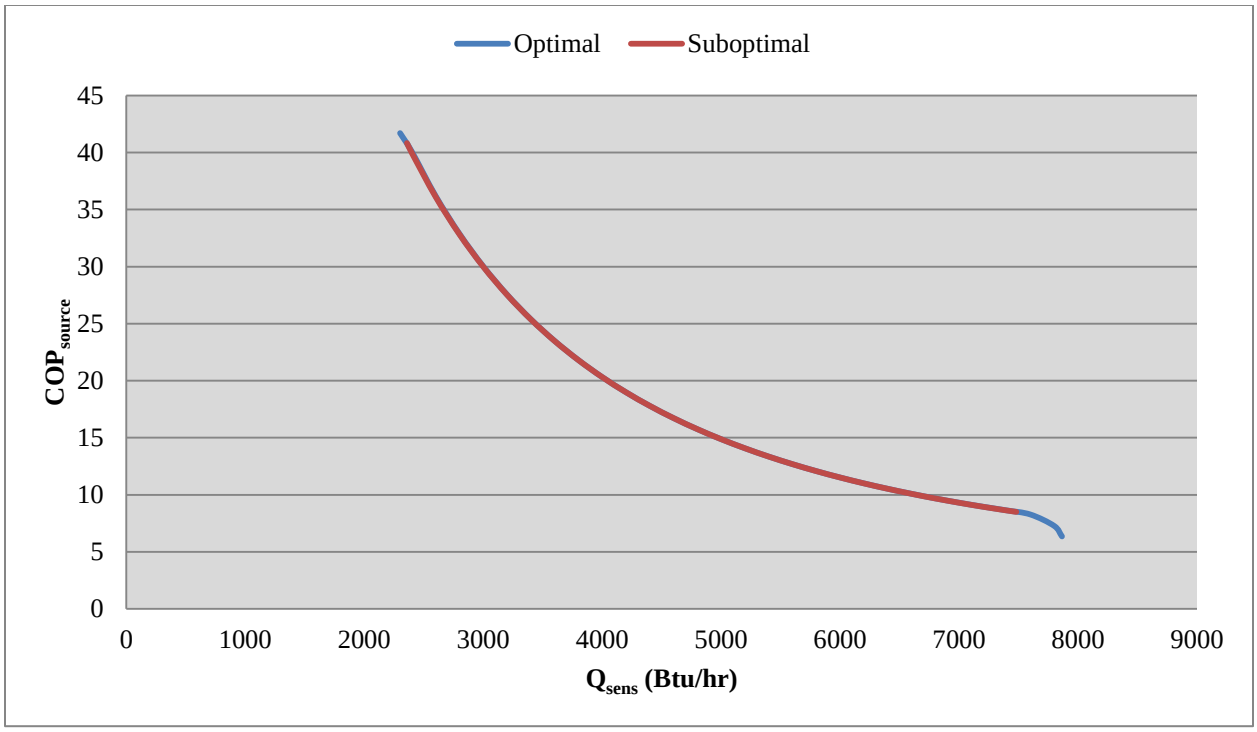

Figure 6.56: Comparison of COP_{source} between optimal and near-optimal trends in IEC mode for typical operating condition (T_{ra} = 75°F, RH_{ra} = 45%, T_{oa} = 90°F, and ω_{oa} = 0.0054 kg/kg)

After examining Figure 6.56, it is determined that there is negligible difference in COP_{source} between optimal and near-optimal control for IEC mode under this combination of return and outdoor air states. Near-optimal control results in greater minimum Q_{sens} and lower maximum Q_{sens} compared to optimal control. This is because near-optimal control does not capture the initial and final trends observed in optimal control where R_{ma} ratio was pegged at 30% and 100%, respectively, while R_{e1} ratio and OAF altered values. Increasing the minimum Q_{sens} is not problematic, but "shaving" the right end of the sensible capacity curve and reducing the maximum Q_{sens} is potentially consequential. However, due to the small amount of Q_{sens} that is lost in doing so, the near-optimal strategy is still satisfactory. Using this combination of return and outdoor air states as an example, near-optimal control results in a reduction in maximum

Q_{sens} that is approximately 400 Btu/hr, which is approximately 5% of the maximum Q_{sens} obtained in optimal control.

A sensitivity analysis is performed on return and outdoor air states to determine how well the near-optimal strategy for IEC mode applies to different circumstances. The return and outdoor air states used in this sensitivity analysis are shown on a psychrometric chart in Figure 6.57.

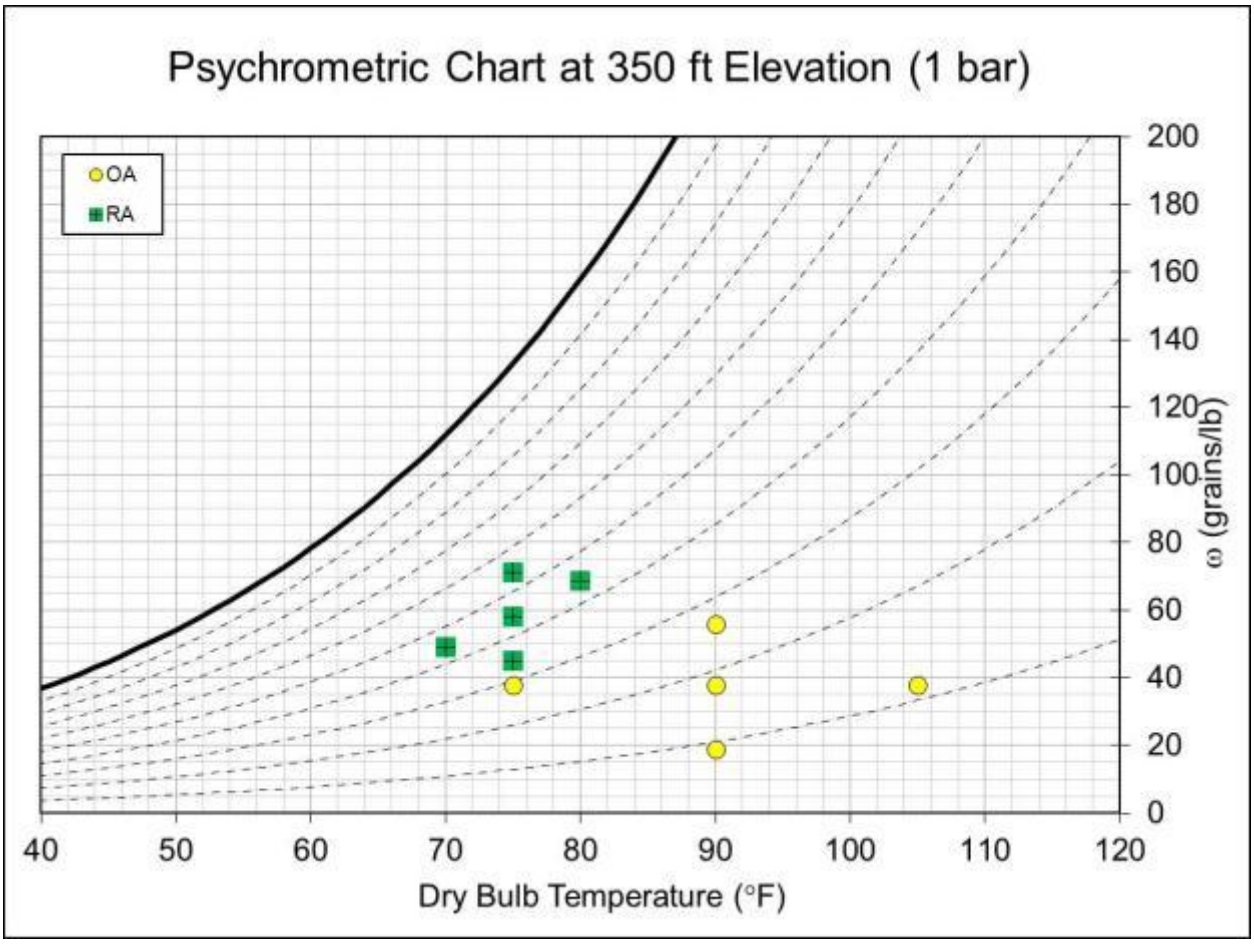

Figure 6.57: Return and outdoor air states used in sensitivity analysis of near-optimal control in IEC mode

These return and outdoor air states were chosen because they encompass the typical operating conditions of IEC mode (T_{ra} = 75°F, RH_{ra} = 45%, T_{oa} = 90°F, and ω_{oa} = 0.0054 kg/kg), as well as allowing for a sensitivity analysis of both temperature and humidity values for each air state. The metric chosen to illustrate the reduction in COP_{source} as a result of near-optimal control is the average percent difference for all instances where optimal and near-optimal control provide equal Q_{sens} values, referred to as $\%\Delta COP_{avg}$. This is because COP_{source} for near-optimal control is always less than that for optimal control, therefore not requiring a metric that squares differences between optimal and near-optimal in order to account for a combination of both positive and negative differences. $\%\Delta COP_{avg}$ is calculated using Equation 6.15.

$$\%\Delta \boldsymbol{COP_{avg}} = \frac{\mathbf{1}}{\boldsymbol{Q_{tot,max} - i}} \sum_{\boldsymbol{Q_{tot} = i}}^{\boldsymbol{Q_{tot,max}}} \frac{\boldsymbol{COP_{suboptimal,i} - COP_{optimal,i}}}{\boldsymbol{COP_{optimal,i}}}$$

Equation 6.15

Calculated values of $\%\Delta COP_{avg}$ for all combinations of return and outdoor air states used in the sensitivity analysis are shown in Figure 6.58.

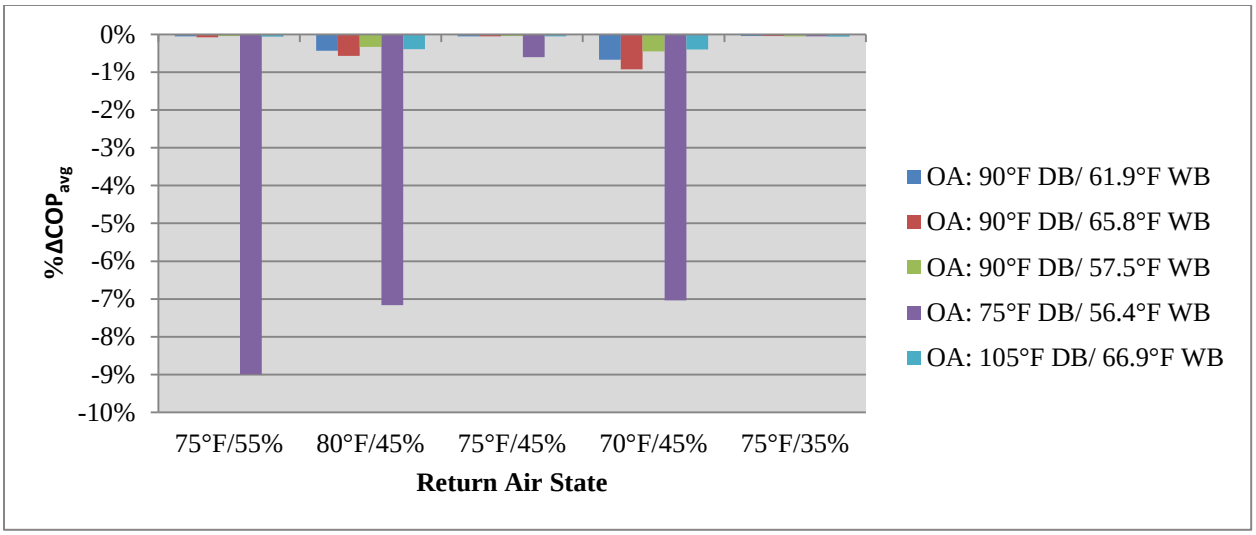

Figure 6.58: Sensitivity analysis results for $\%\Delta COP_{avg}$ between optimal and near-optimal control in IEC mode

From Figure 6.58, it is determined that the near-optimal control strategy developed for IEC mode is satisfactory for all combinations of return and outdoor air states except when T_{oa} = 75°F. This is because the optimal trends for both R_{e1} ratio and OAF are erratic and change behavior depending upon RH_{ra} when T_{oa} is equal to or less than 75°F, therefore making it difficult to capture optimal behavior in these situations. This is not an issue, however, due to the fact that IEC mode is not likely to be used when T_{oa} is at or below a typical cooling set point temperature of 75°F. For all other outdoor air states, the near-optimal strategy yields very satisfactory results, with $\%\Delta COP_{avg}$ values ranging from nearly 0% to a 0.9% loss.

Lower $\%\Delta COP_{avg}$ values occur for T_{ra} = 75°F because the near-optimal strategy was developed in a way that mimicked optimal behavior when T_{ra} = 75°F. As stated previously, the average of the $R_{e1,near\text{-}opt,IEC}$ and $OAF_{near\text{-}opt,IEC}$ values for the three different T_{ra} values will be nearly identical to the $R_{e1,near\text{-}opt,IEC}$ and $OAF_{near\text{-}opt,IEC}$ values for T_{ra} = 75°F, since there is a small linear change in these values as T_{ra} increases from 70°F to 80°F. This also explains why higher

$\%\Delta COP_{avg}$ values occur for T_{ra} = 80°F and T_{ra} = 70°F. This is not problematic, however, since DEVap is much more likely to operate when return air temperature reaches a typical cooling set point of 75°F with small deadband variation.

Another impact of the near-optimal strategy that requires analysis is the reduction in maximum Q_{sens} provided. The metric used to describe this impact is the percent reduction in maximum Q_{sens} provided, referred to as $\%\Delta Q_{sens,max}$ and calculated using Equation 6.16.

$$\%\Delta \boldsymbol{Q_{sens,max}} = \frac{\boldsymbol{Q_{sens,max,near-optimal}} - \boldsymbol{Q_{sens,max,optimal}}}{\boldsymbol{Q_{sens,max,optimal}}}$$

Equation 6.16

Using this definition, $\%\Delta Q_{sens,max}$ will be negative for all cases since $Q_{sens,max}$ in the near-optimal strategy will always be lower than $Q_{sens,max}$ under optimal control. Calculated values of $\%\Delta Q_{sens,max}$ for all combinations of return and outdoor air states used in the sensitivity analysis are shown in Figure 6.59.

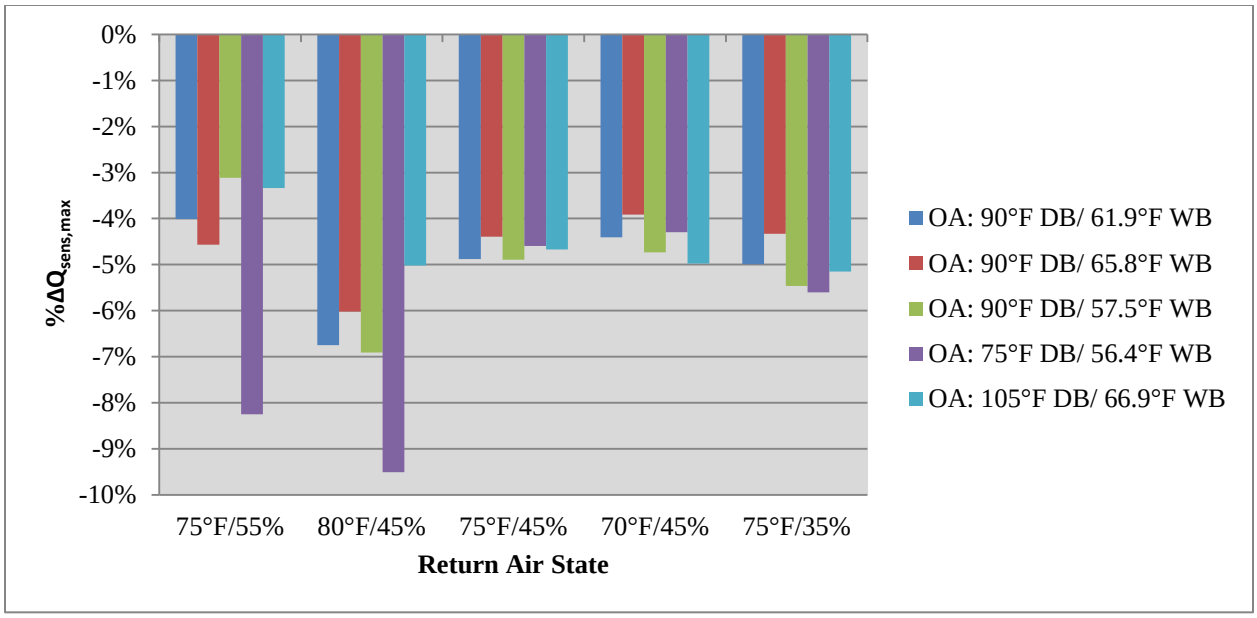

Figure 6.59: Sensitivity analysis results for $\%\Delta Q_{sens,max}$ between optimal and near-optimal control in IEC mode

From Figure 6.59, it is determined that the near-optimal control strategy developed for IEC mode results in approximately constant relative reduction in maximum Q_{sens} for all combinations of return and outdoor air states. For cases when T_{oa} = 75°F, there is greater reduction because the optimal trends for both R_{e1} ratio and OAF are erratic and change behavior depending upon RH_{ra} when T_{oa} is equal to or less than 75°F, therefore making it difficult to capture optimal behavior in these situations. This again is not an issue, however, due to the fact that IEC mode is not likely to be used when T_{oa} is at or below a typical cooling set point temperature of 75°F. For all other outdoor air states, the near-optimal strategy yields very satisfactory results, with $\%\Delta Q_{sens,max}$ values ranging from nearly 3% to a 6% loss. The results of this sensitivity analysis on return and outdoor air states prove that the near-optimal control strategy developed for IEC mode is satisfactory in terms of both impact on COP_{source} and maximum Q_{sens} provided.

6.3 Standard Mode

For standard mode, both return and outdoor air states affect performance and all four control variables are of interest (R_{ma} ratio, R_{e1} ratio, OAF, and $C_{LD,in,DEVap}$). Any control strategies that were previously developed for dehumidification mode and indirect evaporative cooling mode should also apply in standard mode. The trends observed for optimal operation of standard mode are described first, followed by the near-optimal operation strategies derived from those optimal trends.

6.3.1 Optimal Trends

As explained in Section 5.1, the Solver tool in Excel was used to incrementally increase cooling load provided while maximizing COP_{source} by adjusting combinations of values for control variables. For standard cooling mode, the cooling load of interest is the combination of total load and SHR provided. It is expected that as both return and outdoor air become hotter and more humid, the total capacity that can be provided by DEVap will increase because there is greater potential to both dehumidify and sensibly cool from a hotter and more humid mixed air state towards the saturation line on a psychrometric chart. Since the cooling potential is greater, this should also translate into hotter and more humid return and outdoor air states yielding a higher COP_{source} compared to colder and drier return and outdoor air states when trying to provide an equal combination of Q_{tot} and SHR.

It is expected that DEVap would operate in standard mode when RH_{ra} reaches 55% and T_{ra} reaches 75°F, since these are typical RH and temperature set points, respectively. An

example of how R_{ma} ratio, R_{e1} ratio, OAF, $C_{LD,in,DEVap}$, $T_{pa,1}$, T_{sa} and COP_{source} change as the total cooling capacity increases for a typical operating condition of T_{ra} = 75°F, RH_{ra} = 55%, T_{oa} = 90°F, ω_{oa} = 0.0160 kg/kg, and SHR = 0.65 is shown in Figure 6.60, which is referred to as a total capacity curve for standard mode. A psychrometric chart showing air states during optimal operation under these conditions is shown in Figure 6.61.

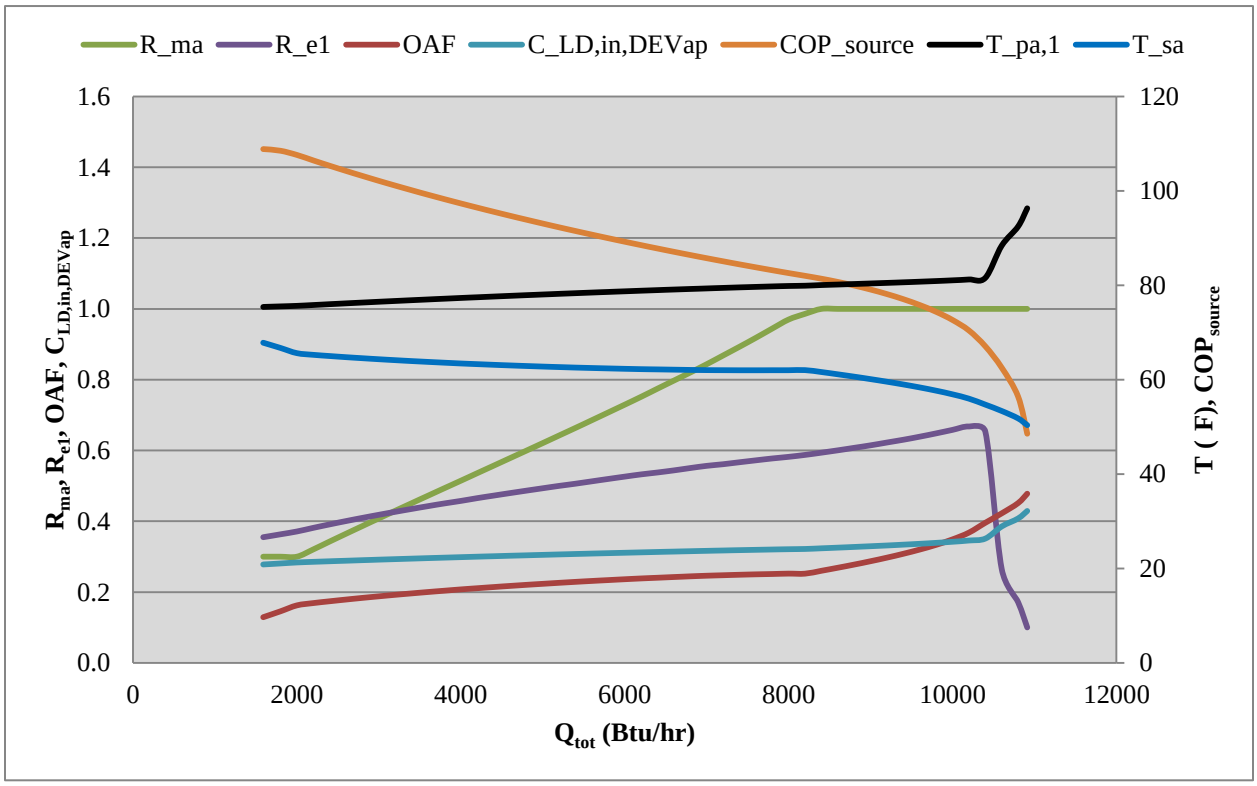

Figure 6.60: Optimal control variable trends for T_{ra} = 75°F, RH_{ra} = 55%, T_{oa} = 90°F, ω_{oa} = 0.0160 kg/kg, and SHR = 0.65 in standard mode

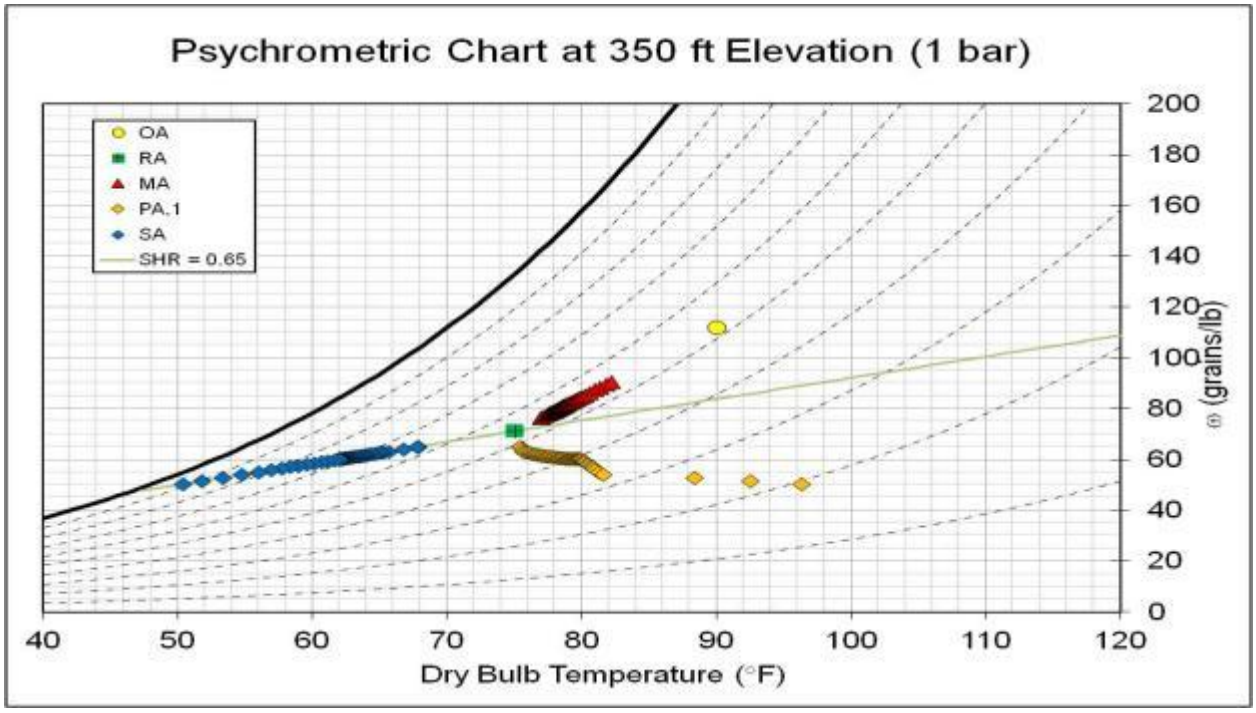

Figure 6.61: Optimal air states for T_{ra} = 75°F, RH_{ra} = 55%, T_{oa} = 90°F, ω_{oa} = 0.0160 kg/kg and SHR = 0.65 in standard mode

From Figure 6.60, it can be determined that for minimum total capacity at the given return and outdoor air states and SHR, it is most efficient to minimize R_{ma} ratio at 30% with a combination of a moderate R_{e1} ratio value and low values for OAF and $C_{LD,in,DEVap}$. This is explained as follows: It is most efficient to provide a low Q_{tot} for a fixed SHR by minimizing the flow rate of air being conditioned as well as the enthalpy change due to conditioning. This results in minimum R_{ma} ratio and low $C_{LD,in,DEVap}$ in order to provide little dehumidification and pass little air through DEVap. A low $C_{LD,in,DEVap}$ value also results in increased COP_{reg}, which in turn increases COP_{source}. Low OAF results in the mixed air state being slightly hotter and more humid than return air, requiring little dehumidification and low $C_{LD,in,DEVap}$, as well as little siphoning of supply air for second stage cooling. A moderate R_{ma} ratio is a result of DEVap being forced to meet a specific SHR. Since there is little dehumidification and second stage

cooling provided, therefore a specific moderate amount of first stage cooling needs to occur to ensure that supply air falls on a SHR line extending from the return air state.

The preceding explanation can also be applied to air states shown in Figure 6.61. The mixed air state associated with this minimum Q_{tot} is closest to return air, since OAF is the lowest throughout the total capacity curve. The process air state exiting the first stage associated with this minimum Q_{tot} is also closest to return air, since a combination of low $C_{LD,in,DEVap}$ and moderate R_{e1} ratio results in little dehumidification and moderate first stage cooling. The supply air state associated with this minimum Q_{tot} is the hottest and most humid, since the most efficient method of providing low total capacity at a fixed SHR is to minimize the enthalpy difference between return and supply air. This is shown by the region where mixed air states are grouped closely together as temperature increases from approximately 77°F to 78°F.

For cases where greater total capacity is required, it is most efficient to increase R_{e1} ratio, OAF, and $C_{LD,in,DEVap}$ as R_{ma} ratio remains at its minimum. This is because it is most efficient to initially increase the enthalpy difference between return and supply air and keep the flow rate of conditioned air at a minimum. This increased enthalpy difference requires a simultaneous increase in both cooling and dehumidification provided in order to maintain SHR, explaining the increase in R_{e1} ratio, OAF, and $C_{LD,in,DEVap}$.

This initial trend of holding minimum R_{ma} ratio while increasing the other three control variables is illustrated in Figure 6.61 as follows: the mixed air state becomes hotter and more humid, resembling the outdoor air state that return air is mixing with. This is shown by the region where mixed air states are grouped closely together as temperature increases from approximately 77°F to 78°F. The process air exiting the first stage becomes slightly hotter and

drier, due to a combination of increasing dehumidification due to increasing $C_{LD,in,DEVap}$ as well as increasingly hotter mixed air entering DEVap. Even though R_{e1} ratio increases, the outdoor air is hot and humid and results in first stage cooling being inefficient compared to if the outdoor air were cold and dry. This is shown by the region where process air states exiting the first stage become quickly dry and slowly hot as temperature increases from approximately 75°F to 76°F. The supply air exiting DEVap becomes colder and drier in a manner that follows a line of constant SHR stemming from the return air state, due to the increase in dehumidification and cooling provided by DEVap. This is shown by the region where supply air states are initially spaced apart as temperature decreases from approximately 68°F to 66°F.

This trend of holding R_{ma} ratio to its minimum continues until an initial transition point is reached at which R_{ma} ratio begins to linearly "ramp" from the minimum 30% of design flow to 100%. As this occurs, OAF and $C_{LD,in,DEVap}$ both increase at a lower rate than previously while R_{e1} ratio increases at the same rate as in the previous trend. This second trend is explained as follows: after increasing the enthalpy change between return and supply air to a specific point, it is most efficient to begin increasing the flow rate of conditioned air being passed through DEVap. Since R_{ma} ratio begins increasing, the heat and mass exchange effect between process air, liquid desiccant, and exhaust air streams is reduced. Therefore, more dehumidification and cooling potential is required to maintain constant enthalpy change between return and supply air, explaining why R_{e1} ratio, OAF, and $C_{LD,in,DEVap}$ all keep increasing during this trend.

This second trend of ramping R_{ma} ratio while increasing the other three control variables is illustrated in Figure 6.61 as follows: the mixed air state still becomes hotter and more humid, but at a lower rate than previously due to the lower rate that OAF increases. This is shown by the region where mixed air states are grouped very closely together as temperature increases

from approximately 78°F to 79°F. The process air exiting the first stage becomes slightly hotter and drier, but at a lower rate than previously. The lower rate at which $C_{LD,in,DEVap}$ increases explains the lower rate at which process air becomes drier, while the lower rate that OAF increases and causes mixed air to become hotter coupled with increasing first stage cooling due to increasing R_{e1} ratio results in process air increasing temperature at a very low rate. This is shown by the region where process air states exiting the first stage maintain almost constant humidity as temperature increases from approximately 76°F to 80°F. The supply air exiting DEVap becomes colder and drier in a manner that follows a line of constant SHR stemming from the return air state, but at a very slow rate. This is shown by the region where supply air states are grouped very closely together as temperature decreases from approximately 66°F to 62°F. This close grouping is due to the slow increase in dehumidification and cooling provided by DEVap during this trend.

This second trend continues until R_{ma} ratio reaches 100%. If more total capacity is still required past this second transition point, it is most efficient to increase both R_{e1} ratio and $C_{LD,in,DEVap}$ at a slightly greater rate than in the previous trend and increase OAF at a higher rate than previously. This third trend is explained as follows: once the rate of process air being passed through DEVap is maximized, it is most efficient to begin increasing the amount of dehumidification and cooling provided at a greater rate than previously. The most efficient method of doing so is to slightly increase the rate at which R_{e1} ratio and $C_{LD,in,DEVap}$ increase and allow OAF to increase at a noticeably higher rate. This is because the benefit of increasing second stage cooling outweighs the negative impact of siphoning supply air and increasing fan energy use.

This third trend of slowly increasing R_{e1} ratio and $C_{LD,in,DEVap}$ while quickly increasing OAF when R_{ma} ratio is pegged at 100% is illustrated in Figure 6.61 as follows: The mixed air state becomes hotter and more humid, but at a higher rate than previously due to the higher rate that OAF increases. This is shown by the region where mixed air states begin to be spaced farther apart as they move towards the outdoor air state as temperature increases from approximately 79°F to 81°F. The process air exiting the first stage becomes hotter at almost the same rate as previously because R_{e1} ratio increases at a slightly higher rate, slightly increasing the amount of first stage cooling provided. However, the process air exiting the first stage becomes drier at a higher rate than previously due to the greater rate at which $C_{LD,in,DEVap}$ increases. This is shown by the region where process air states exiting the first stage begin to be spaced farther apart as they become drier at a higher rate as temperature increases from approximately 80°F to 82°F. The supply air exiting DEVap becomes colder and drier in a manner that follows a line of constant SHR stemming from the return air state, but at a greater rate than previously. This is shown by the region where supply air states become spaced farther apart as temperature decreases from approximately 62°F to 55°F.

This third trend continues until a third and final transition point is reached, at which point it is most efficient to very quickly decrease R_{e1} ratio, increase $C_{LD,in,DEVap}$ at a greater rate than previously, and increase OAF at approximately the same rate as previously. This trend continues until the maximum Q_{tot} is provided when R_{e1} ratio reaches its minimum value of 10%. This final trend is explained as follows: there is a point where the only way to keep increasing Q_{tot} and maintain SHR is to greatly increase the amount of dehumidification and second stage cooling provided and greatly decrease the amount of first stage cooling provided. When $C_{LD,in,DEVap}$ increases at a greater rate than previously, more dehumidification is provided in the first stage.

As process air becomes drier, second stage cooling uses drier air that is more effective as an evaporative sink, resulting in increased cooling potential in the second stage. This increased cooling potential results in a large temperature difference between process air exiting the first stage and supply air exiting DEVap. In order to maintain SHR, this results in the necessity of process air exiting the first stage to become hotter at a faster rate, which translates to much less first stage cooling. This explains why the maximum Q_{tot} is provided when R_{e1} ratio reaches its minimum value of 10%, since the amount of first stage cooling provided cannot be reduced any further. Even though the high values for OAF during this final trend result in high amounts of siphoning from the supply air stream, the benefit of increasing the enthalpy change from return to supply air still outweigh the negative impacts. It should be noted, however, that in Figure 6.60 COP_{source} declines at a higher rate during this final trend than during any other portion of the total capacity curve.

This final trend of very quickly decreasing R_{e1} ratio, increasing $C_{LD,in,DEVap}$ at a greater rate than previously, and increasing OAF at approximately the same rate is illustrated in Figure 6.61 as follows: the mixed air state becomes hotter and more humid at the same rate as in the previous trend. Since OAF is highest during this trend, mixed air is closest to outdoor air during this trend, shown by the region where mixed air states are the hottest and most humid as temperature increases from approximately 81°F to 82°F. The process air exiting the first stage becomes hotter at a very high rate due to the rapid decrease in R_{e1} ratio and drier at a slightly higher rate than previously due to $C_{LD,in,DEVap}$ increasing at a greater rate than previously. This is shown by the region where process air states exiting the first stage are spaced far apart as they become slowly drier and quickly hotter as temperature increases from approximately 82°F to 96°F. The supply air exiting DEVap becomes colder and drier in a manner that follows a line of

constant SHR stemming from the return air state, but at a greater rate than previously. This is shown by the region of coldest and driest supply air states spaced apart as temperature decreases from approximately 55°F to 50°F.

It is important to note that the "ramping" phase for R_{ma} ratio as it increases from 30% to 100% is still the majority of the total capacity curve as it was the majority of the sensible capacity curve in IEC mode, occupying Q_{tot} values ranging from approximately 18% up to 76% of maximum Q_{tot}. However, the final two trends in standard mode account for the final 24% of maximum Q_{tot}, which is a larger portion than witnessed in IEC mode. This indicates that one or both final trends need to be captured in the near-optimal strategy and can't be overlooked.

6.3.2 Sensitivity of Optimal Trends to Return Air State

To determine if these trends are true for other combinations of return and outdoor air states and SHRs, a total capacity curve for each control variable is plotted. First, the impacts of adjusting return air states for a constant outdoor air state and SHR are analyzed. Optimal trends for R_{ma} ratio, R_{e1} ratio, OAF, $C_{LD,in,DEVap}$, and COP_{source} for a typical operating outdoor air state of T_{oa} = 90°F and ω_{oa} = 0.0160 under all simulated return air states expressed as T_{ra}/ RH_{ra} are shown in Figure 6.62 through Figure 6.66. As stated in Section 6.3.1, it is expected that as return air becomes hotter and more humid, the total capacity and COP_{source} that can be provided by DEVap will increase because there is greater potential to both dehumidify and sensibly cool from a hotter and more humid mixed air state towards the appropriate SHR line on a psychrometric chart.

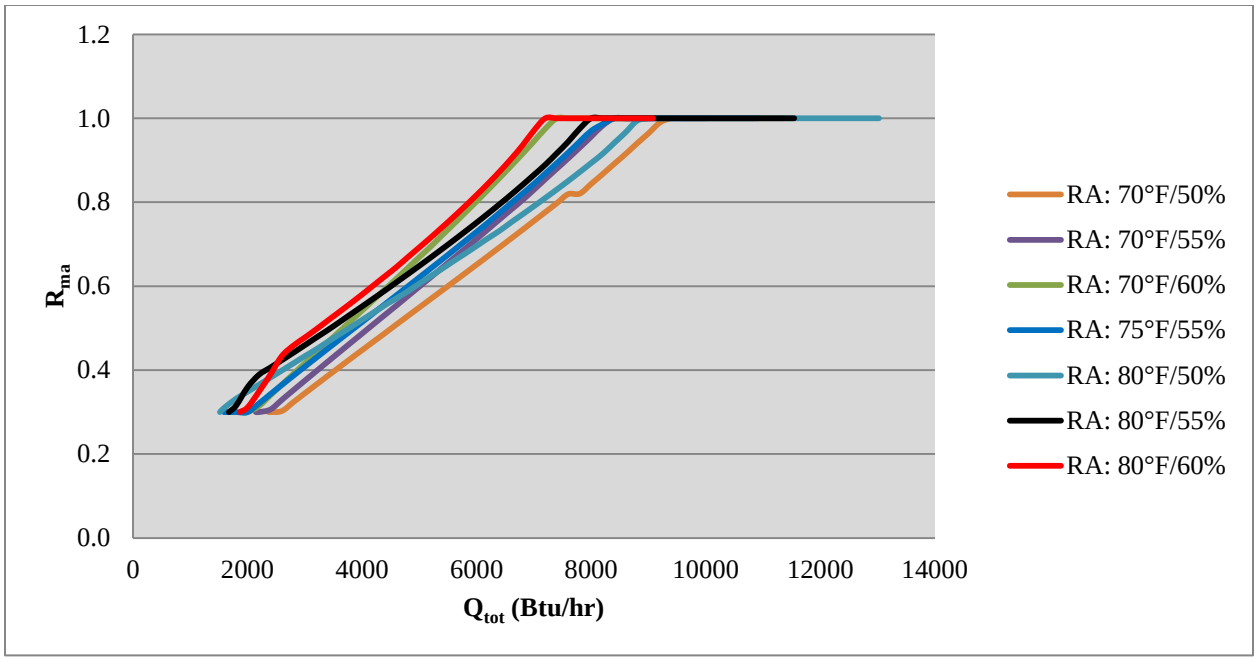

Figure 6.62: Optimal R_{ma} ratio trends in standard mode for T_{oa} = 90°F, ω_{oa} = 0.0160 kg/kg, and SHR = 0.65 at variable return air states

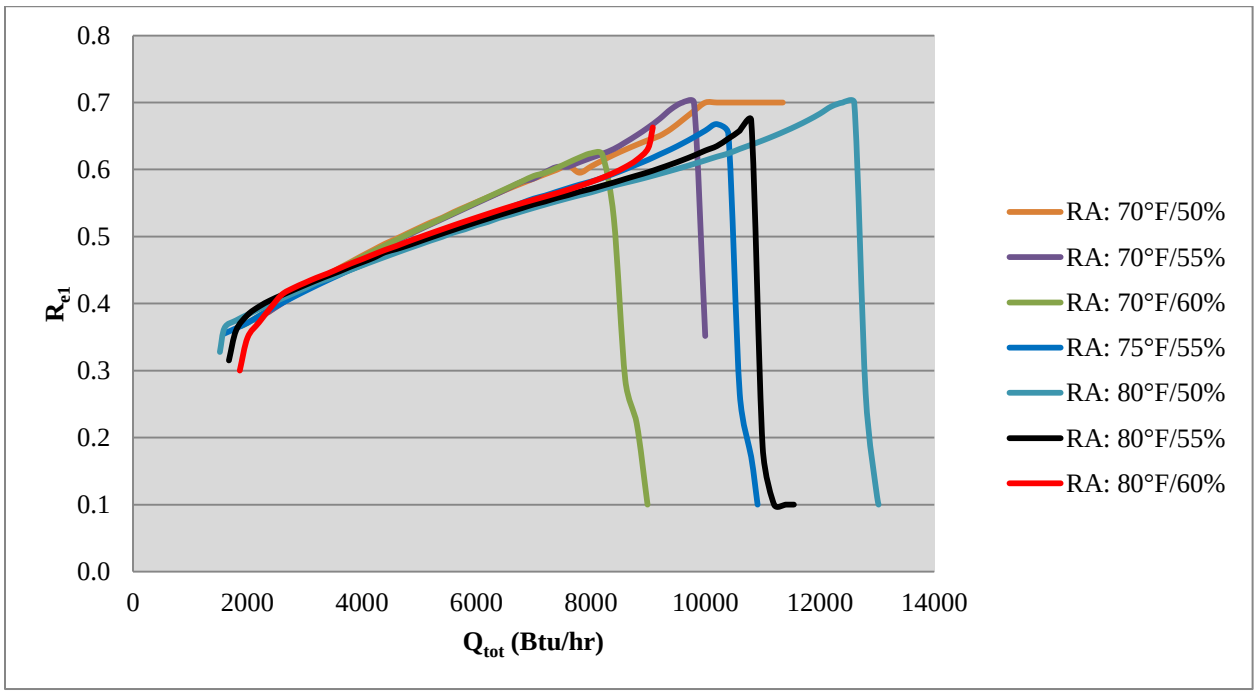

Figure 6.63: Optimal R_{e1} ratio trends in standard mode for T_{oa} = 90°F, ω_{oa} = 0.0160 kg/kg, and SHR = 0.65 at variable return air states

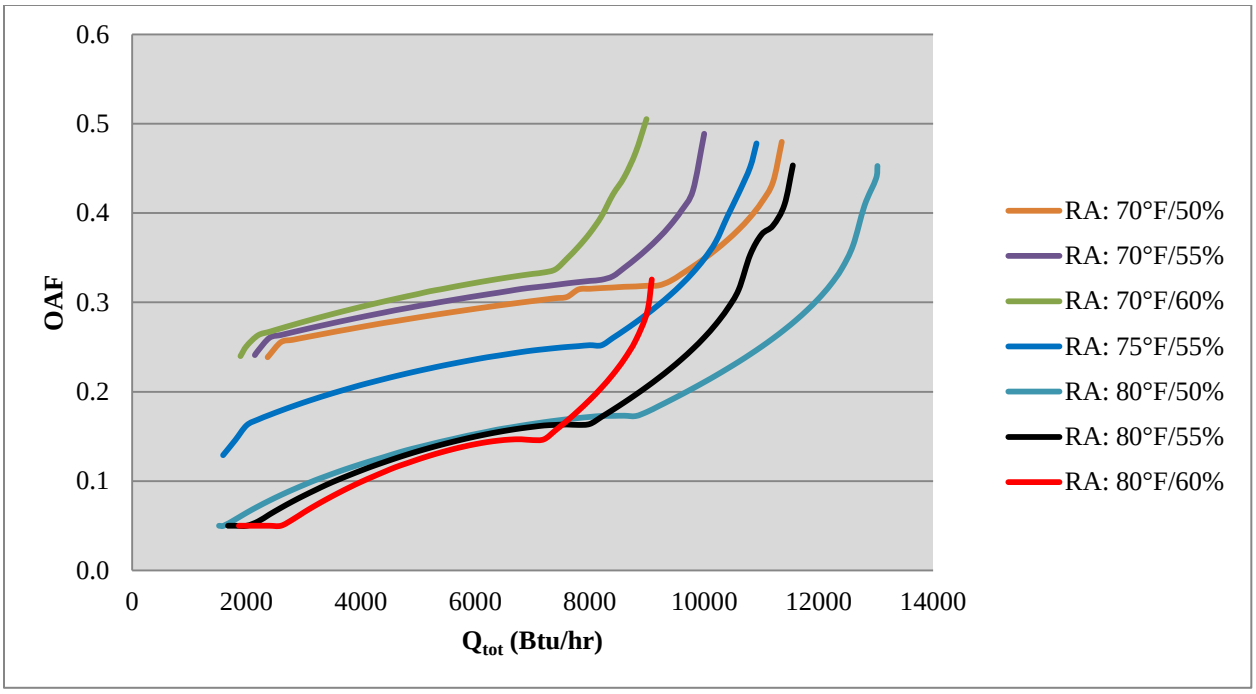

Figure 6.64: Optimal OAF trends in standard mode for T_{oa} = 90°F, ω_{oa} = 0.0160 kg/kg, and SHR = 0.65 at variable return air states

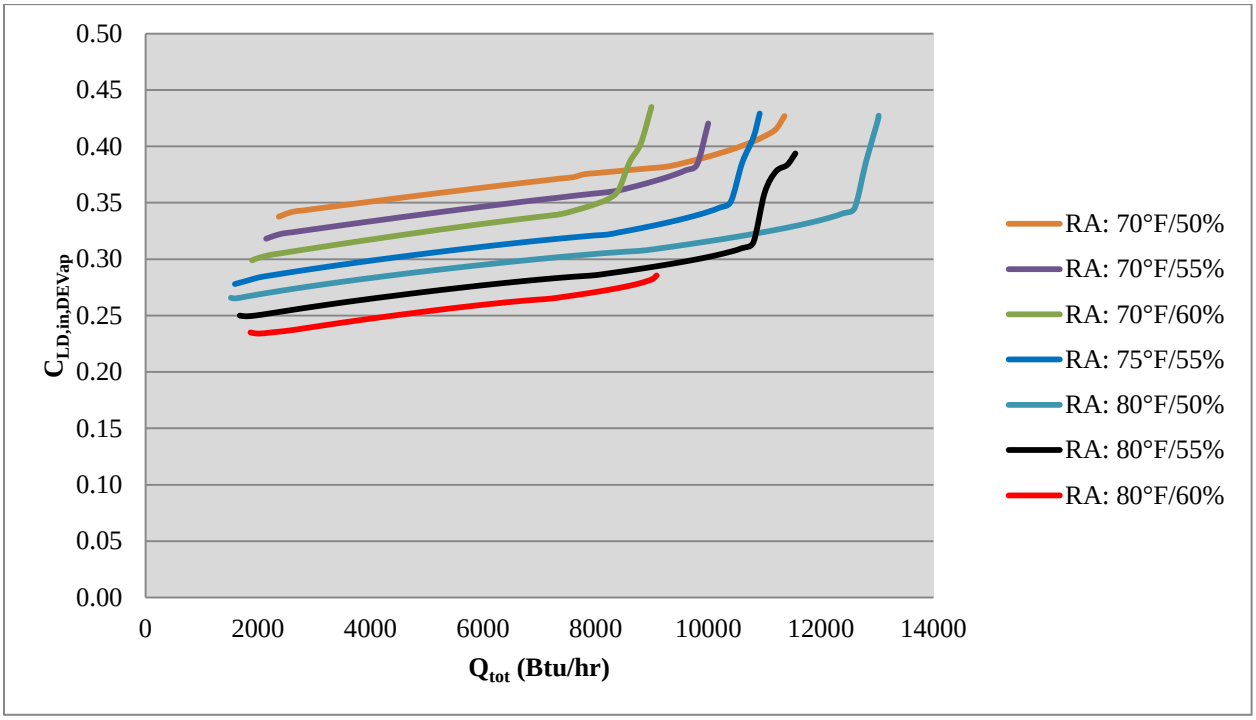

Figure 6.65: Optimal $C_{LD,in,DEVap}$ trends in standard mode for T_{oa} = 90°F, ω_{oa} = 0.0160 kg/kg, and SHR = 0.65 at variable return air states

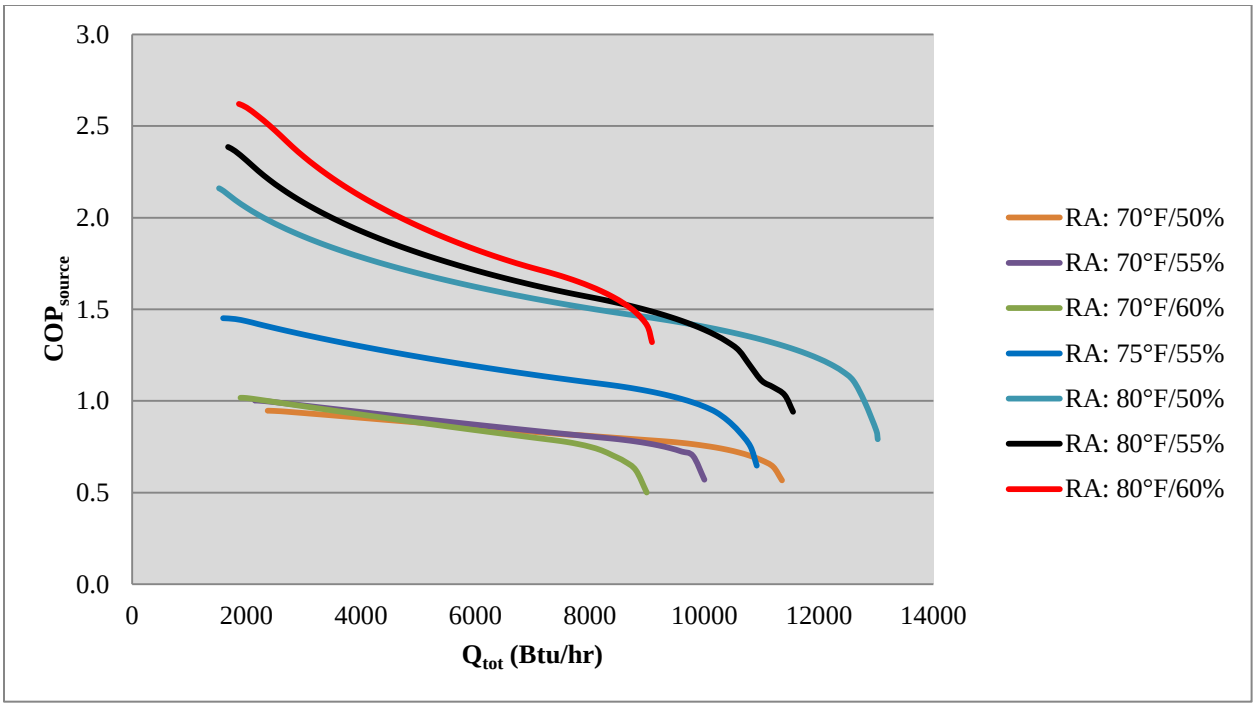

Figure 6.66: Optimal COP_{source} trends in standard mode for T_{oa} = 90°F, ω_{oa} = 0.0160 kg/kg, and SHR = 0.65 at variable return air states

From examining Figure 6.62, it is determined that the trend of linearly ramping R_{ma} ratio from 30% to 100% is applicable to all return air states. Some return air states have a slightly longer region where R_{ma} ratio is pegged at 100%, but the majority of the total capacity curve for each return air state is occupied by R_{ma} ratio linearly ramping from 30% to 100% as OAF and $C_{LD,in,DEVap}$ remain relatively constant and R_{e1} ratio increases. It should be noted that R_{ma} ratio reaches 100% at lower Q_{tot} values as return air becomes more humid. This indicates that it is harder for DEVap to maintain a relatively constant enthalpy change as flow rate of process air increases as mixed air becomes more humid. This is explained by the use of lower $C_{LD,in,DEVap}$ values as RH_{ra} increases, as shown by Figure 6.65. When liquid desiccant is at lower concentrations, there is less moisture transferred from the process air into the liquid desiccant. This also results in less nearly adiabatic heating of the process air as it passes through the first

stage. This reduced heating of the process air results in less cooling potential, minimizing the Q_{tot} that can be provided.

From Figure 6.63, it is determined that the same trends observed previously for R_{e1} ratio behavior hold true for most return air states. Initially R_{e1} ratio is set to a moderate value and increases linearly for all return air states, but the final trend of sharply decreasing R_{e1} ratio as Q_{tot} approaches its maximum value applies to most return air states. In cases where return air is hot and humid, R_{e1} ratio ends at a high value instead of at a low value. This is explained as follows: as T_{ra} increases, OAF decreases, as shown in Figure 6.64, and $C_{LD,in,DEVap}$ decreases, as shown in Figure 6.65. Hotter return air states result in hotter mixed air states. Since little dehumidification and nearly adiabatic heating of this hotter air occurs in the first stage, corresponding process air states exiting the first stage are closer to the desired SHR line and require low second stage cooling. Lower OAF values yield less second stage cooling, therefore more first stage cooling is required.

In cases where return air is cold and "dry" (since RH_{ra} is at its minimum value, which is still a high value of 50%), R_{e1} ratio also ends at a high value instead of at a low value. This is explained as follows: this cold and "dry" return air results in mixed air states that are colder and drier, requiring a high $C_{LD,in,DEVap}$ in order to provide dehumidification potential. This high $C_{LD,in,DEVap}$ value results in high amounts of dehumidification and nearly adiabatic heating of process air in the first stage, requiring more first stage cooling and higher values for R_{ma} ratio.

From Figure 6.64, it is determined that as T_{ra} increases, OAF values decrease, as stated and explained previously. As RH_{ra} changes value for a constant T_{ra}, there is little change in OAF values in the first two trends where R_{ma} is kept at a minimum and where R_{ma} ratio ramps up to

100%. Once R_{ma} ratio reaches 100%, OAF begins to increase at a greater rate until maximum Q_{tot} is achieved, which is similar to behavior observed previously.

From Figure 6.65, it is determined that as both T_{ra} and RH_{ra} increases, $C_{LD,in,DEVap}$ values decrease, as stated and explained previously. There is a more noticeable change in $C_{LD,in,DEVap}$ values as RH_{ra} changes value for constant T_{ra} compared to the change in OAF values observed in Figure 6.64.

From Figure 6.66, it can be determined that the assumption of increased Q_{tot} and COP_{source} for hotter and more humid return air states expressed earlier is partially correct. Hotter return air states yield higher COP_{source} and maximum Q_{tot} values in general, with more humid return air states yielding higher COP_{source} values at lower values of Q_{tot}. At higher values of Q_{tot}, the final trend of rapidly increasing OAF creates a rapid decrease in COP_{source}. However, more humid return air states also yield lower values for maximum Q_{tot}. This is explained as follows: DEVap can achieve better operation under hotter and drier return air states because less dehumidification and second stage cooling is required, as shown by the trend of decreasing $C_{LD,in,DEVap}$ and OAF. This simultaneously results in improved regenerator performance and decreased siphoning of conditioned air for second stage cooling, improving the overall performance of DEVap. Greater Q_{tot} values can also be achieved for hotter and drier return air states because using the same high values for both $C_{LD,in,DEVap}$ and OAF as under colder and more humid return air states yields greater dehumidification and second stage cooling.

6.3.3 Sensitivity of Optimal Trends to Outdoor Air State

Since outdoor air states affect both the mixed air state entering DEVap and the cooling potential in the first stage, they are expected to have a larger impact on optimal control variable

trends than return air states. Optimal trends for R_{ma} ratio, R_{e1} ratio, OAF, $C_{LD,in,DEVap}$, and COP_{source} for a typical operating return air state of T_{ra} = 75°F and RH_{ra} = 55% under all simulated outdoor air states expressed as T_{oa}/ WB_{oa} are shown in Figure 6.67 through Figure 6.71. As stated in Section 6.3.1, it is expected that as outdoor air becomes hotter and more humid, the total capacity and COP_{source} that can be provided by DEVap will increase because there is greater potential to both dehumidify and sensibly cool from a hotter and more humid mixed air state towards the appropriate SHR line on a psychrometric chart.

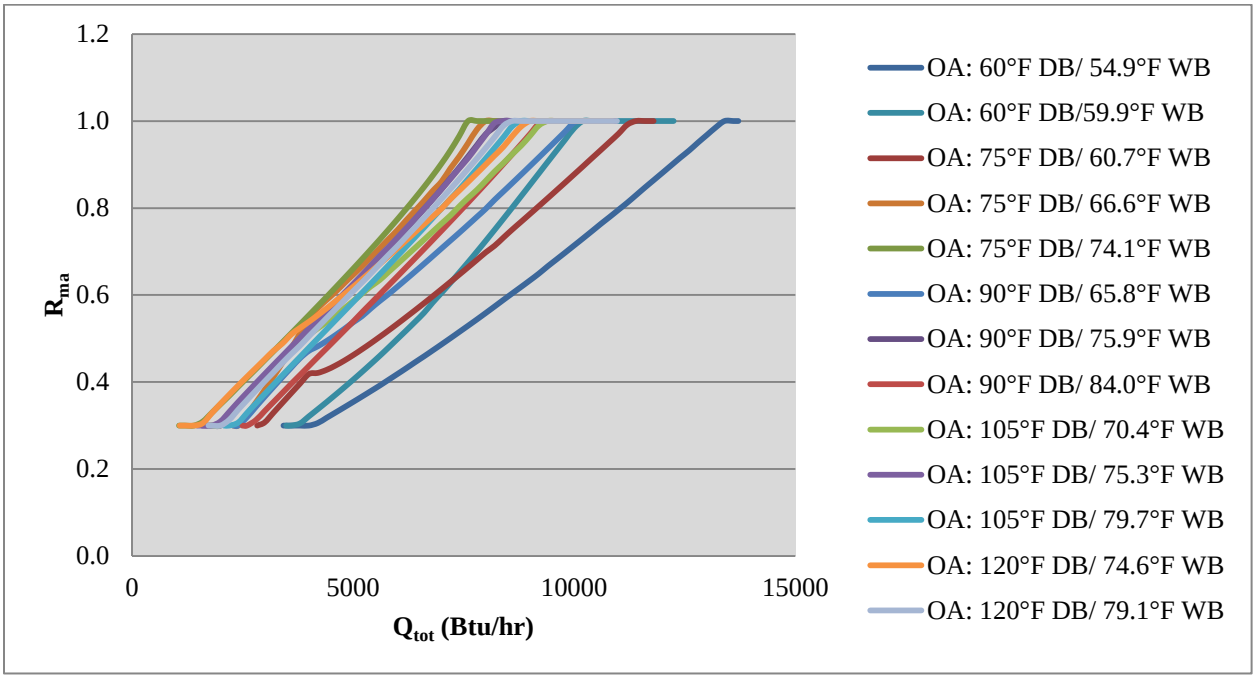

Figure 6.67: Optimal R_{ma} ratio trends in standard mode for T_{ra} = 75°F, RH_{ra} = 55%, and SHR = 0.65 at variable outdoor air states

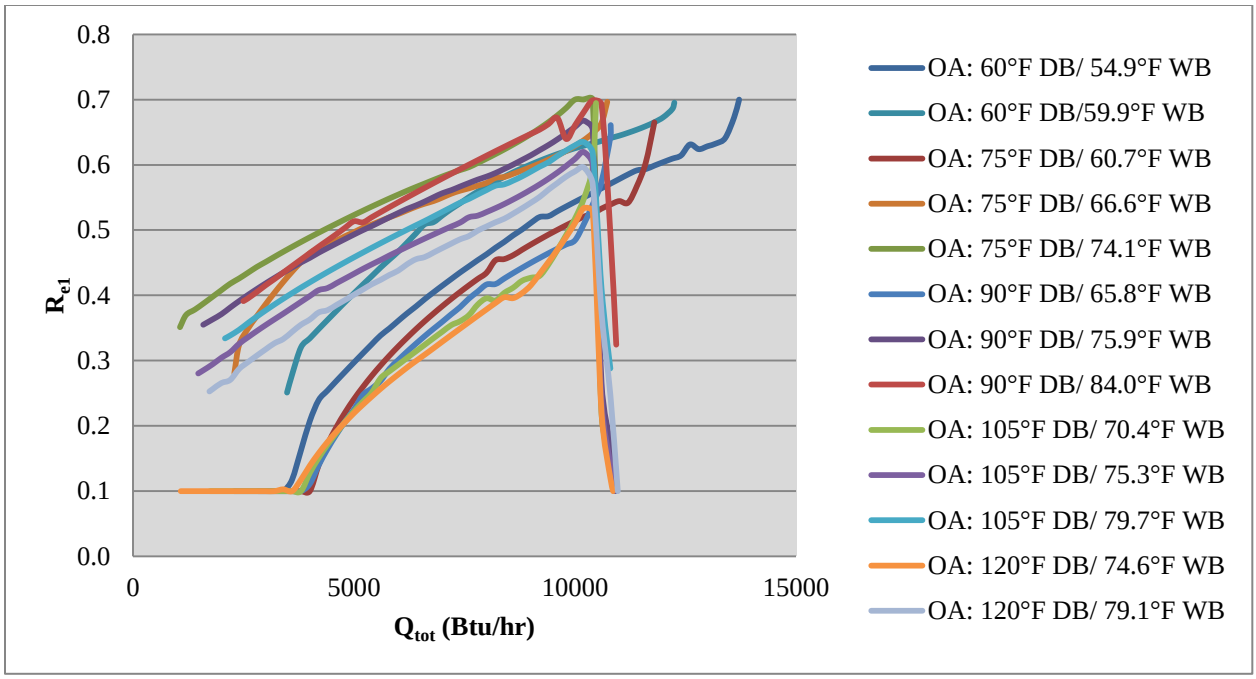

Figure 6.68: Optimal R_{e1} ratio trends in standard mode for T_{ra} = 75°F, RH_{ra} = 55%, and SHR = 0.65 at variable outdoor air states

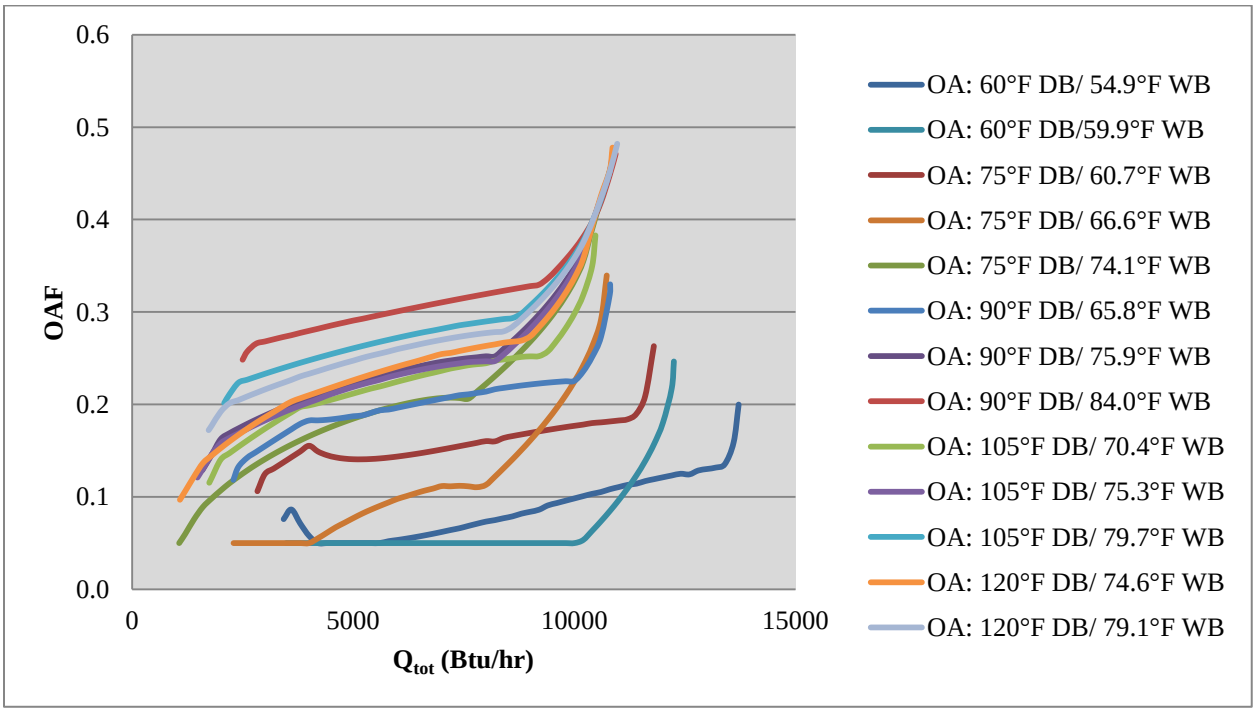

Figure 6.69: Optimal OAF trends in standard mode for T_{ra} = 75°F, RH_{ra} = 55%, and SHR = 0.65 at variable outdoor air states

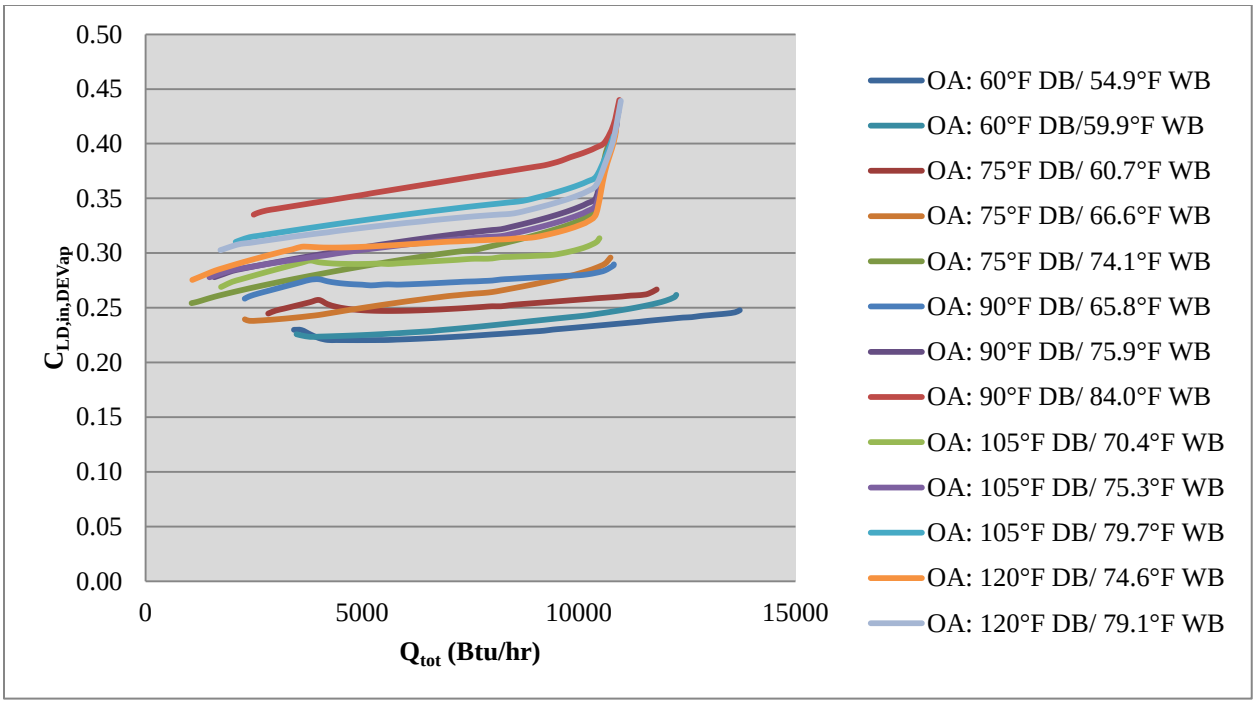

Figure 6.70: Optimal $C_{LD,in,DEVap}$ trends in standard mode for T_{ra} = 75°F, RH_{ra} = 55%, and SHR = 0.65 at variable outdoor air states

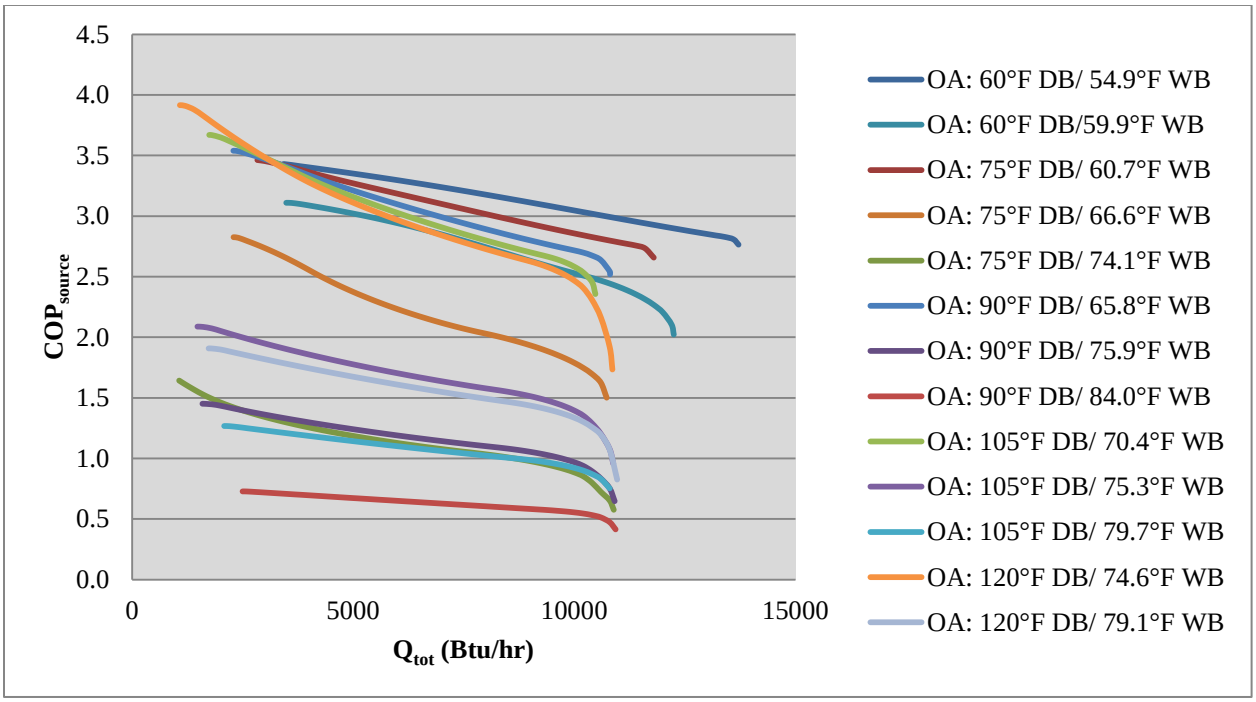

Figure 6.71: Optimal COP_{source} trends in standard mode for T_{ra} = 75°F, RH_{ra} = 55%, and SHR = 0.65 at variable outdoor air states

From examining Figure 6.67, it is determined that the trend of linearly ramping R_{ma} ratio from 30% to 100% is applicable to all outdoor air states. Most outdoor air states have a long region where R_{ma} ratio is pegged at 100%, but the majority of the total capacity curve for each outdoor air state is occupied by R_{ma} ratio linearly ramping from 30% to 100% as OAF and $C_{LD,in,DEVap}$ remain relatively constant and R_{e1} ratio increases. It should be noted that in general, R_{ma} ratio reaches 100% at lower Q_{tot} values as outdoor air becomes hotter and more humid. This indicates that it is harder for DEVap to maintain a relatively constant enthalpy change as flow rate of process air increases as mixed air becomes hotter and more humid.

From Figure 6.68, it is determined that the same trends observed previously for R_{e1} ratio behavior hold true for most outdoor air states. Initially R_{e1} ratio is set to a moderate value and increases linearly for outdoor air states with humidity ratios above the minimum value of 0.008, in which case R_{e1} ratio is initially at its minimum value of 10% and remains there even while R_{ma} ratio is ramping. This is explained as follows: dry outdoor air results in an effective evaporative sink used in first stage cooling. This increase in first stage cooling potential results in the ability to provide the same amount of cooling at a lower exhaust flow rate.

The final trend of sharply decreasing R_{e1} ratio as Q_{tot} approaches its maximum value also applies to most outdoor air states. In cases where outdoor air is cold and dry, R_{e1} ratio ends at a high value instead of at a low value. This is explained as follows: colder and drier outdoor air results in an effective evaporative sink used in first stage cooling. This increase in first stage cooling potential results in first stage cooling being more beneficial than second stage cooling. This also explains why cold and dry outdoor air states have lower OAF values, as shown in Figure 6.69.

From Figure 6.69, it is determined that OAF values generally decrease as outdoor air is colder and drier, as stated and explained previously. For instances where T_{oa} is greater than 75°F, there is less dramatic change in OAF values compared to instances where T_{oa} is equal to or less than 75°F. This is beneficial when developing the near-optimal strategy, since it should capture optimal trends when outdoor air is hot and cooling is likely to be required.

From Figure 6.70, it is determined that there is a strong correlation between increased $C_{LD,in,DEVap}$ values and increased WB_{oa} values, which is the opposite trend observed for return air states. This is explained as follows: as the WB_{oa} increases, the effectiveness of outdoor air as an evaporative sink in first stage cooling decreases. This results in second stage cooling being more beneficial than first stage cooling, which results in higher OAF values. Since more second stage cooling is provided, higher $C_{LD,in,DEVap}$ values are required in order to increase the amount of nearly adiabatic heating of process air that occurs in dehumidification in order to achieve the appropriate SHR.

From Figure 6.71, it can be determined that the assumption of increased Q_{tot} and COP_{source} for hotter and more humid outdoor air states expressed earlier is incorrect. Instead, greater Q_{tot} and COP_{source} values are attained for outdoor air states with low WB_{oa} values. This is explained by the trend of high OAF and $C_{LD,in,DEVap}$ values associated with high WB_{oa} values, since this results in more siphoning of supply air and decreased regenerator performance.

6.3.4 Sensitivity of Optimal Trends to Sensible Heat Ratio

Since SHR affects the amount of sensible and latent cooling that is provided, it dictates what values control variable must be set to in order to produce specific supply air states exiting DEVap. Optimal trends for R_{ma} ratio, R_{ma} ratio, OAF, $C_{LD,in,DEVap}$, and COP_{source} for a typical

operating condition of T_{ra} = 75°F, RH_{ra} = 55%,T_{oa} = 90°F, and ω_{oa} = 0.0160 for the three SHR values simulated are shown in Figure 6.72 through Figure 6.76. It is expected that as SHR increases, less dehumidification and more sensible cooling in both stages will be required, resulting in decreased $C_{LD,in,DEVap}$ and increased R_{e1} ratio and OAF values. As a result, it is expected that increasing SHR values will result in decreasing COP_{source} values due to the increasing amount of supply air siphoned off for second stage cooling.

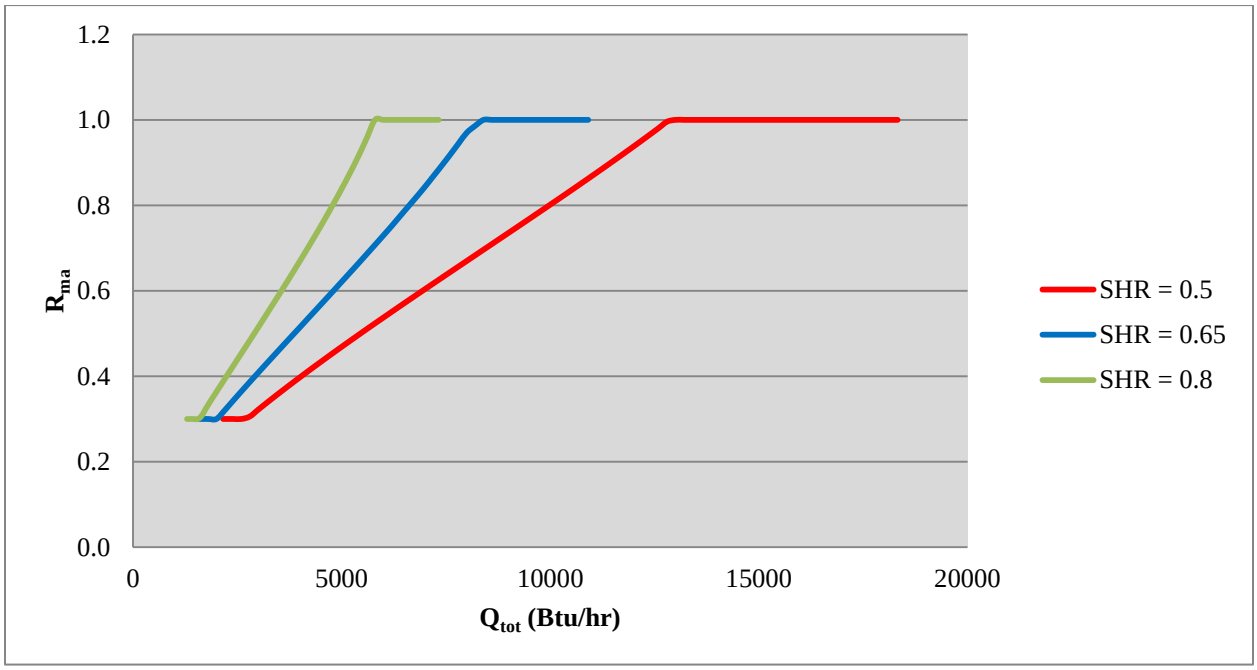

Figure 6.72: Optimal R_{ma} ratio trends in standard mode for T_{ra} = 75°F, RH_{ra} = 55%, T_{oa} = 90°F, and ω_{oa} = 0.0160 kg/kg at variable SHR values

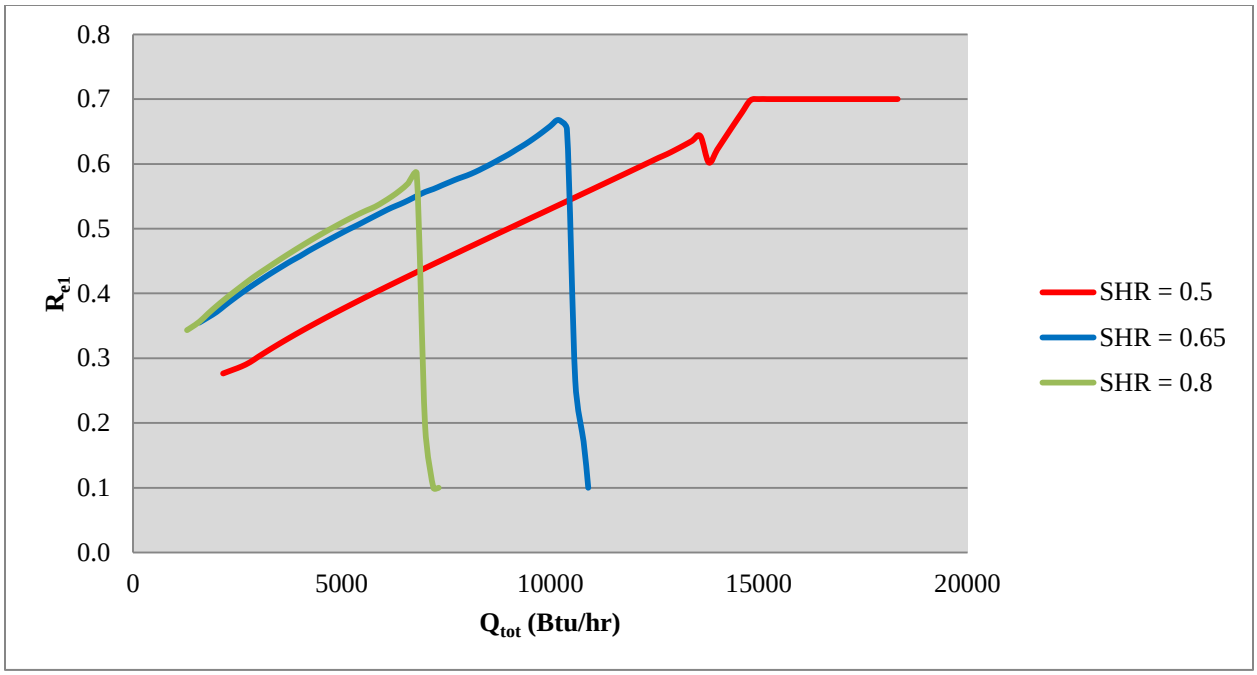

Figure 6.73: Optimal R_{e1} ratio trends in standard mode for T_{ra} = 75°F, RH_{ra} = 55%, T_{oa} = 90°F, ω_{oa} = 0.0160 kg/kg at variable SHR values

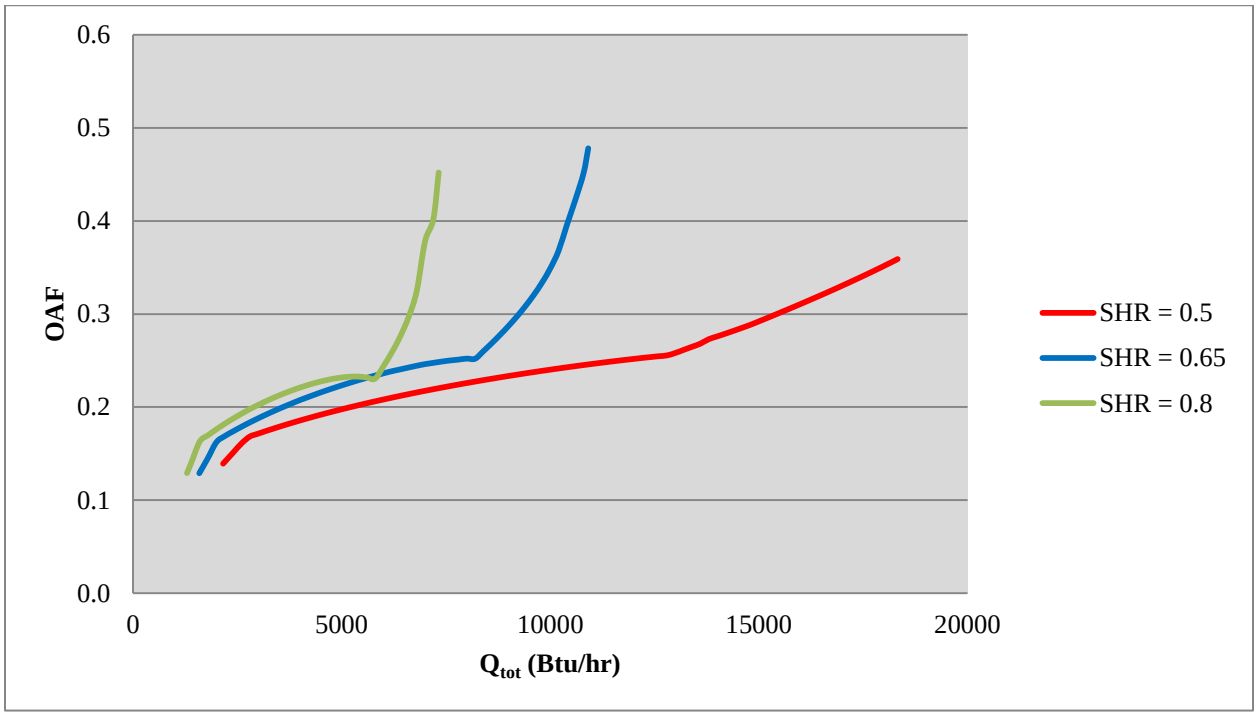

Figure 6.74: Optimal OAF trends in standard mode for T_{ra} = 75°F, RH_{ra} = 55%, T_{oa} = 90°F, ω_{oa} = 0.0160 kg/kg at variable SHR values

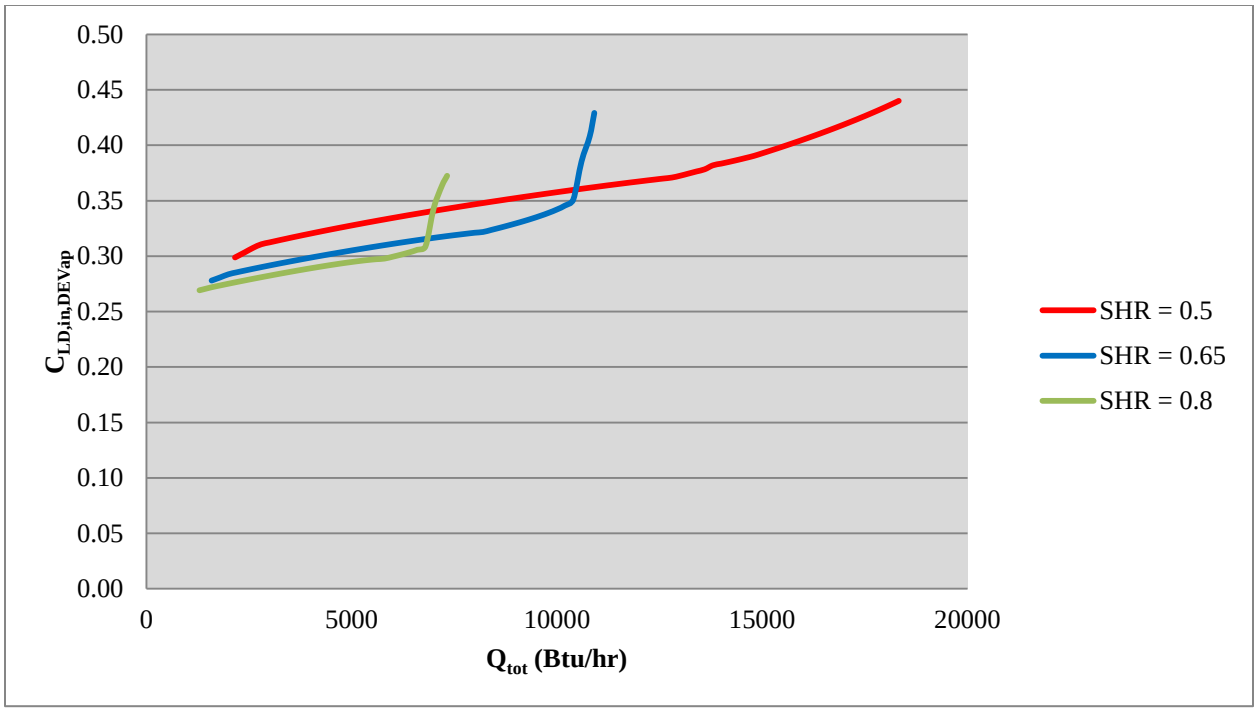

Figure 6.75: Optimal $C_{LD,in,DEVap}$ trends in standard mode for T_{ra} = 75°F, RH_{ra} = 55%, T_{oa} = 90°F, ω_{oa} = 0.0160 kg/kg at variable SHR values

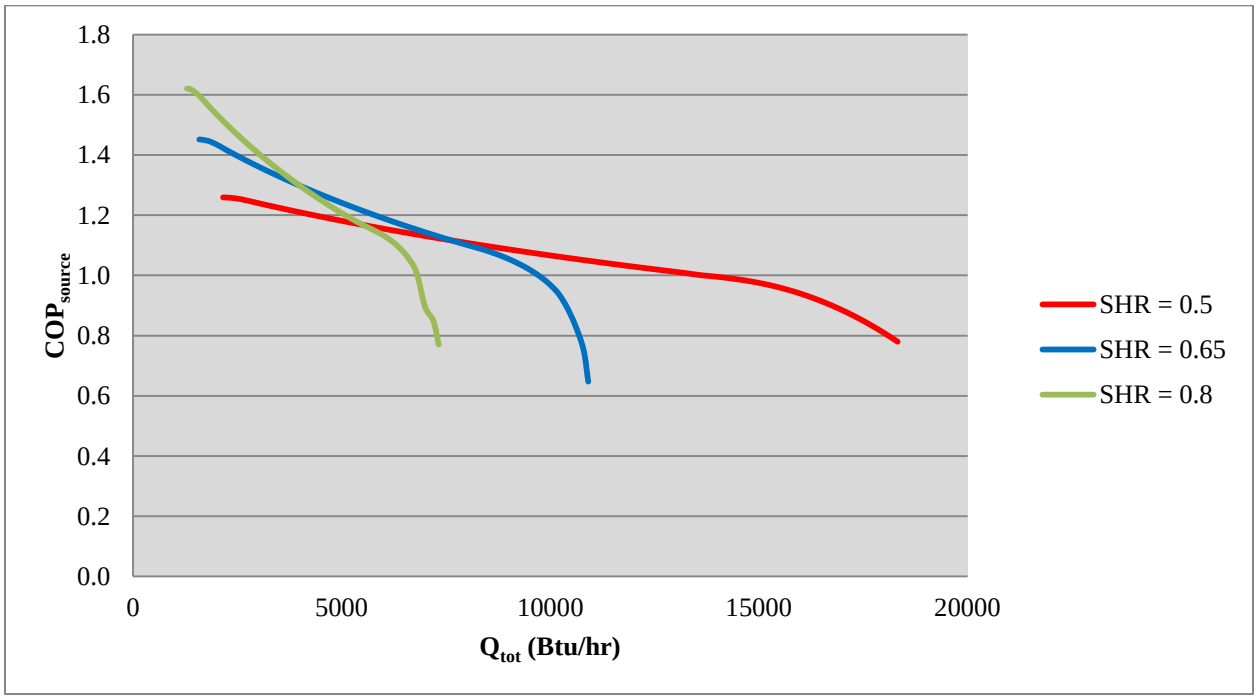

Figure 6.76: Optimal COP_{source} trends in standard mode for T_{ra} = 75°F, RH_{ra} = 55%, T_{oa} = 90°F, ω_{oa} = 0.0160 kg/kg at variable SHR values

From examining Figure 6.72, it is determined that the trend of linearly ramping R_{ma} ratio from 30% to 100% is applicable to all SHR values. Total capacity curves for all SHR values have a long region where R_{ma} ratio is pegged at 100% compared to sensible capacity curves observed in IEC mode, with the relative amount of the total capacity curve that this region occupies ranging from 20% of maximum Q_{tot} at low SHR to 30% of maximum Q_{tot} at high SHR. This indicates that capturing the final optimal trends in the near-optimal strategy for standard mode is important regardless of SHR value.

The majority of the total capacity curve for each SHR value is still occupied by R_{ma} ratio linearly ramping from 30% to 100% as OAF and $C_{LD,in,DEVap}$ remain relatively constant and R_{e1} ratio increases. It should be noted that in general, R_{ma} ratio reaches 100% at lower Q_{tot} values for higher SHR values. This indicates that it is harder for DEVap to simultaneously provide increased sensible cooling and decreased dehumidification. This is explained as follows: increased OAF values are required for higher SHR values in order to provide more second stage cooling. However, this simultaneously results in more siphoning of supply air, reducing the total load that can be provided.

From Figure 6.73, it is determined that the same initial trends observed previously where R_{e1} is initially set to a moderate value and increases linearly occur for all SHR values, although there is a significant reduction in the initial R_{e1} ratio value at the lowest SHR value. This is explained as follows: to maintain a low SHR value, less sensible cooling must be provided. This results in low R_{e1} ratio and OAF values for low SHR values. The significant shift in R_{e1} ratio values between low and moderate SHR values is indicative of a significant shift in the methods that DEVap must employ to provide the correct ratio of sensible and latent cooling. This also explains the significant reduction in OAF value from moderate to low SHR values in Figure 6.74

and the significant increase in $C_{LD,in,DEVap}$ values from moderate to low SHR values in Figure 6.75.

The final trend of sharply decreasing R_{e1} ratio as Q_{tot} approaches its maximum value also applies to higher SHR values. For the lowest SHR value, R_{e1} ratio ends at its maximum value of 70% instead of at a low value. This is explained as follows: for low SHR values, low amounts of sensible cooling are required. Once R_{ma} ratio reaches 100%, the most effective way to maintain low SHR is to slowly increase second stage cooling and dehumidification potential instead of rapidly increase as observed for higher SHR values. This is why OAF values are lower during the final trends for low SHR compared to higher SHR values. This decrease in second stage cooling results in the need for more first stage cooling.

From Figure 6.74, it is determined that OAF values increase as SHR increases, as previously predicted. This is because more sensible cooling is required for higher SHR values, so the amount of second stage cooling provided increases as a result. From Figure 6.75, it is determined that $C_{LD,in,DEVap}$ values decrease as SHR increases, as previously predicted. This is because less latent cooling is required for higher SHR values, so the dehumidification potential provided in the first stage decreases as a result.

From Figure 6.76, it can be determined that the assumption of decreased COP_{source} values for increased SHR values is true for higher Q_{tot} values. However, at lower Q_{tot} values higher COP_{source} values are attained for higher SHR values. This is explained by the trend of low initial OAF and $C_{LD,in,DEVap}$ values associated with low Q_{tot} values, since this results in less siphoning of supply air and increased regenerator performance. Once R_{ma} ratio reaches 100% and both OAF and $C_{LD,in,DEVap}$ begin increasing at higher rates, COP_{source} quickly declines for all SHR values.

All of the air states associated with the trends for each control variable as SHR changes are illustrated on a psychrometric chart in Figure 6.77. As SHR increases, process air exiting the first stage and supply air exiting DEVap become drier due to thereduction in latent cooling.

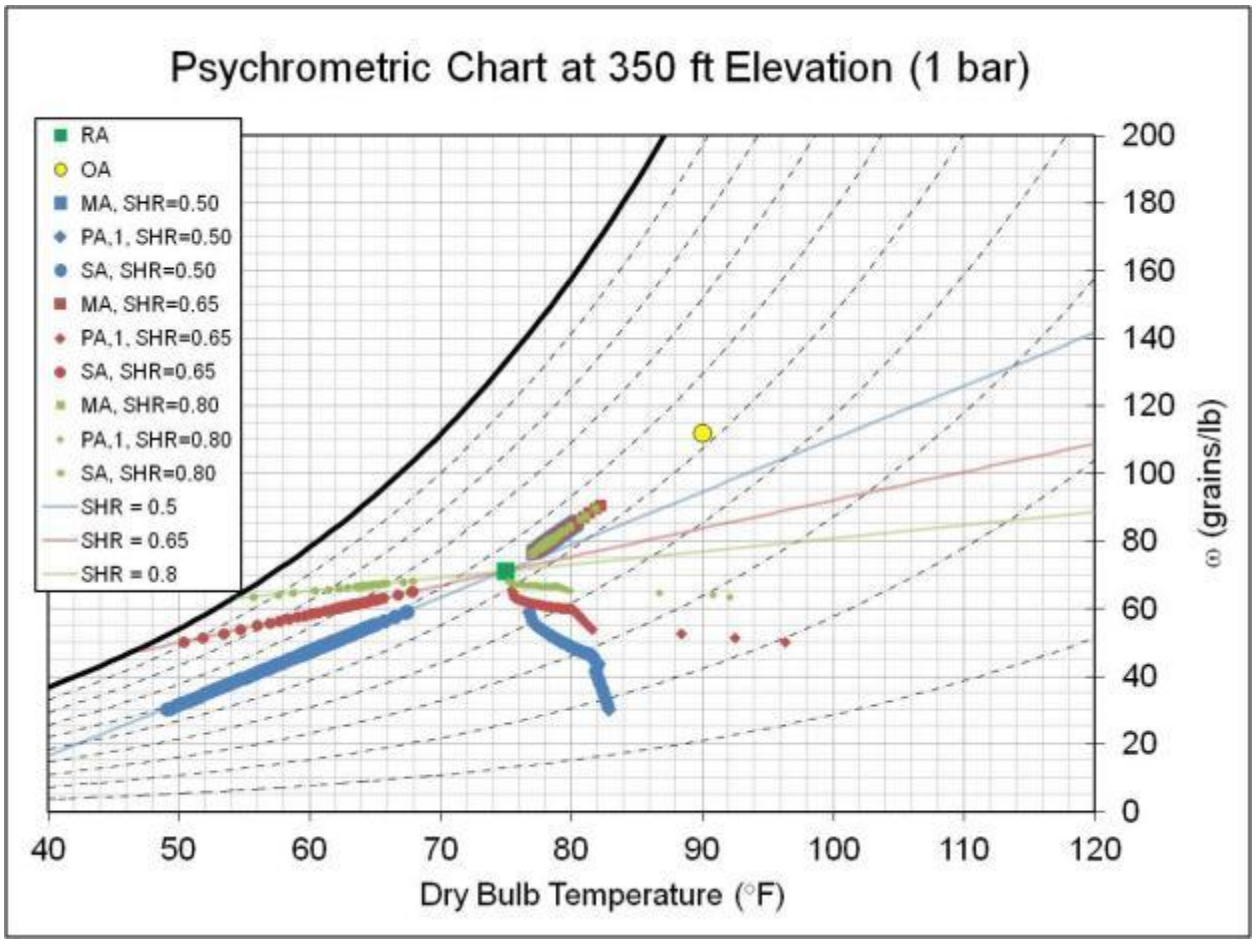

Figure 6.77: Air states for variable SHR values in standard mode

(T_{ra} = 75°F, RH_{ra} = 55%, T_{oa} = 90°F, and ω_{oa} = 0.0160 kg/kg)

6.3.5 Near-optimal Strategy: Ramping Phase

Using the previously discussed logic for near-optimal control strategies from Section 6.1.4, the initial optimal trends of adjusting R_{e1} ratio, OAF, and $C_{LD,in,DEVap}$ while holding R_{ma} ratio to its minimum value can be discarded. This is because this trend accounts for the initial

10% of the total capacity curve, and increasing minimum Q_{tot} can be mitigated through cycling of DEVap. The majority of the total capacity curve is occupied by the "ramping" phase for R_{ma} ratio as it increases from 30% to 100%, which ranges from 60% to 70% of the total capacity curve for low and high SHR values, respectively. The final trend of adjusting R_{e1} ratio, OAF, and $C_{LD,in,DEVap}$ while holding R_{ma} ratio to its maximum value is significant, accounting for 20% to 30% of the total capacity curve for high and low SHR values, respectively. Therefore, the near-optimal strategy for standard mode has the intent of creating a simple method of knowing what values to hold constant for R_{e1} ratio, OAF, and $C_{LD,in,DEVap}$ while R_{ma} ratio ramps from 30% to 100% as well as how to adjust R_{e1} ratio, OAF, and $C_{LD,in,DEVap}$ while maintaining R_{ma} ratio at its maximum value in order to provide higher maximum Q_{tot} values. This section discusses the methods used to develop a near-optimal strategy for the ramping region.

It is important to note that R_{e1} ratio linearly increases as R_{ma} ratio ramps, indicating that both variables can be controlled to "ramp" together. After examining Figure 6.63, R_{e1} ratio displayed the same behavior regardless of return air state where it ramps from an initial value of approximately 35% as R_{ma} ratio begins to increase from 30% and reaches a final value of approximately 60% as R_{ma} ratio reaches its maximum value of 100%. After examining Figure 6.68, the same behavior is observed for outdoor air states that are hotter than return air, which is when DEVap will likely be in operation. After examining Figure 6.73, similar behavior is observed for different SHR. For a high SHR, R_{e1} ratio reaches approximately 50% instead of 60% when R_{ma} ratio reaches 100%. For a low SHR, R_{e1} ratio begins ramping at approximately 30% instead of 35%, but still reaches approximately 60% when R_{ma} ratio reaches 100%. This is regarded as slight deviation from near-optimal ramping strategy for R_{e1} ratio that shouldn't have a large impact on near-optimal performance.

Since the values for OAF and $C_{LD,in,DEVap}$ while R_{ma} ratio ramps are relatively constant, the same near-optimal strategy used for R_{e1} ratio and OAF in IEC mode can be applied again, where the average of all values over the region of the total capacity curve where R_{ma} ratio ramps for each control variable is used as the value to hold constant in the near-optimal strategy. This usually translates to the value for each control variable when R_{ma} ratio = 65%, since there is approximately a linear change in each control variable's value while R_{ma} ratio ramps. These values to hold constant in the near-optimal strategy for standard mode are referred to as $OAF_{near-opt,standard}$ and $C_{LD,in,DEVap,near-opt,standard}$. If $OAF_{near-opt,standard}$ and $C_{LD,in,DEVap,near-opt,standard}$ are plotted for all combinations of return and outdoor air states and SHR values, the most efficient graphing method is to use bar charts to display value for all outdoor air states on a psychrometric chart with varying SHR values, similar to the method used for IEC mode in Figure 6.50 and Figure 6.51. Examples of these charts for a typical operating condition of T_{ra} = 75°F and RH_{ra} = 55% are shown in Figure 6.78 and Figure 6.79. Using this methodology, seven $OAF_{near-opt,standard}$ charts and seven $C_{LD,in,DEVap,near-opt,standard}$ charts are required, one of each for each return air state that was simulated. All of these charts are shown in Appendix C.

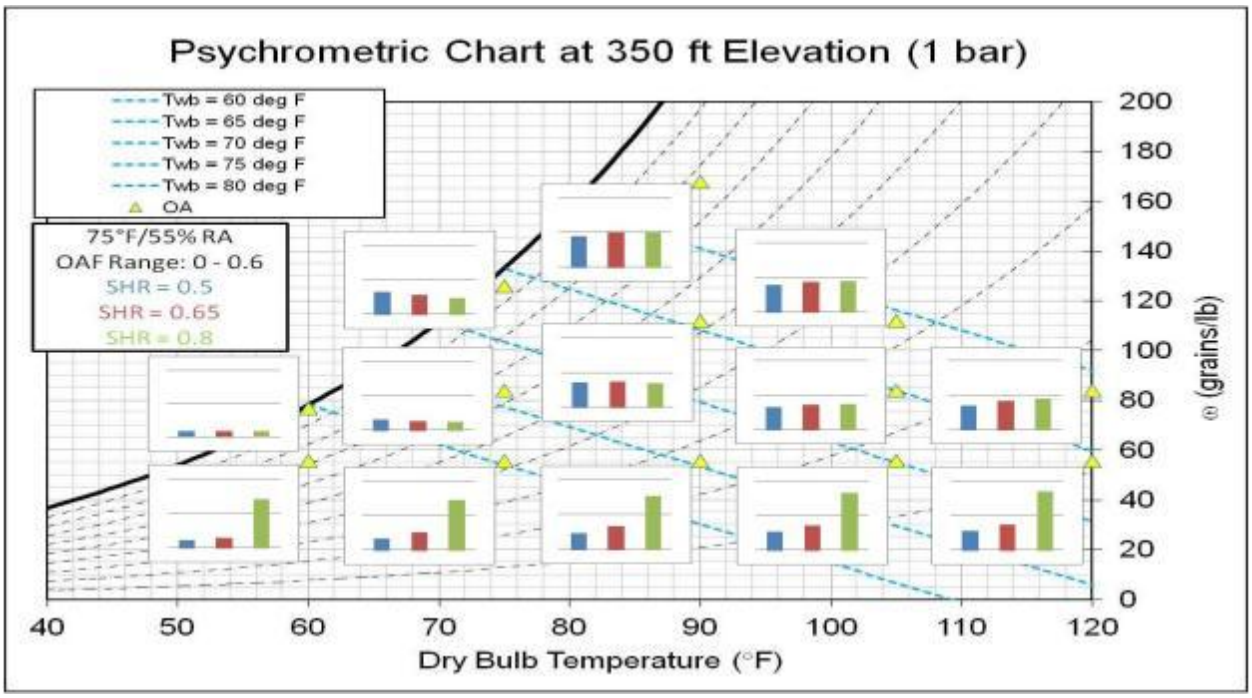

Figure 6.78: Values held constant for $OAF_{near\text{-}opt,standard}$ for T_{ra} = 75°F and RH_{ra} = 55% under variable SHR values and outdoor air states

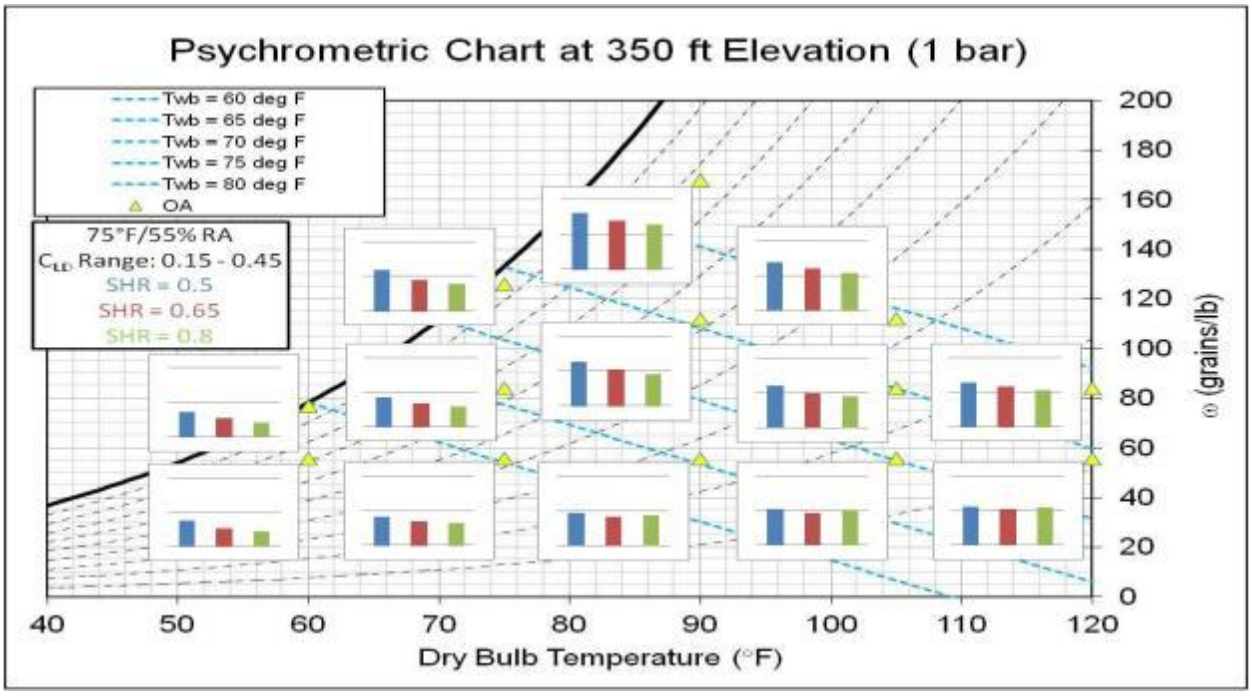

Figure 6.79: Values held constant for $C_{LD,in,DEVap,near\text{-}opt,standard}$ for T_{ra} = 75°F and RH_{ra} = 55% under variable SHR values and outdoor air states

Both of these figures show the inverse relationship between OAF and $C_{LD,in,DEVap}$. As observed earlier in Figure 6.69 and Figure 6.70, $OAF_{near\text{-}opt,standard}$ and $C_{LD,in,DEVap,near\text{-}opt,standard}$ both increase as WB_{oa} increases. They also show that as SHR increases, $OAF_{near\text{-}opt,standard}$ increases for cases where T_{oa} is greater than T_{ra} and $C_{LD,in,DEVap,near\text{-}opt,standard}$ decreases for all cases. However, for high SHR values when outdoor air is hot and dry, $OAF_{near\text{-}opt,standard}$ greatly increases and $C_{LD,in,DEVap,near\text{-}opt,standard}$ reverses trend and slightly increases. A psychrometric chart showing the air states for the three SHR values under this combination of return and outdoor air is shown in Figure 6.80.

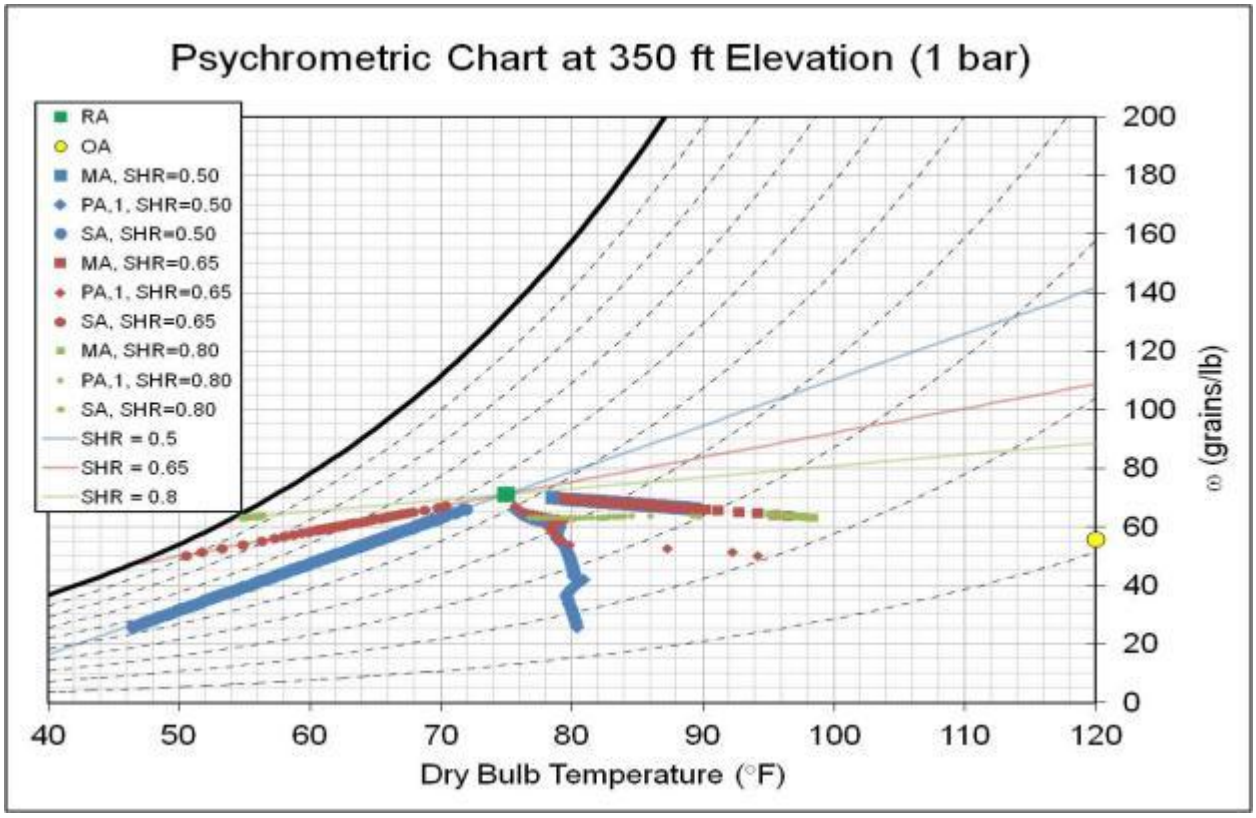

Figure 6.80: Air states for variable SHR values in standard mode

(T_{ra} = 75°F, RH_{ra} = 55%, T_{oa} = 120°F, and ω_{oa} = 0.0080 kg/kg)

From Figure 6.80, it is determined that a high OAF value is required due to the hot and dry outdoor air state that return air is mixing with. Since the mixed air is dry, it will result in dry supply air that serves as an effective evaporative sink in the second stage. This increased second stage cooling potential results in a large temperature difference between process air exiting the first stage and supply air. Since mixed air is so hot and dry, greater dehumidification potential is required and $C_{LD,in,DEVap}$ must increase as a result.

Upon examining the three charts for $OAF_{near\text{-}opt,standard}$ and $C_{LD,in,DEVap,near\text{-}opt,standard}$ for T_{ra} = 80°F found in Appendix C, it is determined that there is little change in both $OAF_{near\text{-}opt,standard}$ and $C_{LD,in,DEVap,near\text{-}opt,standard}$ values as RH_{ra} changes value from 50% to 60%. The same trend is also observed for charts where T_{ra} = 70°F, indicating that both $OAF_{near\text{-}opt,standard}$ and $C_{LD,in,DEVap,near\text{-}opt,standard}$ values are generally insensitive to RH_{ra}.

It is beneficial to condense all of this information such that one chart each for $OAF_{near\text{-}opt,standard}$ and $C_{LD,in,DEVap,near\text{-}opt,standard}$ can represent the seven charts developed for each control variable and simplify near-optimal control. As previously stated, $OAF_{near\text{-}opt,standard}$ and $C_{LD,in,DEVap,near\text{-}opt,standard}$ are generally insensitive to RH_{ra}, so averaging together the three values for T_{ra} = 80°F and T_{ra} = 70°F creates one value to plot for all RH_{ra} values for each temperature that resembles the value for RH_{ra} = 55%. This narrows down the amount of charts for each control variable from seven to three, one for each T_{ra} value. In order to condense information further, the three values for each T_{ra} value are averaged together, resulting in one value to plot for all T_{ra} and RH_{ra} values. From this averaging process, the near-optimal strategy for the ramping phase of standard mode will mimic optimal trends for T_{ra} = 75°F and RH_{ra} = 55%. This is beneficial since these are typical cooling temperature and humidity set points.

The two graphs resulting from the averaging of optimal trends contain all information concerning what values to hold for OAF and $C_{LD,in,DEVap}$ as R_{ma} ratio and R_{e1} ratio proportionally ramp together under all simulated return and outdoor air states and SHR values. If DEVap operates in an outdoor air state and SHR value not shown in these figures, then linear interpolation can be used to determine what values to set for OAF and $C_{LD,in,DEVap}$.

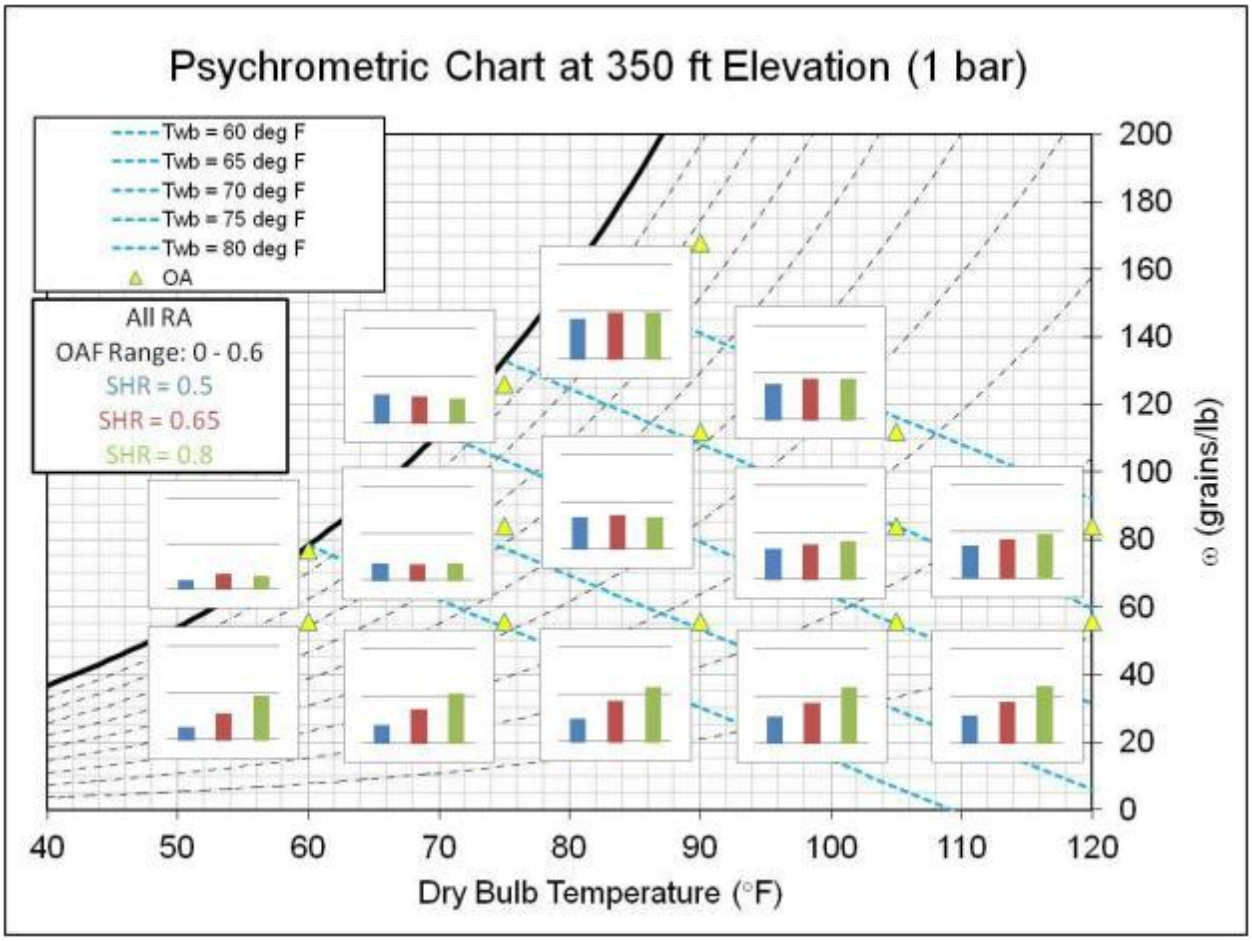

Figure 6.81: Average values held constant for $OAF_{near\text{-}opt,standard}$ across all return air states under variable outdoor air states and SHR values

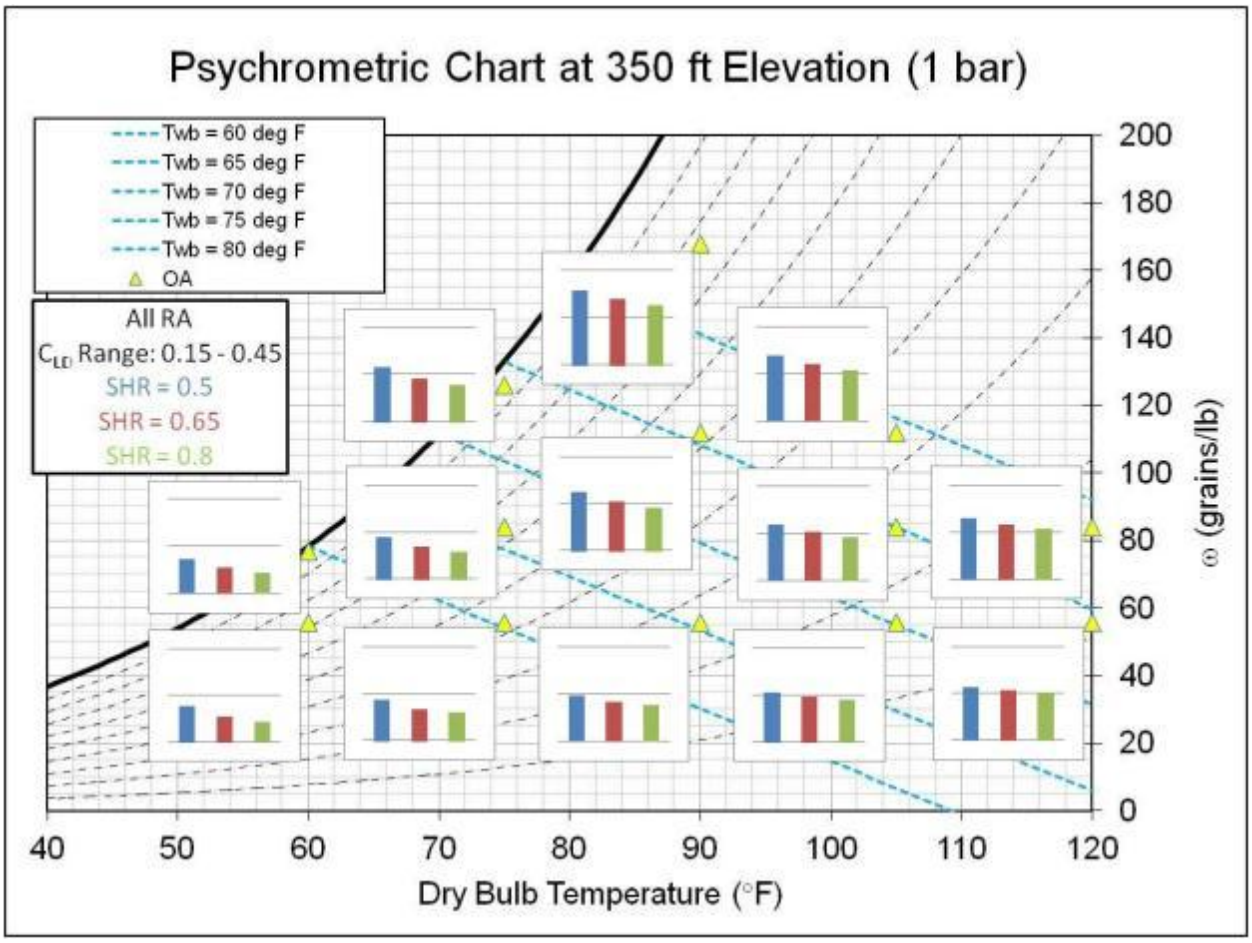

Figure 6.82: Average values held constant for $C_{LD,in,DEVap,near\text{-}opt,standard}$ across all return air states under variable outdoor air states and SHR values

It should be noted that the same trends observed in Figure 6.78 and Figure 6.79 occur in Figure 6.81 and Figure 6.82, indicating a near-optimal strategy that mimics optimal trends. The final near-optimal strategy for the ramping phase of standard mode is outlined as follows:

- Knowing values for T_{oa}, ω_{oa}, and SHR, set OAF and $C_{LD,in,DEVap}$ to values according to Figure 6.81 and Figure 6.82, respectively

- Begin to initially provide Q_{tot} and SHR by setting R_{ma} ratio to 30% and R_{e1} ratio to 35%

- If greater values of Q_{tot} are required, accordingly increase R_{ma} ratio and R_{e1} ratio proportionally so that R_{ma} ratio reaches 100% and R_{e1} ratio reaches 70% simultaneously

- The greatest Q_{tot} that can be provided at the end of this ramping region is achieved when R_{ma} ratio reaches 100% and R_{e1} ratio reaches 70%

An example of how near-optimal values for R_{ma} ratio, R_{e1} ratio, OAF, $C_{LD,in,DEVap}$, $T_{pa,1}$, T_{sa}, and COP_{source} change during the ramping phase as the total cooling capacity increases under the typical standard mode operating condition of T_{ra} = 75°F, RH_{ra} = 55%, T_{oa} = 90°F, and ω_{oa} = 0.0160 kg/kg is shown in Figure 6.83. A psychrometric chart outlining all process air states during near-optimal control of the ramping phase of standard mode for the same return and outdoor air state is shown in Figure 6.84.

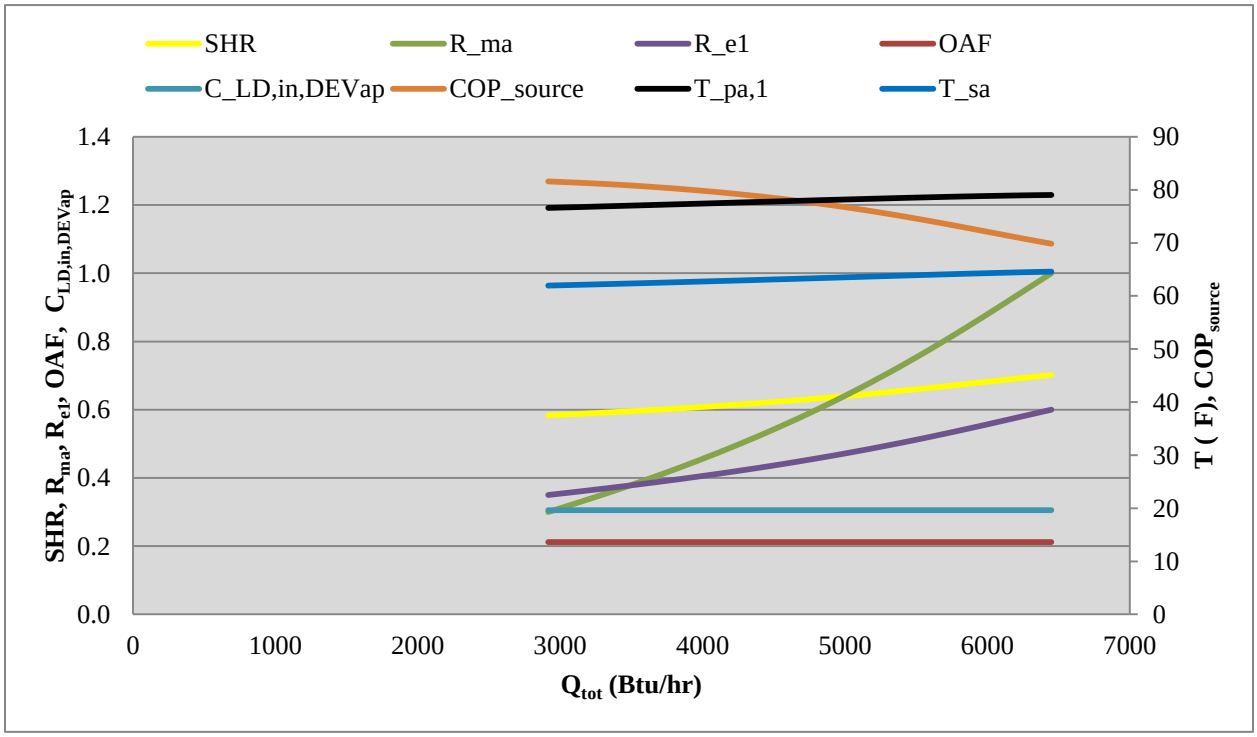

Figure 6.83: Near-optimal control variable trends for T_{ra} = 75°F, RH_{ra} = 55%, T_{oa} = 90°F, and ω_{oa} = 0.0054 kg/kg in standard mode

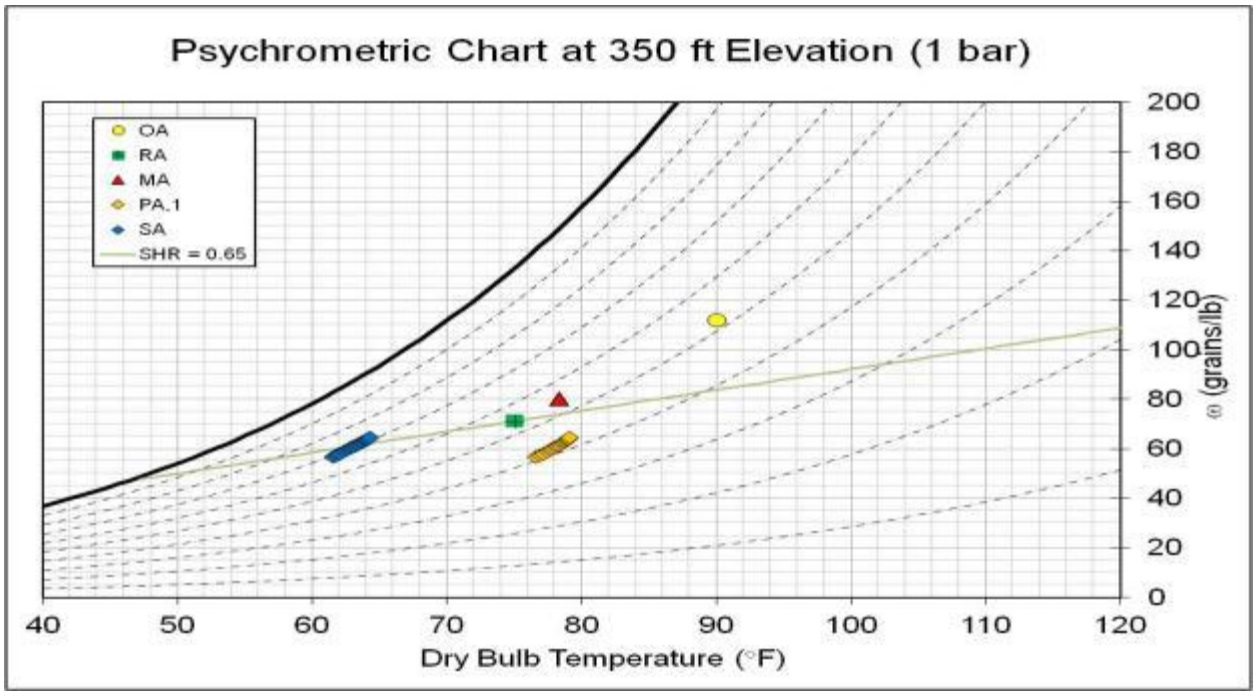

Figure 6.84: Near-optimal air states for T_{ra} = 75°F, RH_{ra} = 55%, T_{oa} = 90°F, and ω_{oa} = 0.0054 kg/kg in standard mode

It is important to illustrate that if a control strategy is simultaneously applied to R_{e1} ratio, OAF and $C_{LD,in,DEVap}$, DEVap can change Q_{tot} values by adjusting R_{ma} ratio but is forced to provide a specific SHR value different from the intended value. This is explained by the degrees of freedom explained in Section 5.4 for standard mode. Since there are only two degrees of freedom, setting three out of the four control variables forces one of the constraints to no longer be met. This is illustrated by the variable SHR values witnessed in both Figure 6.83 and Figure 6.84. For this reason, a near-optimal strategy during the ramping phase of R_{ma} ratio must set a combination of two control variables. To determine the best option, a sensitivity analysis is conducted. This sensitivity analysis is explained in the following section.

6.3.6 Sensitivity Analysis of Near-optimal Performance in Ramping Phase

In order to analyze the performance of the near-optimal strategy for standard mode, the Solver tool must be used in a similar fashion as the optimization process described in Chapter 5. The difference is that for this analysis, either OAF or $C_{LD,in,DEVap}$ can be set to values according to Figure 6.81 and Figure 6.82, respectively, or R_{e1} ratio can be forced to proportionally ramp with R_{ma} ratio. As explained earlier, two of these three control variables must be set, which leaves no degrees of freedom for the Solver tool in Excel to set the value of Q_{tot} and SHR provided using a specific combination of R_{ma} ra and the third control variable that was allowed to float. Using Solver allows for Q_{tot} to incrementally increase in the same manner as described in Chapter 5, which allows for a comparison of COP_{source} values between optimal control and near-optimal control at equal Q_{tot} values.

A sensitivity analysis is required in order to determine which of the three possible combinations of two control variables results in the least impact on both COP_{source} and maximum Q_{tot}. A sensitivity analysis is also required to determine how well the near-optimal strategy for standard mode applies to different outdoor air states and SHR values. It should be noted that since two control variables have a control strategy applied to them, the third control variable that is allowed to float potentially has values that follow different trends from those witnessed earlier. The return and outdoor air states used in this sensitivity analysis are shown on a psychrometric chart in Figure 6.85.

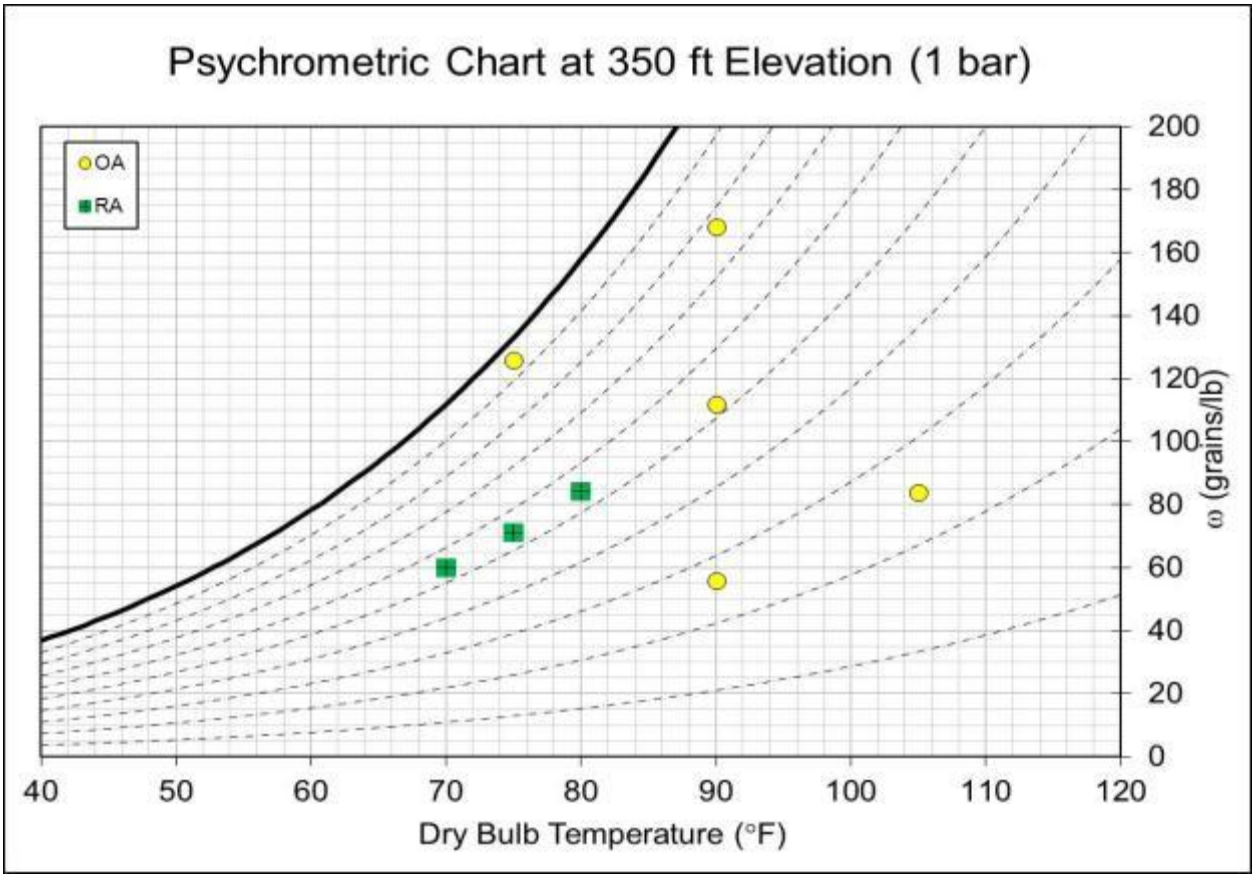

Figure 6.85: Return and outdoor air states used in sensitivity analysis of near-optimal control of ramping phase in standard mode

These return and outdoor air states were chosen because they encompass the typical operating conditions of standard mode (T_{ra} = 75°F, RH_{ra} = 55%, T_{oa} = 90°F, and ω_{oa} = 0.0160 kg/kg), as well as allowing for a sensitivity analysis of both temperature and humidity values for outdoor air. Only temperature values vary for return air since only RH_{ra} = 55% was simulated during the optimization process for T_{ra} = 75°F. The metric chosen to illustrate the reduction in COP_{source} as a result of near-optimal control is $\%\Delta COP_{avg}$, as defined by Equation 6.15 in Section 6.2.5. Calculated values of $\%\Delta COP_{avg}$ for all combinations of return and outdoor air states from Figure 6.85 and SHR = 0.65 are shown in Figure 6.86.

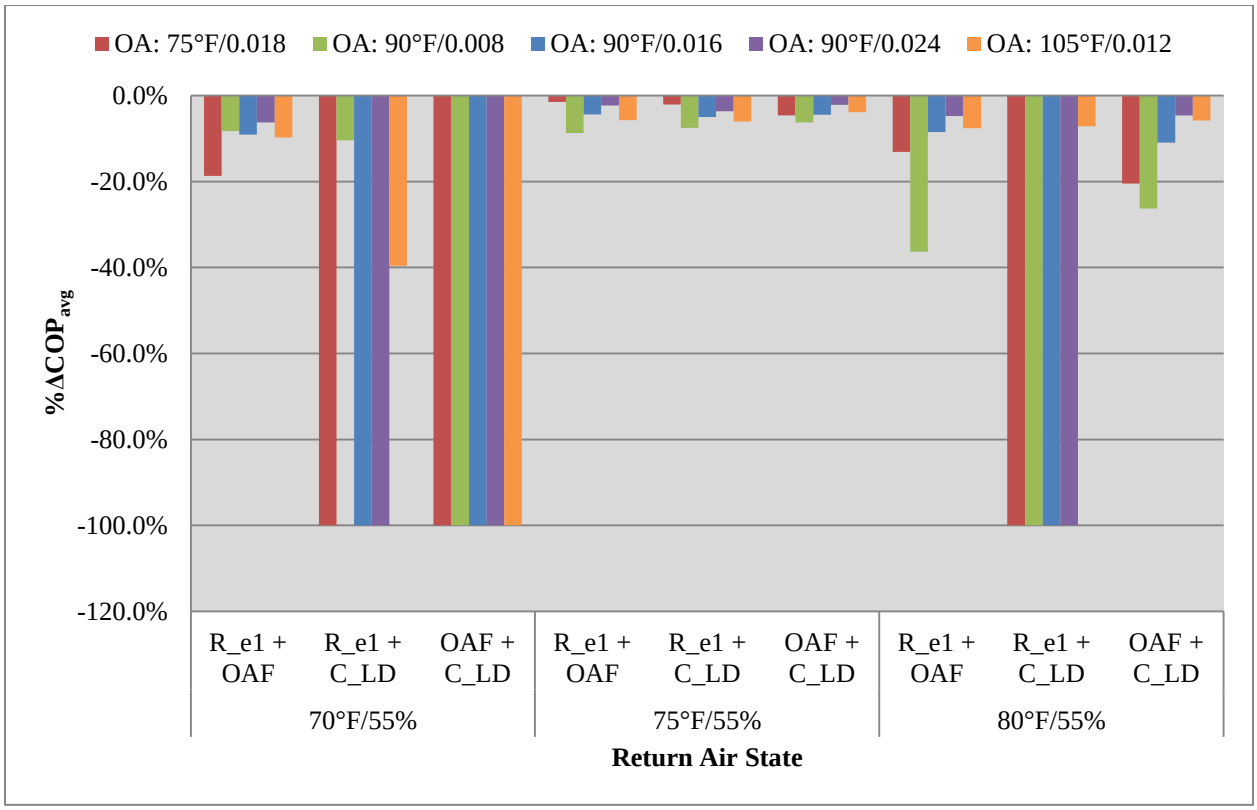

Figure 6.86: Sensitivity analysis results for $\%\Delta COP_{avg}$ between optimal and near-optimal control of ramping phase in standard mode for SHR = 0.65

In Figure 6.86, (R_e1 + OAF) represents a simulation where both R_{e1} ratio and OAF values are controlled together. Also, a value of 100% indicates that a simulation yielded no possible combinations of control variables that could attain the desired SHR value. With this information, it is determined from Figure 6.86 that the near-optimal control strategy where both R_{e1} ratio and OAF values are controlled together is the best option for the ramping phase of standard mode. This is because the other two options cannot attain the desired SHR value as often for T_{ra} values other than 75°F. When T_{ra} = 75°F, the strategy where both OAF and $C_{LD,in,DEVap}$ values are controlled together performs slightly better for most outdoor air states compared to the strategy of controlling R_{e1} ratio and OAF together. However, this slightly increased performance cannot overcome the fact that this strategy cannot attain SHR = 0.65 for

any outdoor air states when T_{ra} = 70°F. Similar results are observed when SHR is set to 0.5 and 0.8, as shown in Appendix C.

Lower $\%\Delta COP_{avg}$ values occur for T_{ra} = 75°F because the near-optimal strategy was developed in a way that mimicked optimal behavior when T_{ra} = 75°F. As stated previously, the average of the $OAF_{near\text{-}opt,standard}$ and $C_{LD,in,DEVap,near\text{-}opt,standard}$ values for the three different T_{ra} values will be nearly identical to the $OAF_{near\text{-}opt,standard}$ and $C_{LD,in,DEVap,opt,standard}$ values for T_{ra} = 75°F, since there is a small linear change in these values as T_{ra} increases from 70°F to 80°F. This also explains why higher $\%\Delta COP_{avg}$ values occur for T_{ra} = 80°F and T_{ra} = 70°F. This is not problematic, however, since DEVap is much more likely to operate when return air temperature reaches a typical cooling set point of 75°F with small deadband variation.

Another impact of the near-optimal strategy that usually requires analysis is the reduction in maximum Q_{tot} provided. However, since the maximum Q_{tot} is achieved in the final phase of the near-optimal strategy, this is not a concern for the ramping phase. Control variable values will linearly change from the values they end at in the ramping phase to the values determined to yield maximum Q_{tot}. The methods used to determine a near-optimal strategy to set control variables to these final values are discussed in the following section.

6.3.7 Near-optimal Strategy: Final Phase

Now that a near-optimal strategy has been developed for the ramping phase of standard mode, the next step is to develop a near-optimal strategy for the final phase of standard mode where high Q_{tot} values are achieved. During this phase of standard mode, R_{ma} ratio is pegged at 100% and the only way to provide greater values of Q_{tot} is to adjust the other three control variables: R_{e1} ratio, OAF, and $C_{LD,in,DEVap}$. All that the near-optimal strategy needs to achieve for

this phase of standard mode is replicate the final values observed for each control variable from where maximum Q_{tot} is achieved from the optimal simulations. The final values for each of these control variables are referred to as R_{e1last}, OAF_{last}, and $C_{LD,in,DEVap,last}$. DEVap will linearly change control variable values from values used at the end of the near-optimal ramping phase to these final values for each variable. This means that OAF will linearly change from $OAF_{near-opt,standard}$ to OAF_{last}, $C_{LD,in,DEVap}$ will linearly change from $C_{LD,in,DEVap,near-opt,standard}$ to $C_{LD,in,DEVap,last}$, and R_{e1} ratio will linearly change from 60% to R_{e1last}.

The same strategy of plotting bar graphs onto a psychrometric chart used for Figure 6.78 can be applied again, except now bars show final control variable values for each SHR value instead of average values. Three of these charts are generated for each return air state simulated, one for each control variable that can be adjusted. Examples of these charts for a typical operating condition of T_{ra} = 75°F and RH_{ra} = 55% are shown in Figure 6.87, Figure 6.88, and Figure 6.89. Using this methodology, a total of 21 charts are required: three for each control variable and seven of each for each return air state that was simulated. All of these charts are shown in Appendix C.

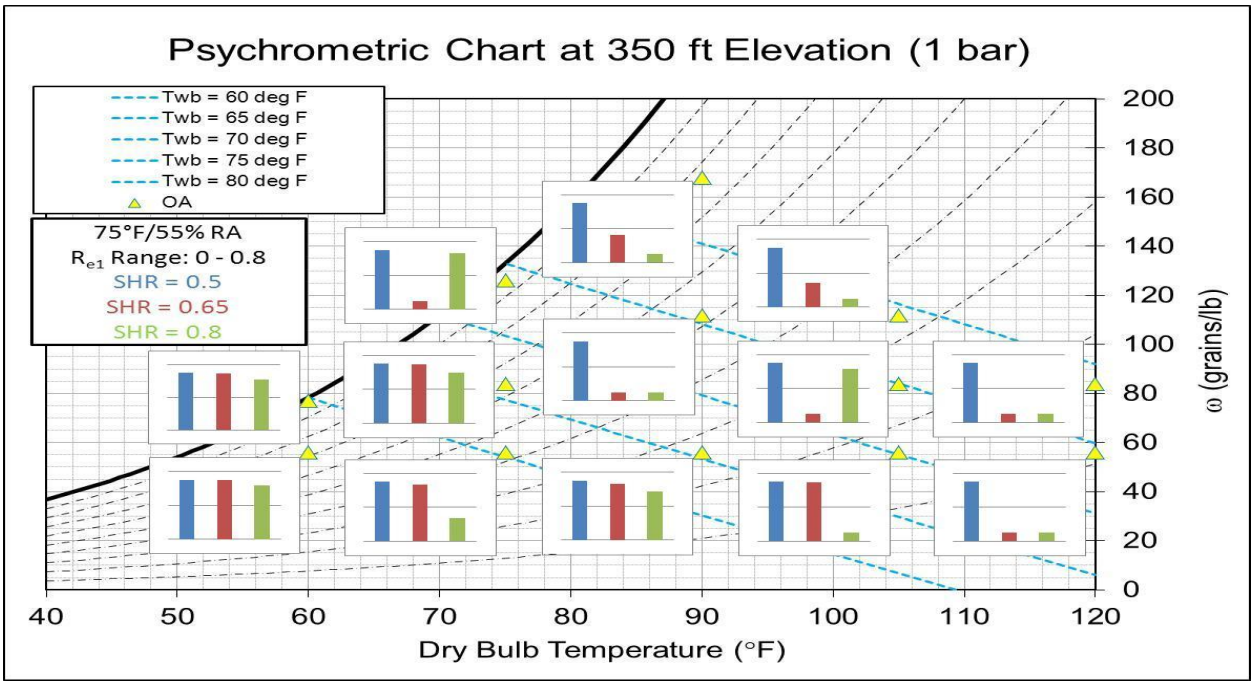

Figure 6.87: $R_{e1,last}$ values for T_{ra} = 75°F and RH_{ra} = 55% under variable SHR values and outdoor air states

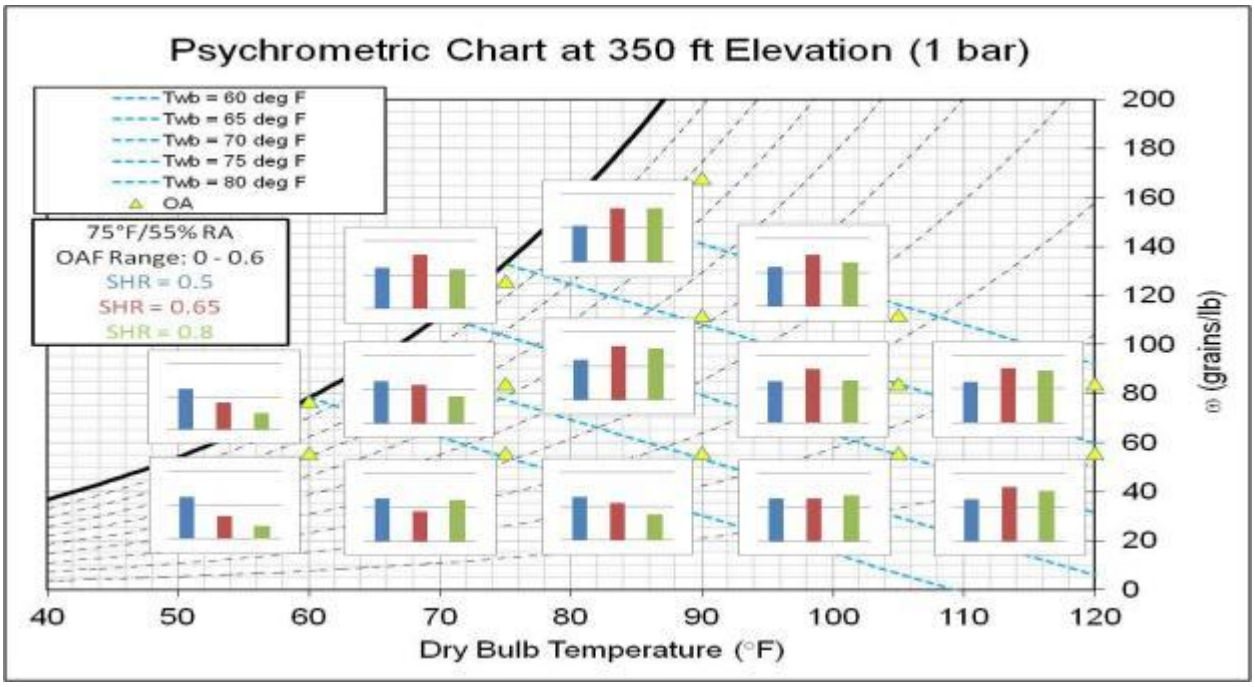

Figure 6.88: OAF_{last} values for T_{ra} = 75°F and RH_{ra} = 55% under variable SHR values and outdoor air states

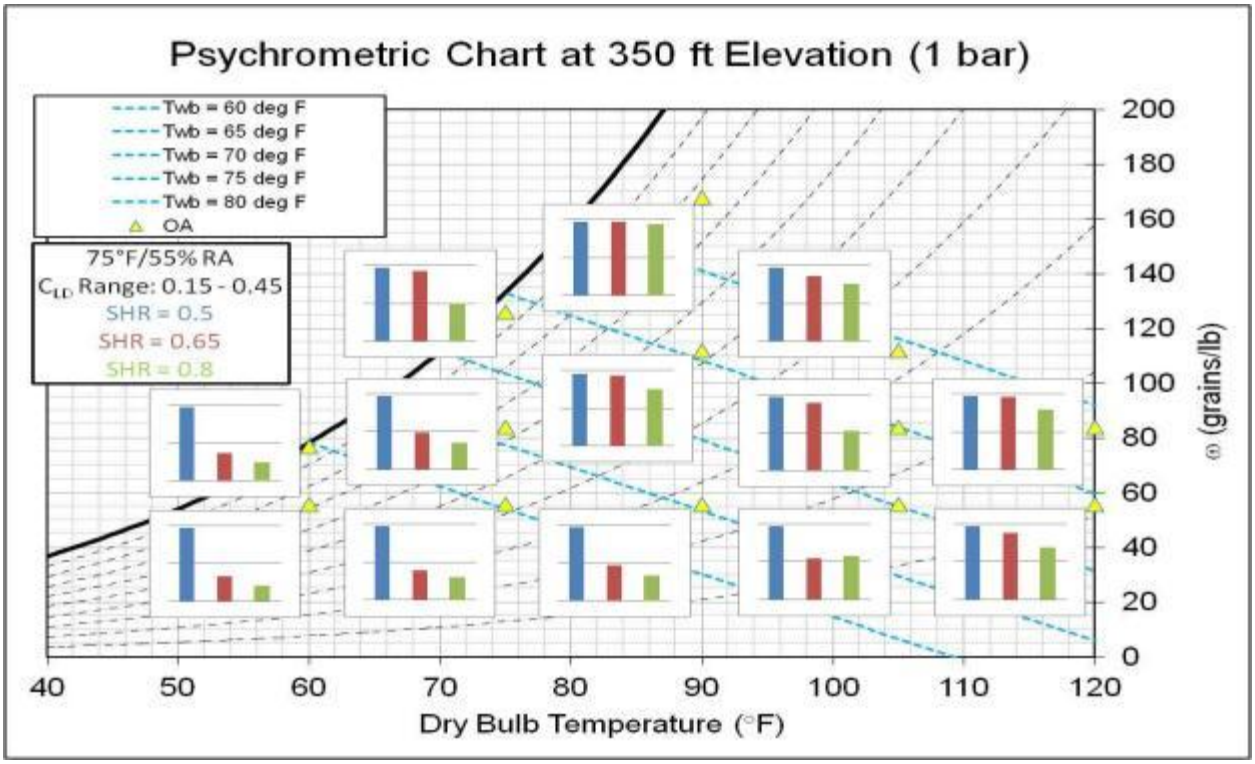

Figure 6.89: $C_{LD,in,DEVap,last}$ values for T_{ra} = 75°F and RH_{ra} = 55% under variable SHR values and outdoor air states

From Figure 6.87, it is determined that R_{e1last} is generally either at its maximum or minimum value when achieving maximum Q_{tot}. In cases where R_{e1last} is low, OAF_{last} is high and vice versa. This signifies that to provide high amounts of cooling, the exhaust stream that will provide more efficient evaporative cooling should be used as much as possible. As SHR increases, $C_{LD,in,DEVap,last}$ decreases due to the reduced need for dehumidification.

If the same strategy of averaging together the three last values for T_{ra} = 80°F and T_{ra} = 70°F, then 21 charts is narrowed down to 9 charts: one chart for each T_{ra} value simulated, three of each for each control variable. The last values for each control variable can then be averaged together again, condensing all information into one chart for each control variable. From this averaging process, the near-optimal strategy for the final phase of standard mode will

mimic optimal trends for T_{ra} = 75°F and RH_{ra} = 55%. This is beneficial since these are typical cooling temperature and humidity set points.

The three graphs resulting from the averaging of optimal trends contain all information concerning what final values to set for R_{e1} ratio, OAF, and $C_{LD,in,DEVap}$ in order to provide maximum Q_{tot} when R_{ma} ratio is at its maximum value under all simulated return and outdoor air states and SHR values. If DEVap operates in an outdoor air state and SHR value not shown in these figures, then linear interpolation can be used to determine what values to set for each control variable.

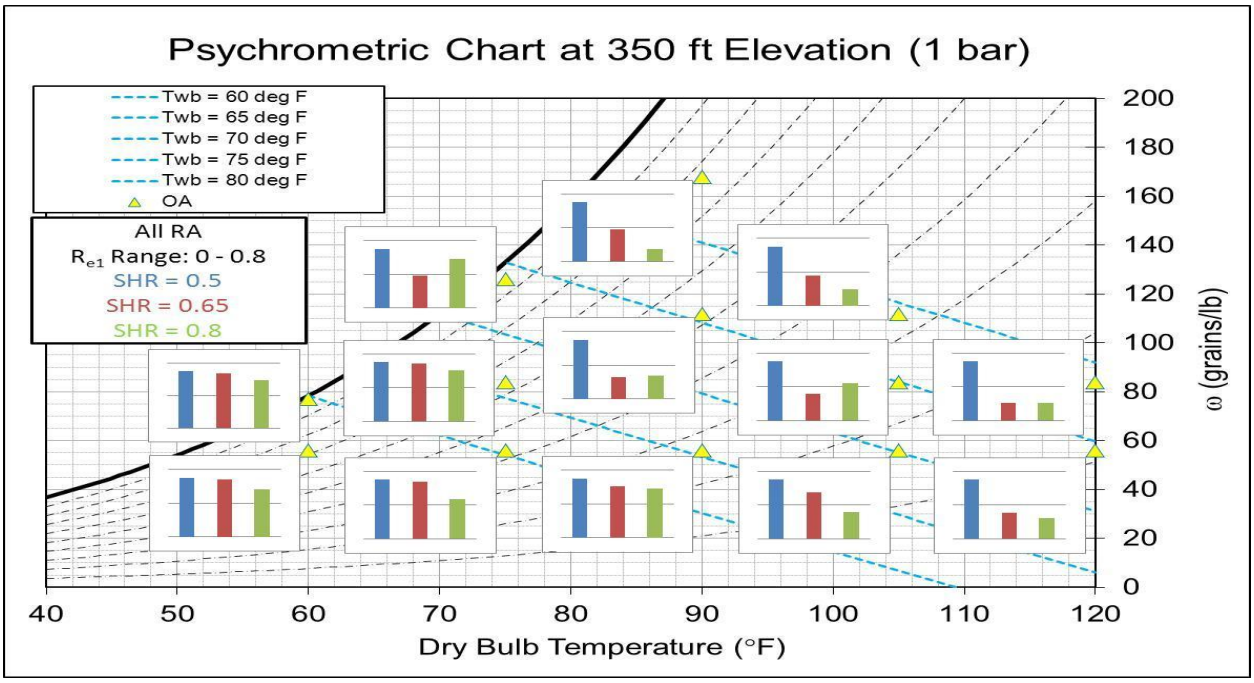

Figure 6.90: Average $R_{e1,last}$ values for all return air states under variable SHR values and outdoor air states

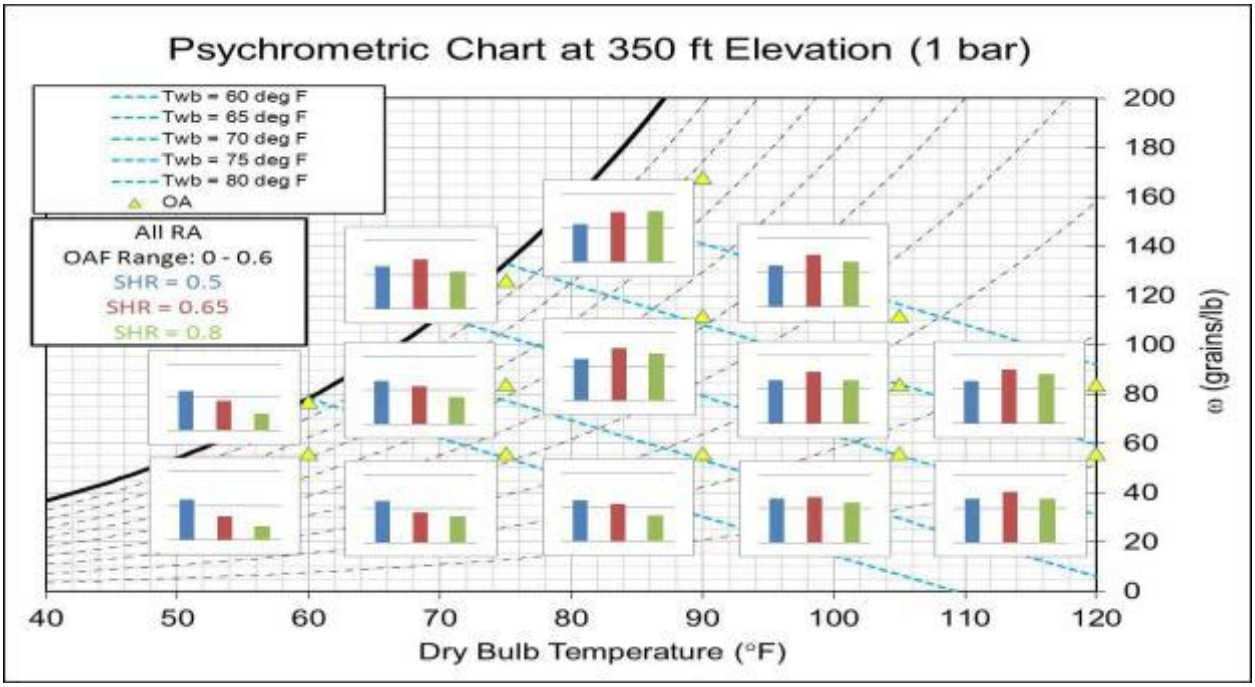

Figure 6.91: Average OAF_{last} values for all return air states under variable SHR values and outdoor air states

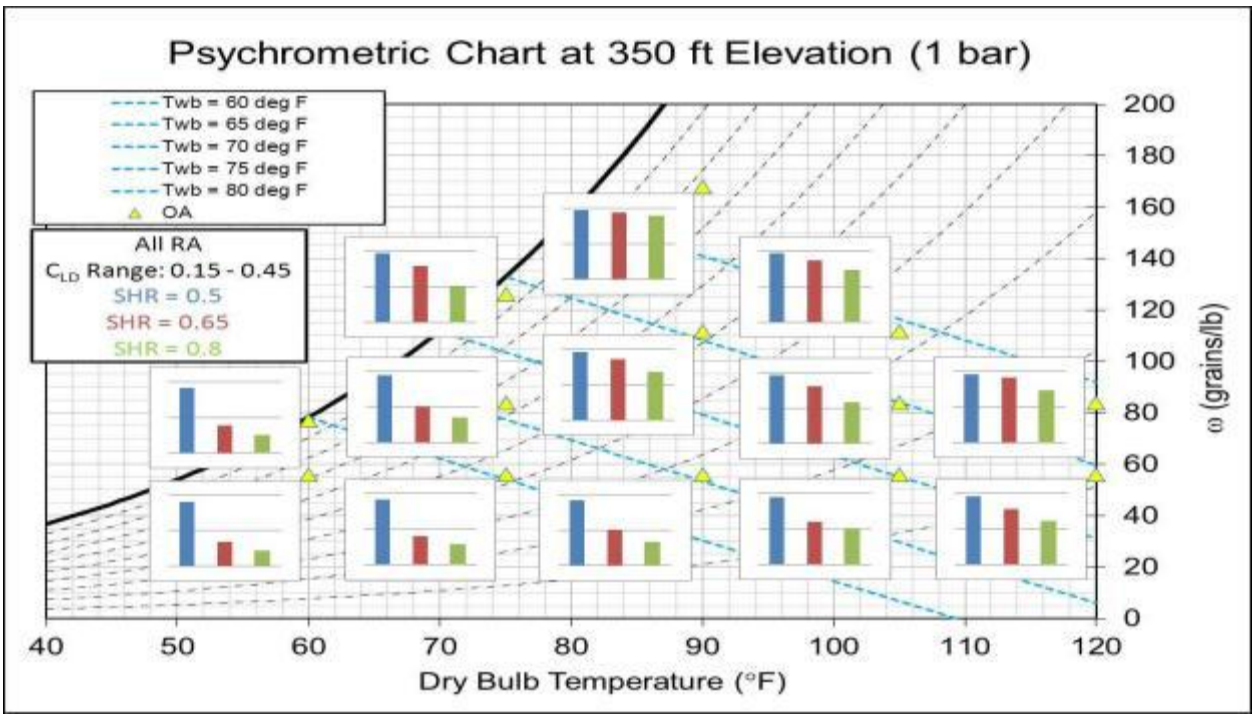

Figure 6.92: Average $C_{LD,in,DEVap,last}$ values for all return air states under variable SHR values and outdoor air states

It should be noted that the same trends observed in Figure 6.87, Figure 6.88, and Figure 6.89 occur in Figure 6.90, Figure 6.91, and Figure 6.92, indicating a near-optimal strategy that mimics optimal trends during the final phase of standard mode. The near-optimal strategy for the final phase of standard mode is outlined as follows:

- R_{e1} ratio, OAF, and $C_{LD,in,DEVap}$ will initially be set to 60%, $OAF_{near\text{-}opt,standard}$, and $C_{LD,in,DEVap,near\text{-}opt,standard}$, respectively, since the final phase begins at the end of the ramping phase

- Knowing values for T_{oa}, ω_{oa}, and SHR, set R_{e1last}, OAF_{last}, and $C_{LD,in,DEVap,last}$ to values according to Figure 6.90, Figure 6.91, and Figure 6.92, respectively

- Linearly change all three control variables from their initial value to their last value while keeping R_{ma} ratio at 100%

- The greatest Q_{tot} that can be provided at the end of this final phase is achieved when all control variables reach their final value

It is important to illustrate that if a control strategy is applied to R_{e1} ratio, OAF and $C_{LD,in,DEVap}$ at the same time, DEVap cannot adjust R_{ma} ratio since it is pegged at 100% during the final phase. In order for Solver to have two degrees of freedom and provide specific Q_{tot} and SHR values while maximizing COP_{source}, only one of the three control variables can be fixed. This allows for the other two control variables to float. For this reason, a near-optimal strategy during the final phase of standard mode where R_{ma} ratio is pegged at 100% must set one control variable. To determine the best option, a sensitivity analysis is conducted and explained in the following section.

6.3.8 Sensitivity Analysis of Near-optimal Performance in Final Phase

In order to analyze the performance of the near-optimal strategy for standard mode, the Solver tool must be used in a similar fashion as the optimization process described in Chapter 5. The difference is that for this analysis, R_{ma} ratio is fixed at 100% and one R_{e1} ratio, OAF, or $C_{LD,in,DEVap}$ can be set to values according to Figure 6.90, Figure 6.91, or Figure 6.92, respectively. As explained earlier, one of these three control variables must be set, which leaves no degrees of freedom for the Solver tool in Excel to set the value of Q_{tot} and SHR provided using a specific combination of the two control variables that are allowed to float. Using Solver allows for determining the combination of control variables that maximizes Q_{tot} and provides the desired SHR value.

A sensitivity analysis is required in order to determine which of the three control variables results in the least impact on maximum Q_{tot} when set to its respective last value. A sensitivity analysis is also required to determine how well the near-optimal strategy for standard mode applies to different outdoor air states and SHR values. The return and outdoor air states used in this sensitivity analysis are the same as those in Figure 6.85. The metric used to describe the impact on maximum Q_{tot} provided is $\%\Delta Q_{tot,max}$, the same metric used in Section 6.2.5 and defined using Equation 6.16. It should be noted that $\%\Delta Q_{tot,max}$ can be negative or positive depending upon the last values of control variables, since the maximum Q_{tot} provided by the near-optimal strategy could be greater than in optimal control. However, this greater maximum Q_{tot} is assured to come at a penalty on COP_{source}. Calculated values of $\%\Delta Q_{tot,max}$ for all combinations of return and outdoor air states and SHR = 0.65 are shown in Figure 6.93.

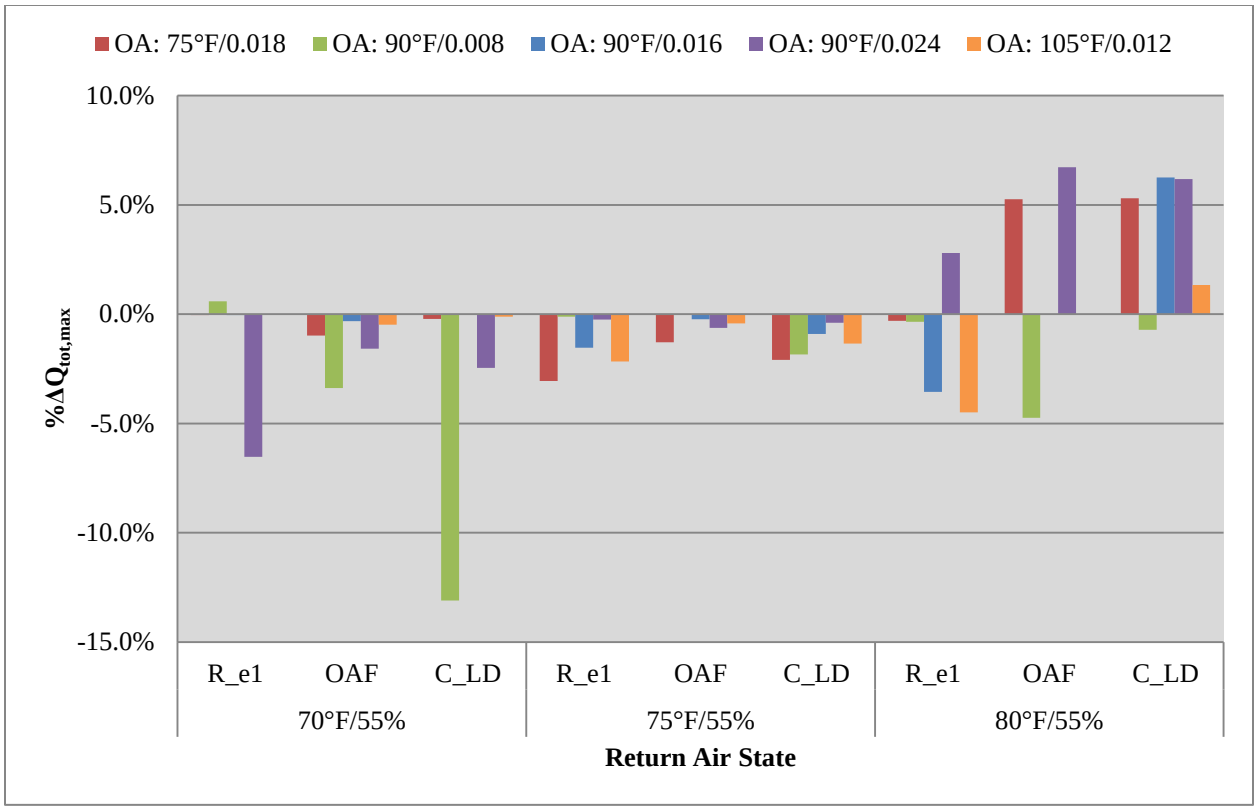

Figure 6.93: Sensitivity analysis results for $\%\Delta Q_{tot,max}$ between optimal and near-optimal control of final phase in standard mode for SHR = 0.65

In Figure 6.93, R_e1 signifies a simulation where R_{e1} ratio is set to its last value according to Figure 6.90 and OAF and $C_{LD,in,DEVap}$ are allowed to float in order to maximize Q_{tot} and provide the desired SHR value. Also, a value of zero indicates that a simulation yielded no possible combinations of control variables that could attain the desired SHR value. With this information, it is determined from Figure 6.93 that the near-optimal control strategy developed for the final phase of standard mode should set OAF to its last value. This is because doing so results in the smallest penalty for maximum Q_{tot} achieved, or a gain in maximum Q_{tot} in some cases. Setting OAF to its last value also results in being able to provide the desired SHR values in more combinations of return and outdoor air states then setting one of the other two control

variables to its respective last value. Similar results are observed when SHR is set to 0.5 and 0.8, as shown in Appendix C.

Now that the near-optimal strategy for both the ramping phase and final phase of standard mode operation is determined, the final near-optimal strategy for operation of standard mode is as follows:

- Knowing values for T_{oa}, ω_{oa}, and SHR, set OAF to $OAF_{near\text{-}opt,standard}$ according to Figure 6.81
- Begin to initially provide Q_{tot} and SHR by setting R_{ma} ratio to 30%, R_{e1} ratio to 35%, and $C_{LD,in,DEVap}$ to the appropriate value
- If greater values of Q_{tot} are required, accordingly increase R_{ma} ratio and R_{e1} ratio proportionally so that R_{ma} ratio reaches 100% and R_{e1} ratio reaches 70% simultaneously. $C_{LD,in,DEVap}$ is allowed to float in order to provide the desired SHR
- The greatest Q_{tot} that can be provided at the end of this ramping region is achieved when R_{ma} ratio reaches 100% and R_{e1} ratio reaches 60%
- Knowing values for T_{oa}, ω_{oa}, and SHR, set OAF_{last} according to Figure 6.91
- Linearly change OAF from $OAF_{near\text{-}opt,standard}$ to OAF_{last} while keeping R_{ma} ratio at 100%. R_{e1} ratio and $C_{LD,in,DEVap}$ are allowed to float in order to provide the desired SHR
- The greatest Q_{tot} that can be provided is achieved at the end of this final phase when OAF reaches OAF_{last}

6.4 Implementation of Control Strategy

During building operation, the cooling load required is never known. Instead, a building operator knows that cooling is required whenever set points are reached and that the amount of cooling increases as return air temperature or humidity increases past its respective set point. Using this knowledge, a general method of incorporating temperature and humidity set points (T_{set} and RH_{set}, respectively) to apply the near-optimal control strategy developed for each of DEVap's modes of operation is analyzed. It is assumed that T_{ra} and RH_{ra} will be kept below 76°F and 55%, respectively, during building operation.

6.4.1 Dehumidification Mode

In dehumidification mode, a humidity set point is met while a temperature set point is not met. Furthermore, the near-optimal strategy developed for dehumidification mode in Section 6.1.4 can be divided into two sections: one where $C_{LD,in,DEVap}$ is held to 37% while R_{ma} ratio ramps, and one where $C_{LD,in,DEVap}$ ramps to 44% while R_{ma} ratio is at its maximum value. Using the same humidity set point and similar proportional control logic found in the original DEVap study [3], the following implementation method is proposed:

- Dehumidification mode initially turns on when $RH_{ra} \geq RH_{set} = 54\%$ and $T_{ra} < T_{set} = 74°F$. At this point, $C_{LD,in,DEVap}$ is set to 37% while R_{ma} is set to 30%

- If RH_{ra} increases, linearly increase R_{ma} such that it reaches 100% when RH_{ra} reaches 55%

- If RH still increases, linearly increase $C_{LD,in,DEVap}$ such that it reaches 44% when RH_{ra} reaches 56%

This implementation method for dehumidification mode is illustrated in Figure 6.94.

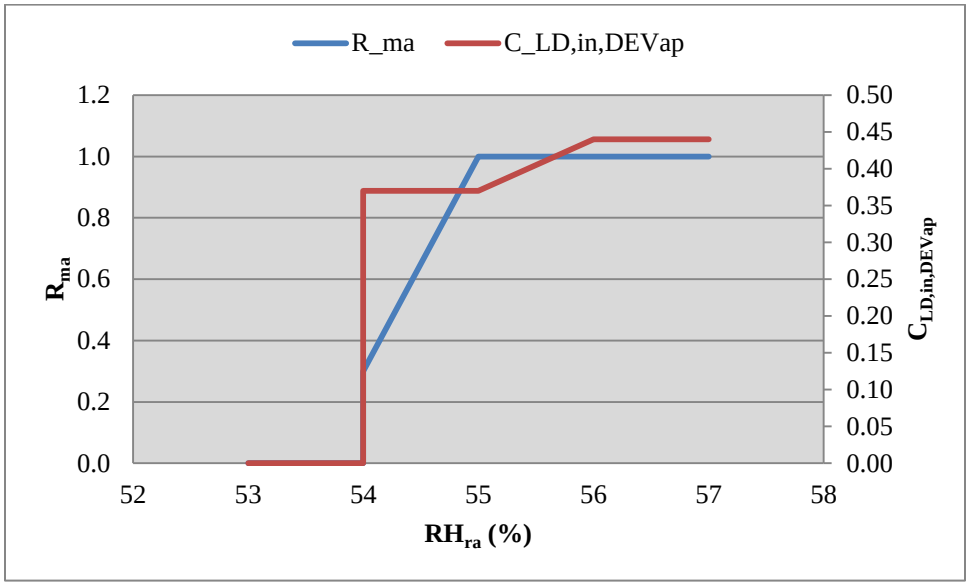

Figure 6.94: Proposed implementation of dehumidification mode

6.4.2 Indirect Evaporative Cooling Mode

In IEC mode, a temperature set point is met while a humidity set point is not met. Furthermore, the near-optimal strategy developed for IEC mode in Section 6.2.4 is composed of one trend where R_{e1} ratio and OAF are held to constant values depending upon RH_{ra} and outdoor air state while R_{ma} ratio ramps. Using the same temperature set point and similar proportional control logic found in the original DEVap study [3], the following implementation method is proposed:

- IEC mode initially turns on when $T_{ra} \geq T_{set} = 74°F$ and $RH_{ra} < RH_{set} = 54\%$. At this point, R_{e1} ratio and OAF are set to values according to Figure 6.52 and Figure 6.53, respectively, while R_{ma} is initially set to 30%

- If T_{ra} increases, linearly increase R_{ma} such that it reaches 100% when T_{ra} reaches 76°F

IEC mode should be used when outdoor air is sufficiently dry, such as when ω_{oa} is at or below 0.0120. This ensures effective use of evaporative cooling. If outdoor air is more humid, low amounts of dehumidification in standard mode will be provided regardless of whether RH_{ra} is at or above RH_{set}. This implementation method for IEC mode is illustrated in Figure 6.95. The actual values to hold constant for R_{e1} ratio and OAF will depend upon RH_{ra} and outdoor air state.

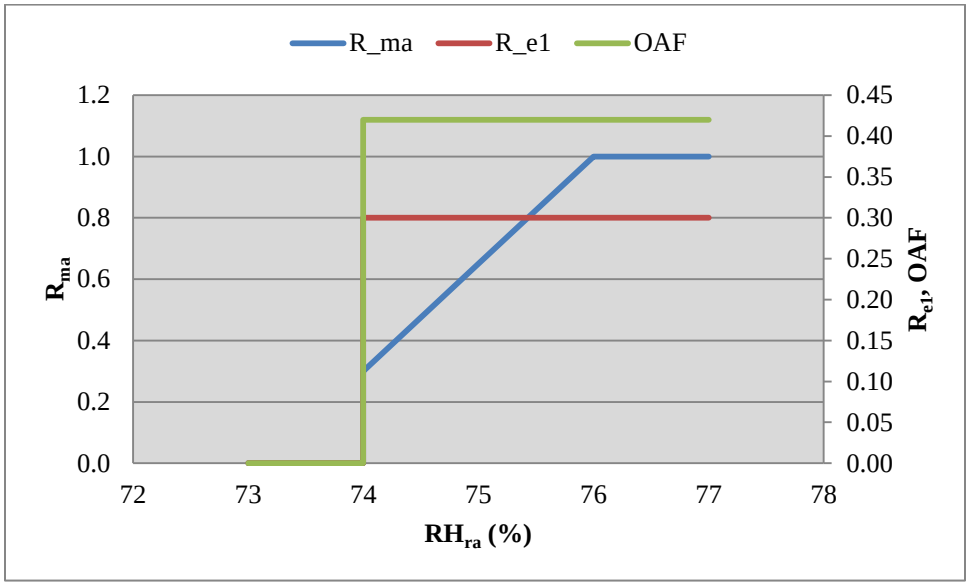

Figure 6.95: Proposed implementation of IEC mode

6.4.3 Standard Mode

In standard mode, both a temperature set point and humidity set point are simultaneously met. Furthermore, the near-optimal strategy developed for standard mode in Section 6.3.8 can be divided into two sections: one where OAF is held to a constant value depending upon outdoor air state while R_{ma} ratio and R_{e1} ratio proportionally ramp together, and one where OAF linearly changes value while R_{ma} ratio is at its maximum value. The values to set for OAF vary depending upon SHR, which is not known during building operation. As a result, the amount of

temperature and humidity deviation from set point will be used as a measure of SHR. Assuming that an initial SHR value of 0.65 is appropriate for when both set points are met, SHR should increase as T_{ra} increases past T_{set} and decreases as RH_{ra} increases past RH_{set}. Knowing that T_{ra} is not expected to surpass 76°F and RH_{ra} is not expected to surpass 56%, and assuming that SHR should be approximately 0.8 when T_{ra} = 76°F and RH_{ra} = RH_{set} and approximately 0.5 when T_{ra} = T_{set} and RH_{ra} = 56%, SHR can be approximated as shown in Equation 6.17. This idea of SHR being a function of T_{ra} and RH_{ra} is illustrated in Figure 6.96.

$$\boldsymbol{SHR \cong 0.65 + \frac{T_{ra} - T_{set}}{12°F} - \frac{RH_{ra} - RH_{set}}{12\%}}$$

Equation 6.17

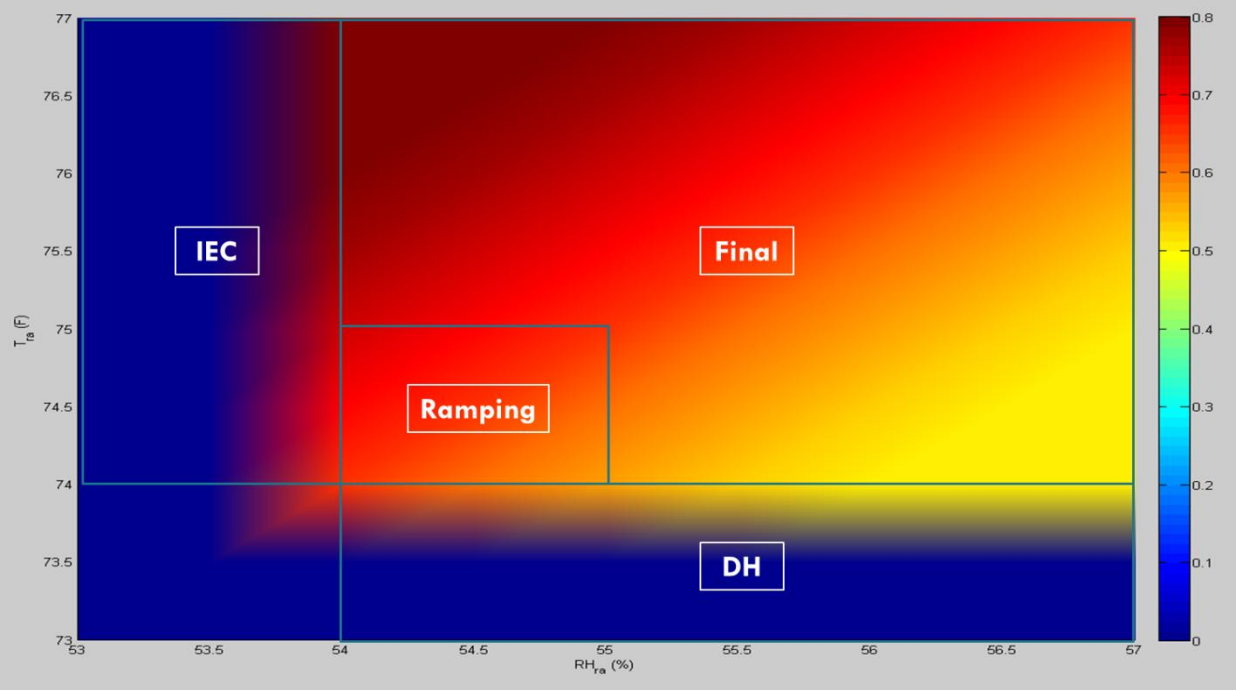

Figure 6.96: Dependence of SHR on T_{ra} and RH_{ra} in standard mode

Using the same temperature and humidity set points and similar proportional control logic found in the original DEVap study [3], the following implementation method is proposed:

- Standard mode initially turns on if $T_{ra} \geq T_{set} = 74°F$ and $RH_{ra} \geq RH_{set} = 54\%$. At this point, OAF is set according to Figure 6.81 depending upon the outdoor air condition and $C_{LD,in,DEVap}$ is allowed to float in order to provide the SHR value calculated by Equation 6.17. This initial start phase coincides with the beginning of the ramping phase, so R_{ma} is initially set to 30% and R_{e1} is initially set to 35%.

- If T_{ra} or RH_{ra} increases, adjust SHR using Equation 6.17 in order to determine the appropriate ramping value to set for OAF using Figure 6.81. $C_{LD,in,DEVap}$ is still allowed to float in order to provide the appropriate SHR. The transition between ramping phase and last phase of standard mode occurs when T_{ra} reaches 75°F or RH_{ra} reaches 55%. As such, linearly increase R_{ma} and R_{e1} such that they are 100% and 60%, respectively, when $T_{ra} = 75°F$ or $RH_{ra} = 55\%$.

- If $T_{ra} \geq 75°F$ or $RH_{ra} \geq 55\%$, hold R_{ma} at 100% and linearly change OAF such that it reaches OAF_{last} using Figure 6.91 when T_{ra} reaches 76°F or RH_{ra} reaches 56%

This implementation method for controlling R_{ma}, R_{e1}, OAF, and $C_{LD,in,DEVap}$ for standard mode when $T_{oa} = 90°F$ and $\omega_{oa} = 0.0080$ kg/kg is illustrated in , Figure 6.98, Figure 6.99, and Figure 6.100, respectively. The actual values for OAF and $C_{LD,in,DEVap}$ will depend upon outdoor air state and SHR approximated using Equation 6.17.

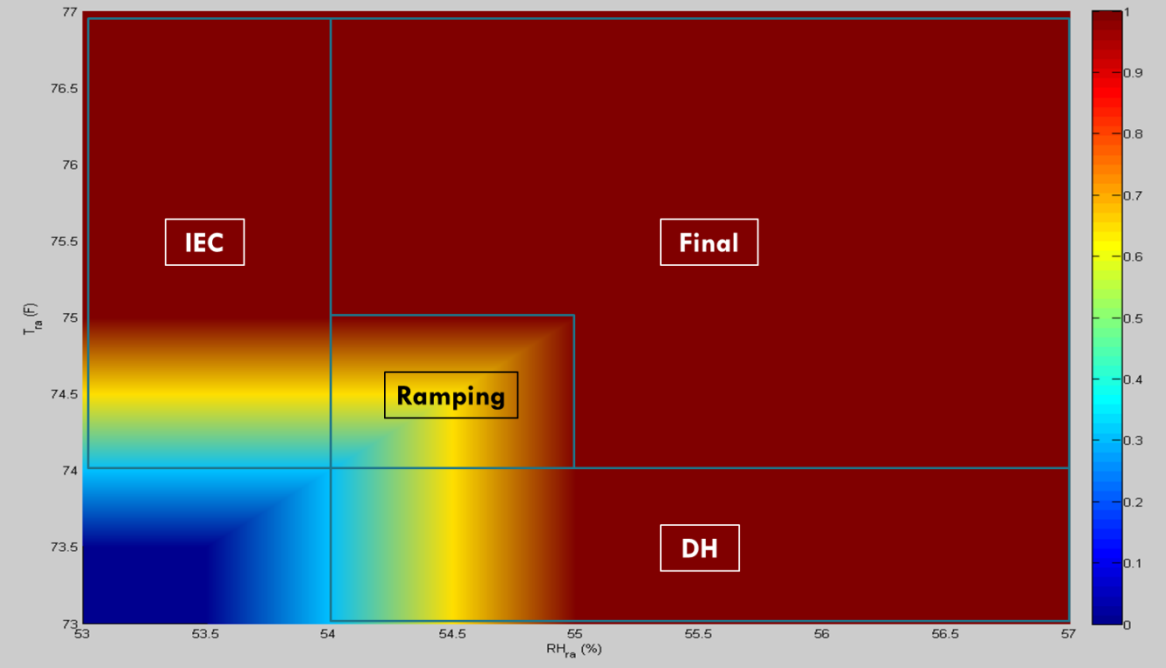

Figure 6.97: Proposed implementation of controlling R_{ma} in standard mode for T_{oa} = 90°F and ω_{oa} = 0.0080 kg/kg

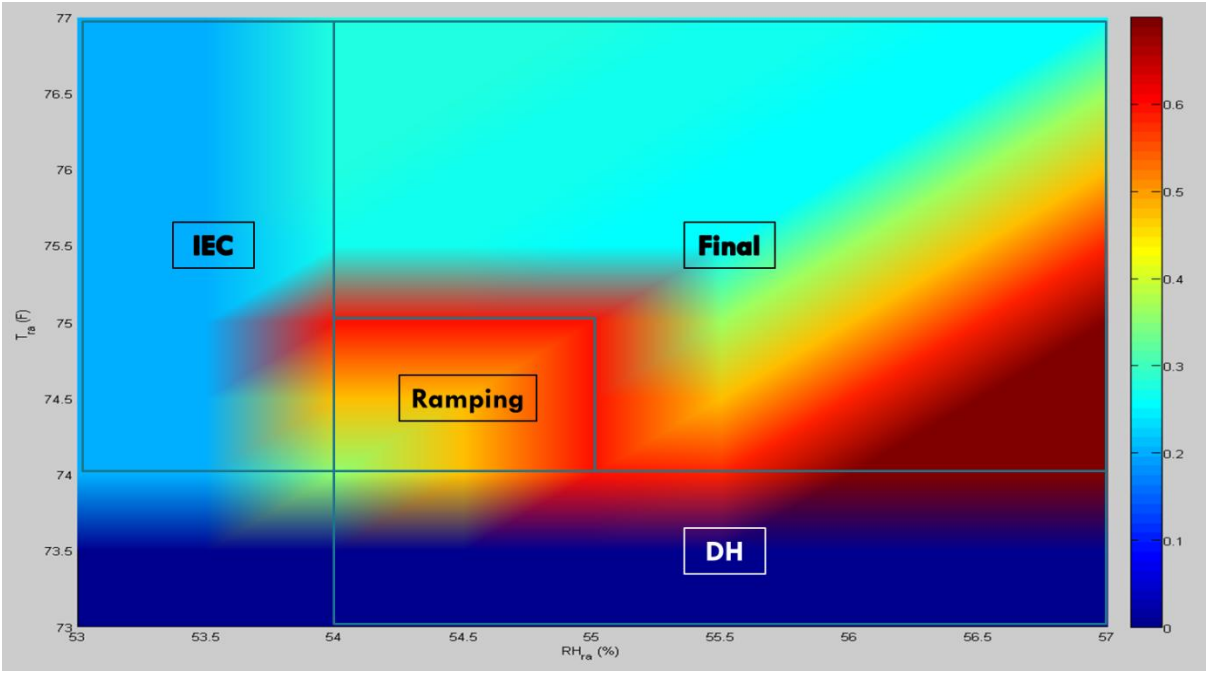

Figure 6.98: Proposed implementation of controlling R_{e1} in standard mode T_{oa} = 90°F and ω_{oa} = 0.0080 kg/kg

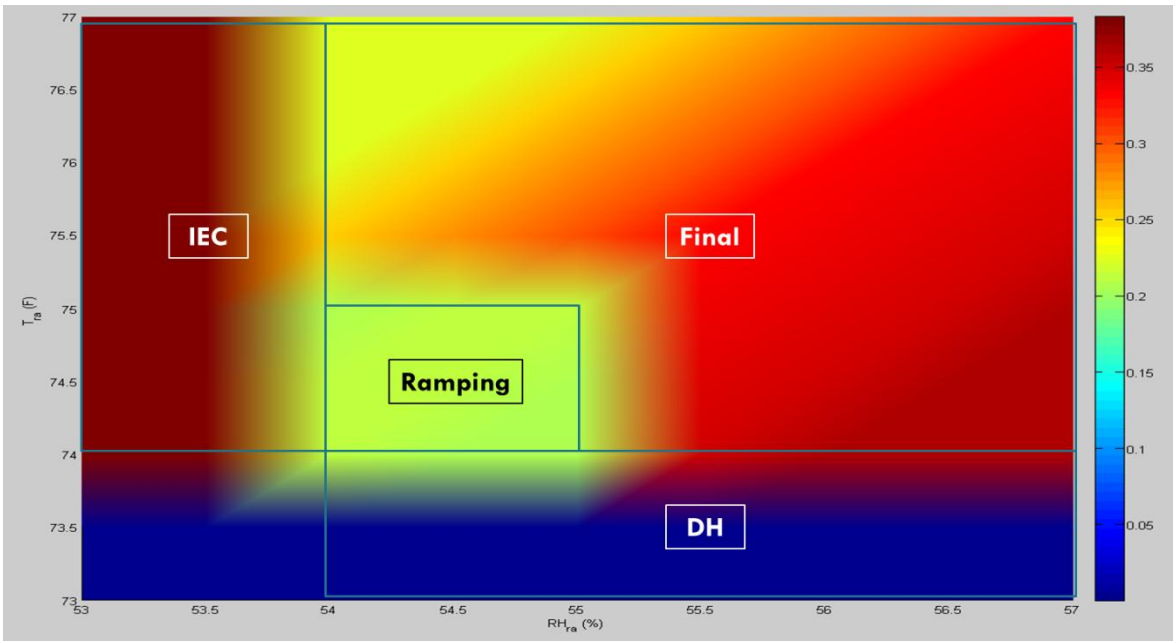

Figure 6.99: Proposed implementation of controlling OAF in standard mode T_{oa} = 90°F and ω_{oa} = 0.0080 kg/kg

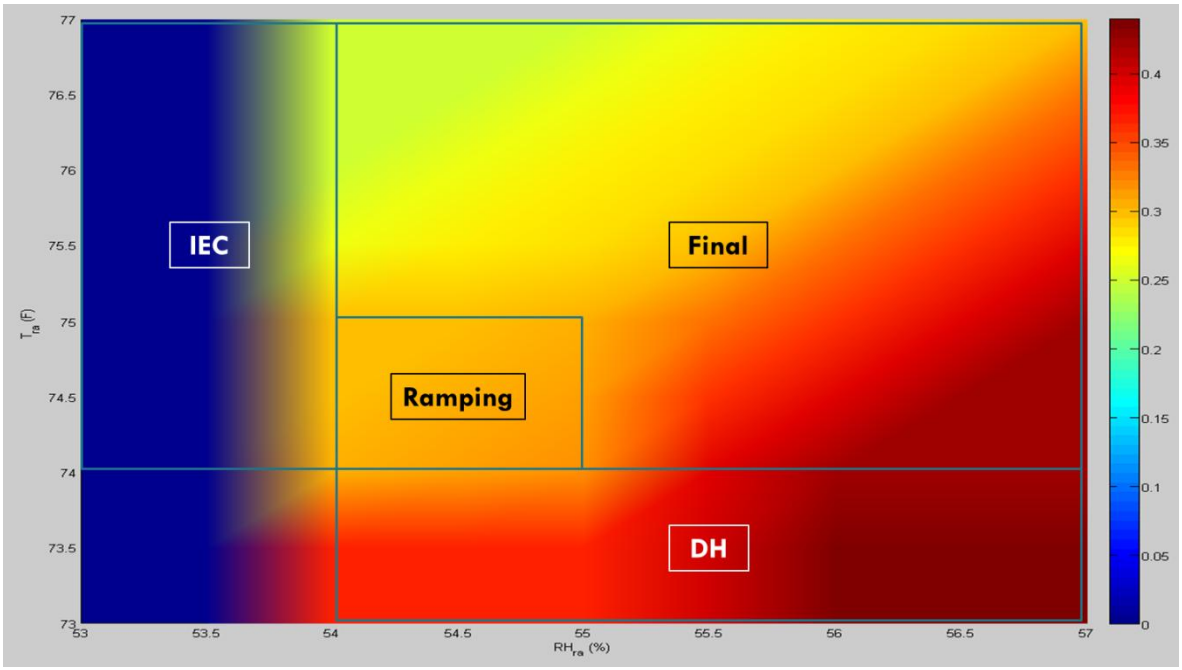

Figure 6.100: Proposed implementation of controlling $C_{LD,in,DEVap}$ in standard mode T_{oa} = 90°F and ω_{oa} = 0.0080 kg/kg

Chapter 7: Conclusions and Future Work

7.1 Conclusions

This thesis has presented a simplified method to control an air conditioning device that combines liquid desiccant dehumidification with indirect evaporative cooling, referred to as DEVap. This near-optimal control strategy was developed based upon control trends observed in simulation results that maximized source coefficient of performance over a wide spectrum of return and outdoor air states and SHR values using four control variables: mixed air flow ratio (R_{ma}), first stage exhaust flow ratio (R_{e1}), outdoor air fraction (OAF), and inlet liquid desiccant concentration ($C_{LD,in,DEVap}$). There were three different modes of operation for DEVap: dehumidification mode, indirect evaporative cooling (IEC) mode, and standard mode where both dehumidification and IEC occur simultaneously.

For dehumidification mode, it was determined that only R_{ma} and $C_{LD,in,DEVap}$ were control variables. During the optimization process, it became apparent that cooling performance was more sensitive to $C_{LD,in,DEVap}$ under higher latent cooling loads. It was determined that the most efficient near-optimal strategy to provide latent capacities for all return air states is as follows:

- Initially set R_{ma} ratio to 30% and $C_{LD,in,DEVap}$ to 37%
- If greater latent capacity is required, linearly ramp R_{ma} ratio to 100%
- If greater latent capacity is still required once R_{ma} ratio reaches 100%, linearly increase $C_{LD,in,DEVap}$ to 44%

For IEC mode, it was determined that R_{ma}, R_{e1}, and OAF were control variables. During the optimization process, it became apparent that cooling performance was most sensitive to R_{e1} and OAF under the majority of sensible cooling loads. In general, a combination of high OAF and low R_{e1} was optimal for different combinations of outdoor air and return air, but values for each control variable were more sensitive to outdoor air. It was observed that as return air became more humid for a constant outdoor air state, the optimal trend was to slightly reduce R_{e1} and slightly increase OAF. It was determined that the most efficient near-optimal strategy to provide sensible capacities under a range of return air and outdoor air states is as follows:

- Knowing values for RH_{ra}, T_{oa}, and ω_{oa}, set R_{e1} ratio and OAF to values according to Figure 6.52 and Figure 6.53, respectively.
- Begin to initially provide Q_{sens} by setting R_{ma} ratio to 30%
- If greater values of Q_{sens} are required, accordingly increase R_{ma} ratio
- The greatest Q_{sens} that can be provided is achieved when R_{ma} ratio reaches 100%

For standard mode, it was determined that R_{ma}, R_{e1}, and OAF $C_{LD,in,DEVap}$ were control variables. During the optimization process, it became apparent that cooling performance was least sensitive to R_{ma} and more sensitive to $C_{LD,in,DEVap}$ than R_{e1} and OAF. It became apparent during the optimization process that there was a necessity for two control phases of standard mode: ramping phase and final phase. Ramping phase would supply lower Q_{tot} capacities by holding OAF and $C_{LD,in,DEVap}$ to a constant value while linearly "ramping" both R_{ma} and R_{e1} together in a proportional fashion. Once R_{ma} and R_{e1} reached their respective maximum values, then the optimal way to supply greater total capacities was to alter OAF. In general, it was

determined that return air had little impact on optimal control variable trends during both phases. In the ramping phase, it was observed that as SHR increased, optimal OAF and $C_{LD,in,DEVap}$ values would increase and decrease, respectively. It was also observed that as outdoor air become hotter, optimal $C_{LD,in,DEVap}$ values would increase. During the final phase, the same optimal trends for both OAF and $C_{LD,in,DEVap}$ during ramping phase were observed. It was also determined that as SHR increases during the final phase, optimal R_{e1} values would decrease. It was determined that the most efficient near-optimal strategy to provide total capacities is separated into a ramping phase and a final phase as follows:

- Knowing values for T_{oa}, ω_{oa}, and SHR, set OAF to $OAF_{near\text{-}opt,standard}$ according to Figure 6.81

- Begin to initially provide Q_{tot} and SHR by setting R_{ma} ratio to 30%, R_{e1} ratio to 35%, and $C_{LD,in,DEVap}$ to the appropriate value

- If greater values of Q_{tot} are required, accordingly increase R_{ma} rat and R_{e1} ratio proportionally so that R_{ma} ratio reaches 100% and R_{e1} ratio reaches 70% simultaneously. $C_{LD,in,DEVap}$ is allowed to float in order to provide the desired SHR

- The greatest Q_{tot} that can be provided at the end of this ramping region is achieved when R_{ma} ratio reaches 100% and R_{e1} ratio reaches 60%

- Knowing values for T_{oa}, ω_{oa}, and SHR, set OAF_{last} according to Figure 6.91

- Linearly change OAF from $OAF_{near\text{-}opt,standard}$ to OAF_{last} while keeping R_{ma} r at 100%. R_{e1} ratio and $C_{LD,in,DEVap}$ are allowed to float in order to provide the desired SHR

- The greatest Q_{tot} that can be provided is achieved at the end of this final phase when OAF reaches OAF_{last}

A practical implementation method that relates the use of temperature and humidity set points to the near-optimal control strategy was also developed. Minimum capacities are provided when set points are initially met and increase until maximum capacities are provided when return air has deviated past set point to an undesirable level.

7.2 Future Work

This thesis has presented a simplified method to control DEVap under a wide spectrum of return and outdoor air states in order to optimize source coefficient of performance. Future work should be applied to comparing this energy optimization to an economic optimization where the life time operating cost of DEVap is minimized. Little economic data is available concerning material costs for the DEVap device, but if the same device was implemented in different locations then this is not an issue. As a result, only the operating costs associated with liquid desiccant use and energy consumption in the form of electricity and natural gas needs an economic analysis.

As DEVap can operate in any climate due to its flexibility in meeting a plethora of combinations of latent and sensible loads, climate specific control optimization is not necessary. If future work is conducted on climate specific control, it is possible to implement a weighting strategy for the return and outdoor air states expected in a specific climate to be applied, giving

weight towards optimal control variable values associated with those common return and outdoor air states.

This thesis has presented a simplified method to control DEVap for a specific set of device dimensions, requiring the process to be replicated whenever these dimensions change. In order to make the optimization process easier and faster to reproduce, future work should be applied towards making the EES model for DEVap less complex. This will cut down simulation time when developing correlations to implement in Excel. However, if the model becomes simple enough that simulation time is not an issue, then the process of developing correlations can be avoided entirely and the optimization process can be performed in EES. One possible method of achieving this is to alter the EES model from a two-dimensional nodal model to an effectiveness-NTU model, since DEVap is essentially an array of channels where heat and mass exchange occurs. This is possible using empirical data from prototype testing in order to develop correlations for effectiveness-NTU relationships.

The regenerator EES model described in this thesis is simple and future work should be applied towards making it more accurate. This can be done by altering the model from a thermodynamic model with control volumes drawn around each component of the regenerator system to a two-dimensional nodal model, similar to the approach used in the DEVap EES model. Incorporating associated pump and fan energy use with regenerator operation should also be completed in future work.

This thesis has presented a simplified method to control DEVap under three distinct modes of operation. Future work should be applied towards the possibility of a fourth mode of operation where DEVap serves as an economizer, mixing outdoor and return air without

providing dehumidification or sensible cooling. There is a possibility that if outdoor air is cold and dry enough, the mixing process alone could provide satisfactory amounts of cooling, avoiding the need to use fan energy to move air through exhaust air stream channels.

Finally, future work should be devoted to accounting for reheating of excessively cold supply air exiting DEVap. Since reheating is applied in conventional direct expansion air conditioners when supply air temperatures drop below approximately 50°F, a fair comparison between DEVap would account for the same process. An energy penalty associated with this reheating will assuredly alter the optimization results, but it will be interesting to determine the impact on the near-optimal control strategy when reheating is accounted for.

References

[1] Incropera, F.P., DeWitt, D.P., Bergman, T.L., Lavine, A.S. Fundamentals of Heat and Mass Transfer. John Wiley & Sons, New Jersey, 6th edition, 2007.

[2] Lowenstein, A.I. Review of Liquid Desiccant Technology for HVAC Applications. ASHRAE HVAC&R Research. Volume 14, Number 6, November 2008.

[3] Kozubal, E., Woods, J., Burch, J., Boranian, A., Merrigan, T. Desiccant Enhanced Evaporativ Air-Conditioning (DEVap): Evaluation of a New Concept in Ultra Efficient Air Conditioning. NREL Report No. TP-5500-49722.

[4] Liu, Xiaohua; Li, Zhen; Jiang, Yi; Lin, Borong. Annual performance of liquid desiccant based independent humidity control HVAC system. *Applied Thermal Engineering*, Vol. 26, pp. 1198-1207, 2006.

[5] Lowenstein, Andy; Slayzak, Steven; Ryan, Joe; Pesaran, Ahmad. Advanced Commercial Liquid-Desiccant Technology Development Study. NREL/TP-550-24688; November 1998.

[6] Lowenstein, Andy; Slayzak, Steven; Kozubal, Eric. A zero-carryover liquid desiccant air conditioner for solar applications. NREL/CP-550-39798; July 2006.

[7] Zhang, L.Z.; Niu, J.L. A pre-cooling Munters environmental control desiccant cooling cycle in combination with chilled-ceiling panels. *Energy;* Vol. 28, pp. 275-292; July 2001.

[8] Tashtoush et al. Thermodynamic behavior of an air-conditioning system employing combined evaporative-water and air coolers. *Applied Energy;* Vol. 70, pp. 305-319; August 2001.

[9] Guo, X. C.; Zhao, T. S. A parametric study of an indirect evaporative air cooler. *Int. Comm. Heat Mass Transfer;* Vol. 25, No. 2, pp. 217-226; 1998.

[10] Saman, W.Y.; Alizadeh, S. Modeling and performance analysis of a cross-flow type plate heat exchanger for dehumidification/cooling. *Solar Energy;* Vol. 70, No. 4, pp. 361-372; July 2000.

[11] Saman, W.Y.; Alizadeh, S. An experimental study of a cross-flow type plate heat exchanger for dehumidification/cooling. *Solar Energy;* Vol. 73, No. 1, pp. 59-71; June 2001.

[12] Fumo, Nelson; Goswami, D. Y. Study of an aqueous lithium chloride desiccant system: air dehumidification and desiccant regeneration. *Solar Energy*, Vol. 72, No. 4, pp. 351-361, 2002.

[13] Liu, X.H.; Chang, X.M.; Xia, J.J.; Jiang, Y. Performance analysis on the internally cooled dehumidifier using liquid desiccant. *Building and Environment;* Vol. 44, pp. 299-308; March 2008.

[14] Liu, X.H.; Zhang, Y.; Qu, K.Y.; Jiang, Y. Experimental study on mass transfer performances of cross flow dehumidifier using liquid desiccant. *Energy Conversion and Management;* Vol. 47, pp. 2682-2692; December 2005.

[15] Vitte, Thibaut; Brau, Jean; Chatagnon, Nadège; Woloszyn, Monika. Proposal for a new hybrid control strategy of a solar desiccant evaporative cooling air handling unit. *Energy and Buildings;* Vol. 40, pp. 896-905; July 2007.

[16] LD Tutorial. AIL Research, Inc. ailr.com/liquid_desiccant_tutorial.htm; Accessed September 15, 2010

[17] Mcquiston, Faye C.; Parker, Jerald D.; Spitler, Jeffrey D. Heating, Ventilating, and Air Conditioning: Analysis and Design. John Wiley & Sons, New Jersey, 6th Edition, 2005.

[18] 2009 ASHRAE Handbook: Fundamentals. American Society of Heating, Refrigeration, and Air-Conditioning Engineers, Atlanta, 2009.

[19] White, Frank M. Fluid Mechanics. McGraw-Hill, New York, 6th Edition, 2008.

[20] Woods, Jason. 2-D Nodal Heat and Mass Exchange EES DEVap Model, August 2010.

[21] Conde, M.R., Properties of aqueous solutions of lithium and calcium chlorides: formulations for use in air conditioning equipment design, Int. J. Therm. Sci. 43 (2004) 367-82.

[22] Lowenstein, Andy. Finite Difference Scavenging Air Regenerator Model, March 2011.

Appendix A: Regenerator Model

```
"Constants"

 m_dot_LD_des=0.02797 [kg/s]                          "Design LD Flow Rate"
 Des$ = 'LiCl'                                        "Desiccant Type"
 P_atm=101.3 [kPa]                                    "Atmospheric Pressure"
 M_w = molarmass(water)                               "Water Molar Mass"
 M_a = MolarMass(air)                                 "Air Molar Mass"

"State 1: Weak LD Directly Exiting DEVap"

{T_LD_1=300 [K]                                       "LD Temperature"}
T_LD_1_F=converttemp(K,F,T_LD_1)
T_LD_1_C=converttemp(K,C,T_LD_1)
{C_LD_1=0.36                                          "LD Concentration"}
m_dot_LD_1=m_dot_LD_des                               "LD Flow Rate"
Call p_vapor_sol(T_LD_1,C_LD_1,Des$:p_v_LD_1)         "LD Vapor Pressure"
omega_LD_1=p_v_LD_1*(M_w/M_a)/(P_atm-p_v_LD_1)  "LD Absolute Humidity"
{delta_C_LD=0.02                                      "Desired Change in LD Concentration from
Regeneration"}

"State 2: Weak LD for Regeneration"

T_LD_2=T_LD_1                                         "LD Temperature"
C_LD_2=C_LD_1                                         "LD Concentration"
m_dot_LD_2=(m_dot_LD_1/4)*Frac_reg                    "LD Flow Rate"
{Frac_reg=1.00                                        "Fraction of Weak LD Leaving DEVap to be
Regenerated"}

"State 3: Weak LD for Mixing with Regenerated LD"

T_LD_3=T_LD_1                                         "LD Temperature"
C_LD_3=C_LD_1                                         "LD Concentration"
m_dot_LD_3=m_dot_LD_1-m_dot_LD_2                      "LD Flow Rate"

"State 4: Weak LD for Regeneration in Boiler before ICHX"

T_LD_4=T_LD_2                                         "LD Temperature"
C_LD_4=C_LD_2                                         "LD Concentration"
m_dot_LD_4=m_dot_LD_2*Frac_boil                       "LD Flow Rate"
{Frac_boil=0.6                                        "Fraction of Regenerated LD sent to Boiler"}
cp_LD_4=Cp_sol(T_LD_4, C_LD_4, Des$)                  "Specific Heat of  LD"

"State 5: Weak LD for Regeneration in Boiler after ICHX"

T_LD_5_F=converttemp(K,F,T_LD_5)
T_LD_5_C=converttemp(K,C,T_LD_5)                      "LD Temperature"
C_LD_5=C_LD_4                                         "LD Concentration"
m_dot_LD_5=m_dot_LD_4                                 "LD Flow Rate"
cp_LD_5=Cp_sol(T_LD_5, C_LD_5, Des$)                  "Specific Heat of  LD"
cp_LD_5_IP=cp_LD_5*convert(J/kg-K,Btu/lbm-F)          "Specific Heat of LD entering Boiler"
Call p_vapor_sol(T_LD_5,C_LD_5,Des$:p_v_LD_5)         "LD Vapor Pressure"
omega_LD_5=p_v_LD_5*(M_w/M_a)/(P_atm-p_v_LD_5)  "LD Absolute Humidity"
```

```
rho_LD_5=Rho_sol(T_LD_5, C_LD_5, Des$)              "Density of Weak LD entering Boiler"

"State 6: Strong LD from Boiler before ICHX"

Call p_vapor_sol(T_LD_6,C_LD_5,Des$:P_atm)          "LD Temperature, set to Boiling Temperature of
LD"
T_LD_6_F=converttemp(K,F,T_LD_6)                    "LD Temperature, set to Boiling Temperature of
LD"
T_LD_6_C=converttemp(K,C,T_LD_6)                    "LD Temperature, set to Boiling Temperature of
LD"
C_LD_6=C_LD_5+delta_C_LD                            "LD Concentration"
cp_LD_6=Cp_sol(T_w_17, C_LD_6, Des$)                "Specific Heat of  LD"
Call p_vapor_sol(T_w_17,C_LD_6,Des$:p_v_LD_6)       "LD Vapor Pressure"
omega_LD_6=p_v_LD_6*(M_w/M_a)/(P_atm-p_v_LD_6)  "LD Absolute Humidity"

"State 7: Strong LD from Boiler after ICHX"

T_LD_7_F=converttemp(K,F,T_LD_7)                    "LD Temperature"
T_LD_7_C=converttemp(K,C,T_LD_7)                    "LD Temperature"
C_LD_7=C_LD_6                                       "LD Concentration"
m_dot_LD_7=m_dot_LD_6                               "LD Flow Rate"
cp_LD_7=Cp_sol(T_LD_7, C_LD_7, Des$)                "Specific Heat of  LD"
Call p_vapor_sol(T_LD_7,C_LD_7,Des$:p_v_LD_7)       "LD Vapor Pressure"
omega_LD_7=p_v_LD_7*(M_w/M_a)/(P_atm-p_v_LD_7)  "LD Absolute Humidity"

"Boiler ICHX Inputs"

epsilon_IC_max=0.80                                 "Effectiveness of ICHX at Max Flow"
V_dot_IC_rat=3.0 [gpm]                              "Rated Max Flow Rate for Max Effectiveness:"
"from AILR site"

"Properties for Boiler ICHX"

cp_LD_4_5=average(cp_LD_4,cp_LD_5)                  "Specific Heat of Weak LD in ICHX"
cp_LD_6_7=average(cp_LD_6,cp_LD_7)                  "Specific Heat of Strong LD in ICHX"
h_mix_5_6=HeatOfMixing(T_LD_6, (C_LD_5+C_LD_6)/2, Des$)  "Heat of Mixing of LD in Boilder"

"Calculations for Boiler ICHX"

M_IC_4_5=m_dot_LD_4*cp_LD_4_5                       "Weak LD Heat Capacity Rate in Boiler ICHX"
M_IC_6_7=m_dot_LD_6*cp_LD_6_7                       "Strong LD Heat Capacity Rate in Boiler ICHX"
M_IC_min=min(M_IC_4_5, M_IC_6_7)                    "Minimum Heat Capacity Rate in Boiler ICHX"
Q_dot_IC=m_dot_LD_4*cp_LD_4_5*(T_LD_5-T_LD_4)  "Heat Gain/Loss in Weak LD in Boiler ICHX"
T_LD_7=T_LD_6-Q_dot_IC/(m_dot_LD_6*cp_LD_6_7)  "Strong LD Temperature after Boiler ICHX"
Ntu_IC = UA_IC/(M_IC_min)                           "NTU for ICHX"
epsilon_IC=(M_IC_6_7*(T_LD_6-T_LD_7))/(M_IC_min*(T_LD_6-T_LD_4))  "Regenerated LD
Temperature"
{ UA_IC=47.91 [J/s-K]                               "ICHX UA Value:"}
epsilon_IC=HX('counterflow', Ntu_IC, M_IC_4_5, M_IC_6_7, 'epsilon')"HX Effectiveness of Boiler ICHX"
V_dot_LD_4_5=(m_dot_LD_4/rho_LD_4_5)*convert(m^3/s,gpm)"Volumetric Flow Rate of Weak LD
through Boiler ICHX"
rho_LD_4_5=Rho_sol((T_LD_4+T_LD_5)/2, C_LD_4, Des$)  "Density of Weak LD through Boiler ICHX"
rho_LD_4_5_IP=rho_LD_4_5*convert(kg/m^3, lbm/gal)    "Density of Weak LD through Boiler ICHX"
```

"Boiler - 1st Stage Regenerator"

"Properties for Boiler"

{m_dot_b_max=0.004147 [kg/s] "Maximum Flow Rate into Boiler"}
eta_b=0.85-(0.85-0.82)*m_dot_LD_5/m_dot_b_max "Boiler Burn Efficiency, Based Upon Ratio of Actual LD Flow throug Boiler to Max LD Flow"
Q_dot_b_max=30000 [Btu/hr]*convert(Btu/hr,W) "Boiler Rated Burn Rate"
cp_LD_avg_b=average(cp_LD_5,cp_LD_6) "Average Specific Heat of LD in Boiler"

"Calculations for Boiler"

m_dot_LD_5*C_LD_5=m_dot_LD_6*C_LD_6 "Species Balance for Boiler"
m_dot_LD_5=m_dot_LD_6+m_dot_steam_8 "Mass Balance for Boiler"
Q_dot_boil=m_dot_steam_8*(h_v_8+h_mix_5_6-cp_LD_5*(T_LD_5-273.15 [K]))+m_dot_LD_6*cp_LD_avg_b*(T_LD_6-T_LD_5) "Energy Rate Balance for LD in Boiler"
Q_dot_boil_sens=m_dot_LD_6*cp_LD_avg_b*(T_LD_6-273.15 [K])-m_dot_LD_5*cp_LD_avg_b*(T_LD_5-273.15 [K]) "Sensible Energy Gain Rate of LD in Boiler"
Q_dot_boil_lat=Q_dot_boil-Q_dot_boil_sens "Latent Energy Loss Rate of LD in Boiler"
Q_dot_rate=Q_dot_boil/eta_b "Boiler Energy Use Rate"
V_dot_LD_5=(m_dot_LD_5/rho_LD_5)*convert(m^3/s,gpm)"Volumetric Flow Rate of Weak LD entering Boiler:"
Q_dot_rate_IP=Q_dot_rate*convert(W,Btu/hr) "Boiler Energy Use Rate"
m_dot_LD_5_IP=m_dot_LD_5*convert(kg/s,lbm/hr) "LD Mass Flow Rate into Boiler"
m_dot_LD_6_IP=m_dot_LD_6*convert(kg/s,lbm/hr) "LD Mass Flow Rate from Boiler"
m_dot_steam_8_IP=m_dot_steam_8*convert(kg/s,lbm/min)"Steam Mass Flow Rate from Boiler"
h_mix_5_6_IP=h_mix_5_6*convert(J/kg,Btu/lbm) "Heat of Mixing of LD in Boiler"
cp_LD_6_IP=cp_LD_6*convert(J/kg-K,Btu/lbm-F) "Specific Heat of LD from Boiler"

"State 8: Steam Leaving Boiler"

T_steam_8=T_LD_6 "Steam Temperature is equal to Boiling Temperature of LD"
T_steam_8_F=converttemp(K,F,T_steam_8) "Steam Temperature, set to Boiling Temperature of LD"
T_steam_8_C=converttemp(K,C,T_steam_8) "Steam Temperature, set to Boiling Temperature of LD"
{h_v_8=enthalpy(water,T=T_steam_8,x=1) "Heat of Vaporization of Steam"}
h_v_8=Enthalpy(Steam,T=T_steam_8,P=P_atm) "Heat of Vaporization of Steam"

"State 9: Weak LD for Regeneration in SAR before ICHX"

T_LD_9=T_LD_2 "LD Temperature"
T_LD_9_F=converttemp(K,F,T_LD_9) "LD Temperature"
T_LD_9_C=converttemp(K,C,T_LD_9) "LD Temperature"
C_LD_9=C_LD_2 "LD Concentration"
m_dot_LD_9=m_dot_LD_2-m_dot_LD_4 "LD Flow Rate"
cp_LD_9=Cp_sol(T_LD_9, C_LD_9, Des$) "Specific Heat of LD"

"State 10: Weak LD for Regeneration in SAR after ICHX"

T_LD_10_F=converttemp(K,F,T_LD_10) "LD Temperature"
T_LD_10_C=converttemp(K,C,T_LD_10) "LD Temperature"
C_LD_10=C_LD_9 "LD Concentration"
m_dot_LD_10=m_dot_LD_9 "LD Flow Rate"
m_dot_LD_10_IP=m_dot_LD_10*convert(kg/s,lbm/min) "LD Flow Rate"

```
cp_LD_10=Cp_sol(T_LD_10, C_LD_10, Des$)              "Specific Heat of  LD"
Call p_vapor_sol(T_LD_10,C_LD_10,Des$:p_v_LD_10) "LD Vapor Pressure"
omega_LD_10=p_v_LD_10*(M_w/M_a)/(P_atm-p_v_LD_10)"LD Absolute Humidity"

"State 11: Strong LD from SAR before ICHX"

T_LD_11=T_w_17                                       "LD Temperature from SAR, set equal to Water
Temperature from Steam Channel in SAR"
T_LD_11_F=converttemp(K,F,T_LD_11)                   "LD Temperature from SAR, set equal to Water
Temperature from Steam Channel in SAR"
T_LD_11_C=converttemp(K,C,T_LD_11)                   "LD Temperature from SAR, set equal to Water
Temperature from Steam Channel in SAR"
C_LD_11=C_LD_10+delta_C_LD                           "LD Concentration"
cp_LD_11=Cp_sol(T_LD_11, C_LD_11, Des$)              "Specific Heat of  LD"
Call p_vapor_sol(T_LD_11,C_LD_11,Des$:p_v_LD_11) "LD Vapor Pressure"
omega_LD_11=p_v_LD_11*(M_w/M_a)/(P_atm-p_v_LD_11)"LD Absolute Humidity"

"State 12: Strong LD from SAR after ICHX"

T_LD_12_F=converttemp(K,F,T_LD_12)                   "LD Temperature"
T_LD_12_C=converttemp(K,C,T_LD_12)                   "LD Temperature"
C_LD_12=C_LD_11                                      "LD Concentration"
m_dot_LD_12=m_dot_LD_11                              "LD Mass Flow Rate"
cp_LD_12=Cp_sol(T_LD_12, C_LD_12, Des$)              "Specific Heat of  LD"
Call p_vapor_sol(T_LD_12,C_LD_12,Des$:p_v_LD_12)   "LD Vapor Pressure"
omega_LD_12=p_v_LD_12*(M_w/M_a)/(P_atm-p_v_LD_12)  "LD Absolute Humidity"

"Properties for SAR ICHX"

cp_LD_9_10=average(cp_LD_9,cp_LD_10)                 "Specific Heat of Weak LD in SAR ICHX"
cp_LD_11_12=average(cp_LD_11,cp_LD_12)               "Specific Heat of Strong LD in SAR ICHX"

"Calculations for SAR ICHX"

M_IC_9_10=m_dot_LD_9*cp_LD_9_10                      "Weak LD Heat Capacity Rate in SAR ICHX"
M_IC_11_12=m_dot_LD_11*cp_LD_11_12                   "Strong LD Heat Capacity Rate in SAR ICHX"
M_IC_min_SAR=min(M_IC_9_10, M_IC_11_12)              "Minimum Heat Capacity Rate in SAR ICHX"
Q_dot_IC_SAR=m_dot_LD_9*cp_LD_9_10*(T_LD_10-T_LD_9)  "Heat Gain/Loss in Weak LD in SAR
ICHX"
T_LD_12=T_LD_11-Q_dot_IC_SAR/(m_dot_LD_11*cp_LD_11_12)  "Strong LD Temperature after SAR
ICHX"
Ntu_IC_SAR = UA_IC_SAR/(M_IC_min_SAR)                "NTU for SAR ICHX"
epsilon_IC_SAR=(M_IC_11_12*(T_LD_11-T_LD_12))/(M_IC_min_SAR*(T_LD_11-T_LD_9))
"Regenerated LD Temperature"
{ UA_IC=47.91 [J/s-K]                                "SAR ICHX UA Value"}
epsilon_IC_SAR=HX('counterflow', Ntu_IC_SAR, M_IC_9_10, M_IC_11_12, 'epsilon')  "HX Effectiveness
of SAR ICHX"
V_dot_9_10=(m_dot_LD_9/rho_LD_9_10)*convert(m^3/s,gpm)  "Volumetric Flow Rate of Weak LD
through ICHX"
rho_LD_9_10=Rho_sol((T_LD_9+T_LD_10)/2, C_LD_9, Des$)  "Density of Weak LD through ICHX"
rho_LD_9_10_IP=rho_LD_9_10*convert(kg/m^3, lbm/gal)  "Density of Weak LD through ICHX"
```

```
"State 13: Cold Air Stream Inlet to AAHX (Ambient Air)"

m_dot_air_13=m_dot_air_13_dry*(1+omega_air_13)      "Dry Air Flow Rate"
{T_air_13=300 [K]                                   "Air Temperature"}
T_air_13=converttemp(F,K,T_air_13_F)                "Air Temperature"
{T_air_13_F=converttemp(K,F,T_air_13)               "Air Temperature"}
T_air_13_C=converttemp(K,C,T_air_13)                "Air Temperature"
{omega_air_13=0.02                                  "Air Humidity Ratio"}
{RH_air_13=0.6                                      "Air Relative Humidity"}
omega_air_13=HumRat(AirH2O,T=T_air_13,r=RH_air_13,P=P_atm)  "Air Humidity Ratio"
h_air_13=enthalpy(AirH2O,T=T_air_13,w=omega_air_13,P=P_atm)  "Air Enthalpy"
cp_air_13=Cp(AirH2O,T=T_air_13,w=omega_air_13,P=P_atm)  "Specific Heat of Air"
V_dot_air_s=12.0 [cfm]                              "Standard CFM"
T_standard=290 [K]                                  "Standard Temperature"
P_standard=100 [kPa]                                "Standard Pressure"
rho_air_s=Density(Air,T=T_standard,P=P_standard)    "Standard Dry Air Density"
rho_air_s_IP=rho_air_s*convert(kg/m^3,lbm/ft^3)     "Dry Air Density"
{m_dot_air_13_dry_IP=V_dot_air_s*rho_air_s_IP*convert(hr,min)"Dry Air Flow"}
m_dot_air_13_dry=m_dot_air_13_dry_IP*convert(lbm/hr,kg/s)  "Dry Air Flow"
rho_air_13=Density(AirH2O,T=T_air_13,W=omega_air_13,P=P_atm)  "Dry Air Density"
rho_air_13_IP=rho_air_13*convert(kg/m^3,lbm/ft^3)   "Dry Air Density"
V_dot_air_13=V_dot_air_s*(P_standard/P_atm)*(T_air_13/T_standard)  "Dry Air CFM"

"State 14: Cold Air Stream Outlet from AAHX into SAR"

m_dot_air_14=m_dot_air_13                           "Mixed Air Flow Rate"
m_dot_air_14_dry=m_dot_air_13_dry                   "Dry Air Flow Rate"
T_air_14_F=converttemp(K,F,T_air_14)                "Air Temperature"
T_air_14_C=converttemp(K,C,T_air_14)                "Air Temperature"
omega_air_14=omega_air_13                           "Air Humidity Ratio"
h_air_14=enthalpy(AirH2O,T=T_air_14,w=omega_air_14,P=P_atm)  "Air Enthalpy"
cp_air_14=Cp(AirH2O,T=T_air_14,w=omega_air_14,P=P_atm)"  Specific Heat of Air"

"State 15: Hot Air Stream Inlet to AAHX from SAR"

m_dot_air_15_dry=m_dot_air_14_dry                   "Dry Air Flow Rate"
m_dot_air_15=m_dot_air_15_dry*(1+omega_air_15)      "Mixed Air Flow Rate"
T_air_15_F=converttemp(K,F,T_air_15)                "Air Temperature"
T_air_15_C=converttemp(K,C,T_air_15)                "Air Temperature"
h_air_15=enthalpy(AirH2O,T=T_air_15,w=omega_air_15,P=P_atm)  "Air Enthalpy"
cp_air_15=Cp(AirH2O,T=T_air_15,w=omega_air_15,P=P_atm)  "Specific Heat of Air"

"State 16: Hot Air Stream Outlet from AAHX to be Exhausted"

m_dot_air_16=m_dot_air_15                           "Mixed Air Flow Rate"
m_dot_air_16_dry=m_dot_air_15_dry                   "Dry Air Flow Rate"
T_air_16_F=converttemp(K,F,T_air_16)                "Air Temperature"
T_air_16_C=converttemp(K,C,T_air_16)                "Air Temperature"
omega_air_16=omega_air_15                           "Air Humidity Ratio"
h_air_16=enthalpy(AirH2O,T=T_air_16,w=omega_air_16,P=P_atm)  "Air Enthalpy"
cp_air_16=Cp(AirH2O,T=T_air_16,w=omega_air_16,P=P_atm)  "Specific Heat of Air"
```

```
"Air to Air Heat Exchanger : AAHX"

"AAHX Inputs"

epsilon_AA_max=0.60                                   "Effectiveness of ICHX at Max Flow"

"Properties for AAHX"

cp_air_13_14=average(cp_air_13,cp_air_14)             "Specific Heat of Cold Air Stream in AAHX"
cp_air_15_16=average(cp_air_15,cp_air_16)             "Specific Heat of Hot Air Stream in AAHX"

"Calculations for AAHX"

M_AA_13_14=m_dot_air_13_dry*cp_air_13_14              "Cold Air Heat Capacity Rate in AAHX:"
M_AA_15_16=m_dot_air_15_dry*cp_air_15_16              "Hot Air Heat Capacity Rate in AAHX:"
M_AA_min=min(M_AA_13_14, M_AA_15_16)                  "Minimum Heat Capacity Rate in AAHX:"
Q_dot_AA=m_dot_air_13_dry*cp_air_13_14*(T_air_14-T_air_13)  "Heat Gain/Loss in Cold Air in AAHX"
T_air_16=T_air_15-Q_dot_AA/(m_dot_air_15_dry*cp_air_15_16)  "Hot Air Temperature after AAHX"
Ntu_AA = UA_AA/(M_AA_min)                             "NTU for AAHX"
epsilon_AA=(M_AA_15_16*(T_air_15-T_air_16))/(M_AA_min*(T_air_15-T_air_13))  "Hot Air Temperature
after Scavenging Air Regenerator"
{h_air_14-h_air_13=h_air_15-h_air_16                  "Enthalpy Change for Cold Air Stream Must
Equal Hot Air Stream"}
epsilon_AA=HX('crossflow_both_unmixed', Ntu_AA, M_AA_13_14, M_AA_15_16, 'epsilon')
"Effectiveness of AAHX at Max Flow"
{ UA_AA=14.27 [J/s-K]                                 "UA Value of AAHX"}
{ T_air_15=T_w_17                                     "Hot Air Temperature after Scavenging Air
Regenerator"}
 RH_air_15=RelHum(AirH2O,T=T_air_15,w=omega_air_15,P=P_atm)  "Relative Humidity of Hot Air
entering AAHX"

"Scavenging Air Regenerator: SAR"

"SAR Inputs"

"LD Parameters"

cp_LD_SAR_avg=average(cp_LD_10,cp_LD_11)              "Average LD Specific Heat in SAR"
h_fg_SAR=enthalpy(water,T=average(T_LD_10,T_LD_11),x=1) -
enthalpy(water,T=average(T_LD_10,T_LD_11),x=0)        "Heat of Evaporation of Water Leaving LD in
SAR"

"State 17: Water Outlet from Steam Flow"

T_w_17=363.15 [K]                                     "Outlet Water Temperature"
T_w_17_F=converttemp(K,F,T_w_17)                      "Air Temperature"
T_w_17_C=converttemp(K,C,T_w_17)                      "Air Temperature"
 h_w_17=Enthalpy(Water,T=T_w_17,P=P_atm)              "Outlet Water Enthalpy"
cp_w_17=Cp(Water,T=T_w_17,x=0)                        "Outlet Water Specific Heat"

"Air Parameters"

cp_air_SAR_avg=average(cp_air_14,cp_air_15)           "Average Air Specific Heat in SAR"
```

"Steam Parameters"

cp_steam_8=Cp(Water,T=T_steam_8,x=1) "Inlet Steam Specific Heat"

"Control Volume Balances"

q_dot_steam=m_dot_steam_8*(h_v_8-h_w_17) "Steam Energy Balance"
m_dot_air_15_dry*h_air_15=m_dot_air_14_dry*h_air_14+q_dot_air+m_dot_v*h_fg_SAR "Air Energy Balance"
{m_dot_air_15_dry*cp_air_15*T_air_15=m_dot_air_14_dry*cp_air_14*T_air_14+q_dot_air "Air Energy Balance"}
q_dot_steam+m_dot_LD_10*cp_LD_SAR_avg*(T_LD_10-273.15 [K])=m_dot_LD_11*cp_LD_SAR_avg*(T_LD_11-273.15 [K])+m_dot_v*(h_fg_SAR+h_mix_5_6)+q_dot_air "LD Energy Balance"
m_dot_air_14_dry*omega_air_14+m_dot_v=m_dot_air_15_dry*omega_air_15 "Air Mass Balance"
m_dot_LD_10=m_dot_LD_11+m_dot_v "LD Mass Balance"
m_dot_LD_10*C_LD_10=m_dot_LD_11*C_LD_11 "LD Species Balance"
p_v_air_SAR = omega_air_15*P_atm / (M_w/M_a+omega_air_15) "Air Vapor Pressure after SAR"
{p_v_air_SAR=eta_SAR*p_v_LD_SAR "Ratio of Air Vapor Pressure to LD Vapor Pressure"}

"Moisture Removal Effectiveness"

m_dot_min=min(m_dot_LD_10, m_dot_air_14_dry) "Minimum Heat Capacity Rate in SAR"
Ntu_SAR_lat = KA_SAR_lat/(m_dot_min) "NTU for AAHX"
{ KA_SAR_lat=1.00 [kg/s]} "Mass Transfer Coefficient"
Call p_vapor_sol(373.15 [K],C_LD_10,Des$:p_v_LD_max) "Max LD Vapor Pressure in SAR"
omega_LD_max=p_v_LD_max*(M_w/M_a)/(P_atm-p_v_LD_max) "Max LD Humidity Ratio SAR"
omega_air_15=omega_air_13+epsilon_SAR_lat*(omega_LD_max -omega_air_13) "Effectiveness of LD Moisture Removal in SAR"
epsilon_SAR_lat=HX('crossflow_both_unmixed', Ntu_SAR_lat, m_dot_air_14_dry, m_dot_LD_10, 'epsilon') "Effectiveness of AAHX at Max Flow"

"Heat Transfer Effectiveness"

M_LD_SAR=average(m_dot_LD_10,m_dot_LD_11)*cp_LD_SAR_avg "LD Heat Capacity Rate in SAR"
M_steam_SAR=m_dot_steam_8*Cp(Steam,T=373.15 [K], P=P_atm) "Steam Heat Capacity Rate in SAR"
M_air_SAR=m_dot_air_15_dry*cp_air_SAR_avg "Air Heat Capacity Rate in SAR"
M_SAR_min=min(M_steam_SAR, M_air_SAR) "Minimum Heat Capacity Rate in SAR"
Q_dot_SAR=q_dot_air_tot "Heat Gain/Loss in Air in SAR"
Ntu_SAR_T = UA_SAR_T/(M_air_SAR) "NTU for AAHX"
{epsilon_SAR_T=Q_dot_SAR/q_dot_steam "SAR Effectiveness at Raising Air Temperature"}
epsilon_SAR_T=(T_air_15-T_air_14)/(373.15 [K] - T_air_14) "Hot Air Temperature after Scavenging Air Regenerator"
epsilon_SAR_T=1-exp(-NTU_SAR_T) "SAR Effectiveness at Raising Air Temperature"
{ UA_SAR_T=14.27 [J/s-K] "UA Value of SAR Temperature Change"}

m_dot_v_IP=m_dot_v*convert(kg/s,lbm/hr) "Water Vapor Mass Flow Rate"
q_dot_air_tot=m_dot_air_15_dry*h_air_15-m_dot_air_14_dry*h_air_14 "Energy rate transfer in air"
q_dot_mix=m_dot_v*h_mix_5_6 "Energy rate transfer due to heat of mixing"
q_dot_LD=m_dot_LD_11*cp_LD_SAR_avg*(T_LD_11-273.15 [K])-m_dot_LD_10*cp_LD_SAR_avg*(T_LD_10-273.15 [K]) "Energy rate transfer in LD stream"
Q_dot_EB_SAR=m_dot_steam_8*(h_v_8-h_w_17)+m_dot_LD_10*cp_LD_SAR_avg*(T_LD_10-273.15 [K])-m_dot_LD_11*cp_LD_SAR_avg*(T_LD_11-273.15 [K])+m_dot_air_14_dry*h_air_14-m_dot_air_15_dry*h_air_15-q_dot_mix

"State 18: Mixing LD Flows after Two ICHXs"

T_LD_18_F=converttemp(K,F,T_LD_18) "LD Temperature"
T_LD_18_C=converttemp(K,C,T_LD_18) "LD Temperature"
m_dot_LD_18=m_dot_LD_7+m_dot_LD_12 "Total LD Flow after ICHX"
m_dot_LD_18*C_LD_18=m_dot_LD_7*C_LD_7+m_dot_LD_12*C_LD_12 "Total Mixed LD Concentration after Regeneration"
m_dot_LD_18*T_LD_18=m_dot_LD_7*T_LD_7+m_dot_LD_12*T_LD_12 "Total Mixed LD Temperature after Regeneration"
Call p_vapor_sol(T_LD_18,C_LD_18,Des$:p_v_LD_18) "LD Vapor Pressure of Mixed Regenerated Flow"
omega_LD_18=p_v_LD_18*(M_w/M_a)/(P_atm-p_v_LD_18) "LD Humidity Ratio of Mixed Regenerated Flow"

"State 19: Mixing Regenerated LD with Weak LD into DEVap"

T_LD_19_F=converttemp(K,F,T_LD_19) "LD Temperature"
T_LD_19_C=converttemp(K,C,T_LD_19) "LD Temperature"
m_dot_LD_19=m_dot_LD_18+m_dot_LD_3 "Total LD Flow after Both ICHX into DEVap"
m_dot_LD_19*C_LD_19=m_dot_LD_18*C_LD_18+m_dot_LD_3*C_LD_3 "Total Mixed LD Concentration after ICHX into DEVap"
m_dot_LD_19*T_LD_19=m_dot_LD_18*T_LD_18+m_dot_LD_3*T_LD_3 "Total Mixed LD Concentration after ICHX into DEVap"
Call p_vapor_sol(T_LD_19,C_LD_19,Des$:p_v_LD_19) "LD Vapor Pressure into DEVap"
omega_LD_19=p_v_LD_19*(M_w/M_a)/(P_atm-p_v_LD_19) "LD Humidity Ratio of Mixed Flow into DEVap"

"COP Calculations"

h_fg_regen= enthalpy(water,T=300,x=1) - enthalpy(water,T=300,x=0) "Regneration Heat of Evaporation, Assumes Room Temperature of 300 K"
COP_reg=m_dot_v_tot*h_fg_regen/Q_dot_rate "Latent COP of 2-Stage Regenerator System"
COP_boil=m_dot_steam_8*h_fg_regen/Q_dot_rate "Latent COP of Boiler"
COP_SAR=m_dot_v*h_fg_regen/q_dot_steam "Latent COP of Scavenging Air Regenerator"
m_dot_v_tot=m_dot_steam_8+m_dot_v "Total Moisture Removal Rate"

Appendix B: Design Expert Correlations

B.1 Dehumidification Mode

Table B.20: Expected Dehumidification Mode Operating Conditions

Parameter	Range
Return air temperature, T_{ra} (°F)	50 – 80
Return air relative humidity, RH_{ra}	0.50 – 1.00
Ratio of mixed air mass flow rate to design mass flow rate, R_{ma}	0.3 – 1.0
Inlet liquid desiccant concentration, $C_{LD,in,DEVap}$	0.30 – 0.44

Table B.21: Dehumidification Mode Design of Experiments Results

T_{ra} (°F)	RH_{ra} (-)	R_{ma} (-)	$C_{LD,in,DEVap}$ (-)	T_{sa} (°F)	ω_{sa} (-)	ΔP_{sa} (in H_2O)
50.00	0.50	0.65	0.37	57.0	0.0024	0.304
50.00	0.75	0.65	0.30	57.3	0.0042	0.306
50.00	0.75	1.00	0.37	62.7	0.0031	0.535
50.00	0.75	0.30	0.37	63.3	0.0029	0.115
65.00	0.50	0.65	0.30	67.6	0.0060	0.318
50.00	0.75	0.65	0.44	68.5	0.0019	0.311
50.00	1.00	0.65	0.37	68.6	0.0037	0.313
65.00	0.50	1.00	0.37	74.4	0.0046	0.558
65.00	0.75	1.00	0.30	74.5	0.0079	0.563
65.00	0.75	0.30	0.30	74.8	0.0078	0.121
65.00	0.50	0.30	0.37	74.8	0.0045	0.120
65.00	1.00	0.65	0.30	81.0	0.0098	0.331
65.00	0.50	0.65	0.44	81.8	0.0031	0.325
65.00	0.75	0.65	0.37	82.8	0.0061	0.328
65.00	1.00	1.00	0.37	89.4	0.0080	0.580
65.00	0.75	1.00	0.44	90.4	0.0046	0.576
65.00	1.00	0.30	0.37	90.4	0.0078	0.125
80.00	0.75	0.65	0.30	91.9	0.0140	0.346
65.00	0.75	0.30	0.44	91.8	0.0044	0.124
80.00	0.50	0.65	0.37	92.2	0.0084	0.341
65.00	1.00	0.65	0.44	99.7	0.0060	0.340
80.00	0.75	1.00	0.37	101.8	0.0120	0.609
80.00	0.75	0.30	0.37	102.7	0.0118	0.131
80.00	1.00	0.65	0.37	110.9	0.0157	0.361
80.00	0.75	0.65	0.44	113.8	0.0095	0.357

Table B.22: Dehumidification Mode Correlation Results

Correlation Term	T_{sa} (°F)	ω_{sa} (-)	ΔP_{sa} (in H_2O)
Exponent	0.2154	0.1640	-3.5030
x_0	0.2154	0.1640	-3.5030
x_A (A: T_{ra})	-0.0021	-0.0009	0.0009
x_B (B: RH_{ra})	-0.0420	-0.0476	-0.0418
x_C (C: R_{ma})	-0.0001	-0.0113	4.5203
x_D (D: C_{LD})	-0.1285	-0.1713	-0.0607
x_A^2	0.0000	0.0000	0.0000
x_B^2	0.0087	-0.0092	-0.0144
x_C^2	0.0006	0.0009	-1.7910
x_D^2	0.0645	-0.2316	-0.0361
x_{AB}	0.0002	0.0016	0.0020
x_{AC}	0.0000	0.0000	0.0000
x_{AD}	0.0002	0.0012	0.0033
x_{BC}	0.0001	0.0045	0.0027
x_{BD}	0.0077	0.0426	0.0503
x_{CD}	0.0009	0.0282	0.0116

Table B.23: Dehumidification Mode Correlation Accuracy

Correlation	Max Δ	Min Δ	Avg Δ	Max %Δ	Min %Δ	Avg %Δ	R^2
T_{sa} (°F)	0.32	-0.43	0.00	0.36%	-0.37%	0.00%	1.000
ω_{sa}	0.0002	-0.0001	0.0000	1.86%	-2.53%	-0.23%	1.000
ΔP_{sa} (in H_2O)	0.001	-0.001	0.000	0.12%	-0.17%	0.00%	1.000

B.2 Indirect Evaporative Cooling Mode

Table B.24: Expected Indirect Evaporative Cooling Mode Operating Conditions

Parameter	Range
Outdoor air fraction, OAF	0.05 – 0.50
Ratio of mixed air mass flow rate to design mass flow rate, R_{ma}	0.3 – 1.0
Ratio of first stage exhaust air mass flow rate to design mass flow rate, R_{e1}	0.1 – 0.7
Return air temperature, T_{ra} (°F)	65 – 80
Return air relative humidity, RH_{ra}	0.15 – 0.65
Outdoor air temperature, T_{oa} (°F)	60 – 120
Outdoor air humidity ratio, ω_{oa}	0.0003 – 0.0110

Table B.25: Indirect Evaporative Cooling Mode Design of Experiments Results

T_{ra} (°F)	RH_{ra} (-)	T_{oa} (°F)	ω_{oa} (-)	R_{ma} (-)	R_{e1} (-)	OAF (-)	$T_{pa,1}$ (°F)	ΔP_{e1} (in H_2O)	ΔP_{s1} (in H_2O)	T_{sa} (°F)	ΔP_{e2} (in H_2O)	ΔP_{s2} (in H_2O)
80	0.4	90	0.00615	0.65	0.07	0.05	76.22	0.03164	0.08904	73.63	0.005164	0.3301
65	0.4	90	0.00615	0.65	0.07	0.05	65.56	0.03081	0.08774	63.65	0.004964	0.3157
72.5	0.4	60	0.0003	0.65	0.38	0.05	50.48	0.1591	0.09071	50.13	0.004771	0.3131
72.5	0.4	62.3	0.012	0.65	0.37	0.05	64.56	0.1642	0.08656	63.17	0.004977	0.3198
72.5	0.15	90	0.00615	1	0.38	0.05	65.96	0.2613	0.08841	63.41	0.008552	0.5494
72.5	0.15	90	0.00615	0.3	0.38	0.05	64.76	0.0785	0.03182	62.33	0.001827	0.1176
72.5	0.65	90	0.00615	1	0.38	0.05	66	0.2635	0.1494	65.34	0.008774	0.5636
72.5	0.65	90	0.00615	0.3	0.38	0.05	64.8	0.07915	0.03344	64.27	0.001875	0.1207
72.5	0.4	120	0.0003	0.65	0.38	0.05	66.96	0.1778	0.1563	65.15	0.005001	0.3215
72.5	0.4	120	0.012	0.65	0.37	0.05	78.23	0.1827	0.08917	75.04	0.005166	0.3267
65	0.4	90	0.00615	0.65	0.68	0.05	63.41	0.3072	0.09109	61.73	0.004934	0.3148
80	0.4	90	0.00615	0.65	0.69	0.05	65.25	0.311	0.08882	64.15	0.005011	0.3256
72.5	0.4	60	0.00615	1	0.07	0.225	66.16	0.04542	0.09051	56.99	0.05864	0.5472
72.5	0.4	60	0.00615	0.3	0.07	0.225	66.15	0.01363	0.0889	56.76	0.01257	0.1173
72.5	0.15	90	0.0003	0.65	0.07	0.225	71.5	0.03095	0.08786	52.66	0.0334	0.3125
72.5	0.65	90	0.0003	0.65	0.07	0.225	71.47	0.03116	0.09103	61.19	0.03447	0.3224
72.5	0.15	90	0.012	0.65	0.07	0.225	75.08	0.03158	0.0324	57.51	0.03407	0.3171
72.5	0.65	90	0.012	0.65	0.07	0.225	75.05	0.03179	0.1522	65.84	0.03514	0.3269
72.5	0.4	120	0.00615	0.3	0.07	0.225	80.17	0.01535	0.08498	60.66	0.0129	0.1203
72.5	0.4	120	0.00615	1	0.07	0.225	80.19	0.05115	0.08752	61.43	0.06017	0.5618
80	0.15	60	0.00615	0.65	0.38	0.225	58.4	0.1614	0.08858	49.89	0.03281	0.3124
65	0.15	60	0.00615	0.65	0.38	0.225	55.27	0.1592	0.09107	46.97	0.03242	0.3048
80	0.5	65	0.005	0.65	0.38	0.25	58.59	0.1635	0.03328	56.93	0.03855	0.321
65	0.65	60	0.00615	0.65	0.38	0.225	55.28	0.1601	0.1561	53.56	0.03322	0.3123
65	0.4	90	0.0003	1	0.38	0.225	59.11	0.2574	0.08851	50.59	0.05708	0.539
80	0.4	90	0.0003	1	0.38	0.225	62.48	0.2609	0.09025	55.66	0.05824	0.5567
65	0.4	90	0.0003	0.3	0.38	0.225	57.19	0.07743	0.0871	49.54	0.01218	0.1154
80	0.4	90	0.0003	0.3	0.38	0.225	59.25	0.07856	0.08978	54.04	0.0124	0.1191
72.5	0.4	90	0.00615	0.65	0.38	0.225	66.15	0.1711	0.03314	57.04	0.0338	0.3186
65	0.4	90	0.012	1	0.37	0.225	70.84	0.2653	0.155	59.06	0.05923	0.5499
65	0.4	90	0.012	0.3	0.37	0.225	70.84	0.07958	0.0871	58.81	0.0127	0.1179
80	0.4	90	0.012	1	0.38	0.225	73.69	0.2687	0.08978	63.34	0.0603	0.5671
80	0.4	90	0.012	0.3	0.38	0.225	72.4	0.08072	0.08601	62.7	0.0129	0.1215
65	0.65	120	0.00615	0.65	0.38	0.225	73.32	0.1809	0.08824	61.23	0.0345	0.3222
80	0.15	120	0.00615	0.65	0.38	0.225	75.32	0.1819	0.08466	56.53	0.03396	0.3218
80	0.65	120	0.00615	0.65	0.38	0.225	75.38	0.1834	0.0866	67.35	0.03535	0.3347
65	0.15	120	0.00615	0.65	0.38	0.225	73.29	0.18	0.0322	54.7	0.03367	0.3147
72.5	0.4	60	0.00615	0.3	0.69	0.225	53.27	0.1342	0.0328	50.67	0.01222	0.1162
72.5	0.4	60	0.00615	1	0.69	0.225	55.69	0.4467	0.03266	52.06	0.05731	0.5432
72.5	0.15	90	0.0003	0.65	0.69	0.225	57.05	0.3032	0.03358	46.78	0.03242	0.3098
72.5	0.65	90	0.0003	0.65	0.69	0.225	57.12	0.3053	0.08848	55.43	0.03347	0.3196
72.5	0.15	90	0.012	0.65	0.68	0.225	71.5	0.314	0.1506	56.48	0.03385	0.3166
72.5	0.65	90	0.012	0.65	0.68	0.225	71.53	0.3161	0.1537	64.87	0.03492	0.3265
72.5	0.4	120	0.00615	0.3	0.69	0.225	72.83	0.1518	0.1533	59.18	0.01274	0.1201
72.5	0.4	120	0.00615	1	0.69	0.225	74	0.5069	0.1584	59.87	0.05954	0.5606
65	0.4	90	0.00615	0.65	0.07	0.4	72.24	0.03126	0.08857	47.83	0.06959	0.3127
80	0.4	90	0.00615	0.65	0.07	0.4	78.64	0.03178	0.09044	53.43	0.07109	0.3214
72.5	0.4	60	0.0003	0.65	0.38	0.4	49.21	0.158	0.08852	40.09	0.06653	0.3045
72.5	0.4	62.3	0.012	0.65	0.38	0.4	63.69	0.1638	0.09073	55.12	0.0704	0.3159
72.5	0.15	90	0.00615	0.3	0.38	0.4	65.71	0.07909	0.08412	41.91	0.02536	0.1156
72.5	0.65	90	0.00615	0.3	0.38	0.4	65.73	0.07949	0.08918	55.54	0.02629	0.1196
72.5	0.65	90	0.00615	1	0.38	0.4	67.61	0.2644	0.03279	56.4	0.123	0.5585
72.5	0.15	90	0.00615	1	0.38	0.4	67.6	0.2631	0.1547	43.86	0.1188	0.5405
72.5	0.4	120	0.0003	0.65	0.38	0.4	70.13	0.1799	0.08436	43.93	0.06873	0.3173
72.5	0.4	120	0.012	0.65	0.38	0.4	80.86	0.1855	0.0904	56.28	0.07182	0.3274
65	0.4	90	0.00615	0.65	0.68	0.4	64.55	0.3091	.0105	47.03	0.06891	0.3123
80	0.4	90	0.00615	0.65	0.69	0.4	65.65	0.3114	0.09039	52.49	0.07003	0.3209
75	0.55	64	0.011	0.65	0.68	0.113	62.94	0.2988	0.03224	61.81	0.01419	0.3229
75	0.55	65	0.00565	0.65	0.69	0.148	56.15	0.2947	0.1513	56.06	0.01962	0.3194
70	0.55	68.5	0.0003	0.53	0.69	0.18	48.21	0.2371	0.08442	48.14	0.01882	0.2401
80	0.55	75	0.011	0.65	0.69	0.104	66.77	0.307	0.0866	65.67	0.01296	0.3289
79.5	0.55	75	0.00565	0.65	0.69	0.13	60.05	0.3021	0.0884	60.01	0.01689	0.3252
76.5	0.55	82.5	0.0003	0.65	0.69	0.16	54.86	0.3011	0.09055	54.75	0.02157	0.3202
75	0.55	90	0.011	0.65	0.07	0.5	79.08	0.03203	0.03319	59.12	0.09597	0.326
80	0.55	90	0.011	0.65	0.07	0.5	80.78	0.03218	0.1557	61.34	0.09674	0.3291
75	0.55	105	0.011	0.65	0.07	0.5	85.13	0.03319	0.08794	59.21	0.09643	0.3296
80	0.55	105	0.011	0.65	0.07	0.5	86.68	0.03335	0.08931	61.4	0.09718	0.3327
75	0.55	120	0.011	0.65	0.07	0.5	90.74	0.03436	0.08852	59.28	0.09684	0.3332
80	0.55	120	0.011	0.65	0.07	0.5	92.13	0.03452	0.08791	61.45	0.09756	0.3363
75	0.55	90	0.00565	0.65	0.07	0.5	77.44	0.03169	0.0908	52.13	0.09394	0.3203
80	0.55	90	0.00565	0.65	0.07	0.5	79.15	0.03185	0.08589	54.75	0.09475	0.3235
75	0.55	105	0.00565	0.65	0.07	0.5	83.46	0.03284	0.08772	52.28	0.09443	0.3239
80	0.55	105	0.00565	0.65	0.07	0.5	85.03	0.03299	0.04194	54.86	0.09521	0.3271
75	0.55	120	0.00565	0.65	0.07	0.5	89.06	0.03399	0.1488	52.4	0.09485	0.3274
80	0.55	120	0.00565	0.65	0.07	0.5	90.46	0.03415	0.033	54.95	0.09561	0.3307
79.5	0.55	90	0.0027	0.65	0.69	0.05	60.87	0.3089	0.1551	60.87	0.004994	0.3264

Table B.26: Indirect Evaporative Cooling Mode Correlation Results – 1st Stage

Correlation Term	$T_{pa,1}$ (°F)	ΔP_{e1} (in H_2O)	ΔP_{s1} (in H_2O)
Exponent	1.27	0.01	0.51
x_0	59.4834	0.9410	0.1299
x_A (A: T_{ma})	-0.5319	0.0000	-0.0010
x_B (B: RH_{ma})	-76.3586	0.0002	-0.0734
x_C (C: R_{ma})	-31.6305	0.0341	0.7057
x_D (D: T_{oa})	1.6856	0.0000	0.0002
x_E (E: ω_{oa})	5224.3222	-0.0012	-0.3034
x_F (F: OAF)	69.7127	-0.0001	-0.0344
x_G (G: R_{e1})	-2.5606	0.0216	0.0013
x_A^2	0.0351	0.0000	0.0000
x_B^2	54.7863	0.0000	0.0035
x_C^2	5.9198	-0.0135	-0.1469
x_D^2	0.0033	0.0000	0.0000
x_E^2	7341.6845	0.2135	0.7177
x_F^2	37.4118	0.0000	0.0079
x_G^2	10.3969	-0.0042	0.0005
x_{AB}	0.5299	0.0000	0.0010
x_{AC}	0.6379	0.0000	0.0009
x_{AD}	-0.0244	0.0000	0.0000
x_{AE}	-24.3898	0.0002	0.0071
x_{AF}	-1.4125	0.0000	0.0004
x_{AG}	-1.1637	0.0000	-0.0001
x_{BC}	-0.7926	-0.0001	0.0222
x_{BD}	0.0380	0.0000	0.0000
x_{BE}	-1986.6245	-0.0091	-0.0715
x_{BF}	20.3220	0.0002	0.0532
x_{BG}	3.3772	0.0000	0.0001
x_{CD}	-0.1953	0.0000	0.0000
x_{CE}	-869.7421	0.0073	0.2435
x_{CF}	-0.1459	0.0000	-0.0211
x_{CG}	4.2978	0.0002	-0.0006
x_{DE}	-4.6522	0.0000	-0.0010
x_{DF}	0.2782	0.0000	-0.0002
x_{DG}	0.3827	0.0000	0.0000
x_{EF}	-680.2760	-0.0101	-0.7985
x_{EG}	1499.1868	0.0037	0.0532
x_{FG}	-1.2838	0.0000	0.0030

Table B.27: Indirect Evaporative Cooling Mode Correlation Results – 2nd Stage

Correlation Term	T_{sa} (°F)	ΔP_{e2} (in H_2O)	ΔP_{s2} (in H_2O)
Exponent	0.77	0.79	0.54
x_0	23.3906	0.0140	0.2866
x_A (A: $T_{pa,1}$)	-0.0370	-0.0001	-0.0026
x_B (B: $RH_{pa,1}$)	-15.6155	-0.0248	0.0111
x_C (C: R_{ma})	0.4894	-0.0167	-0.0008
x_D (D: OAF)	-34.2984	0.0000	-0.0261
x_A^2	0.0012	-0.1598	0.0000
x_B^2	0.6434	-0.0497	-0.0013
x_C^2	-0.2634	0.0003	-0.0009
x_D^2	9.2999	0.0000	0.0412
x_{AB}	0.2187	0.0019	-0.0001
x_{AC}	0.0000	0.0015	0.0000
x_{AD}	0.0261	0.0000	0.0003
x_{BC}	-0.4892	-1.0693	-0.0006
x_{BD}	30.4071	-0.0106	-0.0106
x_{CD}	1.1934	0.0003	0.0026

Table B.28: Indirect Evaporative Cooling Mode Correlation Accuracy

Correlation	Max Δ	Min Δ	Avg Δ	Max %Δ	Min %Δ	Avg %Δ	R^2
$T_{pa,1}$ (°F)	1.56	-1.35	0.03	2.45%	-2.20%	0.06%	0.996
ΔP_{e1} (in H_2O)	0.002	-0.001	0.000	0.44%	-0.37%	0.02%	1.000
ΔP_{s1} (in H_2O)	0.001	-0.002	0.000	0.36%	-0.41%	0.05%	1.000
T_{sa} (°F)	1.35	-2.01	0.09	2.39%	-2.68%	0.18%	0.991
ΔP_{e2} (in H_2O)	0.001	-0.001	0.000	1.22%	-1.36%	0.31%	0.992
ΔP_{s2} (in H_2O)	0.002	-0.003	0.000	1.41%	-1.27%	0.26%	0.990

B.3 Standard Mode

Table B.29: Expected Standard Mode Operating Conditions

Parameter	Range
Outdoor air fraction, OAF	0.05 – 0.50
Inlet liquid desiccant concentration to DEVap, $C_{LD,in,DEVap}$	0.20 – 0.44
Ratio of mixed air mass flow rate to design mass flow rate, R_{ma}	0.3 – 1.0
Ratio of first stage exhaust air mass flow rate to design mass flow rate, R_{e1}	0.1 – 0.7
Return air temperature, T_{ra} (°F)	65 – 80
Return air relative humidity, RH_{ra}	0.15 – 0.65
Outdoor air temperature, T_{oa} (°F)	60 – 120
Outdoor air humidity ratio, ω_{oa}	0.0076 – 0.0267
Outdoor air humidity ratio, WB_{oa} (°F)	56 – 84

Table B.30: Standard Mode Design of Experiments Results

T_{ra} (°F)	RH_{ra} (-)	T_{oa} (°F)	ω_{oa} (-)	R_{ma} (-)	R_{e1} (-)	OAF (-)	$C_{LD,in,DEVap}$ (-)	$T_{pa,1}$ (°F)	ω_{sa} (-)	ΔP_{e1} (in H_2O)	ΔP_{s1} (in H_2O)	T_{sa} (°F)	ΔP_{e2} (in H_2O)	ΔP_{s2} (in H_2O)
72.5	0.4	90	0.01695	0.65	0.1	0.3	0.3	79.15	0.009151	0.07269	0.08904	59.83	0.05015	0.235
65	0.4	90	0.01695	0.65	0.4	0.1	0.3	74.22	0.007449	0.287	0.08774	68.9	0.01237	0.2324
80	0.4	90	0.01695	0.65	0.4	0.1	0.3	78.08	0.008874	0.2905	0.09071	72.22	0.01254	0.2399
72.5	0.18	90	0.0076	0.65	0.4	0.3	0.3	66.16	0.005744	0.2788	0.08656	51.72	0.04828	0.2277
72.5	0.65	90	0.0076	0.65	0.4	0.3	0.3	70.75	0.007165	0.2819	0.08841	55.24	0.04902	0.2333
72.5	0.4	60	0.0093	0.3	0.4	0.3	0.3	58.88	0.004493	0.2643	0.03182	47.28	0.0176	0.08397
72.5	0.4	60	0.0093	1	0.4	0.3	0.3	64.48	0.005757	0.2663	0.1494	51.63	0.08353	0.3945
72.5	0.4	120	0.0128	0.3	0.4	0.3	0.3	79.97	0.009346	0.3022	0.03344	59.5	0.01868	0.08796
72.5	0.4	120	0.0128	1	0.4	0.3	0.3	80.48	0.009479	0.3027	0.1563	61.01	0.08734	0.4112
72.5	0.15	85	0.02668	0.65	0.4	0.3	0.3	83.38	0.01031	0.2961	0.08917	62.16	0.05073	0.2354
72.5	0.65	85	0.02668	0.65	0.4	0.3	0.3	86.79	0.0121	0.2987	0.09109	65.36	0.05142	0.2412
65	0.4	90	0.01695	0.65	0.4	0.5	0.3	78.65	0.009135	0.2908	0.08882	55.32	0.09488	0.2343
80	0.4	90	0.01695	0.65	0.4	0.5	0.3	80.61	0.009983	0.2924	0.09051	57.52	0.09563	0.2385
72.5	0.4	90	0.01695	0.65	0.7	0.3	0.3	77.54	0.008705	0.5077	0.0889	58.9	0.04992	0.2346
72.5	0.15	90	0.01695	0.65	0.1	0.1	0.37	74.36	0.004391	0.07194	0.08786	67.49	0.01224	0.2323
72.5	0.65	90	0.01695	0.65	0.1	0.1	0.37	86.58	0.007294	0.07376	0.09103	76.58	0.01272	0.2419
72.5	0.4	90	0.0076	0.3	0.1	0.3	0.37	72.31	0.004324	0.07111	0.0324	49.63	0.01798	0.08537
72.5	0.4	90	0.0076	1	0.1	0.3	0.37	78.85	0.005551	0.07126	0.1522	54.11	0.0853	0.4012
65	0.4	60	0.0093	0.65	0.1	0.3	0.37	68.82	0.003848	0.06707	0.08498	48.77	0.04797	0.2246
80	0.4	60	0.0093	0.65	0.1	0.3	0.37	76.83	0.00537	0.06831	0.08752	52.81	0.04894	0.2311
65	0.4	120	0.0128	0.65	0.1	0.3	0.37	83.73	0.006333	0.07609	0.08858	55.38	0.04966	0.2333
80	0.4	120	0.0128	0.65	0.1	0.3	0.37	89.9	0.008108	0.07718	0.09107	58.92	0.05049	0.2396
72.5	0.4	85	0.02668	0.3	0.1	0.3	0.37	88.66	0.007568	0.07527	0.03328	56.92	0.01869	0.08799
72.5	0.4	85	0.02668	1	0.1	0.3	0.37	91.83	0.008795	0.07516	0.1561	61.06	0.08818	0.413
72.5	0.15	90	0.01695	0.65	0.1	0.5	0.37	85.73	0.007007	0.07374	0.08851	49.6	0.09392	0.233
72.5	0.65	90	0.01695	0.65	0.1	0.5	0.37	91.29	0.008829	0.07455	0.09025	54.77	0.09563	0.2382
72.5	0.4	60	0.0093	0.65	0.4	0.108	0.37	64.22	0.003398	0.2674	0.0871	59.1	0.01311	0.2305
72.5	0.4	120	0.0128	0.65	0.4	0.1	0.37	80.98	0.005757	0.3027	0.08978	72.56	0.01249	0.2378
72.5	0.4	90	0.01695	0.3	0.4	0.103	0.37	77.28	0.004993	0.2902	0.03314	69.55	0.00477	0.08785
72.5	0.4	90	0.01695	1	0.4	0.1	0.37	79.38	0.005636	0.2908	0.155	71.48	0.02159	0.4109
72.5	0.4	60	0.0093	0.65	0.4	0.107	0.37	64.22	0.003398	0.2674	0.0871	59.15	0.01295	0.2305
72.5	0.4	120	0.0128	0.65	0.4	0.1	0.37	80.98	0.005757	0.3027	0.08978	72.56	0.01249	0.2378
65	0.4	90	0.0076	0.65	0.4	0.3	0.37	68.77	0.003826	0.2806	0.08601	48.79	0.04797	0.2268
80	0.4	90	0.0076	0.65	0.4	0.3	0.37	72.23	0.004582	0.2835	0.08824	50.83	0.04843	0.2324
72.5	0.15	60	0.0093	0.65	0.4	0.3	0.37	61.41	0.002913	0.2653	0.08466	45.25	0.04712	0.2232
72.5	0.65	60	0.0093	0.65	0.4	0.3	0.37	67.07	0.003994	0.2691	0.0866	48.75	0.04788	0.2291
65	0.15	90	0.01695	0.3	0.4	0.3	0.37	76.92	0.004892	0.2896	0.0322	51.23	0.01816	0.08494
80	0.15	90	0.01695	0.3	0.4	0.3	0.37	77.43	0.005035	0.2907	0.0328	51.57	0.01819	0.08633
65	0.65	90	0.01695	0.3	0.4	0.3	0.37	77.95	0.005195	0.2912	0.03266	51.98	0.01822	0.08635
80	0.65	90	0.01695	0.3	0.4	0.3	0.37	79.15	0.005569	0.2932	0.03358	52.84	0.01829	0.08876
72.5	0.4	90	0.01695	0.65	0.4	0.3	0.37	80.38	0.005905	0.2922	0.08848	54.36	0.04935	0.2336
65	0.15	90	0.01695	1	0.4	0.3	0.37	77.64	0.005147	0.2897	0.1506	53.26	0.08498	0.3974
80	0.15	90	0.01695	1	0.4	0.3	0.37	80.48	0.005863	0.292	0.1537	54.92	0.08564	0.4048
65	0.65	90	0.01695	1	0.4	0.3	0.37	82.25	0.006621	0.2924	0.1533	56.5	0.0862	0.4056
80	0.65	90	0.01695	1	0.4	0.3	0.37	87.5	0.008549	0.296	0.1584	60.32	0.08766	0.4187
72.5	0.15	120	0.0128	0.65	0.4	0.3	0.37	80.79	0.00565	0.303	0.08857	53.86	0.0493	0.2327
72.5	0.65	120	0.0128	0.65	0.4	0.3	0.37	84.7	0.007006	0.3059	0.09044	56.7	0.04991	0.2384
65	0.4	85	0.02668	0.65	0.4	0.3	0.37	86.84	0.007241	0.2985	0.08852	57.3	0.0501	0.2343
80	0.4	85	0.02668	0.65	0.4	0.3	0.37	89.19	0.008174	0.3008	0.09073	59.09	0.05049	0.2398
72.5	0.4	61	0.0077	0.65	0.4	0.489	0.37	62.28	0.003189	0.2659	0.08412	36.17	0.08646	0.2216
72.5	0.4	120	0.0076	0.65	0.4	0.5	0.37	78.89	0.005595	0.3	0.08918	45.04	0.09232	0.2335
72.5	0.4	90	0.01695	0.3	0.4	0.5	0.37	78.38	0.005326	0.2921	0.03279	42.99	0.0342	0.08635
72.5	0.4	90	0.01695	1	0.4	0.5	0.37	84.41	0.007295	0.2942	0.1547	51.14	0.1633	0.4078
72.5	0.4	60	0.0093	0.65	0.4	0.5	0.37	64.39	0.003461	0.2672	0.08436	36.96	0.0893	0.2224
72.5	0.4	120	0.0128	0.65	0.4	0.5	0.37	84.47	0.006871	0.3062	0.0904	49.15	0.09373	0.2371
72.5	0.15	90	0.01695	0.65	0.7	0.1	0.37	76.1	0.004653	0.5057	0.08803	75.94	0.01923	0.01923
72.5	0.65	90	0.01695	0.65	0.7	0.1	0.37	79.98	0.005936	0.5106	0.09039	72.04	0.01247	0.2401
72.5	0.4	90	0.0076	0.3	0.7	0.3	0.37	66.05	0.003348	0.4894	0.03224	46.89	0.01771	0.08493
72.5	0.4	90	0.0076	1	0.7	0.3	0.37	70.98	0.004408	0.4928	0.1513	50.76	0.08381	0.3987
65	0.4	60	0.0093	0.65	0.7	0.3	0.37	60.78	0.002922	0.4628	0.08442	45.13	0.04707	0.223
80	0.4	60	0.0093	0.65	0.7	0.3	0.37	63.59	0.003439	0.4666	0.0866	46.91	0.04745	0.2285
65	0.4	120	0.0128	0.65	0.7	0.3	0.37	81.03	0.005808	0.531	0.0884	54.2	0.04936	0.2328
80	0.4	120	0.0128	0.65	0.7	0.3	0.37	82.89	0.006473	0.5338	0.09055	55.6	0.04966	0.2382
72.5	0.4	85	0.02668	0.3	0.7	0.3	0.37	85.62	0.006756	0.5224	0.03319	55.35	0.01855	0.08776
72.5	0.4	85	0.02668	1	0.7	0.3	0.37	88.2	0.008057	0.5235	0.1557	59.56	0.08749	0.4118
72.5	0.15	90	0.01695	0.65	0.7	0.5	0.37	79.51	0.005744	0.5104	0.08794	45.58	0.09249	0.2314
72.5	0.65	90	0.01695	0.65	0.7	0.5	0.37	81.61	0.00654	0.5128	0.08931	48.14	0.09327	0.2356
72.5	0.4	90	0.01695	0.65	0.1	0.3	0.44	89.85	0.004592	0.07443	0.08852	52.88	0.04953	0.2338
65	0.4	90	0.01695	0.65	0.4	0.1	0.44	78.62	0.002876	0.2905	0.08791	69.62	0.0123	0.2335
80	0.4	90	0.01695	0.65	0.4	0.1	0.44	82.23	0.003568	0.2941	0.0908	72.24	0.01244	0.2409
72.5	0.15	90	0.0076	0.65	0.4	0.3	0.44	69.23	0.002044	0.2815	0.08589	45.55	0.04752	0.226
72.5	0.65	90	0.0076	0.65	0.4	0.3	0.44	74.33	0.002866	0.2852	0.08772	48.08	0.04812	0.2316
72.5	0.403	65	0.0093	0.373	0.4	0.3	0.44	62.43	0.001575	0.2696	0.04194	42.82	0.02303	0.1107
72.5	0.4	60	0.0093	1	0.4	0.3	0.44	69.77	0.002573	0.2697	0.1488	47.15	0.08278	0.3931
72.5	0.4	120	0.0128	0.3	0.4	0.3	0.44	81.08	0.003055	0.3045	0.033	48.25	0.01807	0.08684
72.5	0.4	120	0.0128	1	0.4	0.3	0.44	87.09	0.00443	0.3069	0.1551	53.25	0.08567	0.4083
72.5	0.15	85	0.02668	0.65	0.4	0.3	0.44	88.2	0.004254	0.3	0.0882	52.2	0.04936	0.233
72.5	0.65	85	0.02668	0.65	0.4	0.3	0.44	91.74	0.005361	0.3027	0.09001	54.52	0.04986	0.2385
65	0.4	90	0.01695	0.65	0.4	0.5	0.44	82.99	0.00379	0.2944	0.08719	39.36	0.09131	0.2297
80	0.4	90	0.01695	0.65	0.4	0.5	0.44	84.85	0.004231	0.2961	0.0888	40.95	0.0918	0.2338
72.5	0.4	90	0.01695	0.65	0.7	0.3	0.44	80.51	0.003364	0.5118	0.088	49.87	0.04867	0.2323

Table B.31: Standard Mode Correlation Results

Correlation Term	$T_{pa,1}$ (°F)	ω_{sa} (-)	ΔP_{e1} (in H_2O)	ΔP_{s1} (in H_2O)
Exponent	1.23	0.31	0.03	0.33
x_0	-102.7523	0.1768	0.8946	0.1775
x_A (A: T_{ma})	1.0614	-0.0001	0.0000	-0.0003
x_B (B: RH_{ma})	80.3763	-0.0144	0.0017	-0.0360
x_C (C: R_{ma})	-116.4845	-0.1291	-0.0012	0.4684
x_D (D: T_{oa})	1.4423	0.0011	0.0001	0.0002
x_E (E: ω_{oa})	2130.3567	1.9752	0.0705	1.1751
x_F (F: R_{e1})	190.0641	0.1089	0.1966	0.0056
x_G (G: $C_{LD,in,DEVap}$)	253.7836	-0.1447	0.0058	0.0339
x_A^2	0.0097	0.0000	0.0000	0.0000
x_B^2	-53.2498	-0.0302	-0.0008	0.0164
x_C^2	-16.3751	-0.0136	-0.0003	-0.1441
x_D^2	-0.0006	0.0000	0.0000	0.0000
x_E^2	-26294.1711	-8.7285	-0.1269	-1.0156
x_F^2	69.2956	0.0389	-0.1267	0.0041
x_G^2	-267.5979	-0.2778	-0.0044	0.0644
x_{AB}	0.2868	0.0009	0.0000	0.0002
x_{AC}	1.8292	0.0017	0.0000	0.0003
x_{AD}	-0.0124	0.0000	0.0000	0.0000
x_{AE}	-22.5021	-0.0149	-0.0003	-0.0099
x_{AF}	-2.8695	-0.0018	0.0000	-0.0001
x_{AG}	-0.1865	-0.0002	0.0000	-0.0009
x_{BC}	74.6064	0.0772	0.0006	0.0094
x_{BD}	-0.1921	-0.0001	0.0000	0.0003
x_{BE}	782.5334	0.3810	0.0052	-0.5273
x_{BF}	-113.3729	-0.0680	-0.0016	-0.0054
x_{BG}	5.7908	0.0248	0.0003	-0.0185
x_{CD}	-0.5366	-0.0004	0.0000	0.0000
x_{CE}	-1907.8969	-1.5566	-0.0226	0.0534
x_{CF}	-9.3352	0.0021	0.0003	-0.0008
x_{CG}	171.8423	0.1676	0.0016	-0.0096
x_{DE}	18.3280	0.0171	0.0003	-0.0003
x_{DF}	0.8223	0.0005	0.0000	0.0000
x_{DG}	0.3764	-0.0007	0.0000	0.0000
x_{EF}	3023.3220	1.8025	0.0572	0.1258
x_{EG}	2760.1646	-1.5370	0.0319	-0.1665
x_{FG}	-316.2328	-0.1639	-0.0050	-0.0074

Table B.32: Standard Mode Correlation Results – 2nd Stage

Correlation Term	T_{sa} (°F)	ΔP_{e2} (in H_2O)	ΔP_{s2} (in H_2O)
Exponent	0.31	0.78	0.39
x_0	3.4797	0.0221	0.2158
x_A (A: $T_{pa,1}$)	0.0097	-0.0003	-0.0002
x_B (B: $RH_{pa,1}$)	-1.2552	-0.0334	-0.0640
x_C (C: R_{ma})	-0.1407	-0.0220	0.6467
x_D (D: OAF)	-3.5439	-0.0403	-0.0513
x_A^2	0.0000	0.0000	0.0000
x_B^2	-0.1720	-0.0015	0.0130
x_C^2	-0.0079	0.0001	-0.1862
x_D^2	1.5895	-0.0260	0.0321
x_{AB}	0.0153	0.0003	0.0005
x_{AC}	0.0017	0.0003	0.0006
x_{AD}	0.0052	0.0005	0.0002
x_{BC}	-0.0273	0.0117	0.0253
x_{BD}	3.0705	0.0471	0.0410
x_{CD}	0.2095	0.4759	-0.0139

Table B.33: Standard Mode Correlation Accuracy

Correlation	Max Δ	Min Δ	Avg Δ	Max %Δ	Min %Δ	Avg %Δ	R^2
$T_{pa,1}$ (°F)	1.46	-1.40	0.00	1.88%	-1.83%	0.01%	0.995
ω_{sa} (-)	0.0003	-0.0003	0.0000	3.89%	-4.29%	0.02%	0.997
ΔP_{e1} (in H_2O)	0.001	-0.001	0.000	0.20%	-0.23%	0.00%	1.000
ΔP_{s1} (in H_2O)	0.001	-0.003	0.000	1.62%	-2.55%	0.00%	1.000
T_{sa} (°F)	2.79	-2.55	0.00	4.72%	-4.65%	0.01%	0.993
ΔP_{e2} (in H_2O)	0.000	0.000	0.000	0.85%	-1.65%	-0.01%	1.000
ΔP_{s2} (in H_2O)	0.004	-0.005	0.000	1.63%	-2.09%	0.00%	1.000

B.4 Regenerator System

Table B.34: Expected Regenerator Operating Conditions

Parameter	Range
Inlet liquid desiccant concentration	0.20 – 0.42
Liquid desiccant concentration change	0.02 – 0.08
Ambient air temperature	60 – 120°F
Ambient air humidity	0.0076 – 0.0260

Table B.35: Regenerator Design of Experiments Results

T_{oa} (°F)	ω_{oa} (-)	$C_{LD,in,reg}$ (-)	$\Delta C_{LD,reg}$ (-)	COP_{reg} (-)
90	0.01695	0.42	0.02	0.8122
85	0.026	0.24	0.08	1.255
90	0.01695	0.31	0.05	1.059
60	0.0093	0.42	0.02	0.812
120	0.0128	0.31	0.05	1.146
90	0.01695	0.31	0.05	1.145
90	0.01695	0.24	0.08	1.255
85	0.02595	0.26	0.06	1.183
90	0.01695	0.25	0.08	1.239
120	0.0128	0.42	0.02	0.8146
90	0.0076	0.31	0.08	1.171
60	0.0093	0.26	0.08	1.221
90	0.0076	0.31	0.03	0.925
85	0.026	0.26	0.06	1.183
85	0.026	0.36	0.05	0.9532
120	0.0128	0.26	0.08	1.223
60	0.0093	0.42	0.02	0.812
60	0.0093	0.36	0.08	1.087
120	0.0128	0.24	0.08	1.255
85	0.026	0.4	0.04	0.9583
120	0.0128	0.39	0.05	1.016
90	0.0076	0.31	0.08	1.171
90	0.0076	0.42	0.02	0.8137
85	0.026	0.42	0.02	0.8098
60	0.0093	0.27	0.08	1.202

Table B.36: Regenerator Correlation Results

Correlation Term	COP_{reg} (-)
Exponent	3.00
x_0	1.1213
x_A (A: $C_{LD,in,reg}$)	-4.8980
x_B (B: $\Delta C_{LD,reg}$)	53.1067
x_A^2	2.6326
x_B^2	-222.2705
x_{AB}	-50.1375

Table B.37: Dehumidification Mode Correlation Accuracy

Correlation	Max Δ	Min Δ	Avg Δ	Max %Δ	Min %Δ	Avg %Δ	R^2
COP_{reg} (-)	0.02	-0.03	0.00	2.69%	-3.74%	0.19%	0.996

Appendix C: Near-optimal Control Variable Values

C.1 IEC Mode

Table C.38: Near-optimal OAF Values to Hold Constant During Ramping Phase of IEC Mode

	OA (T_{oa}/ ω_{oa})											
RA (T_{ra}/ RH_{ra})	60°F/ 0.0003	60°F/ 0.0054	60°F/ 0.0110	75°F/ 0.0003	75°F/ 0.0054	75°F/ 0.0110	90°F/ 0.0027	90°F/ 0.0054	90°F/ 0.0080	105°F/ 0.0054	120°F/ 0.0003	120°F/ 0.0110
80°F/ 55%	0.192	0.052	0.062	0.139	0.050	0.145	0.453	0.419	0.356	0.445	0.482	0.427
75°F/ 55%	0.161	0.050	0.116	0.090	0.050	0.207	0.461	0.430	0.383	0.456	0.490	0.443
70°F/ 55%	0.112	0.050	0.167	0.484	0.367	0.259	0.475	0.448	0.412	0.472	0.503	0.467
80°F/ 45%	0.076	0.050	0.146	0.050	0.061	0.213	0.397	0.352	0.312	0.396	0.447	0.381
75°F/ 45%	0.050	0.052	0.181	0.424	0.269	0.245	0.417	0.380	0.343	0.415	0.461	0.403
70°F/ 45%	0.050	0.154	0.213	0.448	0.344	0.278	0.440	0.408	0.375	0.438	0.478	0.430
80°F/ 35%	0.050	0.083	0.206	0.362	0.270	0.247	0.364	0.332	0.308	0.365	0.416	0.354
75°F/ 35%	0.050	0.214	0.225	0.394	0.308	0.267	0.389	0.358	0.332	0.388	0.435	0.377
70°F/ 35%	0.388	0.270	0.245	0.423	0.343	0.290	0.415	0.386	0.360	0.413	0.456	0.405
80°F/ 25%	0.316	0.257	0.241	0.356	0.297	0.267	0.350	0.326	0.308	0.348	0.393	0.337
75°F/ 25%	0.354	0.281	0.254	0.382	0.320	0.282	0.374	0.349	0.329	0.370	0.414	0.360
70°F/ 25%	0.387	0.307	0.268	0.408	0.346	0.300	0.399	0.374	0.353	0.396	0.438	0.388
Avg/ 55%	0.155	0.051	0.115	0.238	0.156	0.204	0.463	0.432	0.383	0.458	0.492	0.446
Avg/ 45%	0.059	0.085	0.180	0.307	0.225	0.245	0.418	0.380	0.343	0.416	0.462	0.405
Avg/ 35%	0.163	0.189	0.225	0.393	0.307	0.268	0.389	0.359	0.333	0.388	0.436	0.379
Avg/ 25%	0.352	0.282	0.254	0.382	0.321	0.283	0.374	0.350	0.330	0.371	0.415	0.362

Table C.39: Near-optimal R_{e1} Values to Hold Constant During Ramping Phase of IEC Mode

	OA (T_{oa}/ ω_{oa})											
RA (T_{ra}/ RH_{ra})	60°F/ 0.0003	60°F/ 0.0054	60°F/ 0.0110	75°F/ 0.0003	75°F/ 0.0054	75°F/ 0.0110	90°F/ 0.0027	90°F/ 0.0054	90°F/ 0.0080	105°F/ 0.0054	120°F/ 0.0003	120°F/ 0.0110
80°F/ 55%	0.292	0.349	0.556	0.362	0.472	0.433	0.157	0.214	0.154	0.188	0.257	0.216
75°F/ 55%	0.322	0.404	0.452	0.396	0.543	0.359	0.168	0.199	0.171	0.201	0.273	0.225
70°F/ 55%	0.359	0.540	0.382	0.161	0.223	0.308	0.175	0.187	0.184	0.211	0.285	0.228
80°F/ 45%	0.375	0.555	0.444	0.472	0.599	0.352	0.245	0.272	0.221	0.239	0.279	0.255
75°F/ 45%	0.421	0.612	0.382	0.204	0.331	0.314	0.232	0.251	0.221	0.240	0.288	0.256
70°F/ 45%	0.545	0.454	0.337	0.204	0.255	0.284	0.223	0.234	0.222	0.241	0.297	0.257
80°F/ 35%	0.591	0.650	0.359	0.256	0.321	0.309	0.270	0.277	0.260	0.268	0.296	0.273
75°F/ 35%	0.679	0.393	0.328	0.240	0.284	0.288	0.257	0.262	0.251	0.263	0.301	0.270
70°F/ 35%	0.235	0.323	0.301	0.232	0.258	0.268	0.246	0.251	0.246	0.261	0.306	0.270
80°F/ 25%	0.295	0.331	0.310	0.268	0.290	0.286	0.278	0.277	0.275	0.281	0.308	0.279
75°F/ 25%	0.262	0.303	0.293	0.256	0.273	0.271	0.266	0.266	0.266	0.275	0.309	0.275
70°F/ 25%	0.241	0.279	0.276	0.247	0.257	0.257	0.257	0.255	0.259	0.271	0.312	0.274
Avg/ 55%	0.324	0.431	0.464	0.306	0.413	0.367	0.166	0.200	0.170	0.200	0.272	0.223
Avg/ 45%	0.447	0.541	0.388	0.293	0.395	0.317	0.233	0.253	0.222	0.240	0.288	0.256
Avg/ 35%	0.501	0.455	0.330	0.243	0.288	0.288	0.258	0.263	0.252	0.264	0.301	0.271
Avg/ 25%	0.266	0.304	0.293	0.257	0.273	0.271	0.267	0.266	0.267	0.276	0.310	0.276

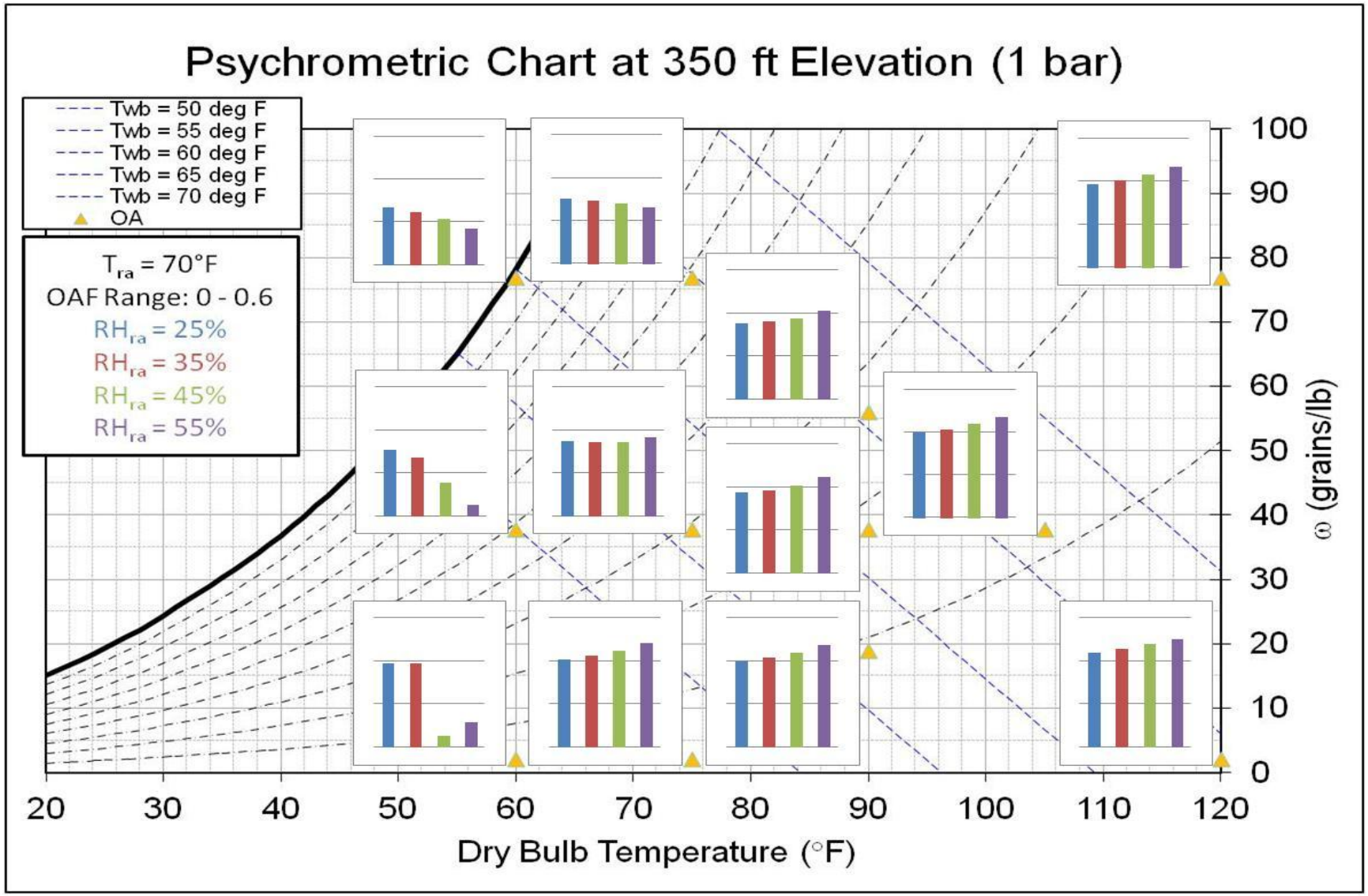

Figure C.101: Values held constant for $OAF_{near\text{-}opt,IEC}$ for T_{ra} = 70°F under variable RH_{ra} and outdoor air states

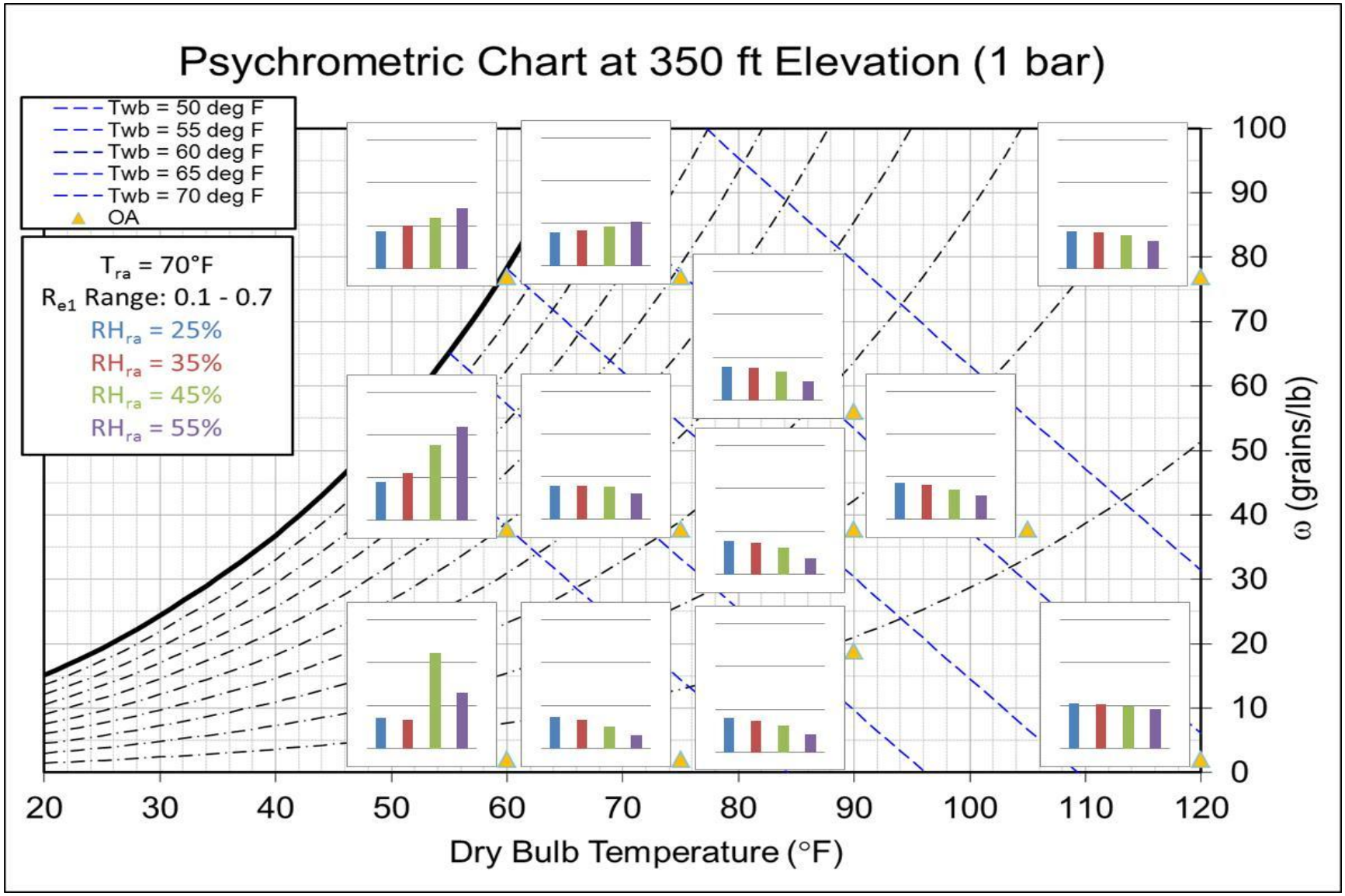

Figure C.102: Values held constant for $R_{e1,near\text{-}opt,IEC}$ for T_{ra} = 70°F under variable RH_{ra} and outdoor air states

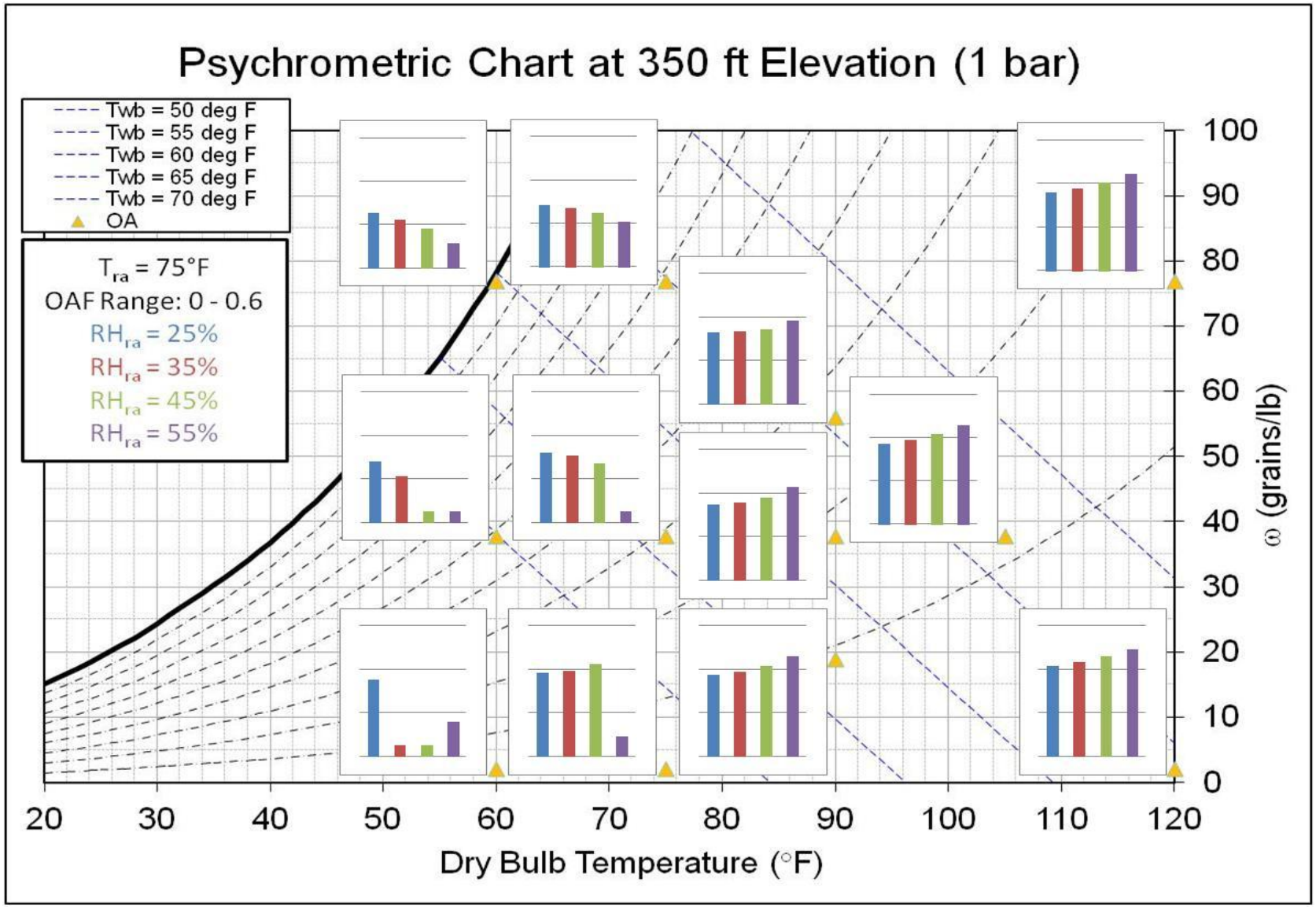

Figure C.103: Values held constant for $OAF_{near\text{-}opt,IEC}$ for T_{ra} = 75°F under variable RH_{ra} and outdoor air states

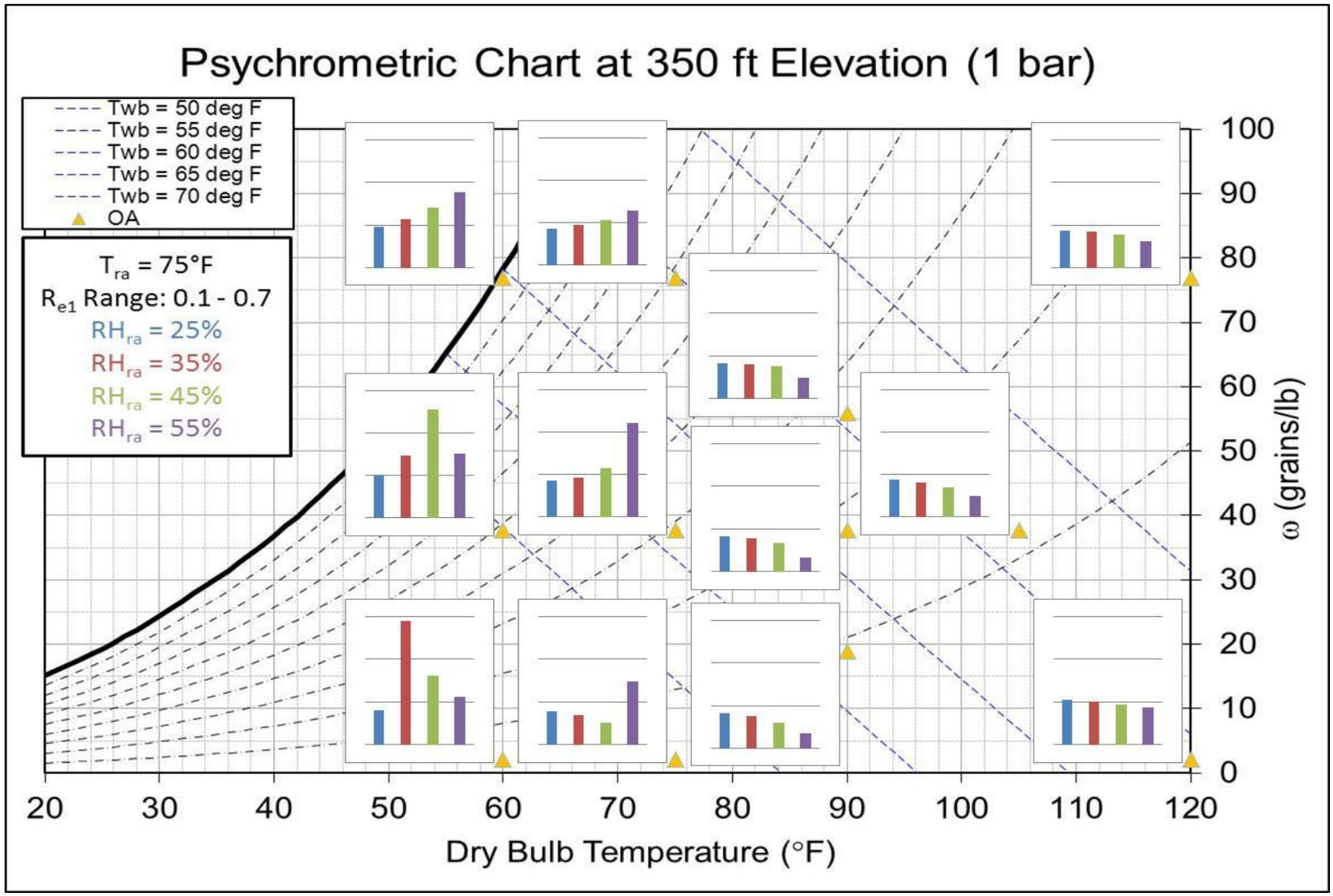

Figure C.104: Values held constant for $R_{e1,near\text{-}opt,IEC}$ for T_{ra} = 75°F under variable RH_{ra} and outdoor air states

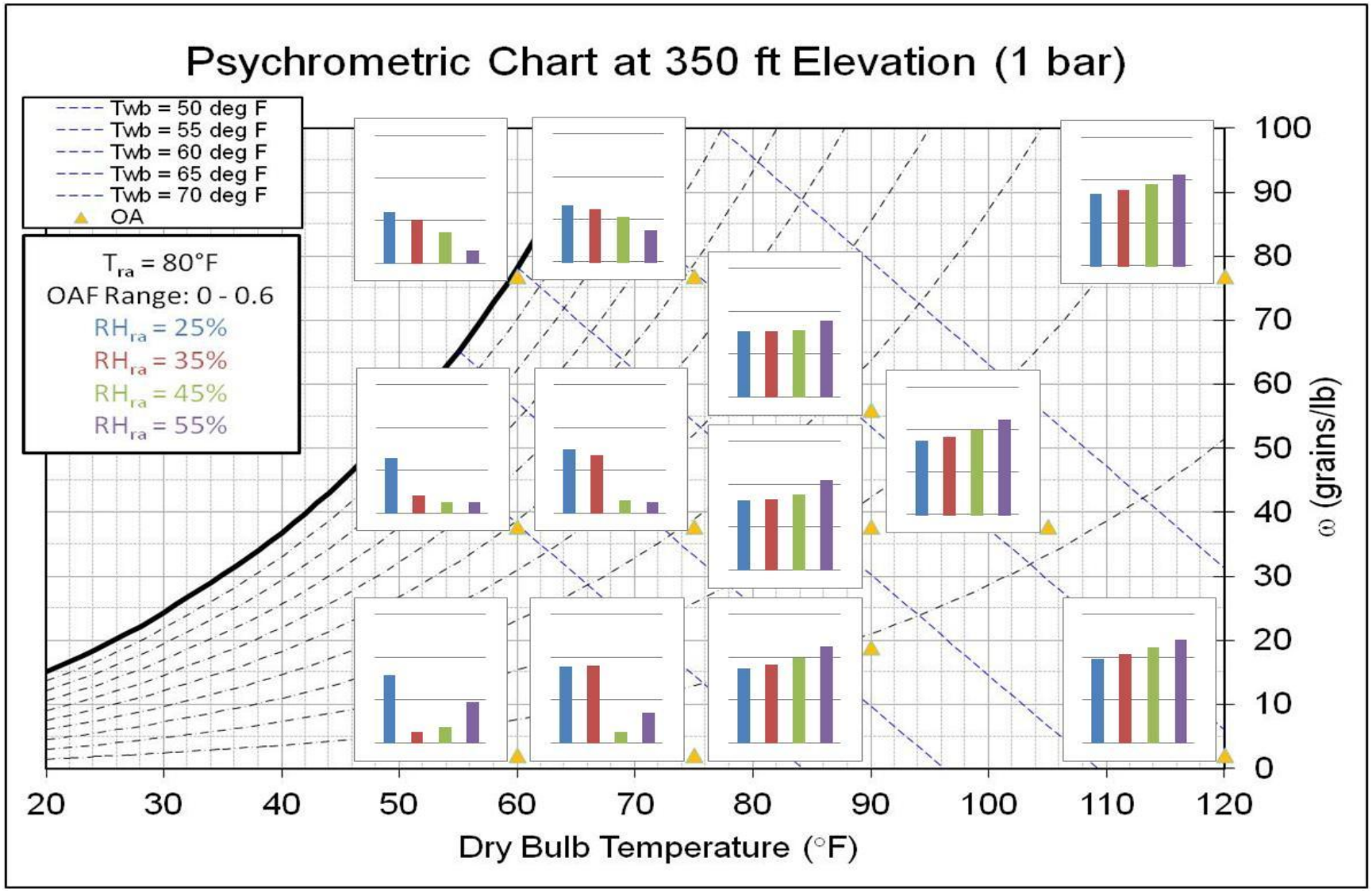

Figure C.105: Values held constant for $OAF_{near\text{-}opt,IEC}$ for T_{ra} = 70°F under variable RH_{ra} and outdoor air states

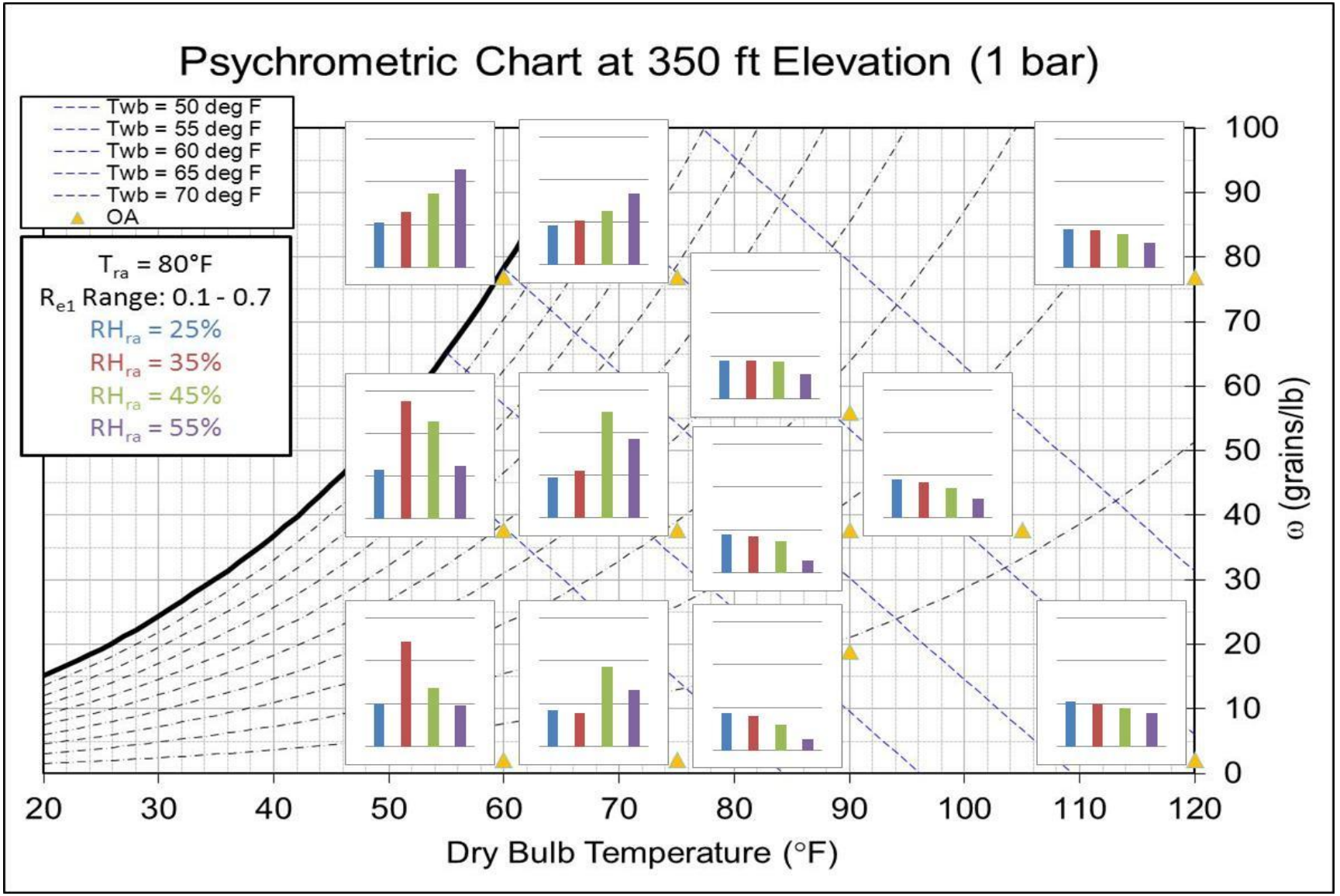

Figure C.106: Values held constant for $R_{e1,near\text{-}opt,IEC}$ for T_{ra} = 70°F under variable RH_{ra} and outdoor air states

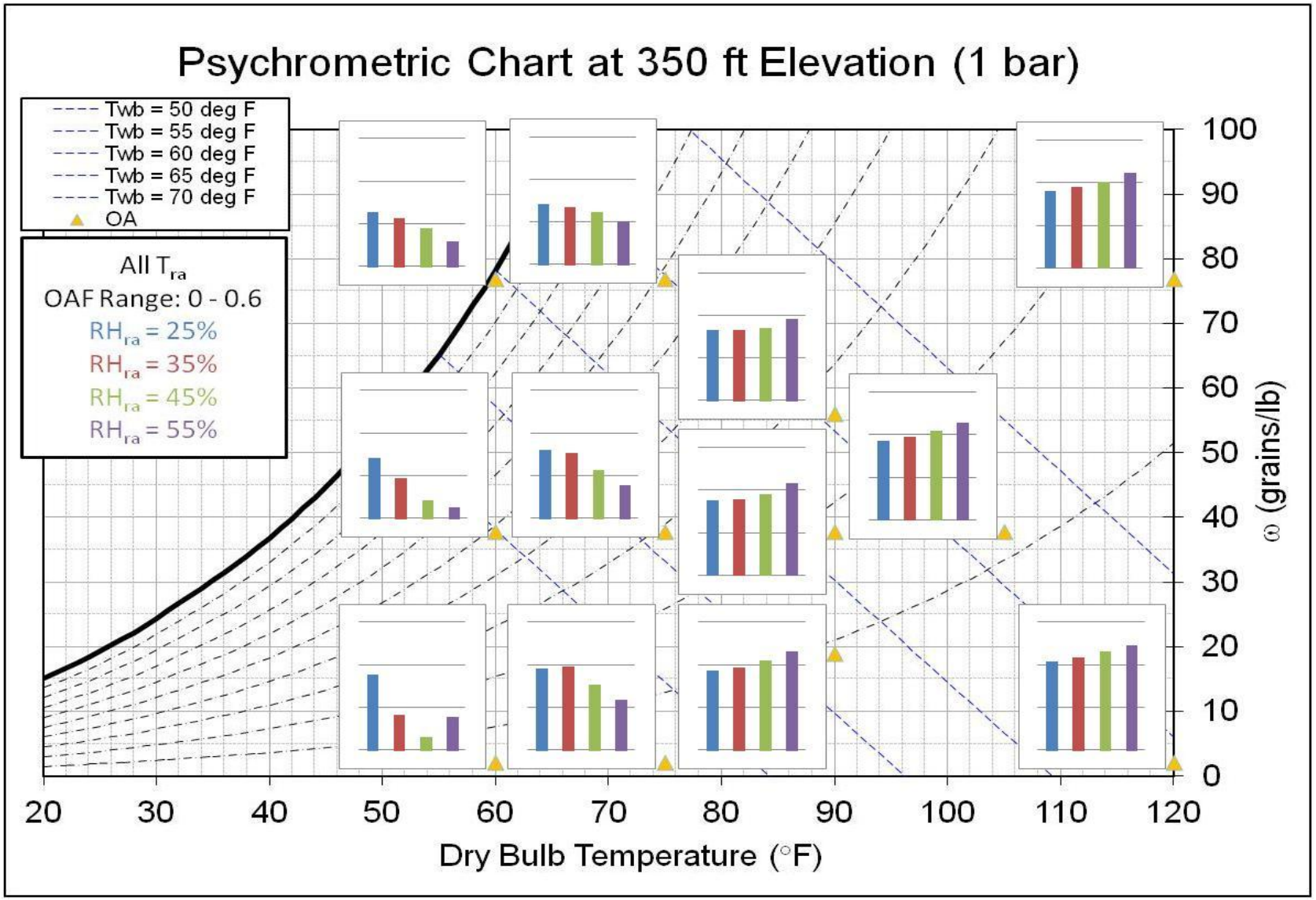

Figure C.107: Average values across all T_{ra} held constant for $OAF_{near\text{-}opt,IEC}$ under variable RH_{ra} and outdoor air states

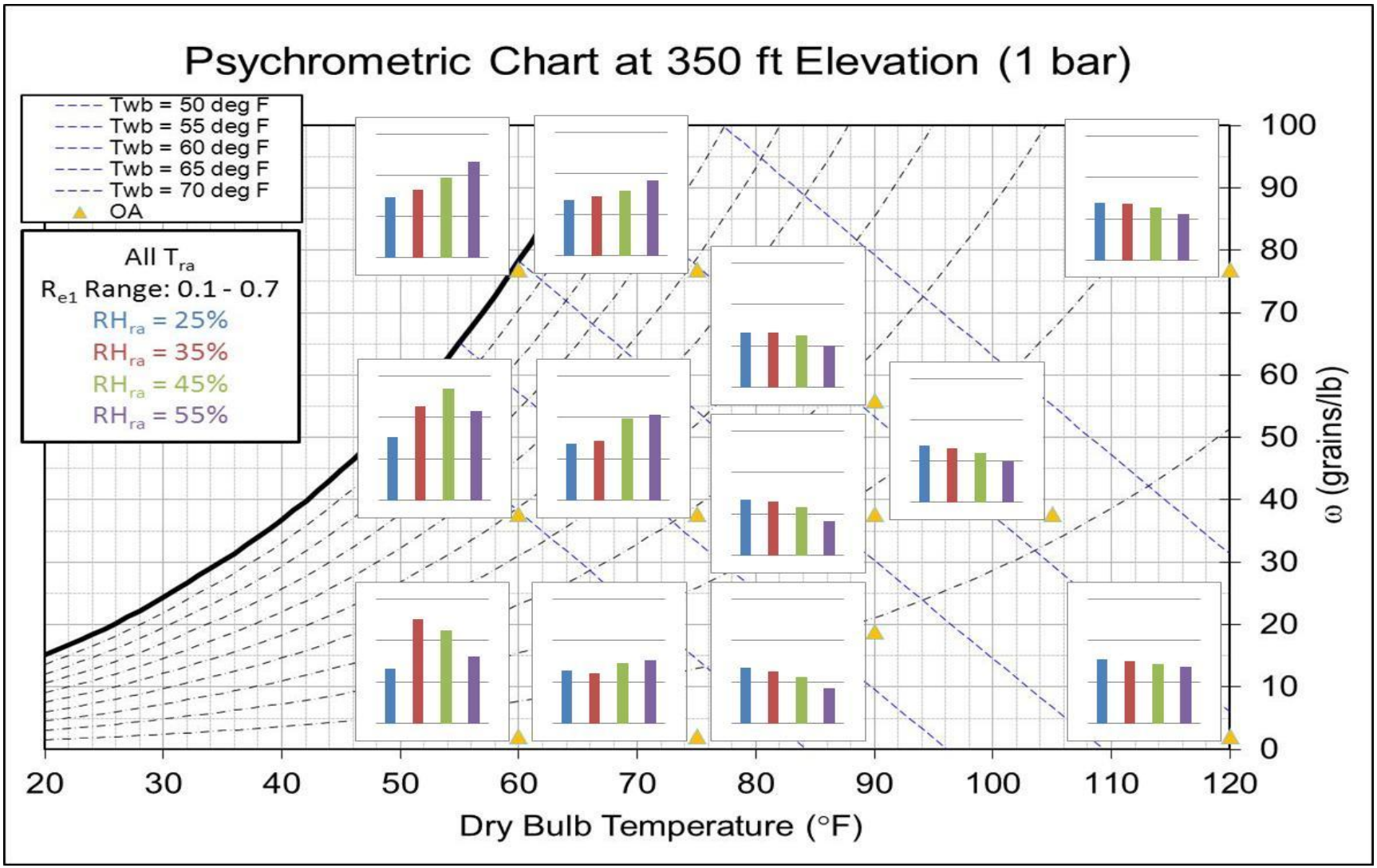

Figure C.108: Average values across all T_{ra} held constant for $R_{e1,near\text{-}opt,IEC}$ under variable RH_{ra} and outdoor air states

C.2 Standard Mode – Ramping Phase

Table C.40: Near-optimal OAF Values to Hold Constant During Ramping Phase of Standard Mode

		OA (T_{oa}/ ω_{oa})												
RA (T_{ra}/ RH_{ra})	**SHR**	60°F/ 0.008	60°F/ 0.011	75°F/ 0.008	75°F/ 0.002	75°F/ 0.018	90°F/ 0.008	90°F/ 0.016	90°F/ 0.024	105°F/ 0.008	105°F/ 0.012	105°F/ 0.016	120°F/ 0.008	120°F/ 0.012
80°F/ 60%	0.5	0.161	0.051	0.167	0.063	0.062	0.168	0.128	0.253	0.168	0.148	0.193	0.166	0.176
	0.65	0.390	0.494	0.395	0.064	0.050	0.411	0.105	0.239	0.455	0.178	0.186	0.477	0.213
	0.8	0.179	0.325	0.179	0.192	0.050	0.179	0.093	0.223	0.161	0.276	0.184	0.128	0.316
80°F/ 55%	0.5	0.081	0.050	0.121	0.065	0.086	0.141	0.136	0.227	0.150	0.141	0.188	0.154	0.167
	0.65	0.484	0.051	0.513	0.062	0.052	0.553	0.120	0.235	0.282	0.159	0.190	0.256	0.193
	0.8	0.273	0.059	0.273	0.064	0.050	0.251	0.110	0.225	0.223	0.189	0.192	0.191	0.235
80°F/ 50%	0.5	0.057	0.050	0.085	0.067	0.102	0.112	0.139	0.205	0.128	0.137	0.179	0.137	0.160
	0.65	0.158	0.051	0.168	0.064	0.070	0.202	0.132	0.230	0.201	0.152	0.192	0.204	0.186
	0.8	0.394	0.051	0.393	0.063	0.052	0.403	0.123	0.225	0.420	0.172	0.192	0.445	0.213
75°F/ 55%	0.5	0.064	0.052	0.101	0.093	0.196	0.136	0.213	0.266	0.157	0.198	0.233	0.170	0.206
	0.65	0.084	0.050	0.157	0.080	0.167	0.197	0.220	0.300	0.213	0.214	0.264	0.222	0.248
	0.8	0.423	0.050	0.434	0.071	0.142	0.462	0.209	0.300	0.497	0.225	0.264	0.511	0.266
70°F/ 60%	0.5	0.070	0.053	0.121	0.156	0.278	0.170	0.282	0.303	0.199	0.255	0.290	0.213	0.270
	0.65	0.075	0.050	0.146	0.122	0.273	0.208	0.303	0.362	0.241	0.288	0.334	0.255	0.316
	0.8	0.252	0.050	0.366	0.100	0.253	0.437	0.293	0.358	0.365	0.295	0.336	0.353	0.330
70°F/ 55%	0.5	0.072	0.064	0.119	0.174	0.255	0.166	0.257	0.268	0.194	0.239	0.260	0.198	0.248
	0.65	0.074	0.050	0.131	0.151	0.279	0.191	0.297	0.344	0.230	0.283	0.323	0.252	0.305
	0.8	0.087	0.050	0.171	0.135	0.262	0.240	0.293	0.348	0.286	0.291	0.326	0.309	0.319
70°F/ 50%	0.5	0.075	0.083	0.121	0.181	0.230	0.165	0.229	0.237	0.174	0.219	0.230	0.192	0.222
	0.65	0.076	0.059	0.132	0.177	0.275	0.189	0.291	0.320	0.225	0.275	0.305	0.247	0.293
	0.8	0.081	0.050	0.152	0.164	0.253	0.218	0.289	0.339	0.262	0.287	0.318	0.289	0.310
All	0.5	0.168	0.101	0.217	0.098	0.167	0.260	0.212	0.292	0.253	0.220	0.258	0.262	0.250
	0.65	0.282	0.082	0.315	0.103	0.150	0.346	0.203	0.291	0.356	0.243	0.260	0.361	0.280
	0.8	0.079	0.056	0.115	0.110	0.178	0.148	0.201	0.254	0.165	0.192	0.227	0.175	0.207

Table C.41: Near-optimal $C_{LD,in,DEVap}$ Values to Hold Constant During Ramping Phase of Standard Mode

		OA (T_{oa}/ ω_{oa})												
RA (T_{ra}/ RH_{ra})	**SHR**	60°F/ 0.008	60°F/ 0.011	75°F/ 0.008	75°F/ 0.002	75°F/ 0.018	90°F/ 0.008	90°F/ 0.016	90°F/ 0.024	105°F/ 0.008	105°F/ 0.012	105°F/ 0.016	120°F/ 0.008	120°F/ 0.012
80°F/ 60%	0.5	0.266	0.234	0.276	0.244	0.251	0.283	0.274	0.343	0.289	0.281	0.307	0.294	0.300
	0.65	0.200	0.200	0.227	0.218	0.233	0.258	0.250	0.304	0.290	0.260	0.277	0.302	0.281
	0.8	0.206	0.200	0.208	0.207	0.223	0.210	0.238	0.288	0.219	0.259	0.265	0.232	0.293
80°F/ 55%	0.5	0.258	0.250	0.275	0.260	0.274	0.289	0.296	0.356	0.299	0.298	0.328	0.307	0.317
	0.65	0.208	0.217	0.232	0.234	0.248	0.258	0.269	0.323	0.294	0.274	0.297	0.305	0.294
	0.8	0.206	0.201	0.209	0.216	0.239	0.226	0.255	0.305	0.242	0.262	0.283	0.254	0.285
80°F/ 50%	0.5	0.269	0.267	0.281	0.279	0.299	0.296	0.319	0.372	0.309	0.318	0.349	0.318	0.337
	0.65	0.251	0.234	0.261	0.252	0.268	0.289	0.289	0.343	0.295	0.292	0.318	0.307	0.312
	0.8	0.212	0.210	0.248	0.234	0.255	0.277	0.274	0.323	0.304	0.278	0.300	0.323	0.299
75°F/ 55%	0.5	0.261	0.258	0.274	0.275	0.325	0.292	0.339	0.395	0.306	0.332	0.360	0.318	0.342
	0.65	0.229	0.231	0.252	0.251	0.283	0.273	0.305	0.360	0.291	0.302	0.332	0.305	0.324
	0.8	0.214	0.211	0.247	0.236	0.265	0.280	0.286	0.343	0.304	0.286	0.313	0.315	0.308
70°F/ 60%	0.5	0.253	0.249	0.269	0.284	0.350	0.290	0.360	0.401	0.309	0.343	0.377	0.323	0.362
	0.65	0.226	0.229	0.246	0.253	0.303	0.269	0.322	0.376	0.291	0.317	0.349	0.308	0.339
	0.8	0.211	0.214	0.244	0.238	0.283	0.277	0.301	0.355	0.300	0.300	0.329	0.318	0.323
70°F/ 55%	0.5	0.268	0.265	0.285	0.311	0.366	0.308	0.374	0.407	0.327	0.360	0.387	0.333	0.374
	0.65	0.241	0.243	0.260	0.275	0.326	0.283	0.342	0.391	0.305	0.335	0.366	0.323	0.355
	0.8	0.220	0.229	0.244	0.258	0.301	0.270	0.318	0.368	0.295	0.315	0.343	0.316	0.336
70°F/ 50%	0.5	0.284	0.287	0.304	0.338	0.379	0.329	0.383	0.412	0.336	0.374	0.393	0.352	0.383
	0.65	0.258	0.259	0.278	0.299	0.348	0.302	0.363	0.406	0.323	0.355	0.382	0.341	0.373
	0.8	0.237	0.245	0.260	0.278	0.312	0.284	0.335	0.383	0.307	0.332	0.359	0.327	0.351
All	0.5	0.265	0.258	0.279	0.282	0.322	0.297	0.336	0.386	0.310	0.330	0.358	0.320	0.344
	0.65	0.230	0.231	0.251	0.254	0.286	0.276	0.305	0.358	0.297	0.304	0.332	0.311	0.325
	0.8	0.215	0.215	0.239	0.238	0.268	0.265	0.287	0.339	0.286	0.289	0.313	0.302	0.312

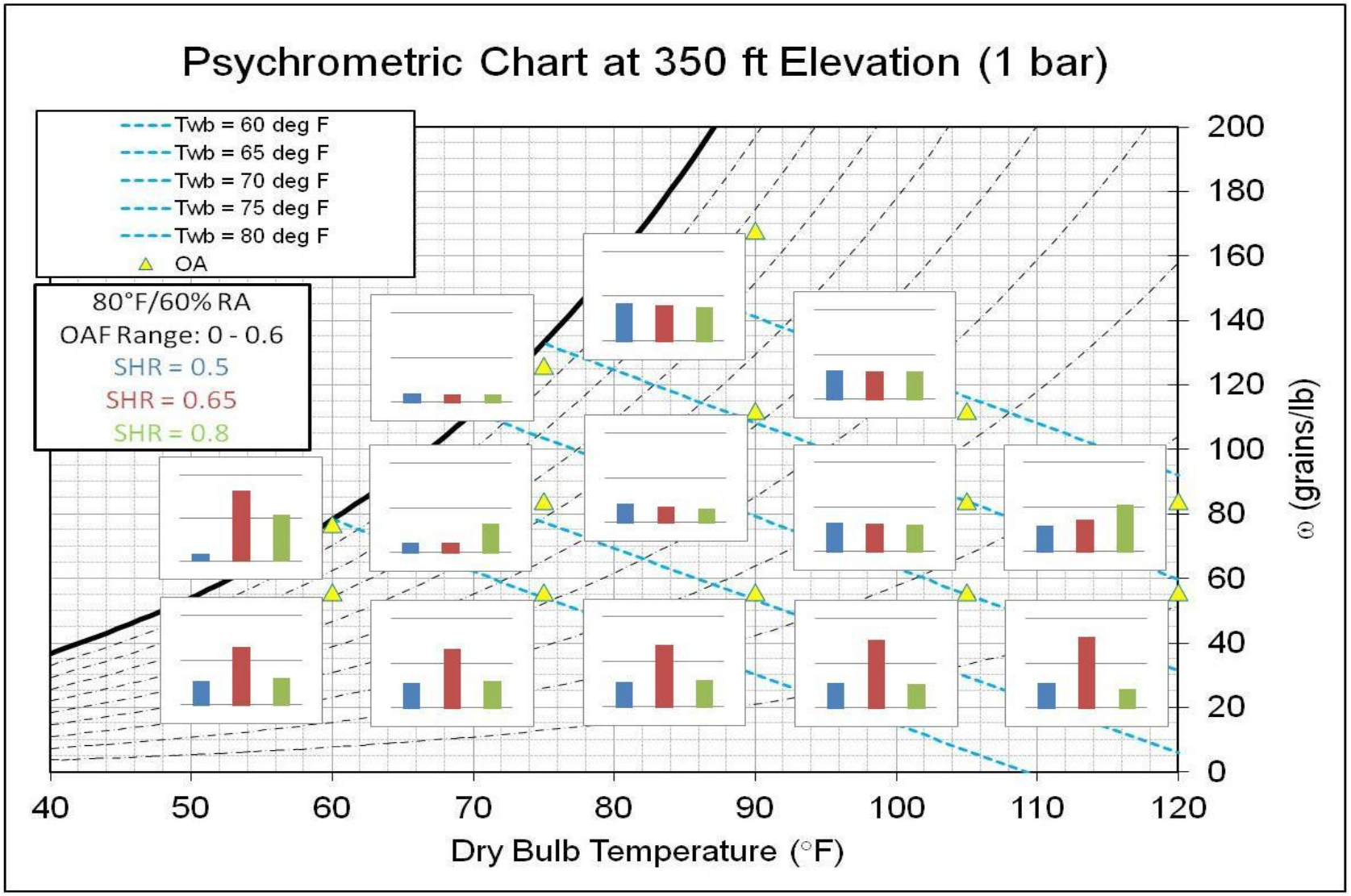

Figure C.109: Values held constant for $OAF_{near\text{-}opt,standard}$ for T_{ra} = 80°F and RH_{ra} = 60% under variable outdoor air states

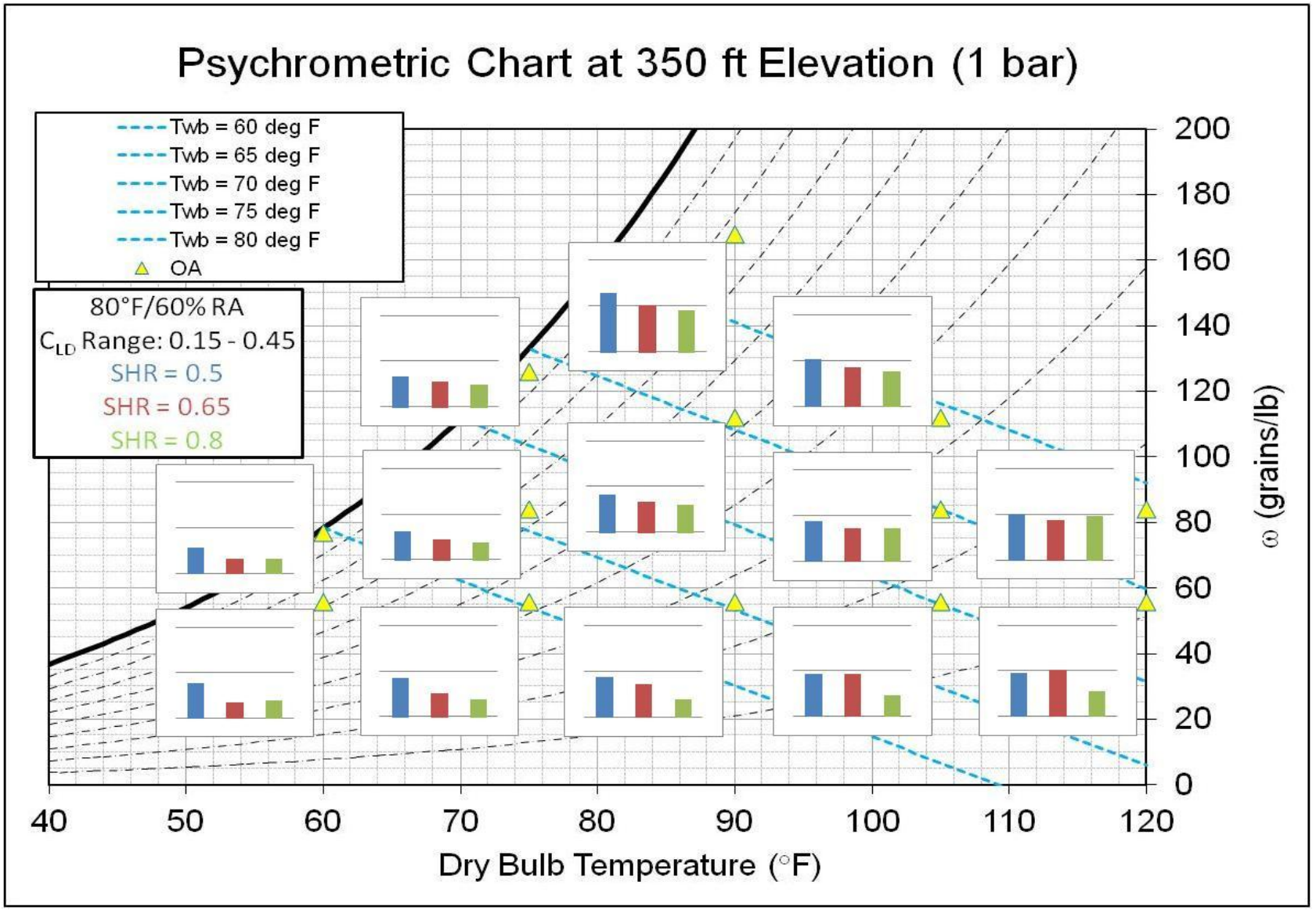

Figure C.110: Values held constant for $C_{LD,in,DEVap,near\text{-}opt,standard}$ for for T_{ra} = 80°F and RH_{ra} = 60% under variable outdoor air states

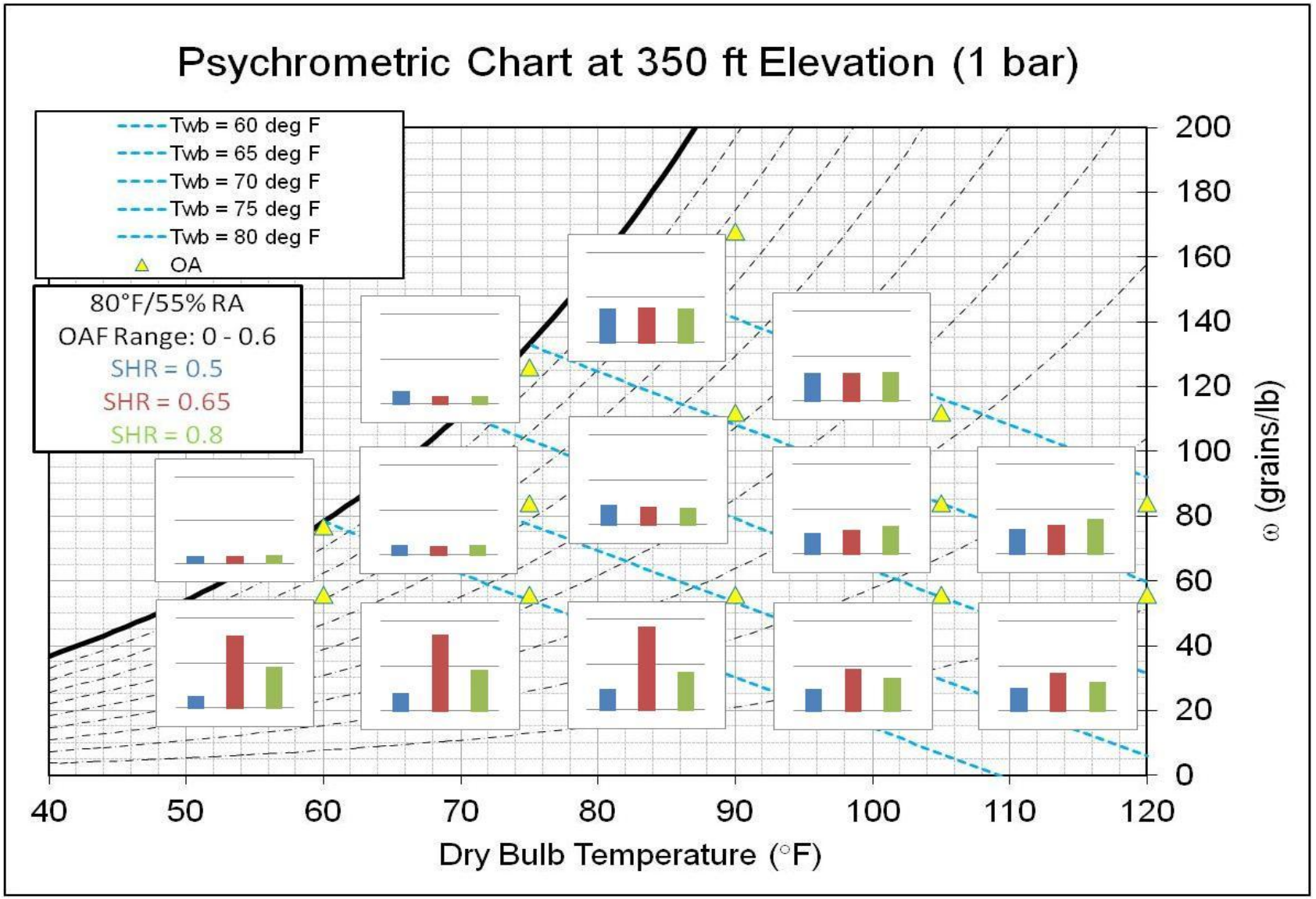

Figure C.111: Values held constant for $OAF_{near\text{-}opt,standard}$ for T_{ra} = 80°F and RH_{ra} = 55% under variable outdoor air states

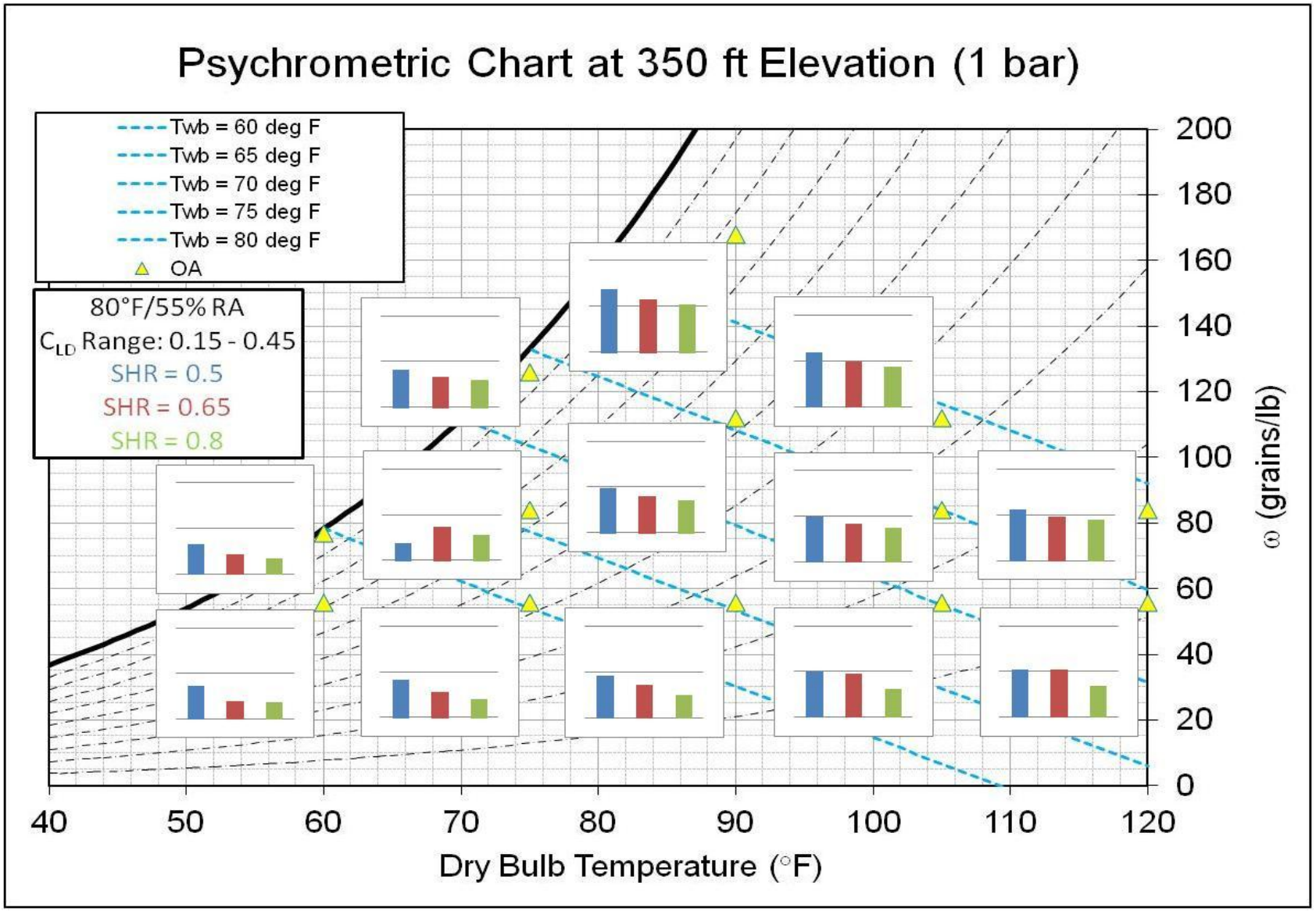

Figure C.112: Values held constant for $C_{LD,in,DEVap,near\text{-}opt,standard}$ for for T_{ra} = 80°F and RH_{ra} = 55% under variable outdoor air states

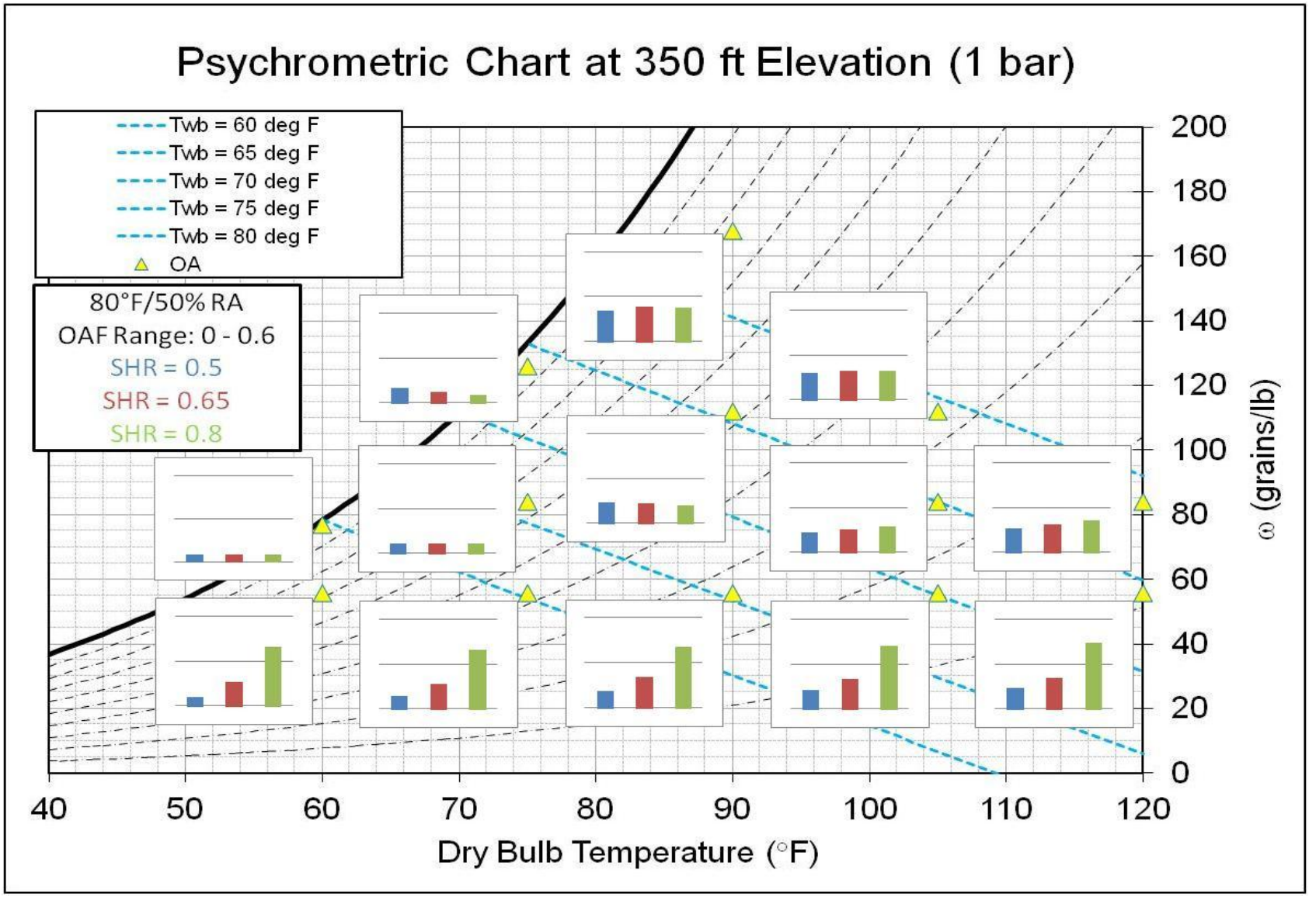

Figure C.113: Values held constant for $OAF_{near\text{-}opt,standard}$ for T_{ra} = 80°F and RH_{ra} = 50% under variable outdoor air states

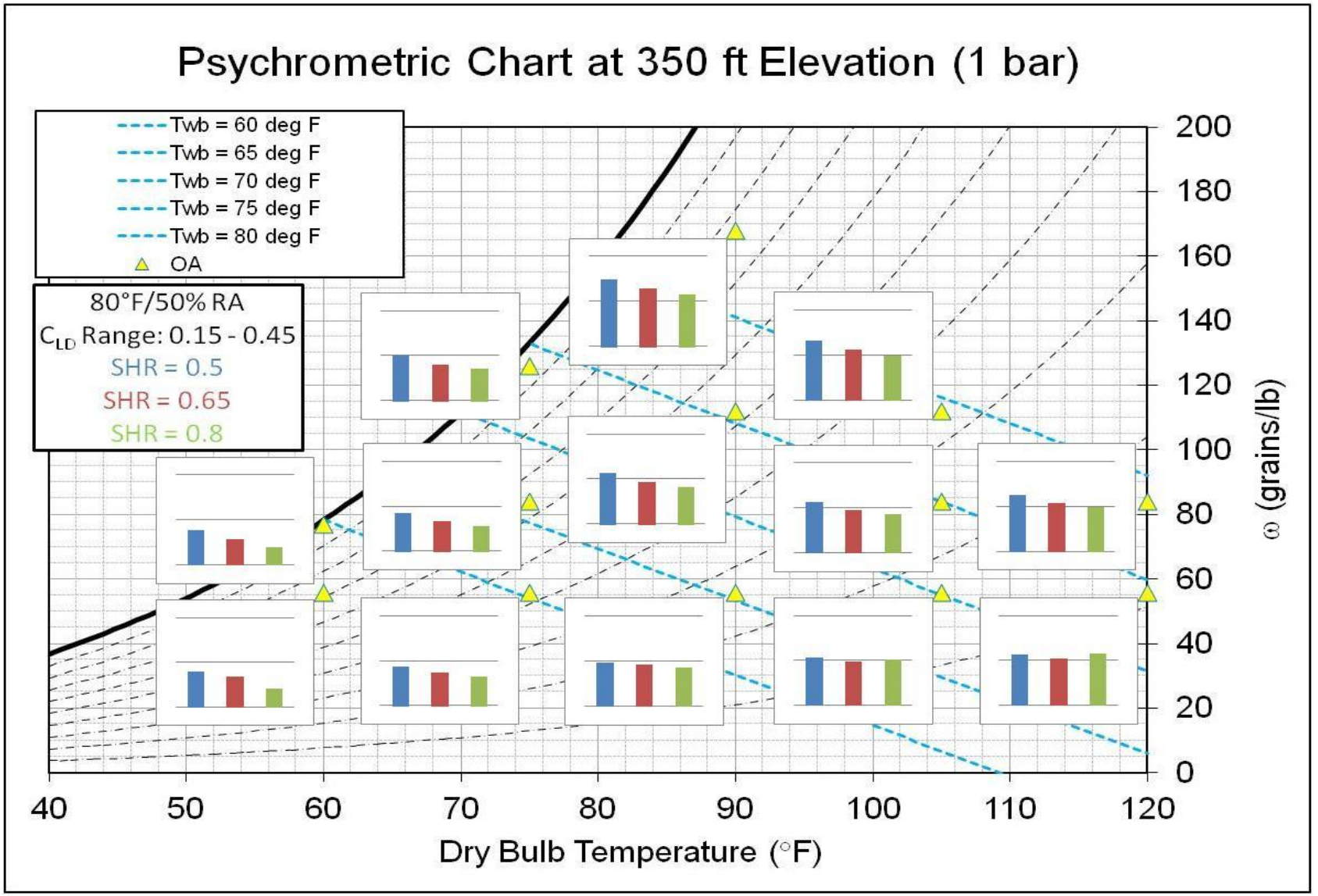

Figure C.114: Values held constant for $C_{LD,in,DEVap,near\text{-}opt,standard}$ for for T_{ra} = 80°F and RH_{ra} = 50% under variable outdoor air states

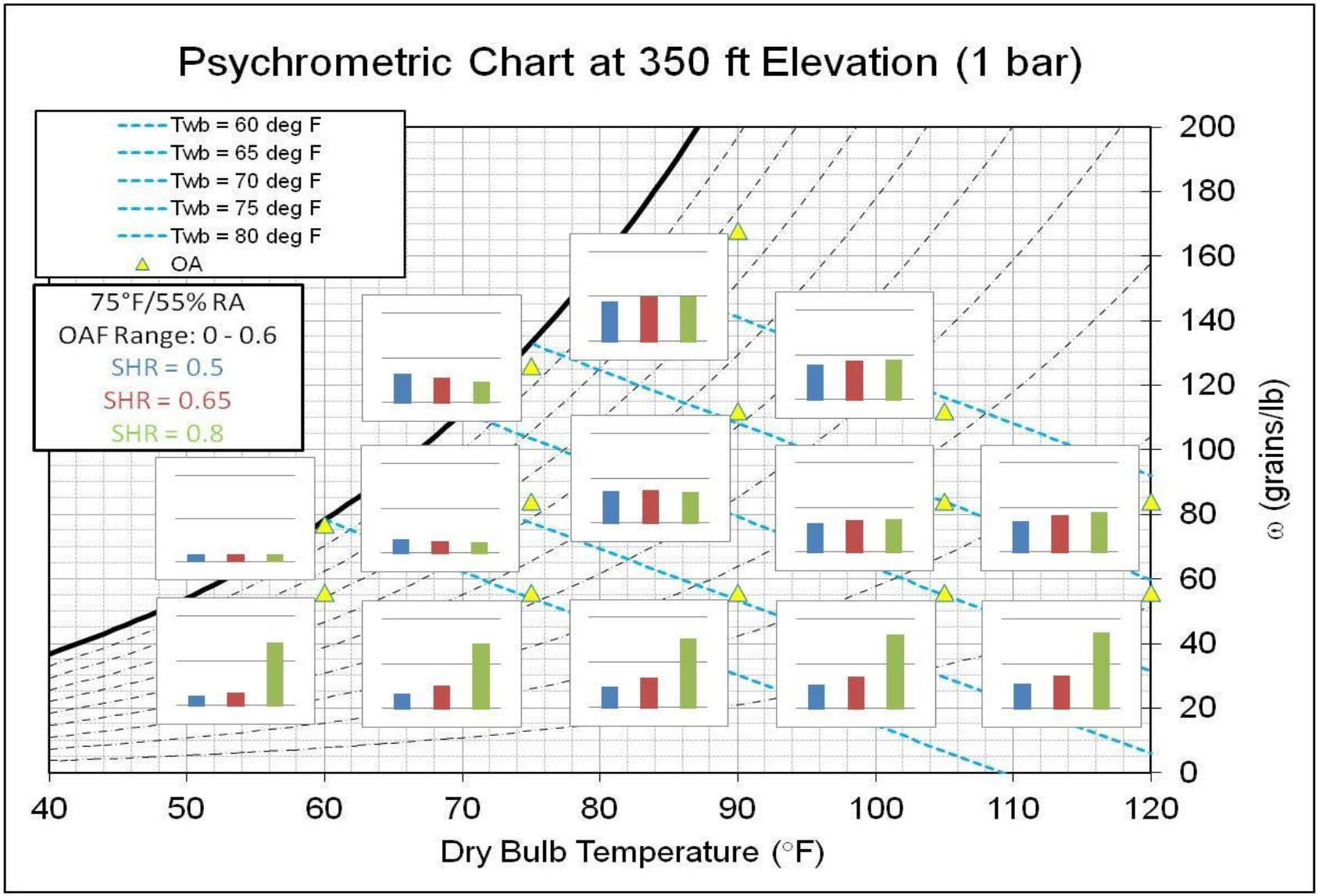

Figure C.115: Values held constant for $OAF_{near\text{-}opt,standard}$ for T_{ra} = 75°F and RH_{ra} = 55% under variable outdoor air states

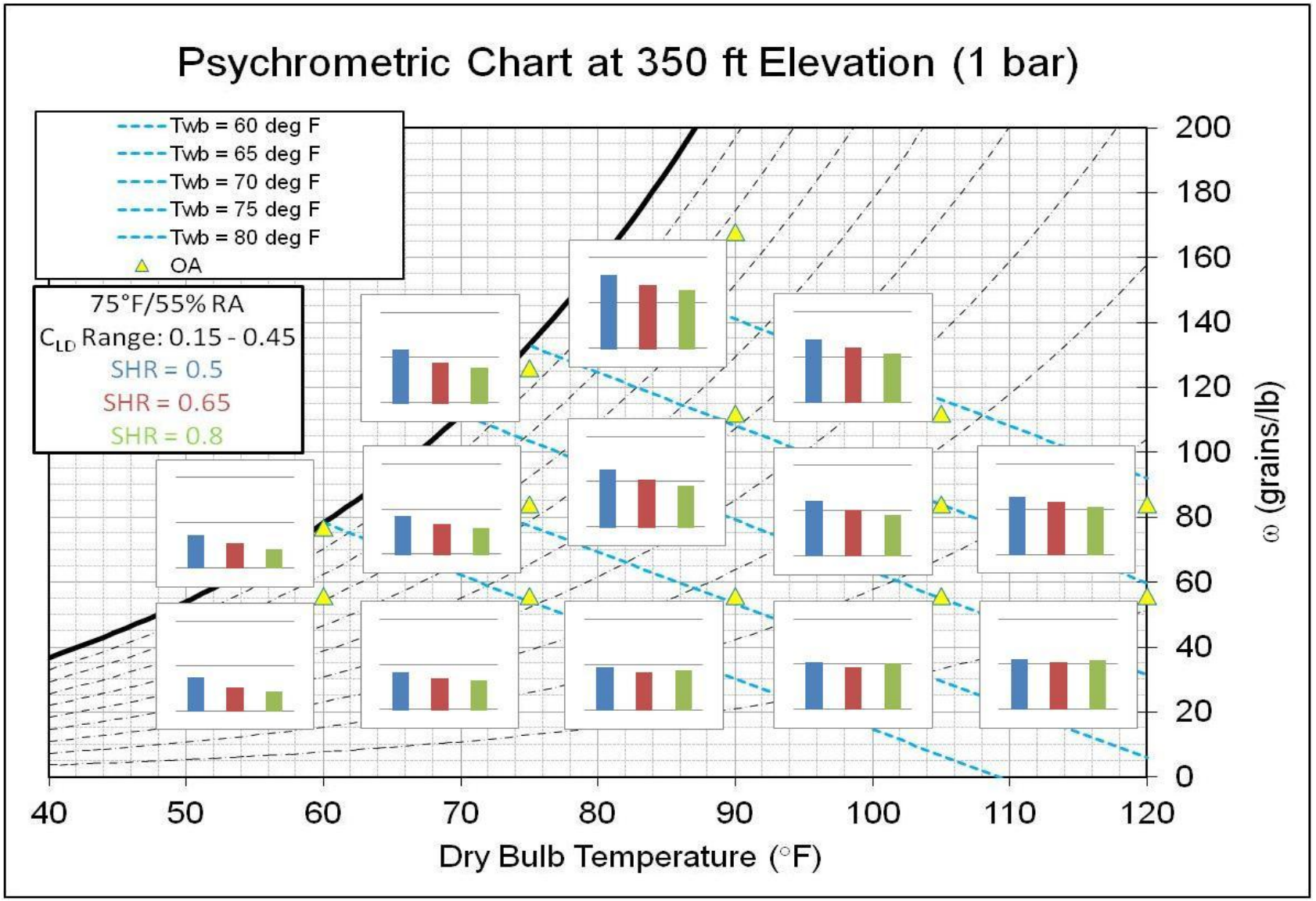

Figure C.116: Values held constant for $C_{LD,in,DEVap,near\text{-}opt,standard}$ for for T_{ra} =75°F and RH_{ra} = 55% under variable outdoor air states

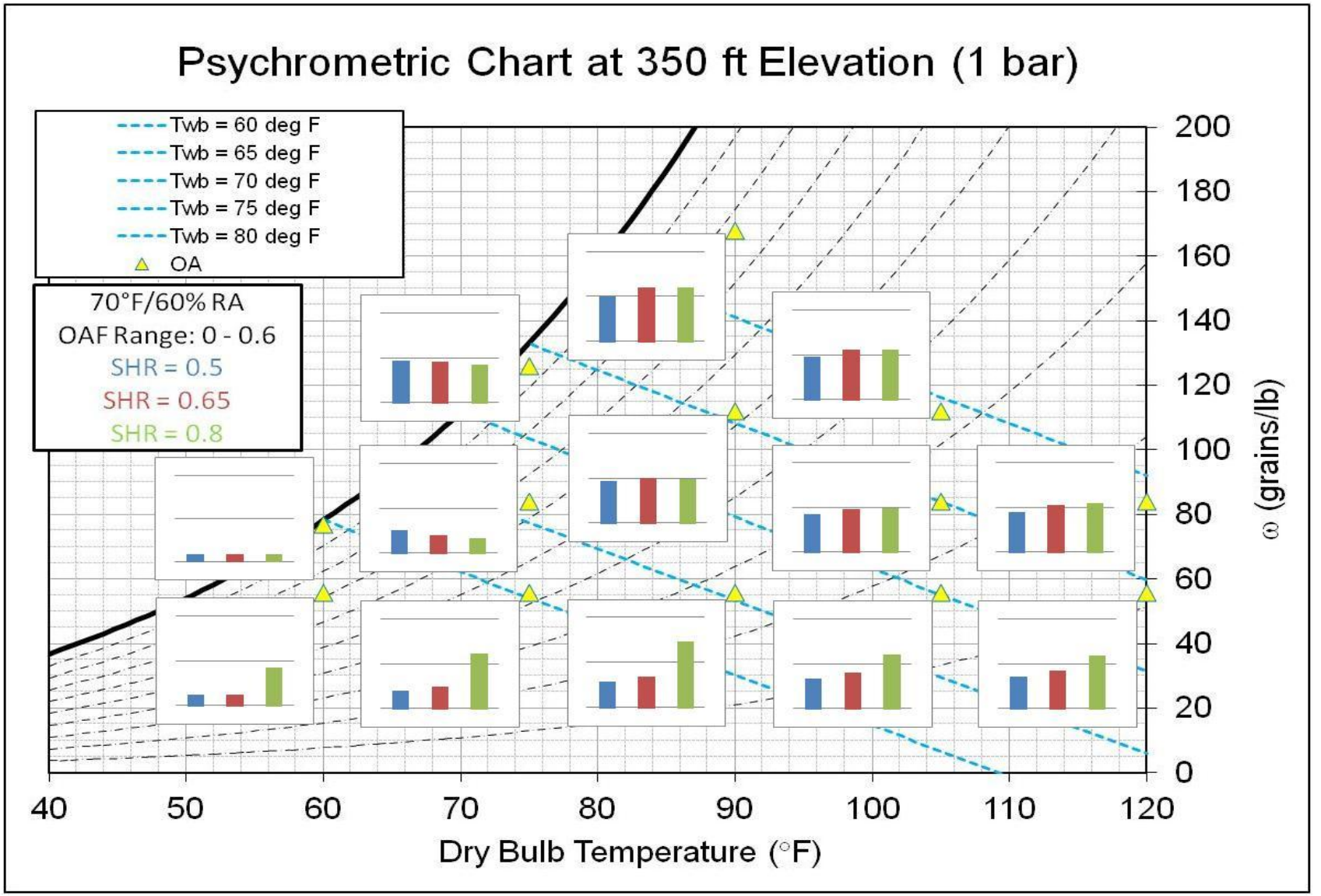

Figure C.117: Values held constant for $OAF_{near\text{-}opt,standard}$ for T_{ra} = 70°F and RH_{ra} = 60% under variable outdoor air states

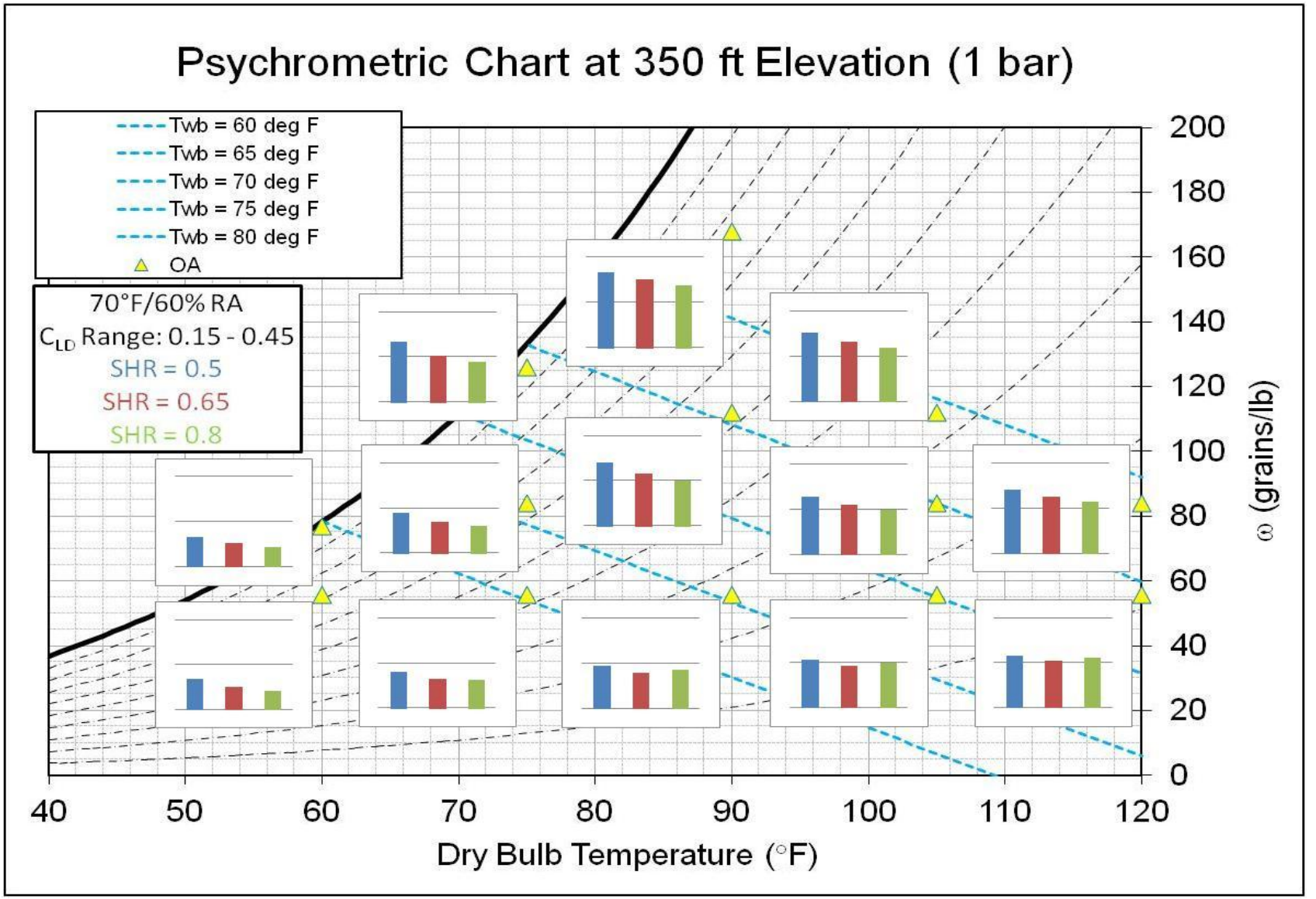

Figure C.118: Values held constant for $C_{LD,in,DEVap,near\text{-}opt,standard}$ for for T_{ra} = 70°F and RH_{ra} = 60% under variable outdoor air states

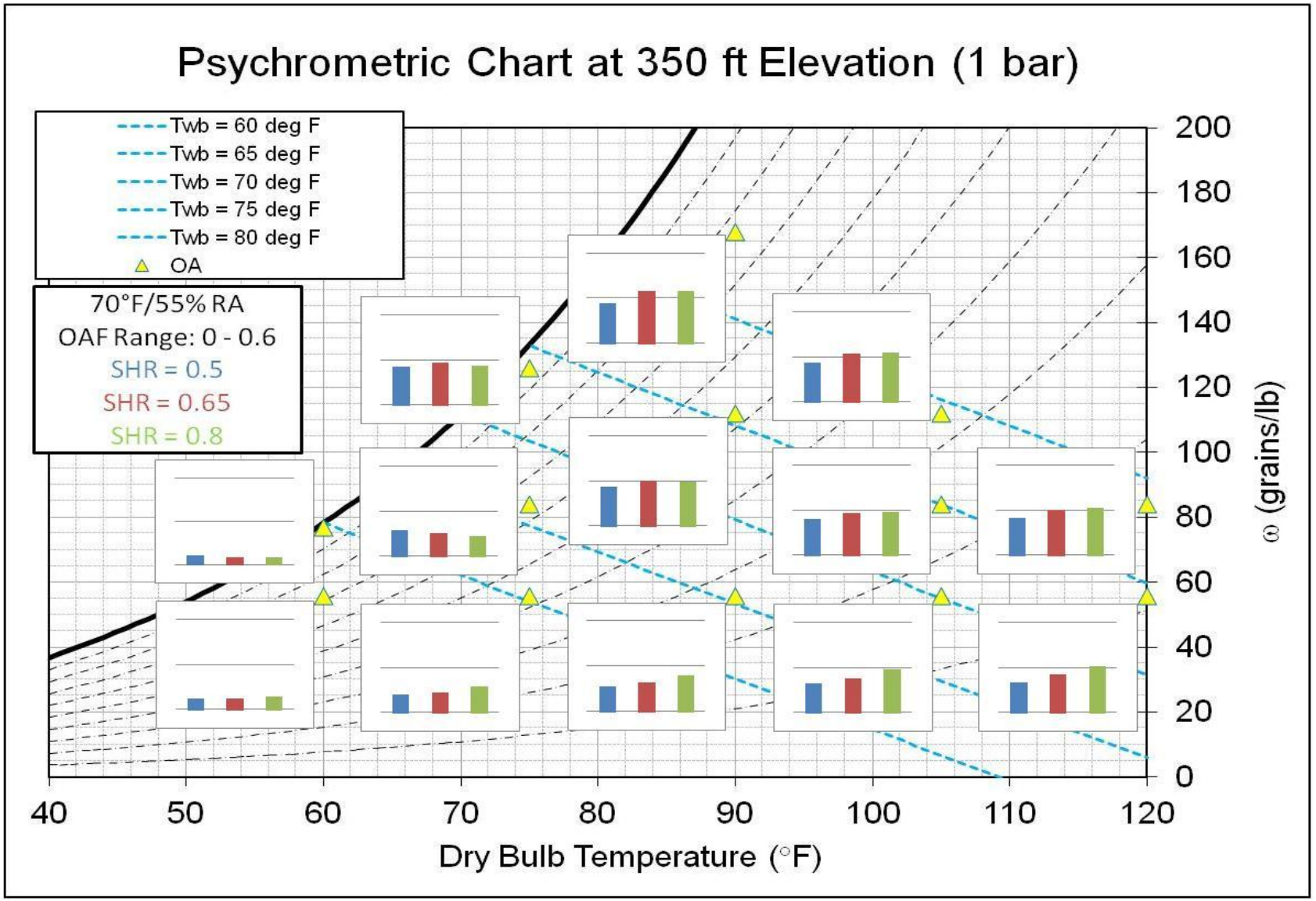

Figure C.119: Values held constant for $OAF_{near\text{-}opt,standard}$ for T_{ra} = 70°F and RH_{ra} = 55% under variable outdoor air states

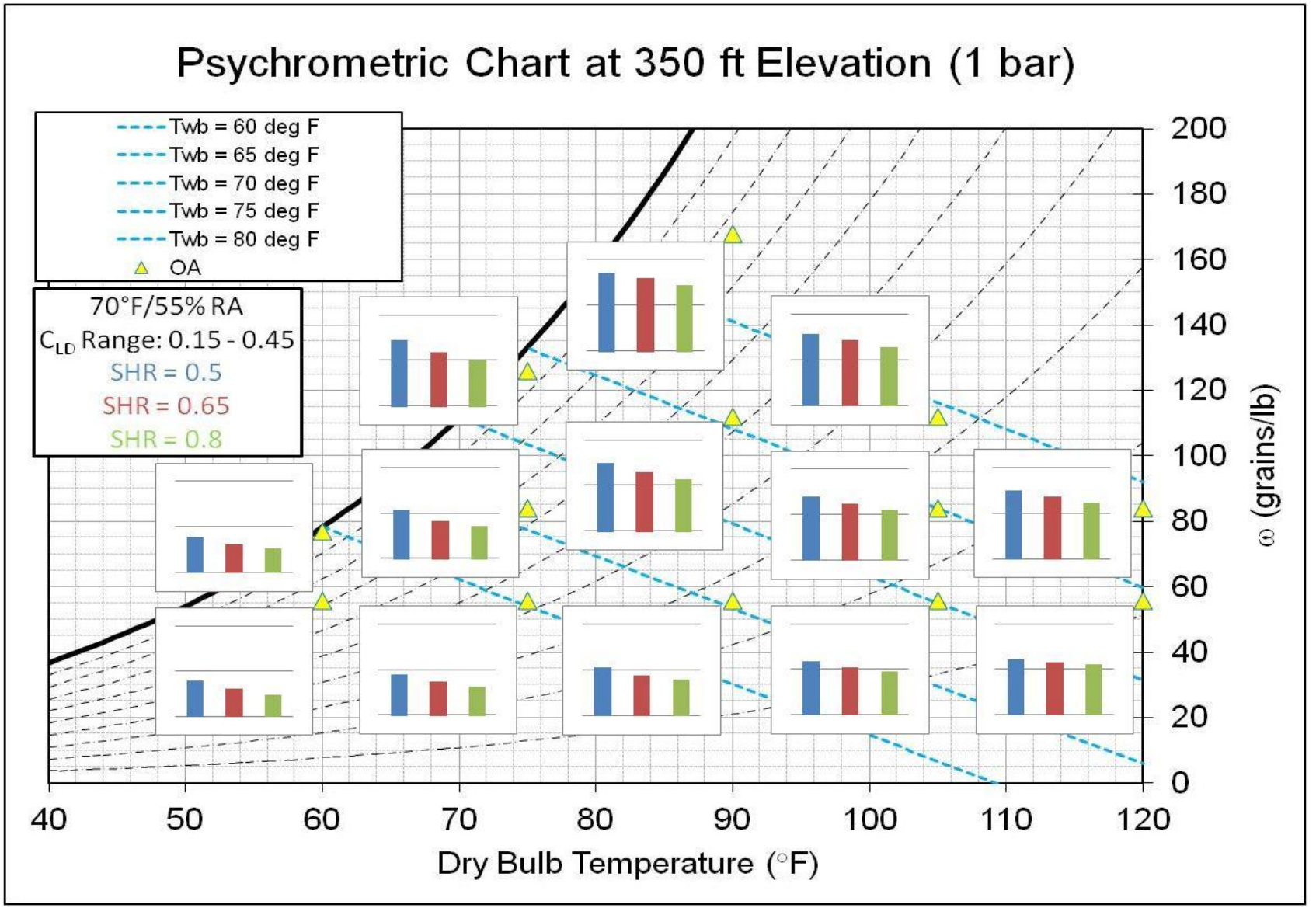

Figure C.120: Values held constant for $C_{LD,in,DEVap,near\text{-}opt,standard}$ for for T_{ra} = 70°F and RH_{ra} = 55% under variable outdoor air states

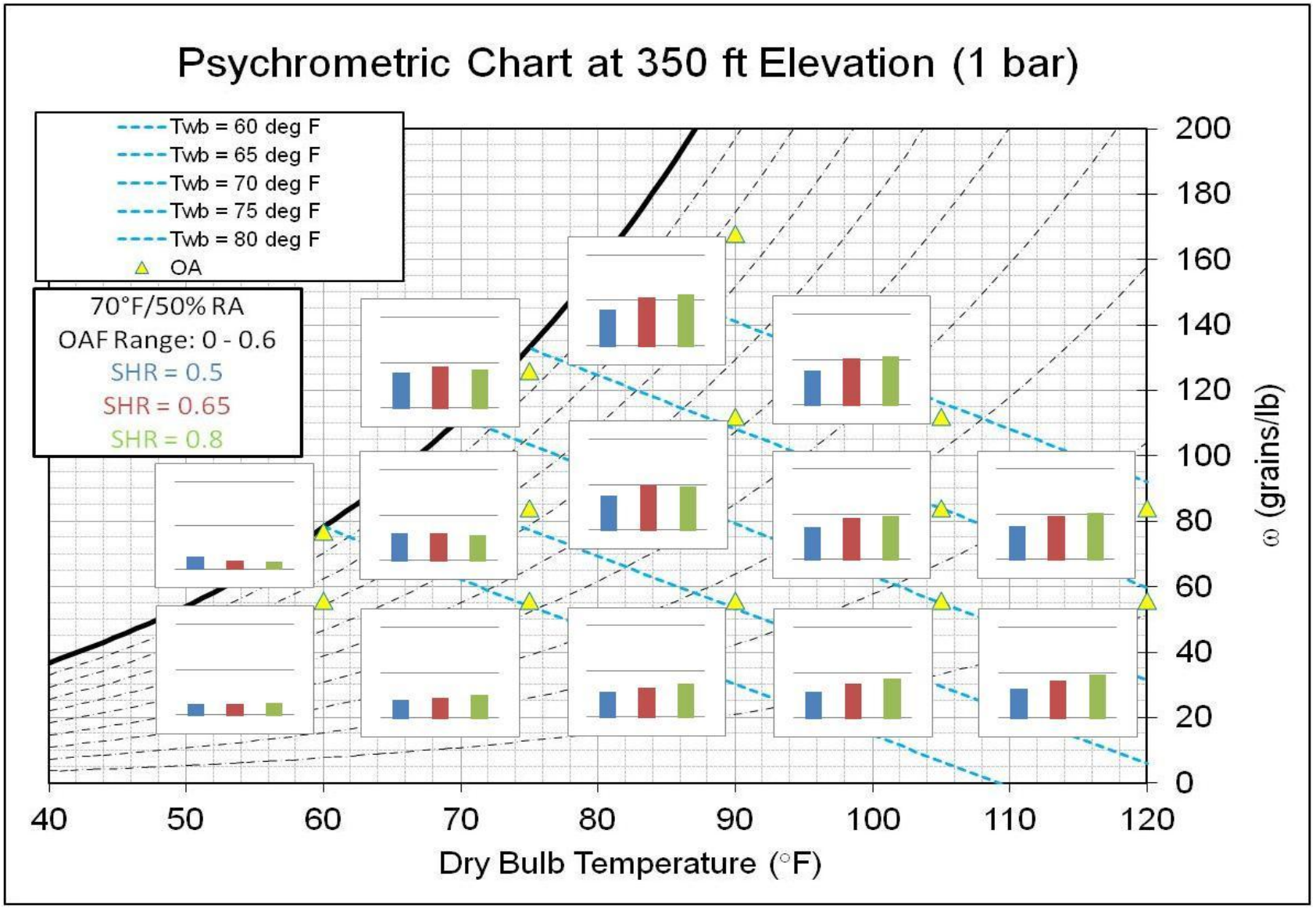

Figure C.121: Values held constant for $OAF_{near\text{-}opt,standard}$ for T_{ra} = 70°F and RH_{ra} = 50% under variable outdoor air states

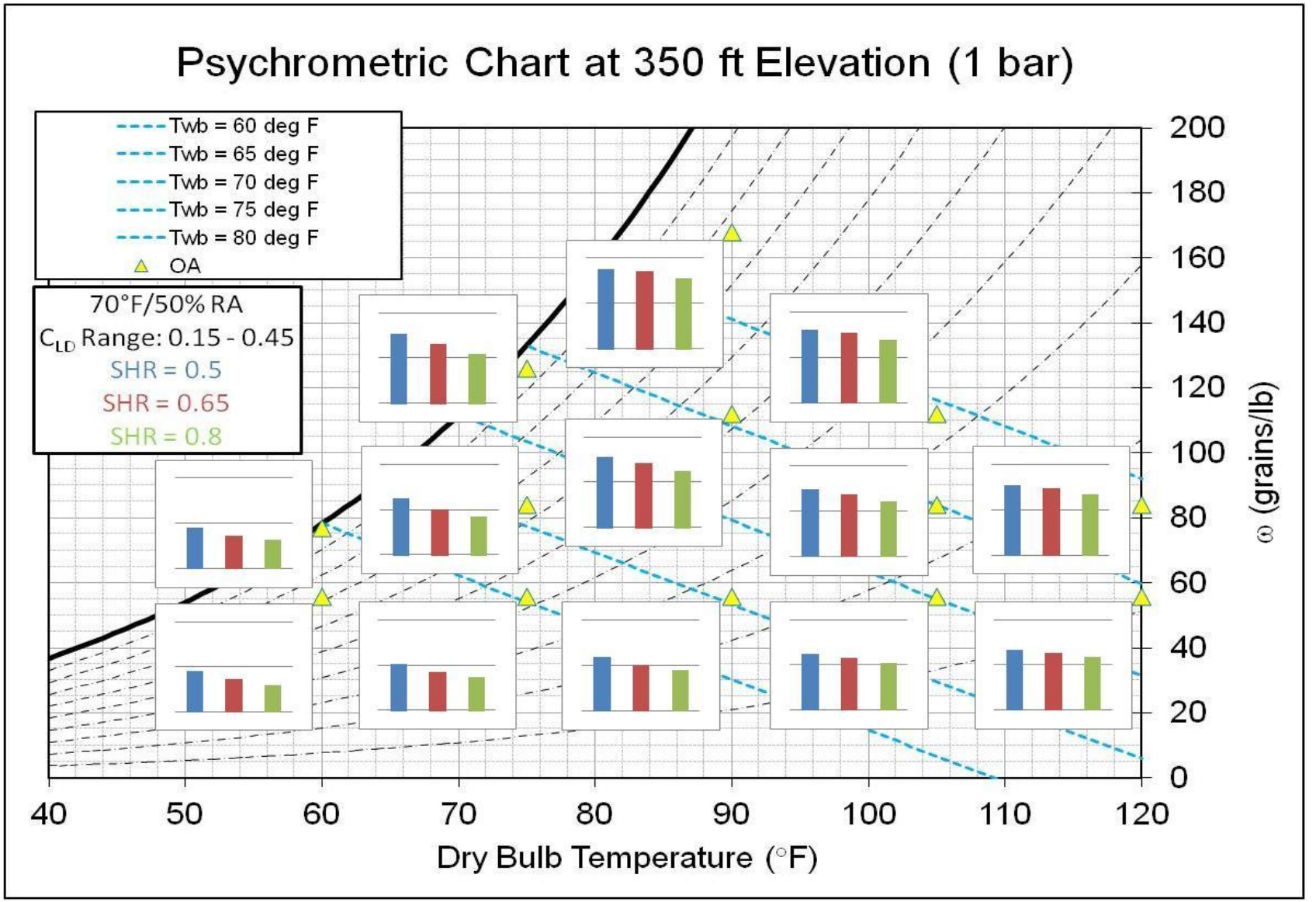

Figure C.122: Values held constant for $C_{LD,in,DEVap,near\text{-}opt,standard}$ for for T_{ra} = 70°F and RH_{ra} = 50% under variable outdoor air states

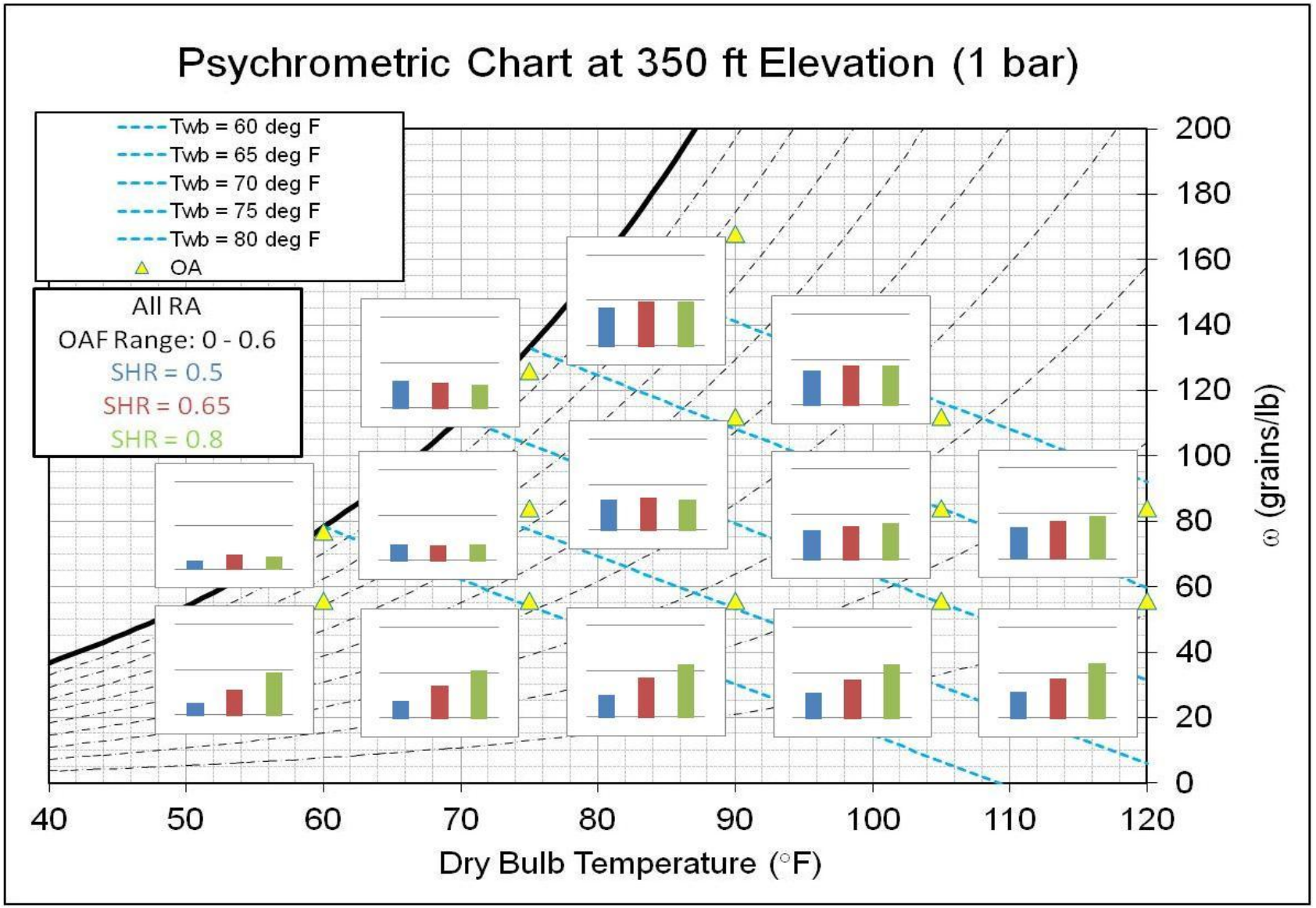

Figure C.123: Average values held constant for $OAF_{near\text{-}opt,standard}$ across all return air states under variable outdoor air states

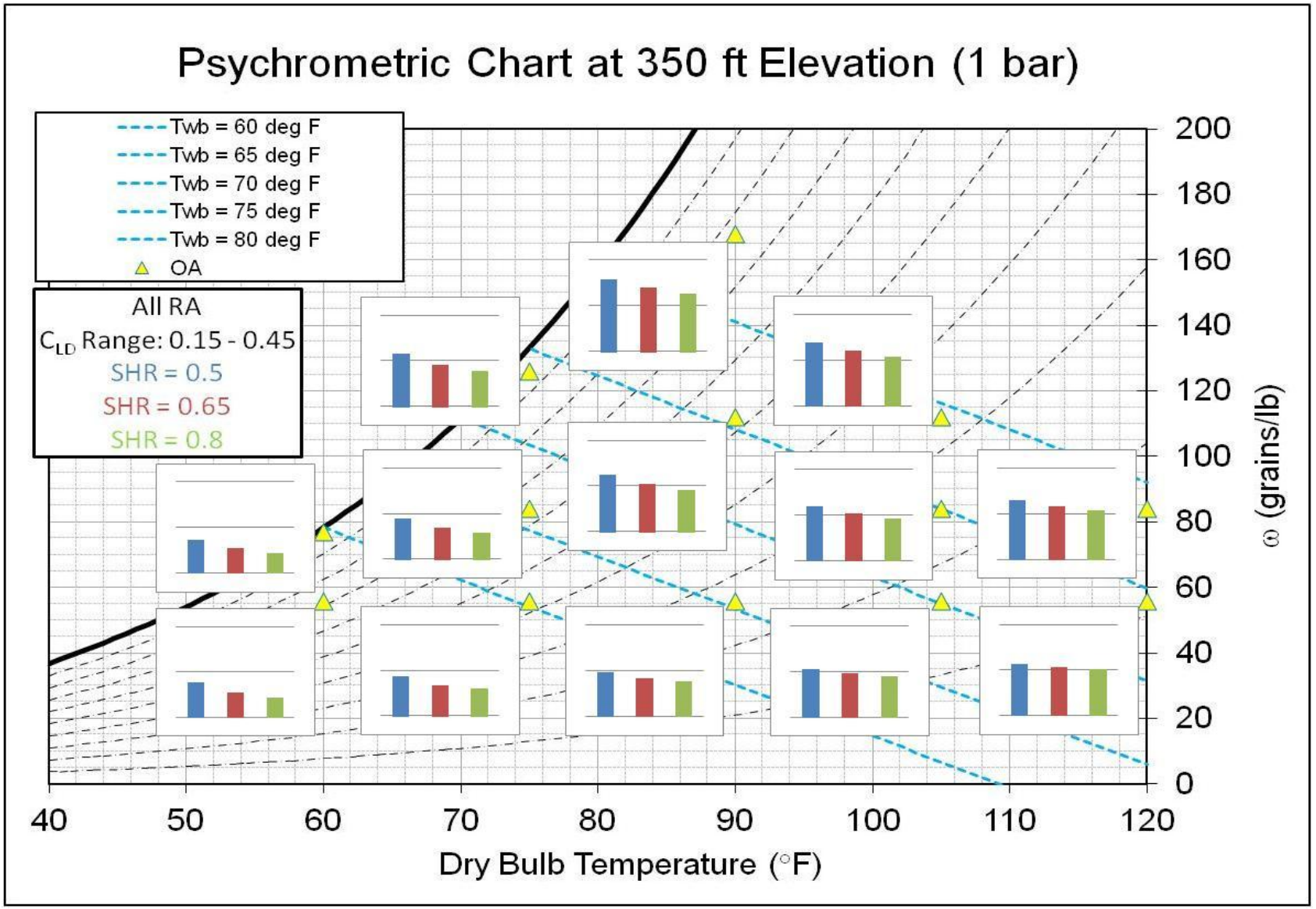

Figure C.124: Average values held constant for $C_{LD,in,DEVap,near\text{-}opt,standard}$ across all return air states under variable outdoor air states

C.3 Standard Mode – Final Phase

Table C.42: Near-optimal R_{e1} Values for Final Phase of Standard Mode

		OA (T_{oa}/ ω_{oa})												
RA (T_{ra}/ RH_{ra})	**SHR**	60°F/ 0.008	60°F/ 0.011	75°F/ 0.008	75°F/ 0.002	75°F/ 0.018	90°F/ 0.008	90°F/ 0.016	90°F/ 0.024	105°F/ 0.008	105°F/ 0.012	105°F/ 0.016	120°F/ 0.008	120°F/ 0.012
80°F/ 60%	0.5	0.700	0.700	0.700	0.700	0.700	0.700	0.700	0.700	0.700	0.700	0.700	0.700	0.700
	0.65	0.597	0.502	0.700	0.669	0.672	0.652	0.663	0.100	0.100	0.644	0.700	0.615	0.100
	0.8	0.293	0.359	0.418	0.620	0.578	0.610	0.594	0.100	0.560	0.571	0.568	0.512	0.589
80°F/ 55%	0.5	0.700	0.700	0.700	0.700	0.700	0.700	0.700	0.700	0.700	0.700	0.700	0.700	0.700
	0.65	0.700	0.700	0.700	0.688	0.700	0.670	0.100	0.260	0.590	0.100	0.100	0.100	0.100
	0.8	0.431	0.676	0.655	0.622	0.629	0.608	0.625	0.167	0.579	0.606	0.100	0.544	0.634
80°F/ 50%	0.5	0.700	0.700	0.700	0.700	0.700	0.700	0.700	0.700	0.700	0.700	0.700	0.700	0.700
	0.65	0.700	0.700	0.700	0.700	0.700	0.700	0.100	0.278	0.700	0.698	0.110	0.700	0.100
	0.8	0.696	0.665	0.650	0.636	0.666	0.620	0.661	0.100	0.100	0.651	0.514	0.100	0.100
75°F/ 55%	0.5	0.700	0.700	0.700	0.700	0.700	0.700	0.700	0.700	0.700	0.700	0.700	0.700	0.700
	0.65	0.700	0.695	0.665	0.697	0.100	0.661	0.100	0.324	0.695	0.100	0.288	0.100	0.100
	0.8	0.637	0.614	0.277	0.595	0.664	0.567	0.100	0.100	0.100	0.629	0.100	0.100	0.100
70°F/ 60%	0.5	0.700	0.700	0.700	0.700	0.700	0.700	0.700	0.700	0.700	0.700	0.700	0.700	0.700
	0.65	0.644	0.653	0.612	0.669	0.100	0.618	0.100	0.402	0.100	0.100	0.146	0.100	0.102
	0.8	0.581	0.567	0.539	0.567	0.700	0.522	0.100	0.114	0.100	0.100	0.101	0.100	0.100
70°F/ 55%	0.5	0.700	0.700	0.700	0.700	0.700	0.700	0.700	0.700	0.700	0.700	0.700	0.700	0.700
	0.65	0.669	0.700	0.662	0.700	0.301	0.100	0.352	0.700	0.700	0.299	0.550	0.300	0.467
	0.8	0.577	0.582	0.551	0.601	0.100	0.555	0.100	0.218	0.592	0.100	0.100	0.100	0.100
70°F/ 50%	0.5	0.700	0.700	0.700	0.700	0.700	0.700	0.700	0.700	0.700	0.700	0.700	0.700	0.700
	0.65	0.700	0.700	0.700	0.700	0.700	0.700	0.700	0.700	0.700	0.700	0.700	0.700	0.700
	0.8	0.585	0.609	0.576	0.641	0.515	0.596	0.100	0.368	0.645	0.100	0.111	0.558	0.100
All	0.5	0.700	0.700	0.700	0.700	0.700	0.700	0.700	0.700	0.700	0.700	0.700	0.700	0.700
	0.65	0.679	0.671	0.674	0.691	0.386	0.603	0.257	0.379	0.553	0.316	0.352	0.313	0.208
	0.8	0.564	0.589	0.469	0.608	0.576	0.579	0.275	0.152	0.320	0.446	0.199	0.246	0.214

Table C.43: Near-optimal OAF Values for Final Phase of Standard Mode

		OA (T_{oa}/ ω_{oa})												
RA (T_{ra}/ RH_{ra})	**SHR**	60°F/ 0.008	60°F/ 0.011	75°F/ 0.008	75°F/ 0.002	75°F/ 0.018	90°F/ 0.008	90°F/ 0.016	90°F/ 0.024	105°F/ 0.008	105°F/ 0.012	105°F/ 0.016	120°F/ 0.008	120°F/ 0.012
80°F/ 60%	0.5	0.500	0.253	0.314	0.347	0.455	0.507	0.258	0.507	0.450	0.476	0.507	0.505	0.507
	0.65	0.650	0.050	0.234	0.107	0.174	0.283	0.156	0.326	0.405	0.395	0.313	0.380	0.276
	0.8	0.800	0.050	0.050	0.050	0.103	0.151	0.077	0.259	0.389	0.129	0.242	0.327	0.125
80°F/ 55%	0.5	0.500	0.442	0.442	0.447	0.439	0.415	0.446	0.411	0.362	0.442	0.422	0.397	0.434
	0.65	0.650	0.134	0.167	0.175	0.244	0.343	0.233	0.453	0.379	0.305	0.452	0.453	0.456
	0.8	0.800	0.050	0.057	0.095	0.159	0.266	0.143	0.305	0.346	0.199	0.293	0.422	0.184
80°F/ 50%	0.5	0.500	0.341	0.342	0.346	0.343	0.330	0.348	0.329	0.296	0.347	0.336	0.320	0.344
	0.65	0.650	0.195	0.234	0.247	0.313	0.386	0.305	0.453	0.448	0.352	0.398	0.450	0.386
	0.8	0.800	0.108	0.141	0.151	0.216	0.312	0.204	0.340	0.430	0.383	0.331	0.218	0.415
75°F/ 55%	0.5	0.500	0.371	0.374	0.378	0.375	0.361	0.381	0.352	0.322	0.380	0.367	0.349	0.377
	0.65	0.650	0.200	0.246	0.263	0.340	0.477	0.330	0.478	0.471	0.383	0.477	0.452	0.478
	0.8	0.800	0.113	0.150	0.365	0.242	0.350	0.228	0.452	0.476	0.409	0.370	0.389	0.450
70°F/ 60%	0.5	0.500	0.399	0.402	0.407	0.405	0.390	0.411	0.387	0.346	0.410	0.397	0.377	0.407
	0.65	0.650	0.211	0.265	0.285	0.374	0.500	0.363	0.505	0.495	0.495	0.504	0.499	0.505
	0.8	0.800	0.119	0.162	0.182	0.279	0.394	0.261	0.485	0.488	0.447	0.482	0.441	0.486
70°F/ 55%	0.5	0.500	0.334	0.339	0.343	0.343	0.333	0.347	0.332	0.302	0.349	0.340	0.325	0.348
	0.65	0.650	0.285	0.342	0.360	0.423	0.489	0.481	0.489	0.472	0.449	0.489	0.489	0.487
	0.8	0.800	0.170	0.220	0.240	0.330	0.481	0.315	0.482	0.483	0.374	0.479	0.490	0.480
70°F/ 50%	0.5	0.500	0.282	0.287	0.290	0.292	0.287	0.295	0.287	0.264	0.298	0.292	0.282	0.299
	0.65	0.650	0.366	0.408	0.418	0.452	0.475	0.448	0.480	0.381	0.464	0.478	0.477	0.473
	0.8	0.800	0.223	0.278	0.295	0.367	0.268	0.356	0.478	0.477	0.399	0.475	0.481	0.429
All	0.5	0.500	0.352	0.361	0.368	0.378	0.372	0.361	0.368	0.332	0.385	0.377	0.361	0.385
	0.65	0.650	0.204	0.265	0.265	0.333	0.434	0.331	0.460	0.444	0.401	0.452	0.456	0.446
	0.8	0.800	0.118	0.151	0.234	0.242	0.325	0.227	0.412	0.449	0.351	0.379	0.394	0.386

Table C.44: Near-optimal $C_{LD,in,DEVap}$ Values for Final Phase of Standard Mode

		OA (T_{oa}/ ω_{oa})												
RA (T_{ra}/ RH_{ra})	**SHR**	60°F/ 0.008	60°F/ 0.011	75°F/ 0.008	75°F/ 0.002	75°F/ 0.018	90°F/ 0.008	90°F/ 0.016	90°F/ 0.024	105°F/ 0.008	105°F/ 0.012	105°F/ 0.016	120°F/ 0.008	120°F/ 0.012
80°F/ 60%	0.5	0.275	0.292	0.300	0.378	0.435	0.294	0.430	0.440	0.391	0.425	0.438	0.422	0.430
	0.65	0.212	0.218	0.220	0.236	0.270	0.233	0.286	0.402	0.310	0.279	0.312	0.266	0.368
	0.8	0.204	0.204	0.204	0.211	0.240	0.209	0.259	0.366	0.224	0.253	0.285	0.236	0.274
80°F/ 55%	0.5	0.440	0.440	0.440	0.440	0.440	0.440	0.440	0.440	0.440	0.440	0.440	0.440	0.440
	0.65	0.227	0.237	0.241	0.261	0.302	0.258	0.394	0.394	0.279	0.385	0.411	0.381	0.406
	0.8	0.207	0.206	0.211	0.230	0.266	0.227	0.281	0.365	0.244	0.275	0.361	0.257	0.296
80°F/ 50%	0.5	0.440	0.440	0.440	0.440	0.440	0.440	0.440	0.440	0.440	0.440	0.440	0.440	0.440
	0.65	0.252	0.265	0.270	0.296	0.340	0.290	0.427	0.440	0.312	0.344	0.440	0.333	0.439
	0.8	0.212	0.224	0.230	0.252	0.292	0.248	0.305	0.416	0.324	0.299	0.310	0.352	0.376
75°F/ 55%	0.5	0.440	0.440	0.440	0.440	0.440	0.440	0.434	0.440	0.440	0.440	0.440	0.440	0.440
	0.65	0.248	0.262	0.267	0.296	0.428	0.290	0.429	0.440	0.314	0.419	0.407	0.413	0.439
	0.8	0.212	0.224	0.241	0.255	0.300	0.250	0.372	0.432	0.323	0.306	0.378	0.356	0.387
70°F/ 60%	0.5	0.440	0.440	0.440	0.440	0.440	0.440	0.440	0.440	0.440	0.440	0.440	0.440	0.440
	0.65	0.245	0.261	0.266	0.300	0.435	0.292	0.435	0.440	0.387	0.422	0.440	0.415	0.440
	0.8	0.212	0.226	0.231	0.261	0.311	0.254	0.384	0.440	0.329	0.371	0.392	0.364	0.394
70°F/ 55%	0.5	0.440	0.440	0.440	0.440	0.440	0.440	0.440	0.440	0.440	0.440	0.440	0.440	0.440
	0.65	0.274	0.295	0.301	0.337	0.424	0.393	0.420	0.440	0.352	0.416	0.420	0.406	0.416
	0.8	0.229	0.246	0.252	0.284	0.403	0.277	0.404	0.440	0.301	0.391	0.423	0.384	0.415
70°F/ 50%	0.5	0.440	0.440	0.440	0.440	0.440	0.440	0.440	0.440	0.440	0.440	0.440	0.440	0.440
	0.65	0.316	0.341	0.345	0.378	0.420	0.369	0.427	0.440	0.389	0.417	0.440	0.405	0.432
	0.8	0.250	0.270	0.275	0.309	0.320	0.301	0.425	0.440	0.325	0.413	0.440	0.348	0.435
All	0.5	0.422	0.424	0.424	0.433	0.439	0.424	0.437	0.440	0.435	0.438	0.440	0.438	0.439
	0.65	0.252	0.267	0.271	0.299	0.386	0.301	0.408	0.431	0.330	0.391	0.409	0.383	0.424
	0.8	0.217	0.228	0.236	0.257	0.304	0.252	0.353	0.418	0.302	0.324	0.372	0.334	0.372

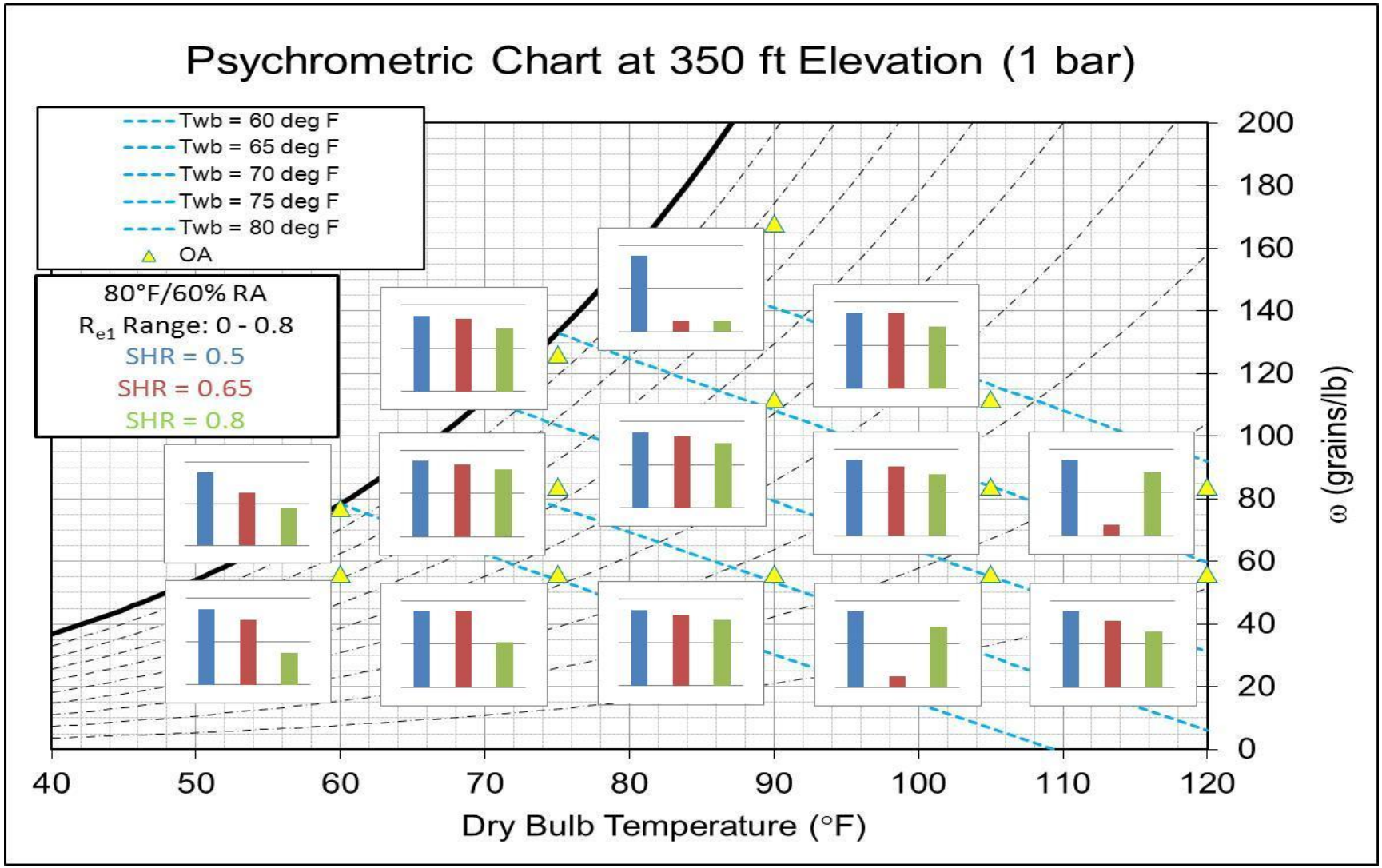

Figure C.125: $R_{e1,last}$ values for T_{ra} = 80°F and RH_{ra} = 60% under variable SHR values and outdoor air states

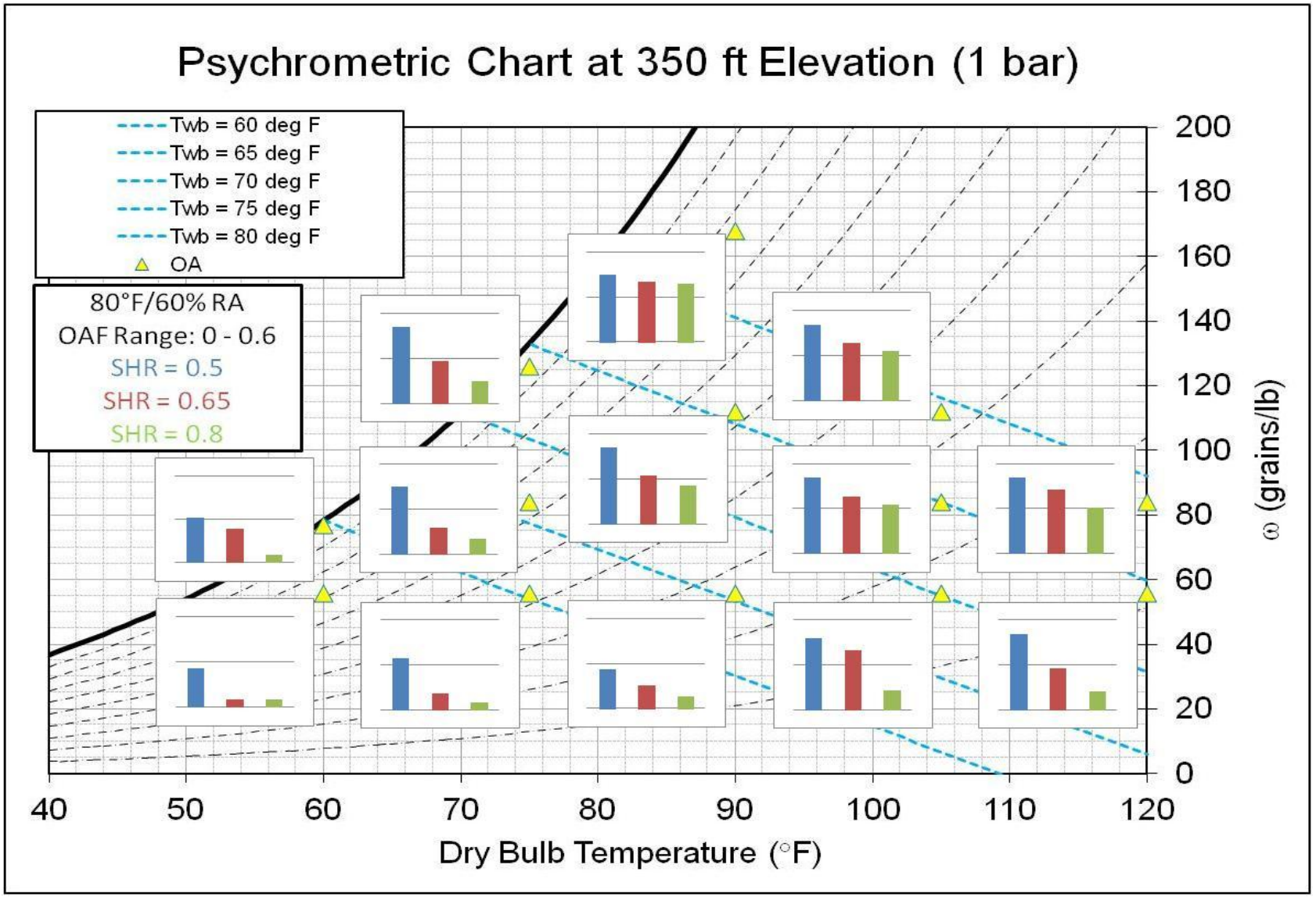

Figure C.126: OAF_{last} values for T_{ra} = 80°F and RH_{ra} = 60% under variable SHR values and outdoor air states

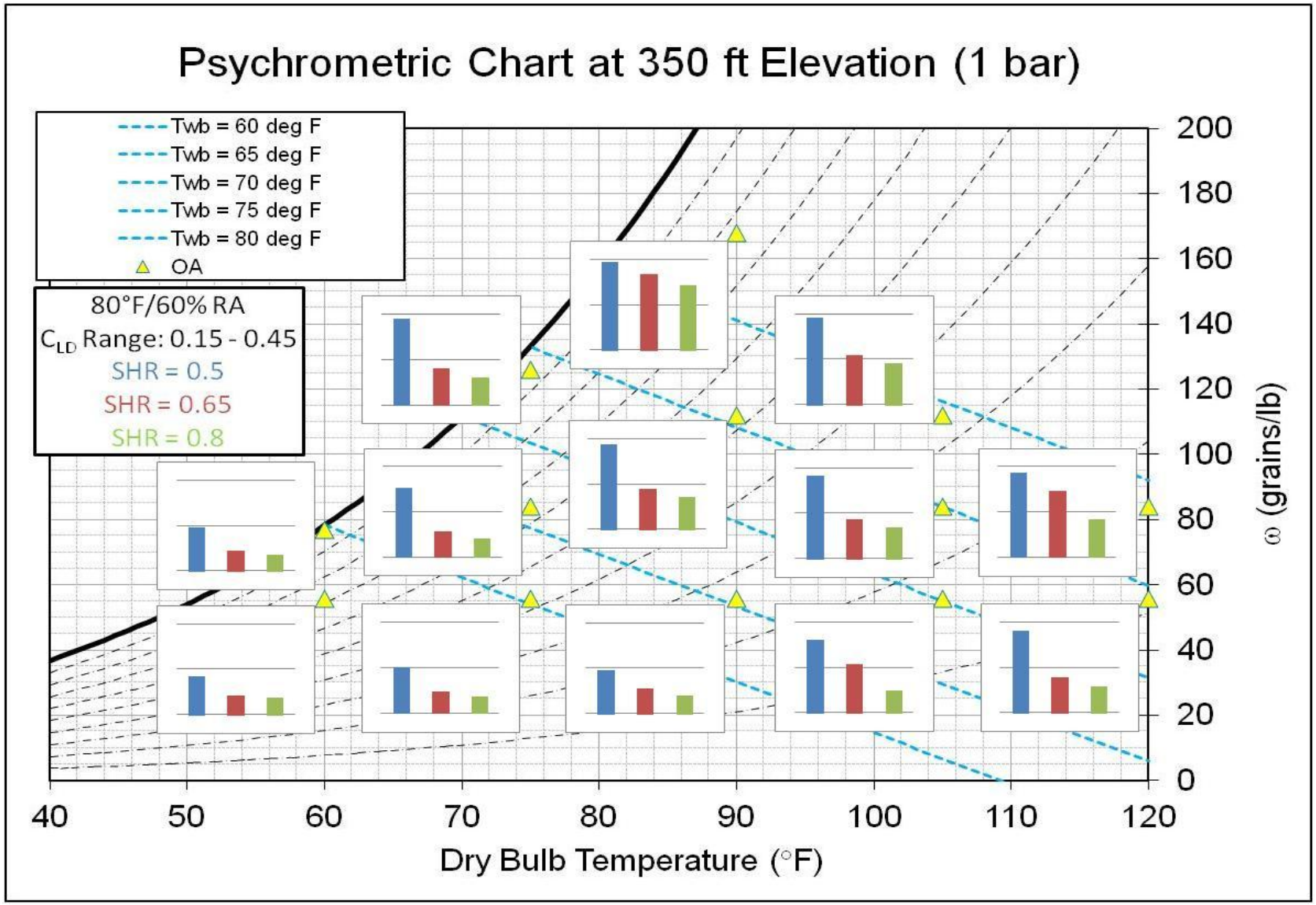

Figure C.127: $C_{LD,in,DEVap,last}$ values for T_{ra} = 80°F and RH_{ra} = 60% under variable SHR values and outdoor air states

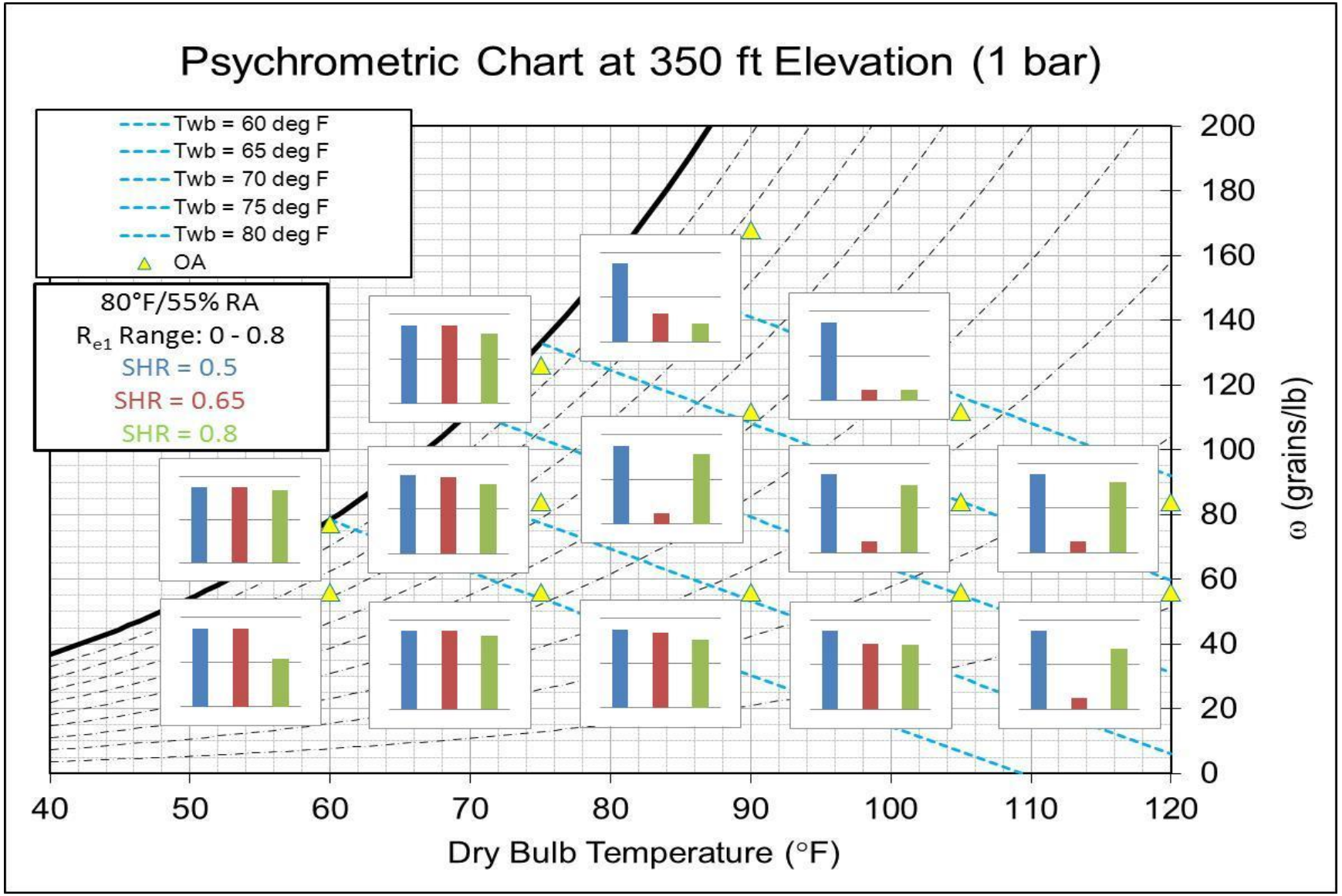

Figure C.128: $R_{e1,last}$ values for T_{ra} = 80°F and RH_{ra} = 55% under variable SHR values and outdoor air states

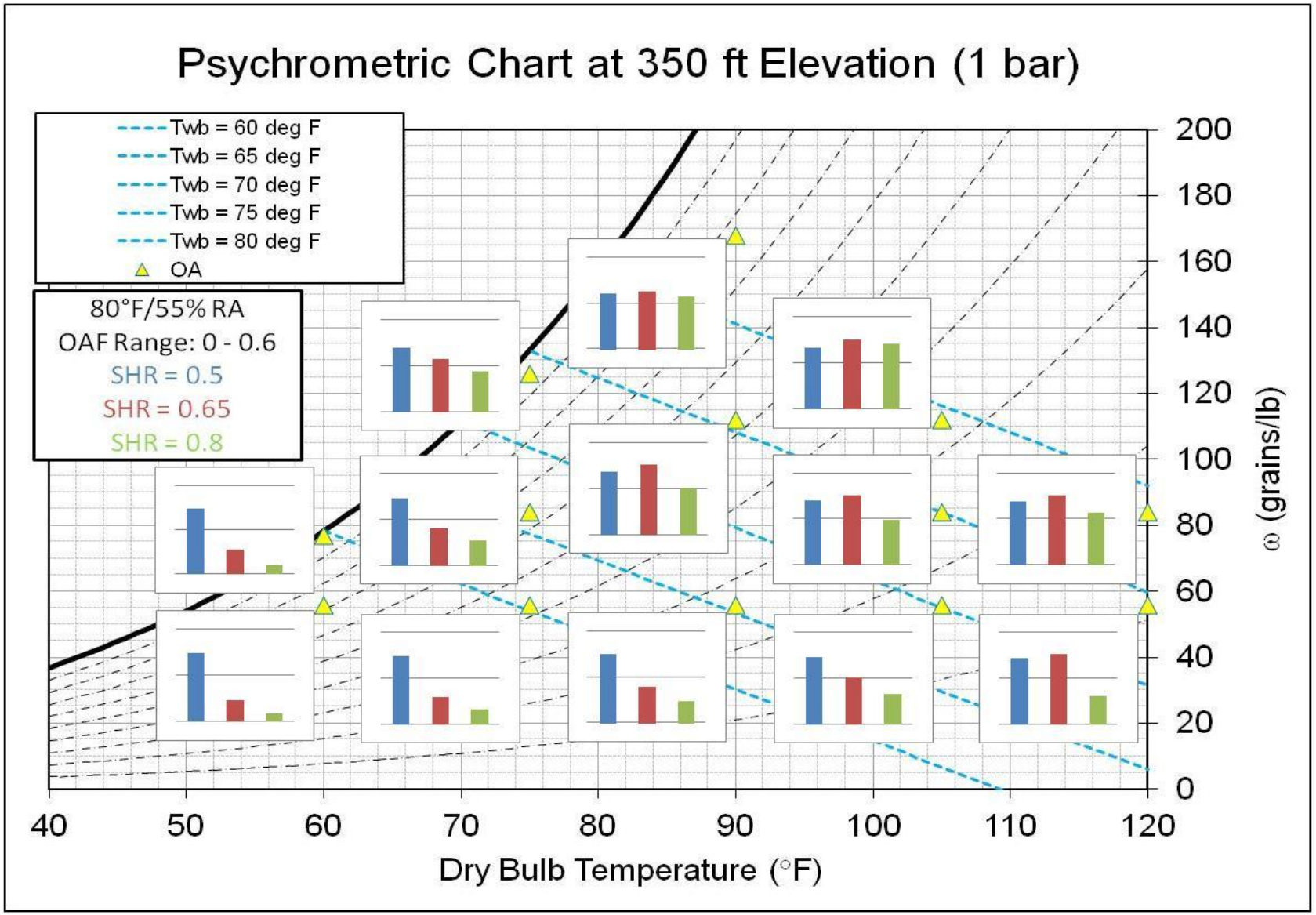

Figure C.129: OAF_{last} values for T_{ra} = T_{ra} = 80°F and RH_{ra} = 55% under variable SHR values and outdoor air states

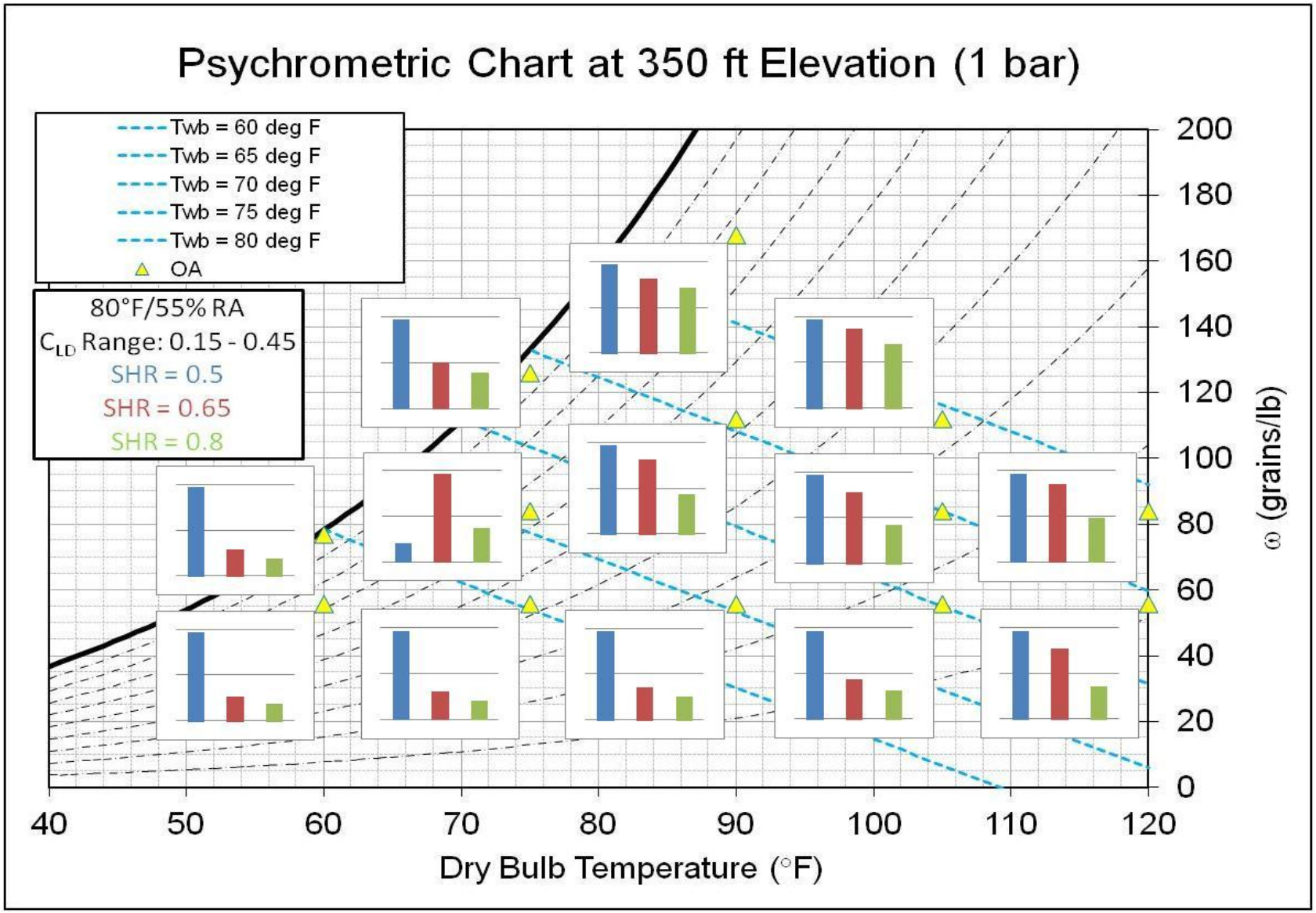

Figure C.130: $C_{LD,in,DEVap,last}$ values for $T_{ra} = T_{ra} = 80°F$ and $RH_{ra} = 55\%$ under variable SHR values and outdoor air states

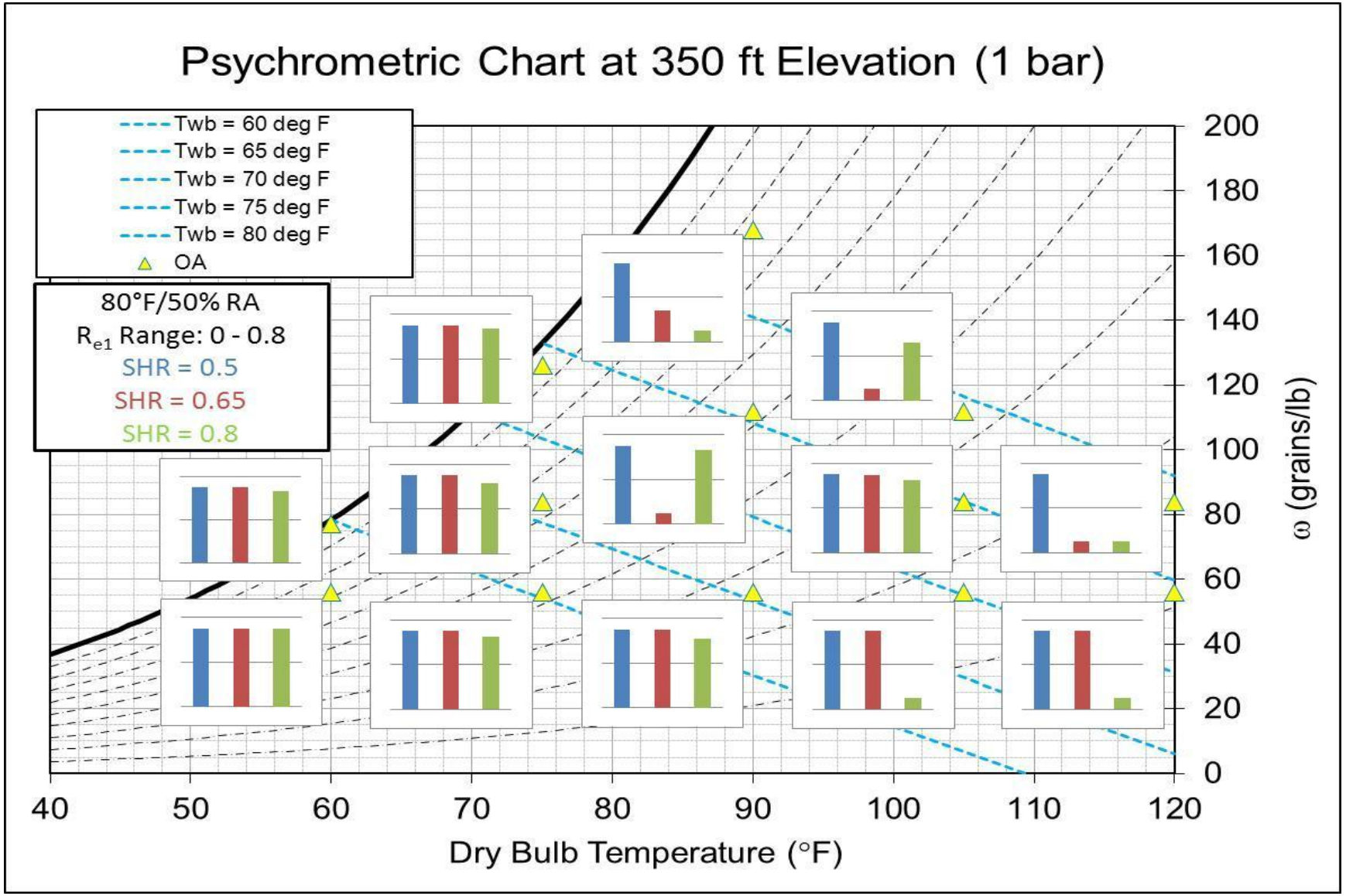

Figure C.131: $R_{e1,last}$ values for T_{ra} = 80°F and RH_{ra} = 50% under variable SHR values and outdoor air states

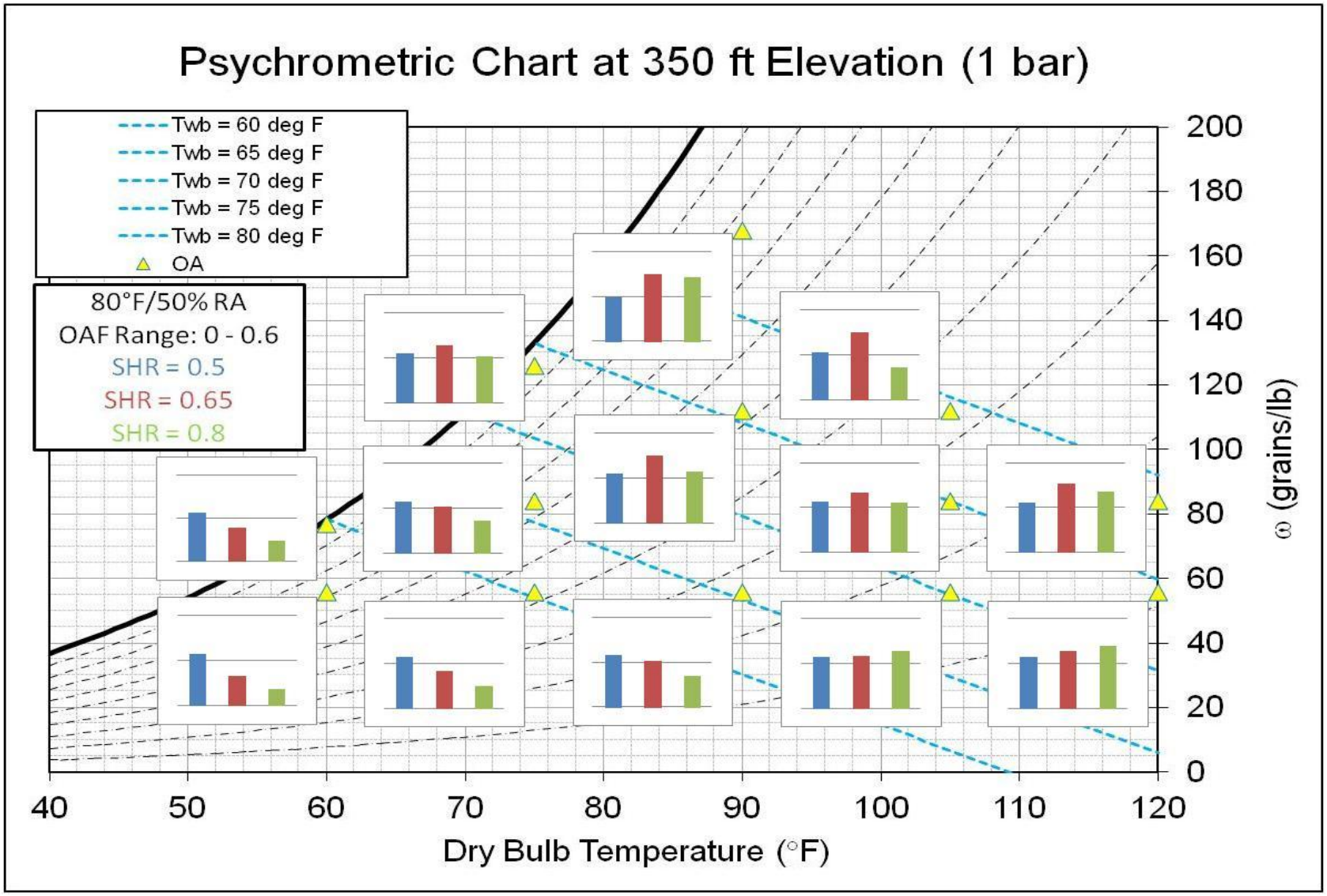

Figure C.132: OAF_{last} values for T_{ra} = 80°F and RH_{ra} = 50% under variable SHR values and outdoor air states

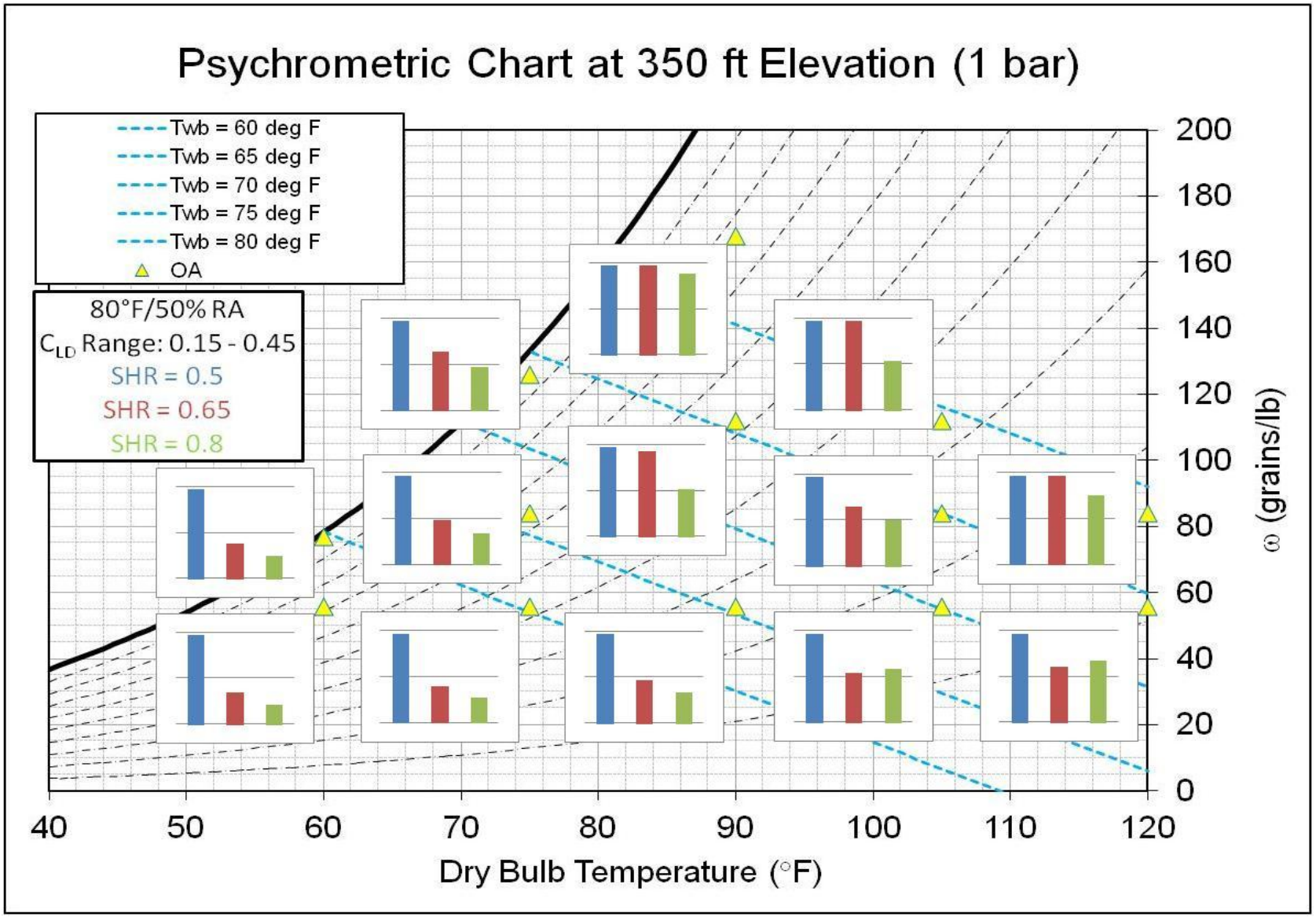

Figure C.133: $C_{LD,in,DEVap,last}$ values for T_{ra} = 80°F and RH_{ra} = 50% under variable SHR values and outdoor air states

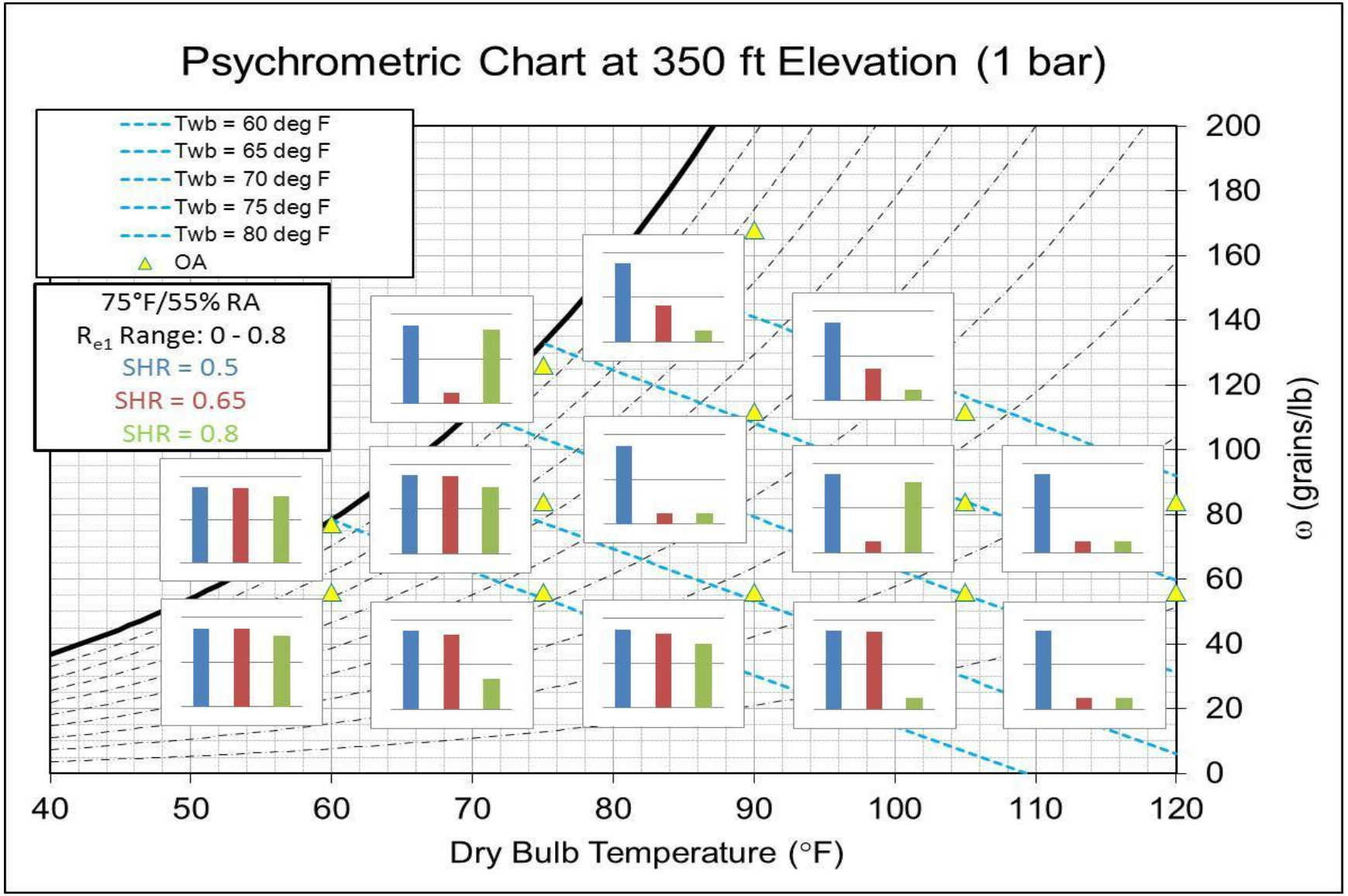

Figure C.134: $R_{e1,last}$ values for T_{ra} = 75°F and RH_{ra} = 55% under variable SHR values and outdoor air states

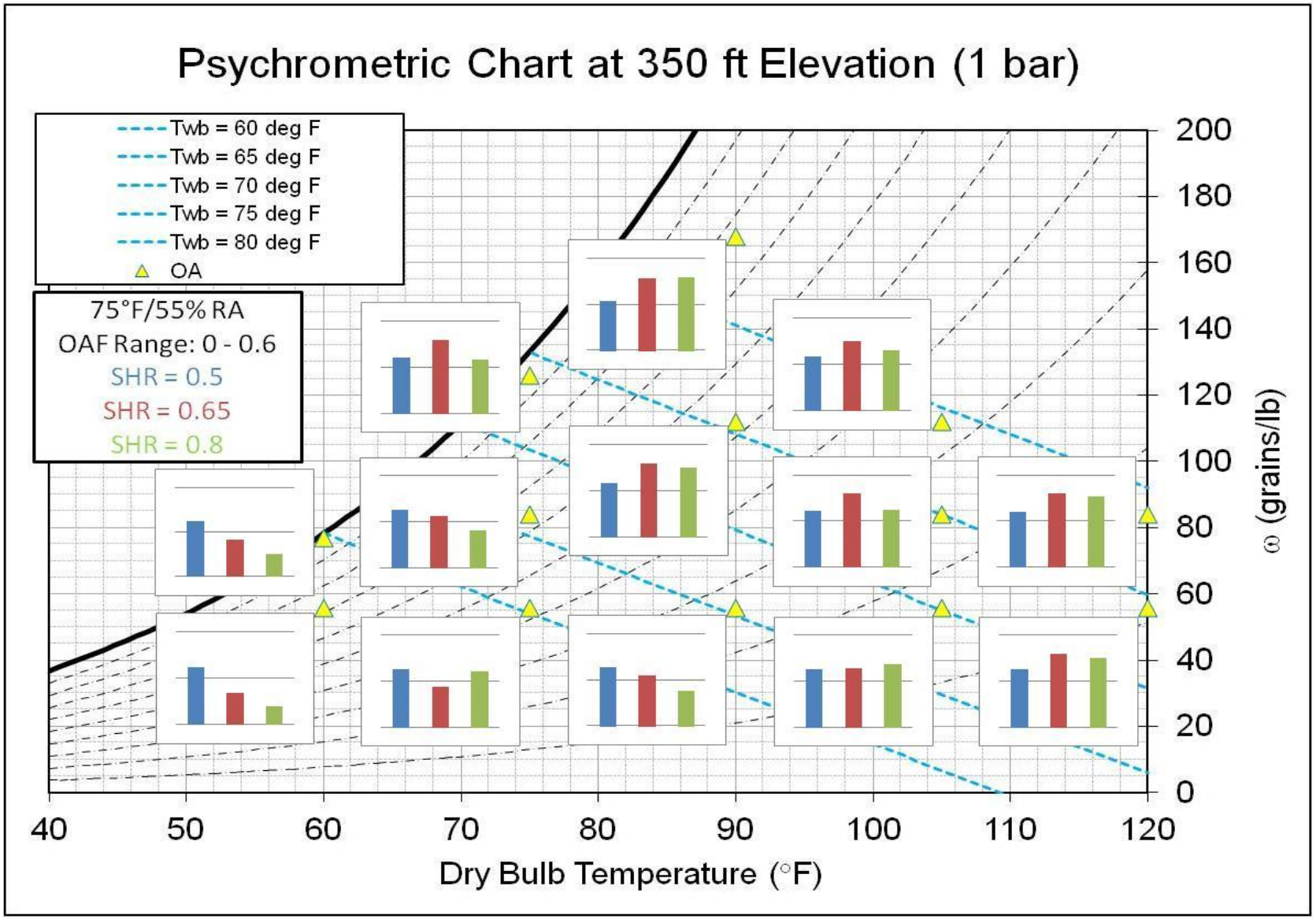

Figure C.135: OAF_{last} values for T_{ra} = 75°F and RH_{ra} = 55% under variable SHR values and outdoor air states

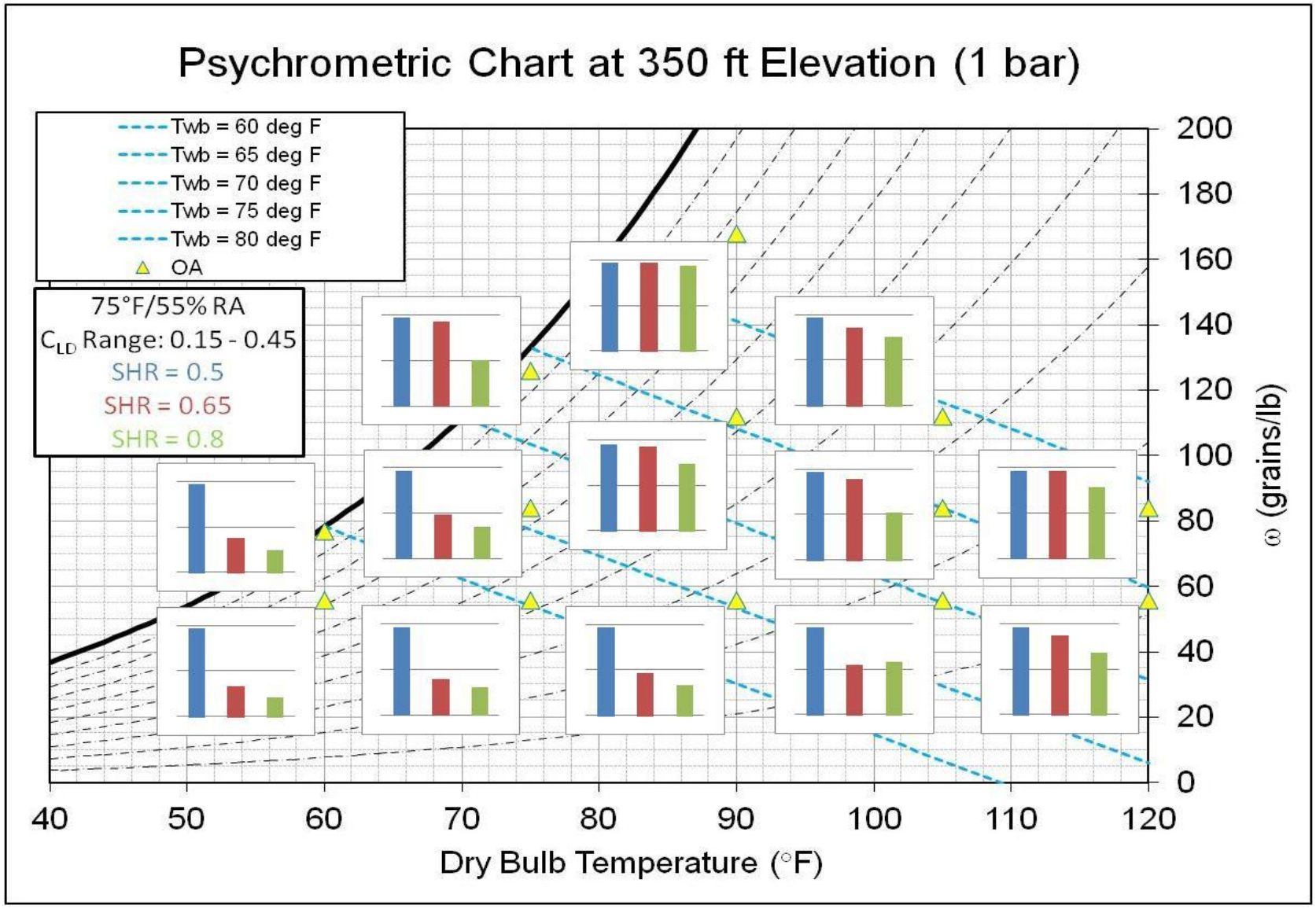

Figure C.136: $C_{LD,in,DEVap,last}$ values for T_{ra} = 75°F and RH_{ra} = 55% under variable SHR values and outdoor air states

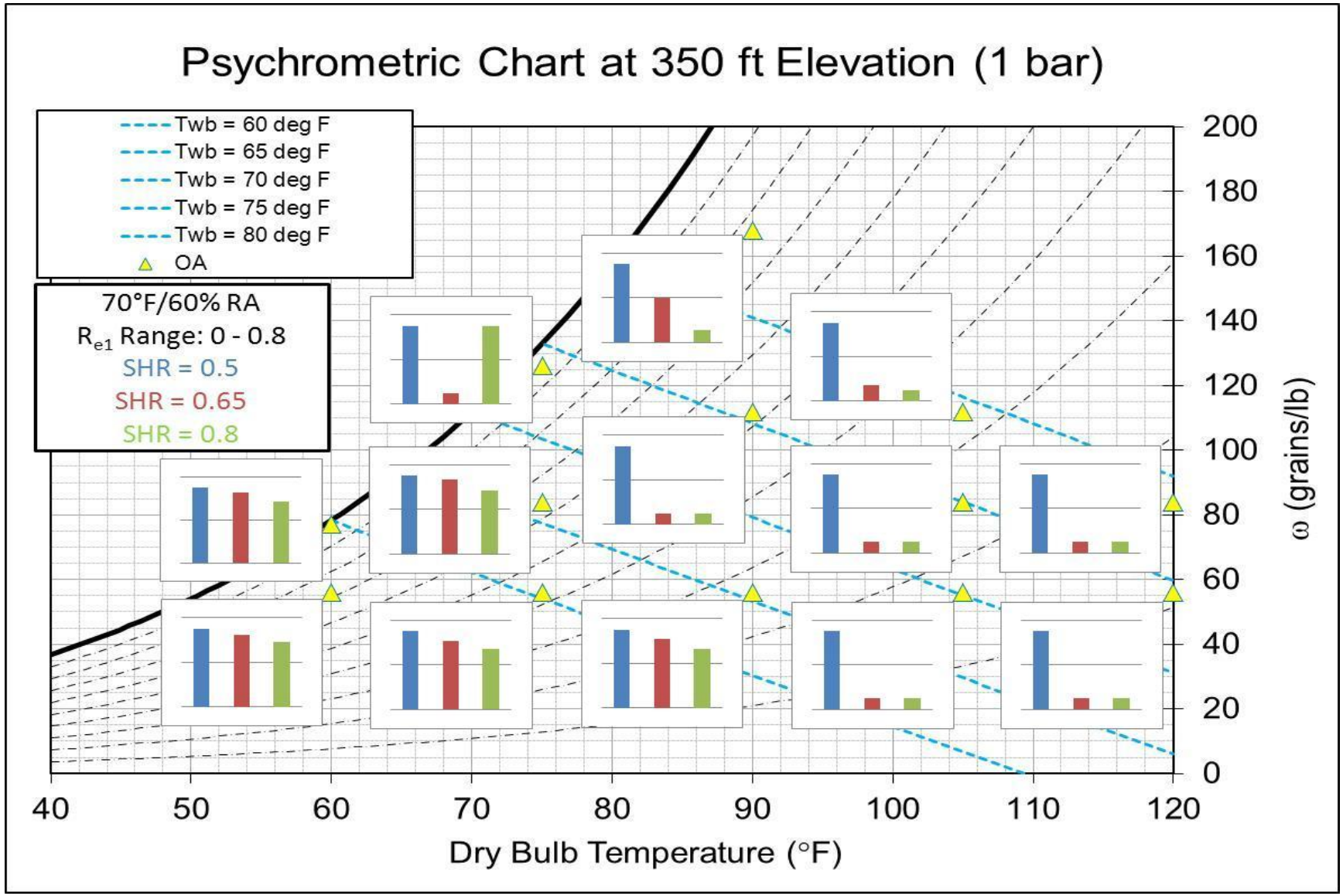

Figure C.137: $R_{e1,last}$ values for T_{ra} = 70°F and RH_{ra} = 60% under variable SHR values and outdoor air states

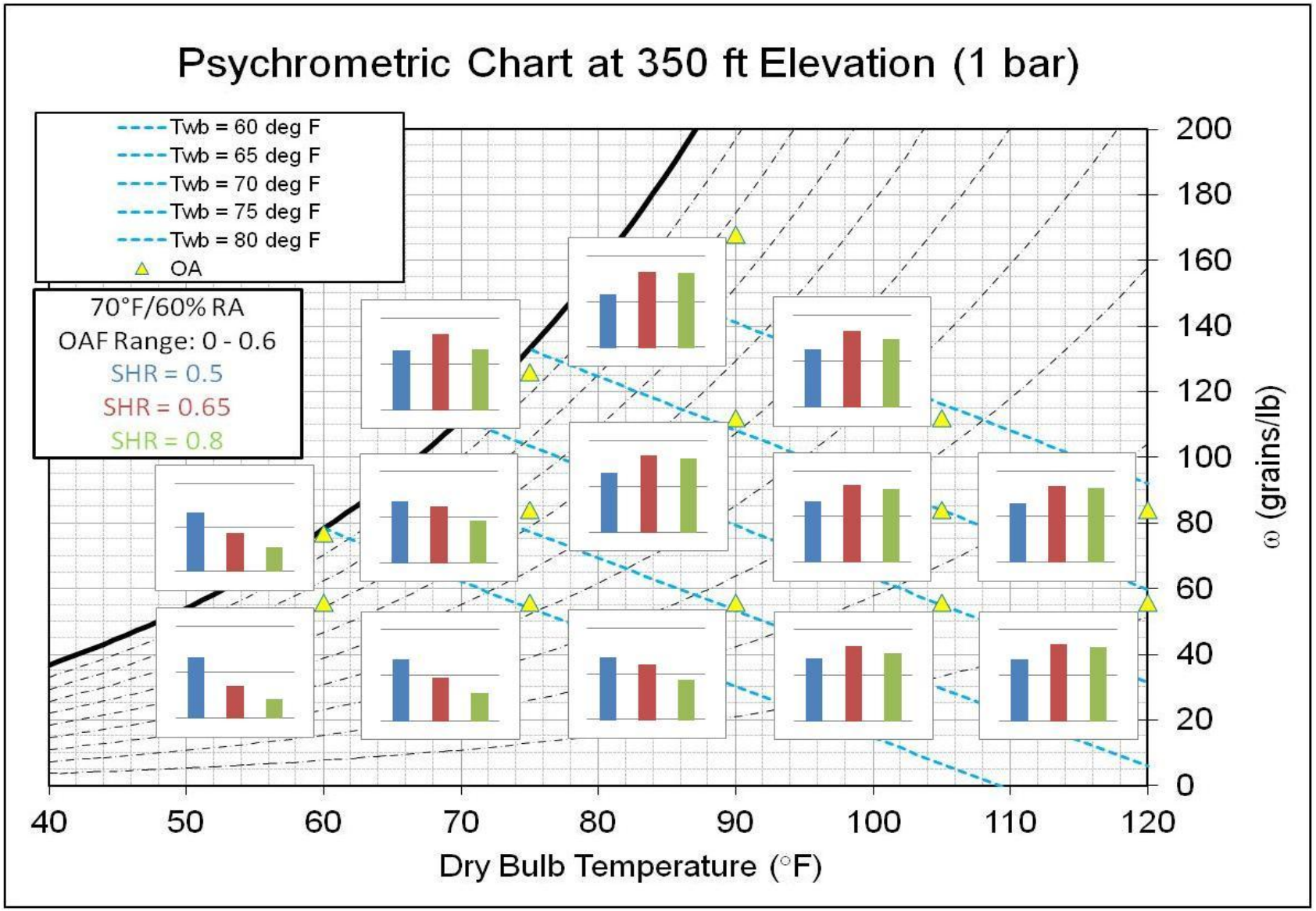

Figure C.138: OAF_{last} values for T_{ra} = 70°F and RH_{ra} = 60% % under variable SHR values and outdoor air states

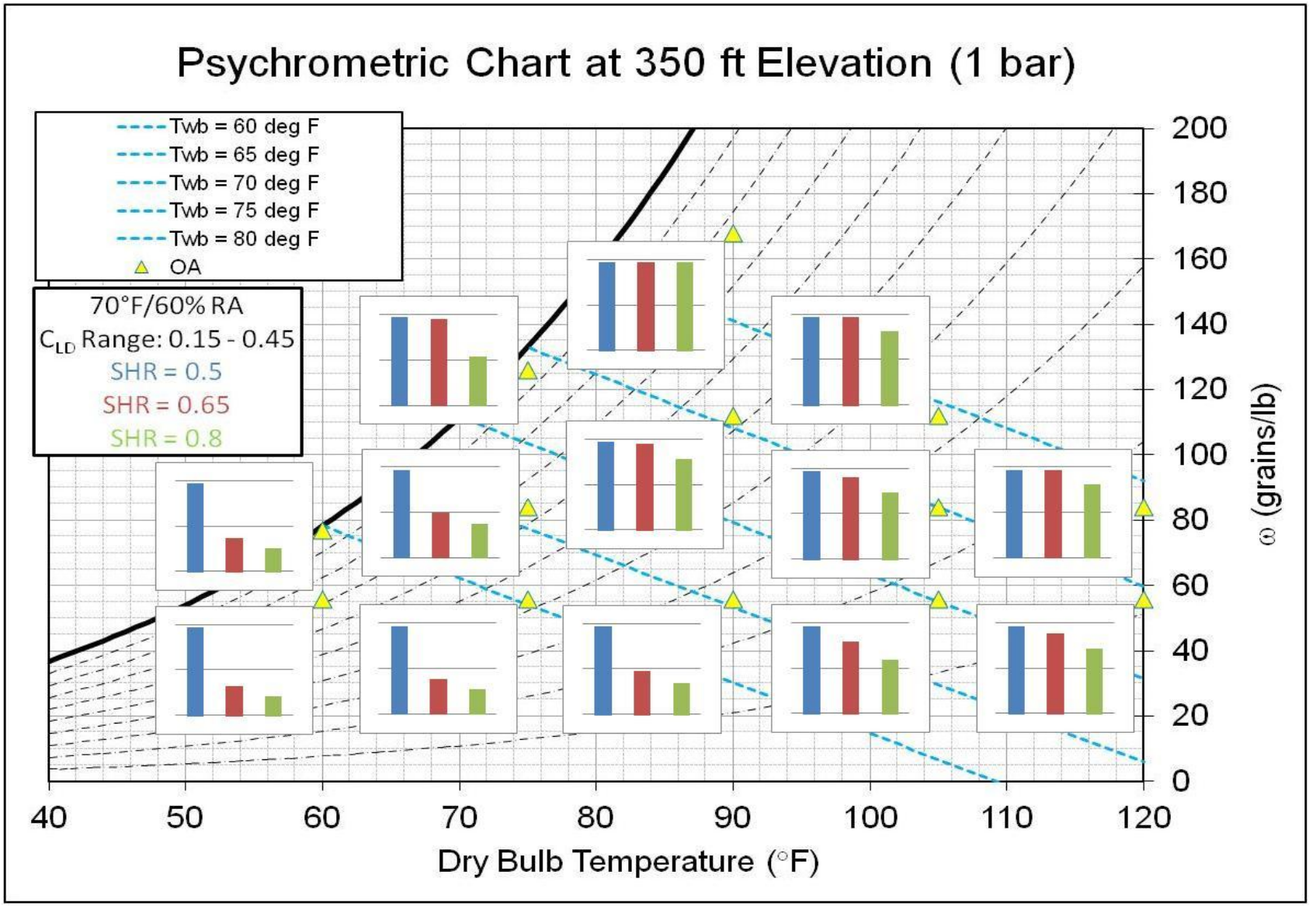

Figure C.139: $C_{LD,in,DEVap,last}$ values for T_{ra} = 70°F and RH_{ra} = 60% under variable SHR values and outdoor air states

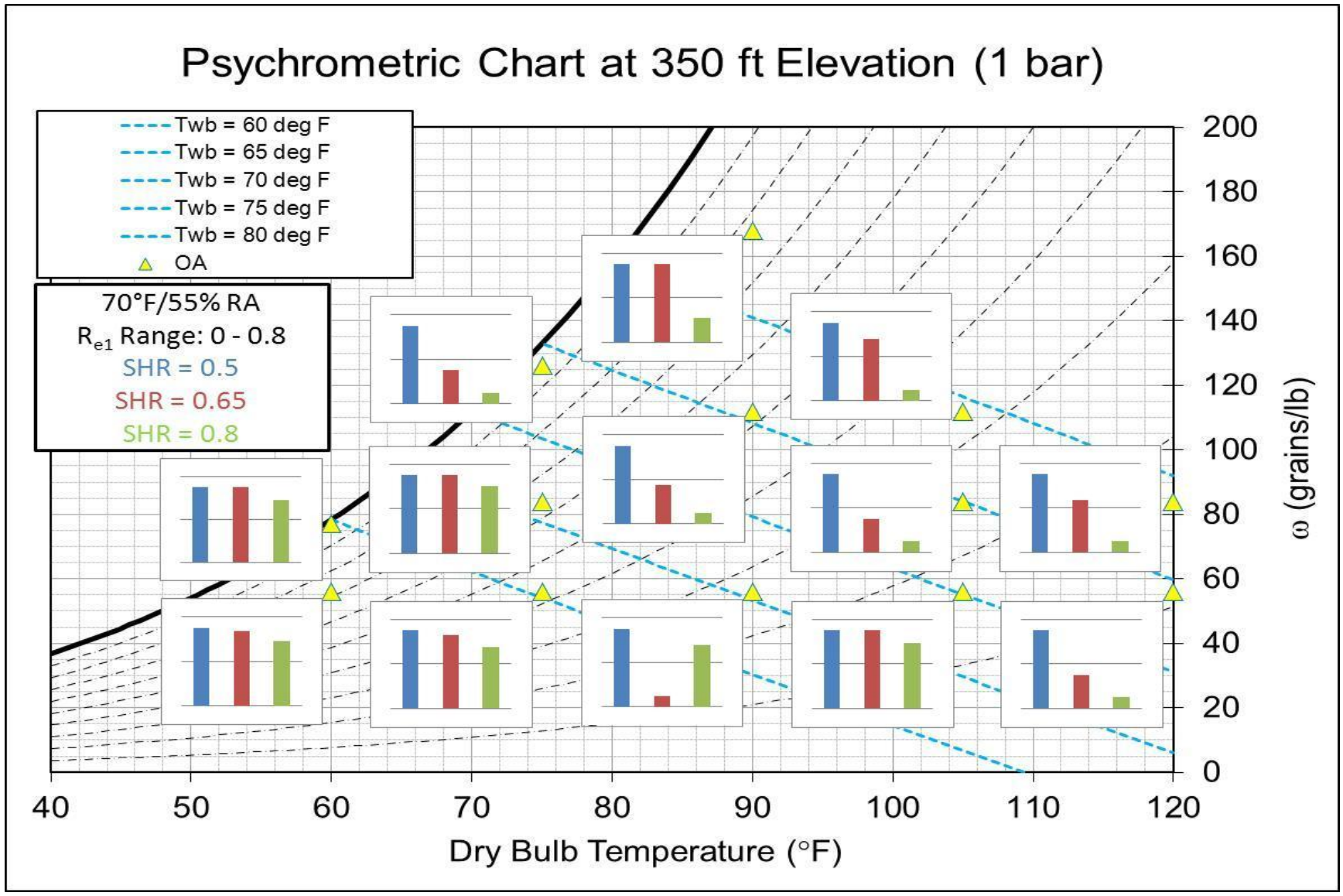

Figure C.140: $R_{e1,last}$ values for T_{ra} = 70°F and RH_{ra} = 55% under variable SHR values and outdoor air states

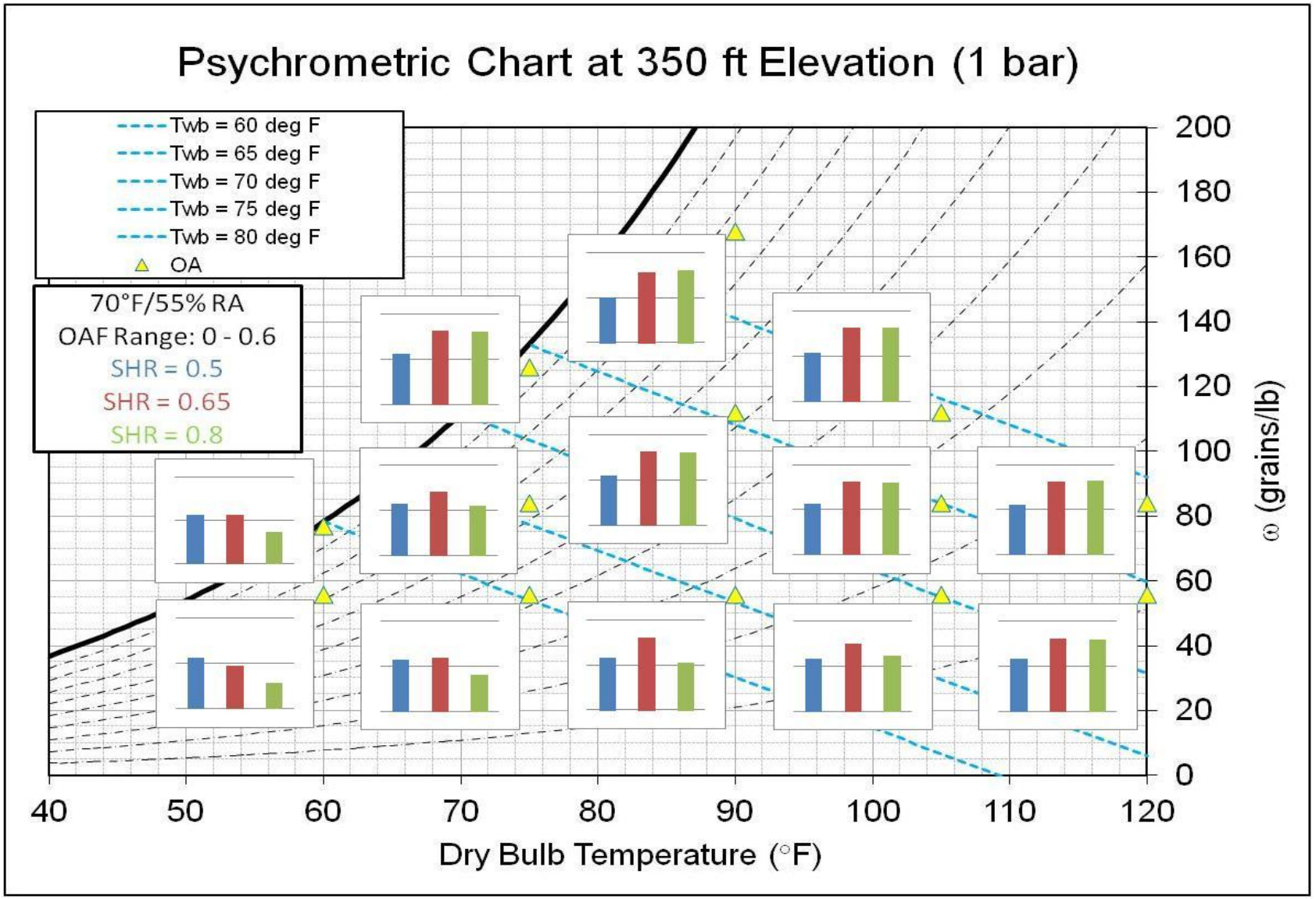

Figure C.141: OAF_{last} values for T_{ra} = 70°F and RH_{ra} = 55% under variable SHR values and outdoor air states

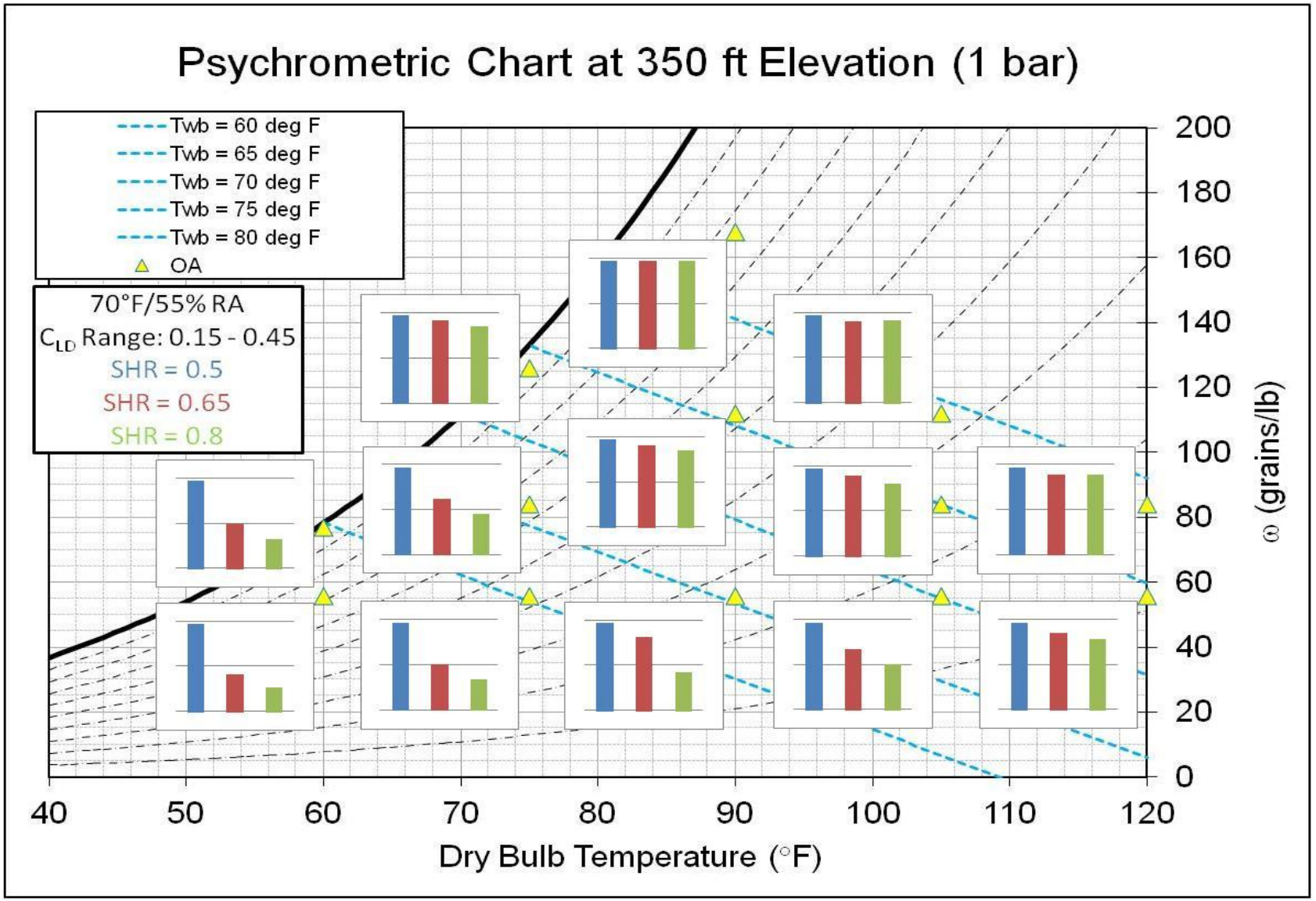

Figure C.142: $C_{LD,in,DEVap,last}$ values for T_{ra} = 70°F and RH_{ra} = 55% under variable SHR values and outdoor air states

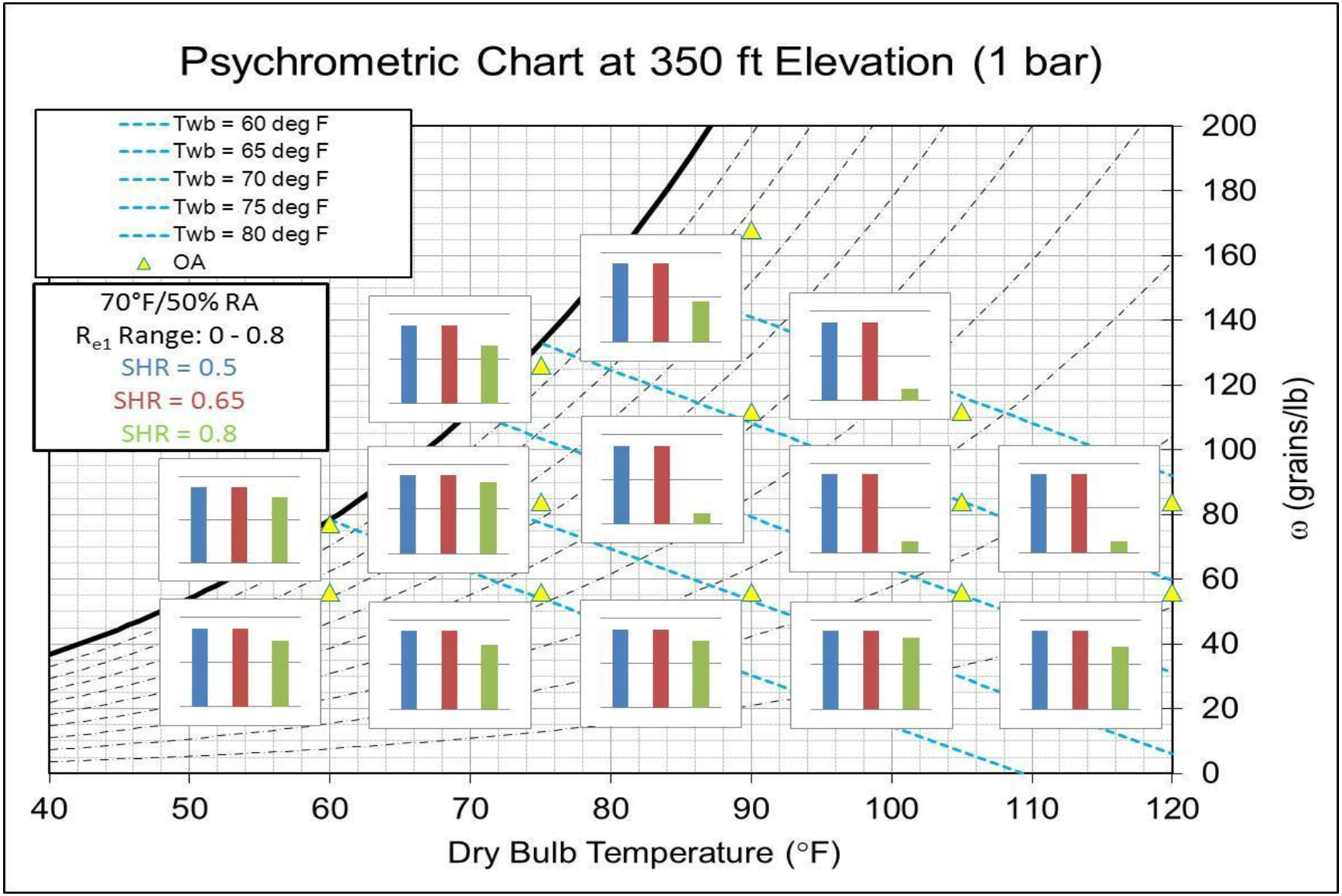

Figure C.143: $R_{e1,last}$ values for T_{ra} = 70°F and RH_{ra} = 50% under variable SHR values and outdoor air states

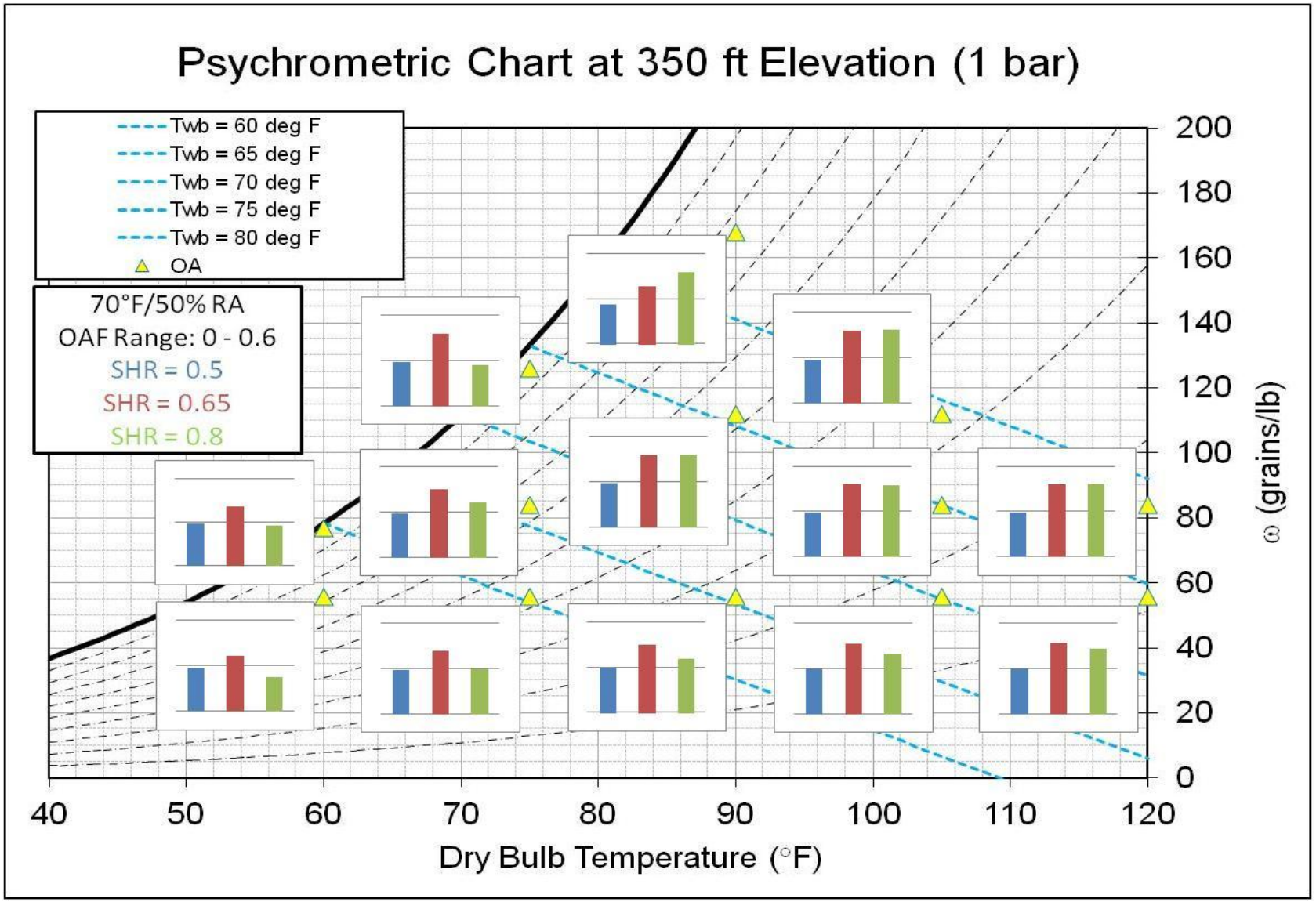

Figure C.144: OAF_{last} values for T_{ra} = 70°F and RH_{ra} = 50% under variable SHR values and outdoor air states

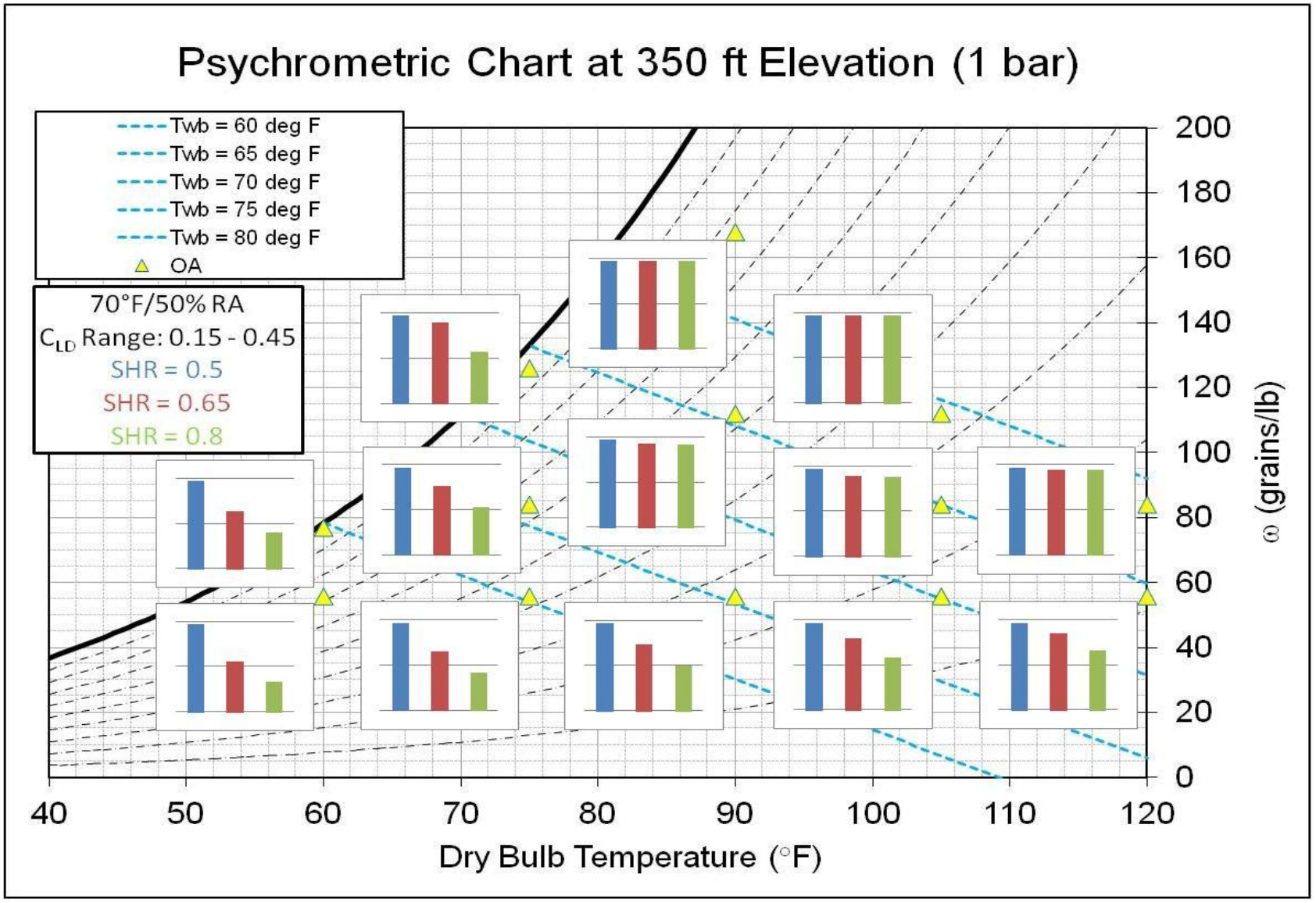

Figure C.145: $C_{LD,in,DEVap,last}$ values for T_{ra} = 70°F and RH_{ra} = 50% under variable SHR values and outdoor air states

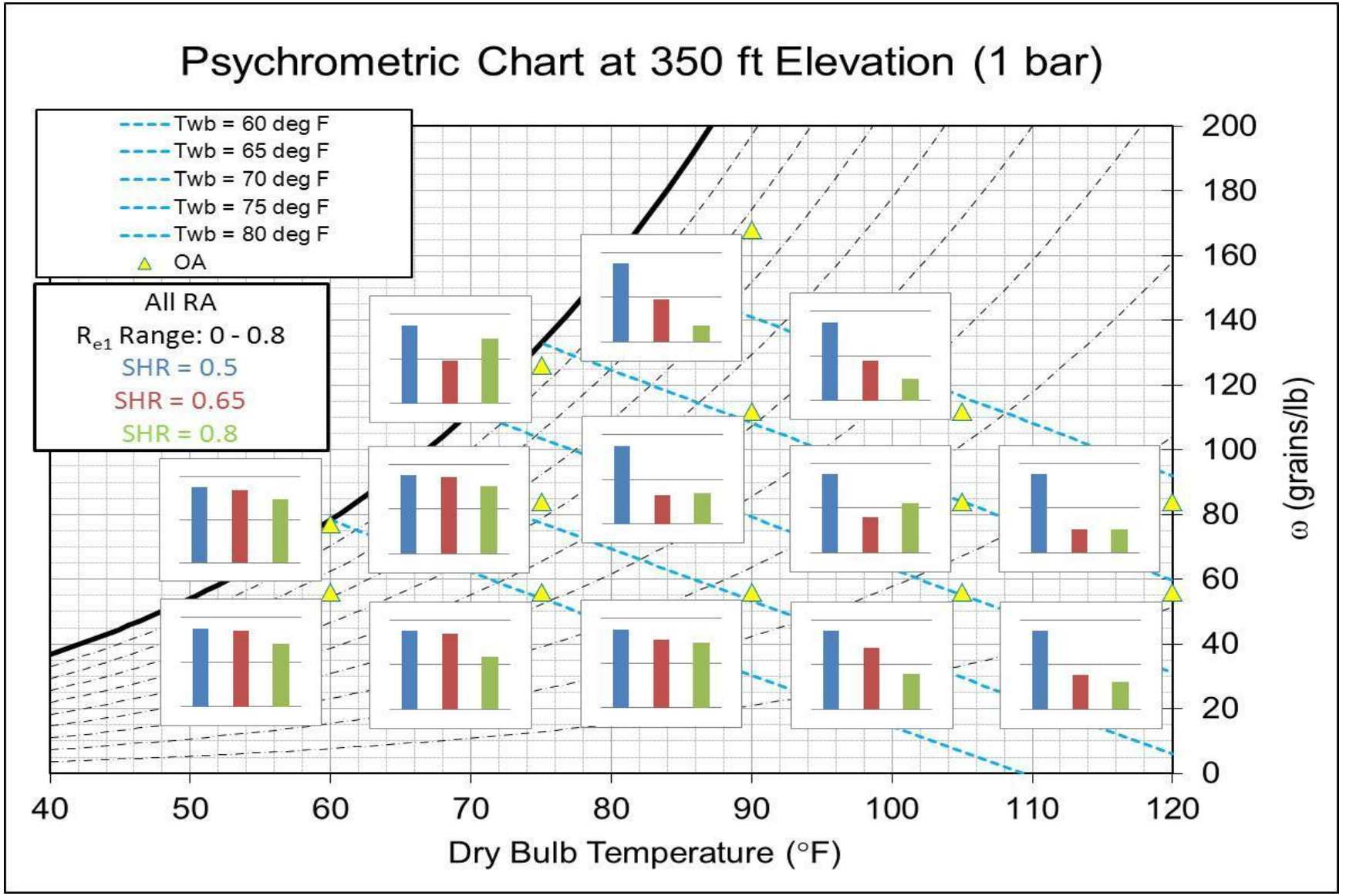

Figure C.146: Average $R_{e1,last}$ values for all return air states under variable SHR values and outdoor air states

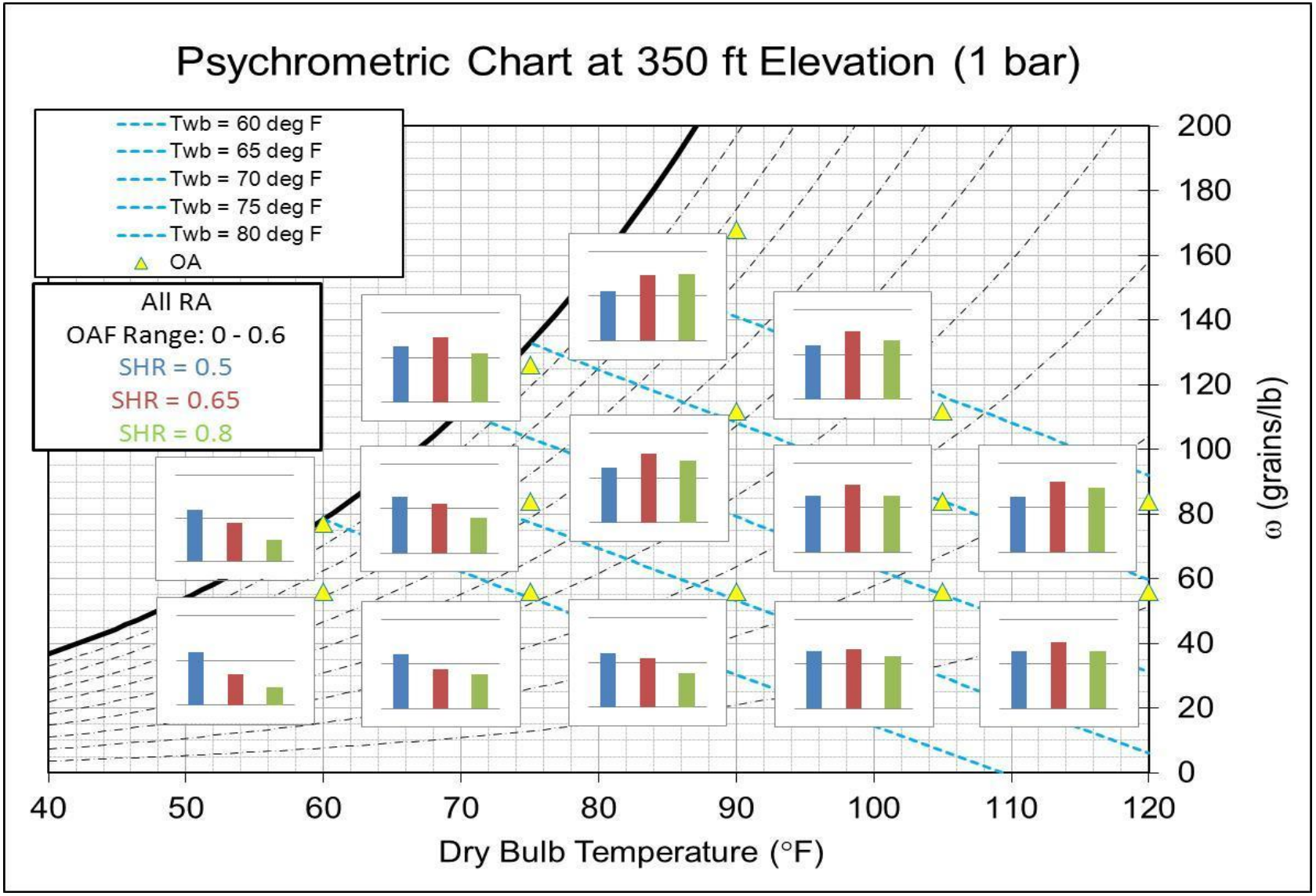

Figure C.147: Average OAF_{last} values for all return air states under variable SHR values and outdoor air states

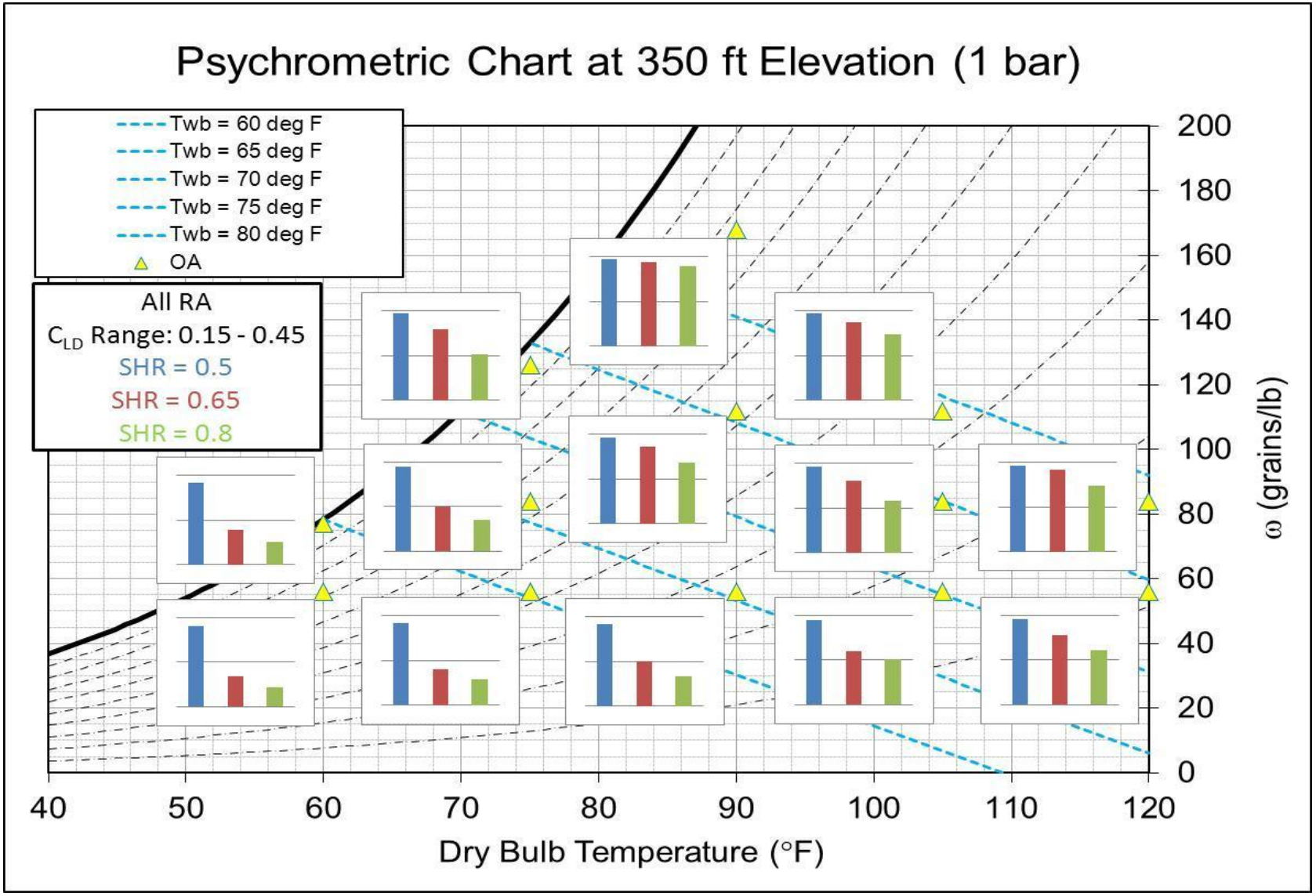

Figure C.148: Average $C_{LD,in,DEVap,last}$ values for all return air states under variable SHR values and outdoor air states